

AD-A141 118



DIGITAL MULTIVARIABLE TRACKER CONTROL  
LAWS FOR THE KC-135A

THESIS

AFIT/GE/EE/83D-40

William J. Locken  
Capt USAF

This document has been approved  
for public release and sale; its  
distribution is unlimited.

DEPARTMENT OF THE AIR FORCE  
AIR UNIVERSITY

**AIR FORCE INSTITUTE OF TECHNOLOGY**

Wright-Patterson Air Force Base, Ohio

DTIC  
ELECTED  
MAY 15 1984  
A

DTIC FILE COPY

84 05 14 114

1

DIGITAL MULTIVARIABLE TRACKER CONTROL  
LAWS FOR THE KC-135A

THESIS

AFIT/GE/EE/83D-40

William J. Locken  
Capt USAF

DTIC  
ELECTE  
MAY 15 1984

DIGITAL MULTIVARIABLE TRACKER CONTROL  
LAWS FOR THE KC-135A

THESIS

Presented to the Faculty of the School of Engineering  
of the Air Force Institute of Technology  
Air University  
in Partial Fulfillment of the  
Requirements for the Degree of  
Master of Science

by

William J. Locken, B.S.E.E.

Capt                      USAF

Graduate Electrical Engineer

December 1983

Accession For	
NTIS GRA&I	<input checked="" type="checkbox"/>
DTIC TAB	<input type="checkbox"/>
Unannounced	<input type="checkbox"/>
Justification	
By	
Distribution/	
Availability Codes	
Dist	Avail and/or
A-1	

## Preface

This thesis topic was suggested and sponsored by the Flight Dynamics Laboratory, Wright-Patterson AFB, Ohio. My choice of this topic was based on two reasons. First, and foremost, the topic parallels my graduate studies in flight control. Second, the topic showed promise of holding both my interest and enthusiasm since I have flown the KC-135A aircraft. Also, being familiar with the aircraft's flight characteristics, I was in a position to evaluate the results obtained.

The theoretical background is based on design techniques developed by Professor Brian Porter from the University of Salford, England. I would like to express my sincere appreciation to my thesis advisor Professor John J. D'Azzo, Deputy Department Head, Department of Electrical Engineering, Air Force Institute of Technology. His guidance and suggestions throughout made this thesis effort achievable.

This research was accomplished in parallel with four fellow students. During the development of this thesis I found the numerous discussions with this group to be most helpful. Special thanks goes to Lt. Jeffrey A. Simmers for his assistance in understanding MULTI's fortran code. My sincere thanks go to the other members of the group, Lt. Mark Hoffman, Lt. Roger S. Feldmann and Lt. Brian H. Mayhew.



Finally, but most of all, I want to express my love and appreciation to my wife, Patricia, for her patience and understanding during this research effort. And to my children, Krista and Nicholas, I Love You.

Capt. William J. Locken

## Contents

	Page
Preface .....	ii
List of Figures .....	vii
List of Tables .....	ix
List of Symbols .....	xii
Abstract .....	xviii
I. Introduction .....	1
Background .....	1
Problem .....	2
Approach .....	3
Assumptions .....	3
Presentation .....	4
II. Control Law Theory .....	5
Introduction .....	5
Unknown Plants .....	8
Known Plants .....	11
Known/Regular Plants .....	14
Known/Irregular Plants .....	18
B* Plants .....	23
Summary .....	25
III. KC-135A Aircraft Model .....	26
Introduction .....	26
Aircraft Description .....	26
System Models .....	28
Sign Convention and Axis System .....	30
Summary .....	34
IV. Time Delay Modification to Computer Program MULTI .....	35
Introduction .....	35
Theory of Computational Time Delay .....	35
Summary of MULTI Code Changes .....	38
Summary .....	43
V. Multivariable Control Law Design .....	44
Introduction .....	44
Requirements .....	45

	Page
Manuevers .....	46
Input/Output Models .....	47
Design Procedures .....	49
Tracker Control Laws For Flight Condition #3 ..	53
Coordinated Turn .....	53
Sideslip .....	59
Normal Climb .....	63
Pitch Pointing .....	70
Tracker Control Laws For Flight Condition #2 ..	76
Coordinated Turn .....	76
Sideslip .....	77
Normal Climb .....	78
Pitch Pointing .....	78
Tracker Control Laws For Flight Condition #1 ..	79
Coordinated Turn .....	79
Sideslip .....	80
Normal Climb .....	80
Pitch Pointing .....	81
Time Delay .....	81
Coordinated Turn Flight Condition #3 .....	82
Sideslip Flight Condition #3 .....	91
Normal Climb Flight Condition #3.....	97
Pitch Pointing Flight Condition #3 .....	102
Modifications to $K_0$ and $K_1$ .....	113
Robustness of The Control Laws .....	115
Coordinated Turn .....	115
Sideslip .....	127
Normal Climb .....	136
Pitch Pointing .....	150
Summary .....	155
VI. Conclusion and Recommendations .....	156
Thesis Summary .....	156
Conclusions .....	157
Recommendations .....	158
Bibliography .....	162
Appendix A: Aircraft Equations of Motion .....	164
Appendix B: Sample Run of Cat Program .....	185
Appendix C: Simulation Results For Flight Conditions #1 and #2 .....	190
Appendix D: Calcomp Plots .....	220
Appendix E: Debugging of MULTI Fortran Code .....	224

	Page
Appendix F: Transformation Matrix .....	225
VITA .....	228

## List of Figures

Figure		Page
2-1	P.I. Controller .....	7
2-2	Block Diagram of Known/Regular Plant/Controller Structure .....	14
2-3	Block Diagram of Known/Irregular Plant /Controller Structure .....	19
3-1	Sign Conventions .....	31
3-2	Lateral Sign Convention .....	32
3-3	Longitudinal Sign Convention .....	33
4-1	Computational Time Delay With Compensator .	37
5-1a-f	Flight Condition #3, Coordinated Turn .....	55-57
5-2a-d	Flight Condition #3, Sideslip .....	61-62
5-3a-h	Flight Condition #3, Normal Climb .....	65-68
5-4a-h	Flight Condition #3, Pitch Pointing .....	72-75
5-5a-f	Flight Condition #3, Coordinated Turn With Time Delay .....	83-85
5-6a-f	Flight Condition #3, Coordinated Turn With Time Delay Redesigned .....	88-90
5-7a-d	Flight Condition #3, Sideslip With Time Delay .....	92-93
5-8a-d	Flight Condition #3, Sideslip With Time Delay Redesigned .....	95-96
5-9a-h	Flight Condition #3, Normal Climb With Time Delay .....	98-101
5-10a-h	Flight Condition #3, Pitch Pointing With Time Delay .....	103-106
5-11a-h	Flight Condition #3, Pitch Pointing With Time Delay Redesigned .....	108-111
5-12a-f	Robust Controller Flight Condition #3 Coordinated Turn .....	117-119

Figure		Page
5-13a-f	Robust Controller Flight Condition #2 Coordinated Turn .....	120-122
5-14a-f	Robust Controller Flight Condition #1 Coordinated Turn .....	123-125
5-15a-d	Robust Controller Flight Condition #3 Sideslip .....	130-131
5-16a-d	Robust Controller Flight Condition #2 Sideslip .....	132-133
5-17a-d	Robust Controller Flight Condition #1 Sideslip .....	134-135
5-18a-h	Robust Controller Flight Condition #3 Normal Climb .....	138-141
5-19a-h	Robust Controller Flight Condition #2 Normal Climb .....	142-145
5-20a-h	Robust Controller Flight Condition #1 Normal Climb .....	146-149
5-21a-h	Flight Condition #3, Pitch Pointing With Time Delay Minimum K .....	151-154
A-1	Geometry of a Climb .....	165
C-1a-f	Flight Condition #2 Coordinated Turn .....	191-193
C-2a-d	Flight Condition #2 Sideslip .....	194-195
C-3a-h	Flight Condition #2 Normal Climb .....	197-200
C-4a-h	Flight Condition #2 Pitch Pointing .....	201-204
C-5a-f	Flight Condition #1 Coordinated Turn .....	206-208
C-6a-d	Flight Condition #1 Sideslip .....	209-210
C-7a-h	Flight Condition #1 Normal Climb .....	212-215
C-8a-h	Flight Condition #1 Pitch Pointing .....	216-219
D-1	Improperly Scaled Calcomp Plot .....	220

## List of Tables

Table		Page
5-1	Simulation Results For Coordinated Turn Flight Condition #3 .....	59
5-2	Simulation Results For Sideslip Flight Condition #3 .....	63
5-3	Simulation Results For Normal Climb Flight Condition #3 .....	70
5-4	Simulation Results For Pitch Pointing Flight Condition #3 .....	76
5-5	Simulation Results For Coordinated Turn With Time Delay Flight Condition #3 .....	86
5-6	Simulation Results For Coordinated Turn With Time Delay Flight Condition #3 (Redesigned) ...	87
5-7	Simulation Results For Sideslip With Time Delay Flight Condition #3 .....	91
5-8	Simulation Results For Sideslip With Time Delay Flight Condition #3 (Redesigned) .....	97
5-9	Simulation Results For Normal Climb With Time Delay Flight Condition #3 .....	97
5-10	Simulation Results For Pitch Pointing With Time Delay Flight Condition #3 .....	102
5-11	Simulation Results For Pitch Pointing With Time Delay Flight Condition #3 (Redesigned) .....	112
5-12	Simulation Results For Robust Controller Condition #3 Coordinated Turn .....	126
5-13	Simulation Results For Robust Controller Condition #2 Coordinated Turn .....	126
5-14	Simulation Results For Robust Controller Condition #1 Coordinated Turn .....	127
5-15	Simulation Results For Robust Controller Condition #3 Sideslip .....	128
5-16	Simulation Results For Robust Controller Condition #2 Sideslip .....	129

Table		Page
5-17	Simulation Results For Robust Controller Condition #1 Sideslip .....	129
5-18	Simulation Results For Robust Controller Condition #3 Normal Climb .....	137
5-19	Simulation Results For Robust Controller Condition #2 Normal Climb .....	137
5-20	Simulation Results For Robust Controller Condition #1 Normal Climb .....	150
5-21	Simulation Results For Pitch Pointing With Time Delay Flight Condition #3 Minimum K .....	155
A-1	KC-135A Aircraft Data .....	175
A-2	Non-dimensional Stability Axis Derivatives For Flight Condition #1 .....	176
A-3	Non-dimensional Stability Axis Derivatives For Flight Condition #2 .....	177
A-4	Non-dimensional Stability Axis Derivatives For Flight Condition #3 .....	178
A-5	Dimensional A and B Matrix Coefficients For Flight Condition #1 .....	179
A-6	Dimensional A and B Matrix Coefficients For Flight Condition #2 .....	180
A-7	Dimensional A and B Matrix Coefficients For Flight Condition #3 .....	181
C-1	Simulation Results For Flight Condition #2 Coordinated Turn .....	190
C-2	Simulation Results For Flight Condition #2 Sideslip .....	190
C-3	Simulation Results For Flight Condition #2 Normal Climb .....	196
C-4	Simulation Results For Flight Condition #2 Pitch Pointing .....	196
C-5	Simulation Results For Flight Condition #1 Coordinated Turn .....	205



Table		Page
C-6	Simulation Results For Flight Condition #1 Sideslip .....	205
C-7	Simulation Results For Flight Condition #1 Normal Climb .....	211
C-8	Simulation Results For Flight Condition #1 Pitch Pointing .....	211

## List of Symbols

A	Continuous-time plant matrix
AC	Aerodynamic center
$\alpha$	Angle of attack, perturbation angle of attack in perturbation equations, Ratio of proportional to integral feedback
$\alpha_0$	Trim angle of attack
B	Continuous-time plant matrix
b	Wing span
$\beta$	Sideslip angle
C	Continuous-time Output Matrix
c	Mean Aerodynamic Cord
CG, cg	Center of gravity
$C_D$	Nondimensional coefficient of drag (along velocity vector)
$C_{D\alpha}$	Nondimensional variation of drag with angle of attack
$C_{D\delta}$	Nondimensional variation of drag with elevator ( $\delta_e$ ) or speed brake ( $\delta_{sb}$ )
$C_{Du}$	Nondimensional variation of drag with forward velocity perturbations from trim velocity
$C_L$	Nondimensional coefficient of lift (normal to velocity vector)
$C_{L\alpha}$	Nondimensional variation of lift with angle of attack
$C_{L\dot{\alpha}}$	Nondimensional variation of lift with the rate of change of angle of attack
$C_{L\delta}$	Nondimensional variation of lift with elevator ( $\delta_e$ ) or speed brakes ( $\delta_{sb}$ )
$C_{L\dot{\alpha}}$	Nondimensional variation of lift with pitch rate
$C_{l\beta}$	Nondimensional variation of rolling moment with sideslip angle

$C_{l_{\delta}}$	Nondimensional variation of rolling moment with control wheel ( $\delta_w$ ) or rudder ( $\delta_r$ )
$C_{l_p}$	Nondimensional variation of rolling moment with roll rate
$C_{l_r}$	Nondimensional variation of rolling moment with yaw rate
$C_m$	Nondimensional variation of pitching moment
$C_{m_{\alpha}}$	Nondimensional variation of pitching moment with angle of attack
$C_{m_{\delta}}$	Nondimensional variation of pitching moment with elevator ( $\delta_e$ ) or speed brakes ( $\delta_{sb}$ )
$C_{m_q}$	Nondimensional variation of pitching moment with pitch rate
$C_{m_u}$	Nondimensional variation of pitching moment with forward velocity perturbations
$C_{n_{\beta}}$	Nondimensional variation of yawing moment with sideslip angle
$C_{n_{\delta}}$	Nondimensional variation of yawing moment with control wheel ( $\delta_w$ ) or rudder ( $\delta_r$ )
$C_{n_p}$	Nondimensional variation of yawing moment with roll rate
$C_{n_r}$	Nondimensional variation of yawing moment with yaw rate
$\cos$	Cosine
$C_{x_{\alpha}}$	Nondimensional variation of x-force with angle of attack
$C_{x_{\delta}}$	Nondimensional variation of x-force with elevator ( $\delta_e$ ) or speed brake ( $\delta_{sb}$ )
$C_{x_q}$	Nondimensional variation of x-force with pitch rate
$C_{x_u}$	Nondimensional variation of x-force with forward velocity perturbations
$C_{y_{\beta}}$	Nondimensional variation of y-force with sideslip angle
$C_{y_{\delta}}$	Nondimensional variation of y-force with control wheel ( $\delta_w$ ) or rudder ( $\delta_r$ )

$C_{y_p}$	Nondimensional variation of y-force with roll rate
$C_{y_r}$	Nondimensional variation of y-force with yaw rate
$C_{z_\alpha}$	Nondimensional variation of z-force with angle of attack
$C_{z_{\dot{\alpha}}}$	Nondimensional variation of z-force with the rate of change of angle of attack
$C_{z_{\delta}}$	Nondimensional variation of z-force with elevator ( $\delta_e$ ) or speed brake ( $\delta_{sb}$ )
$C_{z_q}$	Nondimensional variation of z-force with pitch rate
$C_{z_u}$	Nondimensional variation of z-force with forward velocity perturbation
deg	Degree
$\delta_w$	Control wheel deflection
$\delta_e$	Elevator deflection
$\delta_{sb}$	Speed brake deflection
$\delta_T$	Percent engine thrust, change from trim
e	Body bending displacement, error vector
e(t)	Error vector
e(kT)	Discrete error vector
$\epsilon$	Epsilon scalar multiplier
ft	Feet
f	Sampling frequency
g	Gravity
G(0)	Transfer function matrix
$I_{xx}$	Moment of inertia about x-axis
$I_{yy}$	Moment of inertia about y-axis
$I_{zz}$	Moment of inertia about z-axis
$I_{xz}$	Product of inertia about xz-axes

$I$	Identity matrix
$K_0$	Proportional control law feedback matrix
$K_1$	Integral control law feedback matrix
lbs	pounds
$L_\beta$	Dimensional variation of rolling moment with sideslip angle
$L_\delta$	Dimensional variation of rolling moment with control wheel ( $\delta_w$ ) or rudder ( $\delta_r$ )
$L_p$	Dimensional variation of rolling moment with roll rate
$L_r$	Dimensional variation of rolling moment with yaw rate
$M$	Measurement matrix
$m$	Aircraft mass, number of inputs
MAC	Mean Aerodynamic Cord
$M_\alpha$	Dimensional variation of pitching moment with angle of attack
$M_{\dot{\alpha}}$	Dimensional variation of pitching moment with the rate of change of angle of attack
$M_c$	Controllability matrix
$M_o$	Observability matrix
$M_q$	Dimensional variation of pitching moment with pitch rate
$M_{\dot{\alpha}}$	Dimensional variation of pitching moment with pitch angle
$M_x$	Moment about the x-axis
$M_y$	Moment about the y-axis
$M_z$	Moment about the z-axis
$n$	Number of states
$N_\beta$	Dimensional variation of yawing moment with sideslip angle

$N_{\delta}$	Dimensional variation of yawing moment with control wheel ( $\delta_w$ ) or rudder ( $\delta_r$ )
$N_r$	Dimensional variation of yawing moment with yaw rate
$N_p$	Dimensional variation of yawing moment with roll rate
$p$	Number of output, roll rate
$q$	Pitch rate
$q$	Dynamic pressure
$r$	Yaw rate
rad	Radians
$S$	Surface area
sec	Seconds
sin	Sine
$\sigma$	Elements of the Sigma ( $\Sigma$ ) matrix
$\Sigma$	Sigma gain weighting matrix
$T$	Transformation matrix, Sampling period, thrust
$U_0$	Equilibrium (trim) x-axis velocity
$u$	Perturbation velocity along x-axis, input vector
$V$	Velocity along y-axis
$v$	Perturbation velocity along y-axis, command input vector
$V_0$	Equilibrium (trim) y-axis velocity
$W_0$	Equilibrium (trim) z-axis velocity
$W$	Aircraft weight
$w$	Perturbation velocity along z-axis
$x$	State vector
$X_{\alpha}$	Dimensional variation of x-force with angle of attack
$X_{\dot{\alpha}}$	Dimensional variation of x-force with rate of change of angle of attack

$x_{\delta}$	Dimensional variation of x-force with elevator ( $\delta_e$ ) or speed brakes ( $\delta_{sb}$ )
$x_q$	Dimensional variation of x-force with pitch rate
$x_u$	Dimensional variation of x-force with forward velocity perturbation
$y$	Output vector
$y_{\beta}$	Dimensional variation of y-force with sideslip angle
$y_{\delta}$	Dimensional variation of y-force with control wheel ( $\delta_w$ ) or rudder ( $\delta_r$ )
$y_p$	Dimensional variation of y-force with roll rate
$y_r$	Dimensional variation of y-force with yaw rate
$z(t), z$	Integral of error vector
$z(kT)$	Discrete integral of error vector
$z_{\alpha}$	Dimensional variation of z-force with angle of attack
$z_{\dot{\alpha}}$	Dimensional variation of z-force with the rate of change of angle of attack
$z_{\delta}$	Dimensional variation of z-force with the elevator ( $\delta_e$ ) or speed brakes ( $\delta_{sb}$ )
$z_q$	Dimensional variation of z-force with pitch rate
$z_u$	Dimensional variation of z-force with forward velocity perturbation
$z_t$	Transmission zeros
$z_{1,2}$	Finite system roots
$z_3$	Infinite system roots
$\theta$	Pitch angle
$\theta_0$	Equilibrium pitch angle
$\phi$	Roll angle
$\psi$	Yaw angle
$\Gamma(\lambda)$	Asymptotic transfer function matrix

## ABSTRACT

### Digital Multivariable Control Laws For The KC-135A

Multivariable design techniques developed by Professor Brian Porter of the University of Salford, England, are used to develop digital control laws for the KC-135A. Control laws are developed for each of three diverse flight conditions. MULTI, a computer program used in the design, is modified to account for computational time delay. The effects of a computational time delay on the controllers developed are presented.

The controllers developed, using these techniques, utilize output feedback with proportional plus integral control. Because of the structure of the system, measurement variables, in addition to the outputs, are necessary. A reduced controller is modeled by setting some of the required feedback gains to zero. A comparison of the results of the reduced controller to the complete controller is presented.

A robustness controller is tested by performing specific maneuvers at more than one flight condition. The robust controller is of the reduced form and is required to perform under the constraints of the computational time delay.

This thesis concludes that actuator dynamics play a significant role in the development of control laws, and as a result, 2nd order or higher actuator models should be used in future studies.



# DIGITAL MULTIVARIABLE TRACKER CONTROL LAWS FOR THE KC-135A

## I. INTRODUCTION

### Background

Aircraft are now being designed with closed-loop fly-by-wire flight control systems. These multiple input/multiple output (MIMO) systems are required to achieve stability and desirable performance while transforming the pilot's command inputs into movement of the flight control surfaces. At the heart of this MIMO system is a digital computer.

Presently, controllers for such MIMO systems are often designed using classical single input/single output (SISO) and Linear Quadratic Gaussian (LQG) methods. Each of these methods have some serious drawbacks. The well known classical SISO method may yield a satisfactory design, however, it allows for examination of only a single input/output combination at any one time. LQG methods can handle the MIMO case, but all internal states have to be accessible for the design method to work. If not accessible, LQG requires the use of complicated state estimators to provide the system with an estimate of the inaccessible states.

Professor Brian Porter and his associates of the University of Salford, England, have suggested the use of four direct design methods capable of synthesizing a

controller which can handle MIMO systems while at the same time providing for a high degree of output decoupling (Ref. 2). These design techniques produce controllers for highly-interactive linear multivariable systems.

Initial attempts to synthesize an aircraft flight control system using Porter's techniques has proven to be successful (Ref. 3 and 4). These investigations found the techniques to be fairly straightforward. Still, much remains to be studied before a final design can be implemented on future aircraft.

AFIT students have developed a computer program called MULTI (Ref. 4) that utilizes the design techniques of Brian Porter. MULTI allows the user to both design and simulate a MIMO controller with the help of a digital computer. The computer provides a means for multiple iterations of the design and simulation to allow the user to achieve a suitable design.

### Problem

The purpose of this thesis is to investigate the development of tracker control laws for the KC-135A aircraft. Controller performance is demonstrated through the use of the computer program MULTI by performing designated flight maneuvers. Controllers are developed for each of three flight conditions. For each flight condition, four maneuvers, two lateral and two longitudinal are

performed. A robust controller is developed which is capable of producing satisfactory responses for a single maneuver for all three flight conditions studied.

This thesis also incorporates a modification to MULTI that allows for the addition of a computational time delay when simulating the results of a controller. Controller performance is tested against this computational time delay.

### Approach

In order to accomplish the desired results, six steps are taken in completion of this thesis.

1. Development of the aircraft equations of motion for three separate flight conditions, including a body bending mode in the longitudinal case.
2. Adding to MULTI the capability to include, at the user's request, a computational time delay when simulating design results.
3. Design of digital multivariable tracker control laws using the appropriate design methods of Chapter II.
4. Evaluation of the effects of computational time delay on each of the controllers developed.
5. Investigation of minimum gain designs where the gain Matrices  $K_0$  and  $K_1$  are minimized for each maneuver.
6. Development of a robust controller capable of performing a single maneuver for all flight conditions.

### Assumptions

It is assumed that computer simulations give a realistic approximation of aircraft motion. Other

assumptions as necessary in the development of certain parts of this thesis are listed as they are needed.

### Presentation

Six chapters are included in this thesis. Chapter II describes the theory underlying the design method used in this study. Chapter III describes the KC-135A aircraft and Appendix A details the development of the necessary aircraft equations of motion. Chapter IV present the computational time delay modification made to MULTI. Chapter V describes the development of tracker control laws for the KC-135A for the three different flight conditions. This includes discussions of the results obtained for flight condition #3 using computational time delays and minimum K designs. Also included in Chapter V is a presentation of the robust controller developed for each of the four maneuvers. Chapter VI is the conclusion and offers recommendations for future studies and suggestions for possible improvements and/or additions to MULTI.

## II. MULTIVARIABLE CONTROL LAW THEORY

### Introduction

The control law theory used in this thesis was developed primarily by Professor Brian Porter, of the University of Salford, England with the help of Doctor A. Bradshaw, also of the University of Salford. Professor Porter's research was performed under a contract sponsored by the Air Force Flight Dynamics Laboratory (AFWAL/FIGL), Wright-Patterson Air Force Base, Ohio. Only a summary of the theory on singular perturbation multivariable controller design is presented in this chapter and in Reference 2. A truly interested reader can trace the development of this theory from its early stages, by researching the bibliography in chronological order.

The multivariable controller design presented here is based on a system whose continuous state and output equations can be defined as:

$$\dot{x}(t) = Ax(t) + Bu(t) + Dd(t) \quad (2-1)$$

$$y(t) = Cx(t) + Fu(t) \quad (2-2)$$

where

A = continuous-time plant matrix (nxn)

B = continuous-time control matrix (nxm)

D = continuous-time disturbance matrix (nxr)

C = continuous-time output matrix (pxn)

$F$  = continuous-time feed forward matrix ( $p \times m$ )

The dimensions  $n$ ,  $m$ ,  $p$  and  $r$  are defined as the number of states, inputs, outputs and disturbances, respectively. This thesis, however, deals entirely with the case where  $m=p$ . (i.e. number of inputs = number of outputs).

Professor Porter's efforts have resulted in design techniques that produce a Proportional Plus Integral (PI) Controller which can be either analog or digital in nature. For the purpose of this thesis, this chapter concentrates on the digital case where the system state and output difference equations assume the form:

$$x[(k+1)T] = \theta x(kt) + \Psi u(kt) + \Delta d(kt) \quad (2-3)$$

$$y(kt) = \Gamma x(kT) + \gamma u(kT) \quad (2-4)$$

where

$\theta$  = sampled-data plant matrix ( $n \times n$ )

$\Psi$  = sampled-data control matrix ( $n \times m$ )

$\Delta$  = sampled-data disturbance matrix ( $n \times r$ )

$\Gamma$  = sampled-data output matrix ( $p \times n$ )

$\gamma$  = sampled-data feed forward matrix

$T$  = sampling period

with

$$\theta = e^{AT} \quad (2-5)$$

$$\Psi = \int_0^T e^{A(T-t)} B dt \quad (2-6)$$

$$\Delta = \int_0^T e^{AT} D dt \quad (2-7)$$

$$\Gamma = C \quad (2-8)$$

$$\gamma = F \quad (2-9)$$

Figure 2-1 represents the Proportional Plus Integral Controller for the digital case. The discrete integrator shown in this figure satisfies Equation (2-15). For this discrete case, samplers are assumed to be placed in the feedback loop and at the command input vector,  $v$ . A zero-order-hold device is placed after the second summer to produce piece-wise constant inputs to the plant. An important advantage of this method of controller design is that after making these assumptions, no further complex design analysis in the "Z" domain is required.

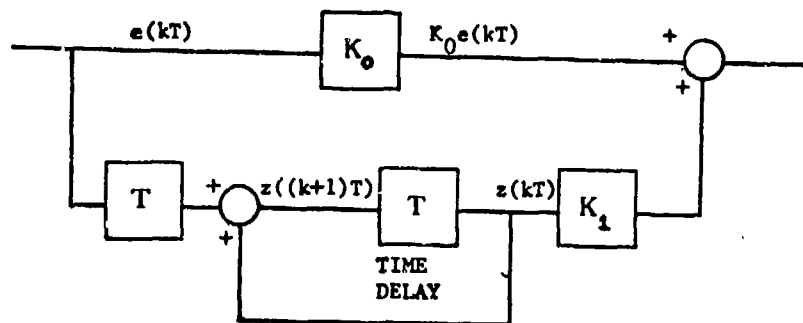


FIGURE 2-1: (PI) Controller

Using this type of system, Professor Porter has developed four separate design procedures with which to synthesize a Proportional Plus Integral Digital Controller.

The first three procedures are based on whether the plant involved is described as unknown, known/regular, or known/irregular. The fourth procedure, known as B\*, provides synthesis of the digital controller to provide enhanced decoupling and/or elimination of any undesirable initial undershooting of the outputs. These four procedures are briefly described in the following paragraphs. It should be noted that even though the designs discussed are for a discrete controller, the continuous state equation given by Equations (2-1) and (2-2) may be used (Ref. 5).

#### Unknown Plants (Ref. 6)

In many cases, very little is known about the dynamical properties which describe the state equation model. In this case exact representation for the matrices A, B, C, D and F of Equations (2-3) thru (2-9) are not available. It can therefore be very expensive and time consuming to develop such a model when one does not already exist. At the same time, the state transfer function matrix,  $G(0)$ , can be easily determined from "off-line" tests. These tests must be done in the absence of the disturbance vector, and can be accomplished only if the open-loop plant is asymptotically stable. Also, it should be noted that when the state equations are available and the designer decides to use this technique,  $G(0)$  can be calculated by Equation (2-11). In either case the matrix transfer function is



$$G(\lambda) = C(\lambda I_n - A)^{-1}B \quad (2-10)$$

and

$$G(0) = -CA^{-1}B \quad (2-11)$$

To preserve stability, the rank of  $G(0)$  must be equal to the number of system outputs. It is further required that the number of system outputs be less than or equal to the number of inputs and that  $G(0)$  have no transmission zeros at the origin or in the right half of the  $s$ -plane.

In this case, the control law equation for an error-actuated Proportional Plus Integral Digital Controller assumes the form:

$$u(kT) = T[\epsilon K_0 e(kT) + \epsilon K_1 z(kT)] \quad (2-12)$$

where

$$K_0 = \alpha K_1 \quad (2-13)$$

$$e(kT) = v(kT) - y(kT) \quad (2-14)$$

$$z[(k+1)T] = z(kT) + Te(kT) \quad (2-15)$$

In these equations,  $\alpha$  determines the ratio of proportional to integral control;  $\epsilon$  is a scalar multiplier;  $T$  is the sampling period;  $v(kT)$  is the command input vector;  $y(kT)$  is the output vector;  $e(kT)$  is the error vector;  $z(kT)$  is the integral of the error vector; and  $K_0$  and  $K_1$  are given by:

$$K_0 = \alpha G^T(0) [G(0)G^T(0)]^{-1} \Sigma \quad (2-16)$$

$$K_1 = G^T(0) [G(0)G^T(0)]^{-1} \Sigma \quad (2-17)$$

where sigma is a weighting matrix whose scalar diagonal elements,  $\sigma_i$  ( $i=1,2,3,\dots,p$ ) are chosen by the designer. If it is further restricted so that the number of outputs equals the number of inputs, as is the case for this thesis, then  $G(0)$  is a square matrix. In this case  $[G(0)G^T(0)]^{-1} = [G^T(0)]^{-1} [G(0)]^{-1}$  and Equations (2-16) and (2-17) reduce to:

$$K_0 = \alpha G(0)^{-1} \Sigma \quad (2-18)$$

$$K_1 = G(0)^{-1} \Sigma \quad (2-19)$$

Equations (2-12) thru (2-19) result in two sets of closed-loop roots,  $z_1$  and  $z_2$  :

$$z_1 = \{\lambda \in \mathbb{C} : |\lambda I_n - I_n - TA + H(T^2)| = 0\} \quad (2-20)$$

$$z_2 = \{\lambda \in \mathbb{C} : |\lambda I_p - I_p + T^2 + H(T^3)| = 0\} \quad (2-21)$$

where

$z_1$  = set of roots due to plant states

$z_2$  = set of roots due to integrator states

$I_n$  = nxn identity matrix

$HT^2$  = analytic expression whose value is a function of  $T^2$

$HT^3$  = analytic expression whose value is a function of  $T^3$

### Known Plant (Ref. 5)

Known plants fall into two categories, regular and irregular. For a plant to be classified as known, the matrices A, B, C, D, and F of Equations (2-1) and (2-2) must be available. To design the controller using Porter's method for known plants, Equations (2-1) and (2-2) may first be put into the form:

$$\begin{bmatrix} \dot{x}_1(t) \\ \dot{x}_2(t) \end{bmatrix} = \begin{bmatrix} A_{11} & A_{12} \\ A_{21} & A_{22} \end{bmatrix} \begin{bmatrix} x_1(t) \\ x_2(t) \end{bmatrix} + \begin{bmatrix} \gamma \\ B_2 \end{bmatrix} u(t) \quad (2-22)$$

and

$$y(t) = [C_1 \quad C_2] \begin{bmatrix} x_1(t) \\ x_2(t) \end{bmatrix} \quad (2-23)$$

where

$A_{11}$  = A matrix partition,  $(n-p) \times (n-p)$

$A_{12}$  = A matrix partition,  $(n-p) \times p$

$A_{21}$  = A matrix partition,  $p \times (n-p)$

$A_{22}$  = A matrix partition,  $p \times p$

$B_2$  = non-zero B matrix partition, full rank,  $p \times p$

$C_1$  = C matrix partition,  $p \times (n-p)$

$C_2$  = C matrix partition,  $p \times p$

If Equations (2-1) and (2-2) cannot be put into the form of (2-22) and (2-23) by reordering the states, they can be transformed by a matrix T into the proper form by

choosing  $T$  in  $x'(t) = Tx(t)$  to meet this requirement.

$$T^{-1}B = \begin{bmatrix} 0 \\ B_2 \end{bmatrix} \quad (2-24)$$

Once  $T^{-1}$  is found that satisfies Equation (2-24), the  $A$  matrix of Equation (2-1) can be transformed using the relationship

$$A' = T^{-1}AT \quad (2-25)$$

and the  $C$  matrix is transformed using

$$C' = CT \quad (2-26)$$

Then Equations (2-1) and (2-2) become:

$$\dot{x}'(t) = A'x(t) + \begin{bmatrix} 0 \\ B_2 \end{bmatrix} u(t) \quad (2-27)$$

$$y(t) = C'x(t) \quad (2-28)$$

which can be made to conform to Equations (2-22) and (2-23). It should be noted, however, that the transformation to the form of Equations (2-22) and (2-23) is not necessary in order to perform the design. This is shown in the example given on page 44 of Reference 5. However, the form of Equations (2-22) and (2-23) are used in the discussion to follow.

If the original system contains a feedforward matrix  $F$  in Equation (2-2), then manipulation of the original system

so as to remove the F matrix is recommended. This allows the system to be represented in the form of Equations (2-22) and (2-23). This can be accomplished by either using outputs which do not contain F terms (F terms are caused by accelerations appearing in the outputs) or by augmenting the original system with the servo dynamics yielding new state equations which do not contain an F matrix.

To successfully design a controller using Porter's techniques, all of the following must hold true:

- (1) The pair (A,B) must be a controllable pair
- (2) The pair (A,C) must be an observable pair
- (3)  $\text{Rank} \begin{bmatrix} A & B \\ -C & D \end{bmatrix} = n+p$
- (4)  $p \leq m$  (for an irregular design  $p=m$ )

In addition the designer must check the rank of the first Markov parameter to determine whether the plant is regular or irregular. The first Markov parameter is defined as  $CB=C B$  for the system described by Equations (2-22) and (2-23). If the system is not in the form of Equations (2-22) and (2-23) then the first Markov parameter is defined as CB. If the rank of this parameter is equal to the number of outputs, p, then the plant is said to be "regular". If the rank is less than p, then the plant is "irregular".

### Known/Regular Plants (Ref. 5)

If the first Markov parameter has full rank (i.e. equal to  $p$ ) the plant is referred to as being "regular" and CB is invertable. When this is true the system can be represented by the block diagram of Figure 2-2. Although a continuous-time integrator is shown in Figures 2-2 and 2-3, a discrete integrator of the form shown in Figure 2-1 is intended.

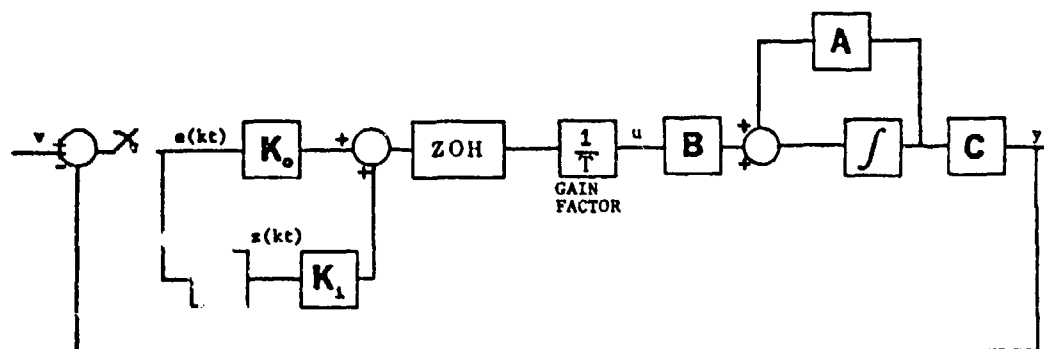


FIGURE 2-2: Block Diagram of Known/Regular Plant/Controller Structure.

For this system the control law equation assumes the form:

$$u(kT) = (1/T) [K_0 e(kT) + K_1 \dot{e}(kT)] \quad (2-29)$$

For tracking constant commands and the rejection of constant disturbance the controller matrices are designed such that:

$$K_0 = \alpha [C_2 B_2]^{-1} \Sigma \quad (2-30)$$

$$K_1 = [C_2 B_2]^{-1} \Sigma = K_0 / \alpha \quad (2-31)$$

where

$$\Sigma = \text{diag}(\sigma_1 \ \sigma_2 \ \dots \ \sigma_p) \quad (2-32)$$

$$\sigma_j \in \mathbb{R} \quad (2-33)$$

The error vector  $e(kT)$  is the difference between the command input vector  $v(kT)$  and the output vector  $y(kT)$  (see Figure 2-2). Since the complete system is augmented with a vector integrator, the steady-state value of the error vector is zero for a constant command vector input, and tracking is achieved (Ref. 5).

Furthermore, this design theory shows that increasingly 'tight' tracking occurs as the sampling frequency,  $f=1/T$ , approaches infinity. It can also be shown (Ref. 5) that as  $T$  approaches zero the closed-loop transfer function matrix  $G(\lambda)$  assumes an asymptotic form:

$$\Gamma(\lambda) = \tilde{\Gamma}(\lambda) + \hat{\Gamma}(\lambda) \quad (2-34)$$

where

$$\tilde{\Gamma}(\lambda) = C_0 (\lambda I_n - I_n - T A_0)^{-1} T B_0 \quad (2-35)$$

$$\hat{\Gamma}(\lambda) = C_2 (\lambda I_p - I_p + g B_2 K_0 C_2)^{-1} g B_2 K_0 \quad (2-36)$$

$$A_0 = \begin{bmatrix} -K_0^{-1} K_1 & 0 \\ A_{12} C_2^{-1} K_0 K_1 & A_{11} - A_2 C_2^{-1} C_1 \end{bmatrix} \quad (2-37)$$

$$B_0 = \begin{bmatrix} 0 \\ A_{12}C_2^{-1} \end{bmatrix} \quad (2-38)$$

$$C_0 = [K_0^{-1}K_1, \quad 0] \quad (2-39)$$

It can be seen from Equations (2-34), (2-35) and (2-37) that  $\tilde{\Gamma}(\lambda)$  contains two sets of roots, associated with what are called the "slow modes". These two sets of roots are:

$$Z_1 = \{\lambda \in \mathbb{C} : |\lambda I_p - I_p + TK_0^{-1}K_1| = 0\} \quad (2-40)$$

and

$$Z_2 = \{\lambda \in \mathbb{C} : |\lambda I_{n-p} - I_{n-p} - TA_{11} + TA_{12}C_2^{-1}C_1| = 0\} \quad (2-41)$$

From Equations (2-34), (2-36), (2-38) and (2-39) it is noted that the poles of  $\hat{\Gamma}(\lambda)$  contains a set of roots associated with the "fast modes". This set of roots is:

$$Z_3 = \{\lambda \in \mathbb{C} : |\lambda I_p - I_p + C_2B_2K_0| = 0\} \quad (2-42)$$

It can be shown (Ref. 5) from Equations (2-37), (2-38), and (2-39) that, as the sampling time  $T$  gets smaller, the slow mode roots associated with the set of roots  $Z_1$  become uncontrollable, and the slow mode roots associated with the set of roots  $Z_2$  (composed of the transmission zeros) become unobservable. Also, the fast modes remain both controllable and observable. Thus, as  $T$  goes to zero, the slow modes disappear from the overall transfer function



$\Gamma(\lambda)$ , and only the fast modes remain:

$$\Gamma(\lambda) = \hat{\Gamma}(\lambda) = [\lambda I_p - I_p + C_2 B_2 K_0]^{-1} C_2 B_2 K_0 \quad (2-43)$$

The roots associated with the fast modes are chosen by the designer to lie within the unit circle of the z-plane by making

$$C_2 B_2 K_0 = \Sigma = \text{diag}(\sigma_1, \sigma_2 \dots \sigma_p) \quad (2-44)$$

and  $K_1$  is found using Equation (2-30). Combining Equations (2-43) and (2-44) yields:

$$\begin{aligned} \Gamma(\lambda) &= [\lambda I_p - I_p + \Sigma]^{-1} \\ &= \text{diag} \left[ \frac{\sigma_1}{\lambda - 1 + \sigma_1}, \frac{\sigma_2}{\lambda - 1 + \sigma_2}, \dots, \frac{\sigma_p}{\lambda - 1 + \sigma_p} \right] \end{aligned} \quad (2-45)$$

and thus Equation (2-45) shows that decoupling is achieved in the asymptotic case.

Transmission zeros of the system are a subset of the slow modes and can be found using Equation (2-41) if the original system has the form of Equations (2-22) and (2-23). If this is not the case, the transmission zeros can be found using a computer program described in Reference 7. Transmission zeros can be a problem since Porter's method requires them to lie within the unit circle in the z-plane. If they are located on or outside the unit circle then a stable controller may not be achievable.

### Known/Irregular Plants (Ref. 5)

If the first Markov parameter is rank deficient (i.e. not equal to  $p$ ) then the plant is said to be "irregular". In this case the product  $CB$  is not invertable and it becomes necessary to introduce measurement equations to compensate for this rank deficiency. When this happens a new feedback vector is defined as:

$$w(t) = [C_1 + MA_{11} \quad C_2 + MA_{12}] \begin{bmatrix} x_1(t) \\ x_2(t) \end{bmatrix} \quad (2-46)$$

$$= [F_1 \quad F_2] \begin{bmatrix} x_1(t) \\ x_2(t) \end{bmatrix} \quad (2-47)$$

where

$M$  = Measurement Matrix,  $p \times (n-p)$

The matrix ' $M$ ' is a measurement matrix which is chosen such that the matrix product  $FB$  has full rank. With the addition of the measurement matrix the system can now be represented by the Block Diagram of Figure 2-3.

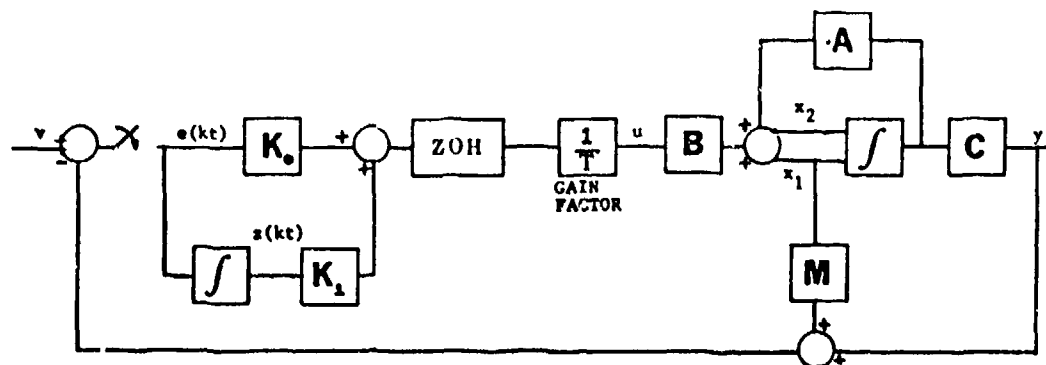


FIGURE 2-3: Block Diagram of Known/Irregular Plant/Controller Structure.

The measurement matrix must be chosen by the designer.

Only through proper choice of this matrix can decoupling of the outputs in the asymptotic case occur. Reference 8 discusses a method for choosing a measurement matrix which allows for decoupling. The method discussed in this paper works only if the system can be put in the form of Equations (2-22) and (2-23). Once in this form a  $B^*$  matrix is formed from the following equation:

$$B^* = \begin{bmatrix} C_1^T A_{11}^{d_1} A_{12} \\ \vdots \\ C_m^T A_{11}^{d_m} A_{12} \end{bmatrix} \quad (2-48)$$

where  $m$  is the number of control inputs,  $C_i^T$  is the  $i$ th row of  $C_1$  and  $d_j = \min(j: C_i^T A_{11}^j A_{12} \neq 0, j=0, 1, 2, \dots, n-1)$  or  $d_j = n-1$  if  $C_i^T A_{11}^j A_{12} = 0$  for all  $j$ . Next  $F_2$  is formed using:

$$F_2 = C_2 + M A_{12} \quad (2-49)$$

and by comparison of Equation (2-48) to (2-49) the  $m$

elements are chosen based upon the non zero elements of  $B^*$ . It should be noted that additional constraints are put on the elements of the  $M$  matrix depending on the rank of  $B^*$  and the row dimension of  $C_1$  as compared to row dimension of  $A_{12}$  and column dimension of  $A_{11}$ . For a complete understanding of the choice of the  $M$  matrix elements the reader must refer to Reference 8. Also it should be pointed out that proper choice of the measurement matrix elements is critical because it affects the location of the transmission zeros of the system. These transmission zeros are now determined by:

$$z_T = \{\lambda \in C : |\lambda I_{n-p} - I_{n-p} - A_{11} + A_{12}F_2^{-1}F_1| = 0\} \quad (2-50)$$

and as with regular plants, the transmission zeros must lie in the left half of the  $s$ -plane or within the unit circle in the  $z$ -plane. Once again, if the system is not represented as in Equations (2-22) and (2-23), then Equation (2-50) can not be used to determine the transmission zeros.

Once the measurement matrix  $M$  is chosen and  $F$  and  $F$  are calculated, the control law is governed by the form:

$$u(kt) = (1/T)[K_0 e(kt) + K_1 z(kt)] \quad (2-51)$$

where

$$K_0 = \alpha(F_2 B_2)^{-1} \Sigma \quad (2-52)$$

$$K_1 = (F_2 B_2)^{-1} \Sigma \quad (2-53)$$

Note that  $C_2$  in Equations (2-30) and (2-31) is replaced by  $F_2$

in Equations (2-52) and (2-53), and that  $F_2 B_2$  does have full rank, by proper choice of  $M$ , and is therefore invertable.

Figure 2-3 shows that the error vector  $e(kT)$  is now given by:

$$e(kT) = v(kT) - w(kT) \quad (2-54)$$

It can also be shown, as before, that for constant inputs, the steady-state value of  $w(kT)$  equals  $y(kT)$ , so that the system still tracks the constant command input, as desired.

As with Known/Regular plants, it can be shown that as the sampling time  $T$  approaches zero the asymptotic closed-loop transfer function  $G(\lambda)$  assumes the form:

$$\Gamma(\lambda) = \tilde{\Gamma}(\lambda) + \hat{\Gamma}(\lambda) \quad (2-55)$$

where

$$\tilde{\Gamma}(\lambda) = C_0 (\lambda I_n - I_n - TA_0)^{-1} TB_0 \quad (2-56)$$

$$\hat{\Gamma}(\lambda) = C_0 (\lambda I_p - I_p - A_4)^{-1} B_2 K_0 \quad (2-57)$$

$$A_0 = \begin{bmatrix} -K_0^{-1} K_1 & 0 \\ A_{12} F_2^{-1} K_0 K_1 & A_{11} - A_{12} F_2^{-1} F_1 \end{bmatrix} \quad (2-58)$$

$$B_0 = \begin{bmatrix} 0 \\ A_{12} F_2^{-1} \end{bmatrix} \quad (2-59)$$

$$C_0 = [C_2 K_2^{-1} K_0^{-1} K_1, \quad C_1 - C_2 F_2^{-1} F_1] \quad (2-60)$$

$$A_4 = B_2 K_0 F_2 \quad (2-61)$$

As expected, these equations are similar to Equations (2-34) thru (2-39) which were developed for Known/Regular plants. Because of this similarity it can be seen that the two sets of "slow mode" roots are now:

$$Z_1 = \{\lambda \in C: |\lambda I_p - I_p + TK_0^{-1}K_1| = 0\} \quad (2-62)$$

and

$$Z_2 = \{\lambda \in C: |\lambda I_{n-p} - I_{n-p} - TA_{11} + TA_{12}F_2^{-1}F_1| = 0\} \quad (2-63)$$

and that the "fast mode" roots become:

$$Z_3 = \{\lambda \in C: |\lambda I_p - I_p + F_2B_2K_0| = 0\} \quad (2-64)$$

Again, analogous to the Known/Regular plant, it can be shown (Ref. 5) that as the sampling time  $T$  gets smaller the slow modes associated with the  $Z_1$  roots become uncontrollable and thus have no contribution to the transfer function. But, unlike the case of the Known/Regular plant, the slow modes associated with the  $Z_2$  roots remain both observable and controllable due to the extra measurements generated by the  $M$  matrix. The fast modes associated with roots ( $Z_3$ ), again remain both controllable and observable as  $T$  gets smaller.

Hence, it is evident that as  $f$  approaches infinity the transfer function matrix  $G(\lambda)$  of the discrete-time tracking system assumes the asymptotic form:

$$\Gamma(\lambda) = (C_1 - C_2 F_2^{-1} F_1) [\lambda I_{n-p} - I_{n-p} - T A_{11} + T A_{12} F_2^{-1} F_1]^{-1} T A_{12} F_2^{-1} \\ + C_2 F_2^{-1} [\lambda I_p - I_p + F_2 B_2 K_0]^{-1} F_2 B_2 K_0 \quad (2-65)$$

The first term of Equation (2-65) contains the slow mode roots (transmission zeros) and the second term contains the fast mode roots.

The fast mode roots are chosen by the designer, using a method similar to that used for Known/Regular plants:

$$F_2 B_2 K_0 = C_2 + M A_{12} B_2 K_0 = \text{diag}(\sigma_1, \sigma_2, \dots, \sigma_p) \quad (2-66)$$

These roots must lie within the unit circle in the z-plane. The transmission zero locations are also set by the designer in Equation (2-63) and are chosen by selection of the measurement matrix M.

It should be noted that the transfer function matrix given in Equation (2-65) does not always result in decoupled outputs and that the measurement matrix M plays a large role in determining decoupling. Again the reader is referred to Reference 8 for help in picking a measurement matrix that allows decoupling of the outputs.

#### B\* Plants (Ref. 9)

For plants in which the three previous designs do not satisfactorily decouple the output and/or undesirable initial undershooting occurs in the time response, this fourth design method is available. A new matrix, B\* is

determined using:

$$B^* = \begin{bmatrix} c_1^T A^{d_1} B \\ c_2^T A^{d_2} B \\ . \\ c_p^T A^{d_p} B \end{bmatrix} \quad (2-67)$$

where  $m$  is the number of control inputs,  $C_p$  is the  $i$ th row of  $C$ , and  $d_p = \min(j: C_p^T A^j B = 0, j=0, 1, \dots, n-1)$  or  $d_p = n-1$  if  $C_p^T A^j B = 0$  for all  $j$ . Note, however, that if  $B^*$  is rank deficient (i.e.  $B^*$  is singular) this design method cannot be used.

When  $B^*$  has full rank, the controller matrices are determined by:

$$K_0 = (B^*)^{-1} \Sigma_1 \quad (2-68)$$

$$K_1 = [G(0)]^{-1} \Sigma_2 \quad (2-69)$$

where  $\Sigma_1$  and  $\Sigma_2$  are both selected as diagonal ( $p \times p$ ) matrices. Once  $K_0$  and  $K_1$  have been determined by Equations (2-66) and (2-67), the control law is governed by the equation:

$$u(kt) = (1/T) [K_0 e(kt) + K_1 z(kt)] \quad (2-70)$$

with

$$e(kt) = v(kt) - Y(kt) \quad (2-71)$$

Analysis of this method reveals that  $K_0$  shapes the



initial output response (i.e. no undershoot) while  $K_1$  shapes the steady-state outputs (i.e. no offset). It is also important to note that  $G(0)$  and  $B^*$  can both be obtained from 'off-line' tests of the open-loop plant by using the unit-step response matrix

$$S(T) = \int_0^T C e^{At} B dt \quad (2-72)$$

such that

$$S(\infty) = G(0), \text{ as in the unknown case} \quad (2-73)$$

$$S(0) = B^* \quad (2-74)$$

### Summary

This chapter presents a summary of the four digital controller design methods developed by Professor Brain Porter. The highly interactive computer program MULTI (Ref. 4) implements the four design methods discussed. It should also be pointed out that, although this chapter emphasises the digital approach, analog controllers can also be designed using the same overall concepts. Chapter III, the next chapter, gives a description of the KC-135A aircraft along with a discussion of the equations of motion, sign convention, and axis system used.

### III. KC-135A AIRCRAFT MODEL

#### Introduction

This thesis deals with the KC-135A aircraft. A linear six degree-of-freedom model is generated for each of the three flight conditions chosen. This results in a set of three linearized constant-coefficient equations of motion, each one representing the aircraft operating within small perturbations about its respective equilibrium. For the purpose of this thesis the three flight conditions are selected so as to represent the aircraft over a wide range of flight operating conditions. This has been done so that one controller, however chosen, could be tested for robustness at the three distinctly different flight conditions. Thus the flight conditions chosen include a high altitude high speed cruise of MACH 0.77 at 45,000 feet; a medium altitude, heavy weight cruise of MACH 0.77 at 28,500 feet; and a landing condition of MACH 0.21 at sea level.

This chapter provides a basic description of the KC-135A aircraft and overviews a general discussion of the linearized equations of motion, sign convention, and axis system used in this thesis.

#### Aircraft Description (Ref. 10)

The KC-135A is a four engine jet-powered tanker/cargo

airplane. The swept wing is mounted low on the fuselage at an incidence of 2 degrees and is tailored for high subsonic cruise speeds. The aircraft has a basic weight of approximately 106,000 pounds, depending on equipment installed, and a maximum gross weight of 287,000 pounds. All control surfaces, except the spoilers, are aerodynamically balanced and operated by means of control tabs. A hydraulically boosted rudder is installed on all aircraft. The lateral control system is composed of integrated aileron and spoiler control surfaces. The spoilers may also be used as speed brakes when operated symmetrically. Movement of the inboard ailerons causes a corresponding movement of the outboard ailerons if the wing flaps are extended beyond the 23 degree point. Such is the case for the flight condition representing the landing phase in this thesis. If the wing flaps are up, a lockout mechanism prevents the outboard ailerons from moving. Lateral trim of both the rudder and ailerons is accomplished manually by rotating a trim wheel which positions trim tabs on respective control surfaces.

Longitudinal control is provided by an all moveable horizontal stabilizer and elevator system. The stabilizer position is set by a trim wheel which can be operated electrically or manually. All three flight conditions used in this thesis assume a horizontal stabilizer setting, which results in no elevator deflection required to maintain that

flight condition. It should also be noted that no flight control surface, either lateral or longitudinal, is modified for the purpose of this thesis and all function as described by the current Tech. Order specification at the time of this thesis (Ref. 11)

The four Pratt and Whitney J57-P-59W or -43WB engines are mounted individually below the wing on forward swept struts. The engines are each rated at 12845 pounds thrust for a standard day at sea level (15 deg. C, 29.29 inches of mercury). Other relative geometric data as found in Reference 10 is as follows:

<u>Characteristic</u>	<u>Symbol</u>	<u>Dimension</u>
Fuselage	F	128.83 ft
Wing Area	S	2433 sq.ft.
Wing Span	b	130.83 ft.
Wing M.A.C.	c	20.16 ft.
Distance from 25% Wing M.A.C. to 25% Horizontal Tail M.A.C.	$l_T$	61.39 ft.

The abbreviation, M.A.C , is for mean aerodynamic chord. Further data for the KC-135A aircraft can be found in References 10 and 11.

### System Models

The aircraft models in this thesis are developed using six degree-of-freedom equations of motion. The equations

are assumed to have no coupling between motion in the lateral directional plane and the longitudinal plane. Therefore, the original six differential motion equations can be decoupled into two sets of three equations each. One set describes motion of the aircraft in the longitudinal plane or plane of symmetry while the other describes motion only in the lateral and directional plane or motion out of the plane of symmetry. Appendix A presents the development of the equations of motion in state form along with other assumptions made about them.

Control inputs available include two lateral controls, the rudder ( $\delta_r$ ) and the ailerons and spoilers ( $\delta_w$ ).  $\delta_w$  is modeled as the control wheel movement and its limits are set at  $\pm 90$  degrees. A control wheel movement would correspond to a combined aileron and spoiler displacement. Movement of the control wheel within its limits would result in both aileron and spoiler movements within their limits.  $\delta_r$  is rudder displacement and its limits are set at  $\pm 17$  degrees. Longitudinal controls include the elevator ( $\delta_e$ ), the speed brakes ( $\delta_{sb}$ ), and the thrust ( $\delta_T$ ).  $\delta_e$  is elevator displacement and its limits are set at  $\pm 25$  degrees. It should be noted that any constant elevator displacement represents an out of trim condition and would normally be trimmed off by an appropriate horizontal stabilizer position. However, this is not possible with the model representation used in this thesis.  $\delta_{sb}$  is speed brake

deflection which is symmetrical spoiler deployment and has a limit of 0 to 60 degrees.  $\delta_T$  is modeled in terms of 100% of available thrust and limits vary depending upon altitude and gross weight.

Since the equations are decoupled and the theory requires that the number of inputs equals the number of outputs, two lateral and up to three longitudinal outputs are chosen. The lateral outputs are the roll angle  $\phi$  and the sideslip angle  $\beta$ . The longitudinal outputs depend on the maneuver being performed and the controls available. This is necessary since, in the case of a constant airspeed climb, the speed brakes are not used and are removed from the model. Chapter V gives a more detailed description of the inputs and outputs used for each maneuver.

#### Sign Convention and Axis System

The sign conventions for forces and moments, as used throughout this thesis, are shown in Figures 3-1, 3-2, and 3-3. Figure 3-2 shows lateral sign conventions while Figure 3-3 shows longitudinal sign conventions.

Rudder ( $\delta_r$ ): Rudder deflection to the left is defined as positive. This produces a positive  $\beta$ , positive V, negative N, and negative R.

Control Wheel ( $\delta_w$ ): Control wheel deflections to the right, which cause right aileron up and right spoiler up along with left aileron down is defined as positive. This



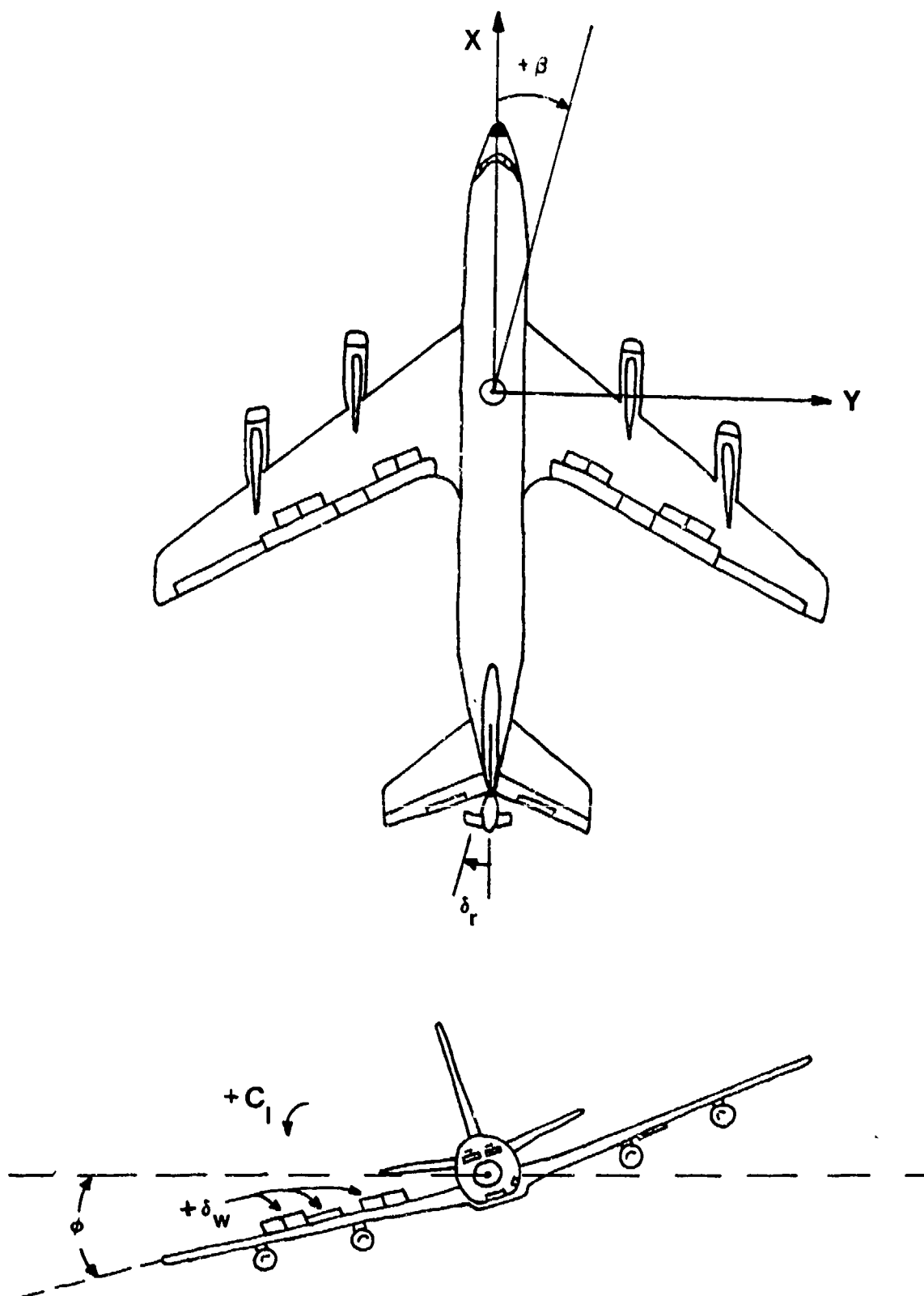


FIGURE 3-2: Lateral Sign Convention



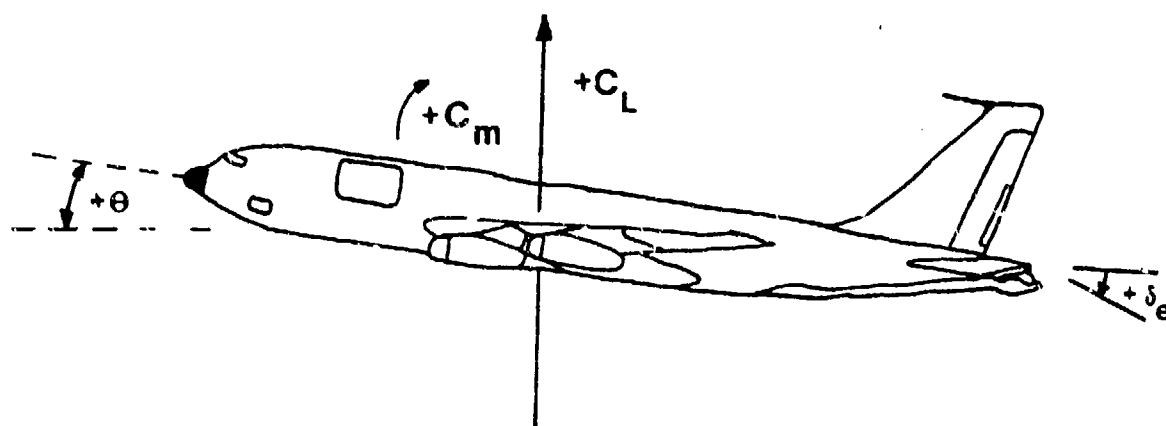


FIGURE 3-3: Longitudinal Sign Convention

produces a positive  $L$ , positive  $\phi$ , and positive  $P$ . Note, that this definition of positive aileron is not standard, but does conform with Reference 12.

Elevator ( $\delta_e$ ): Control column movement forward which caused down elevator is defined as positive. This positive elevator produces a negative  $\theta$ , negative  $M$ , and negative  $Q$ .

Speed Brakes ( $\delta_{sb}$ ): Spoilers when used symmetrically are defined as speed brakes, which when deflected positive are up.

Thrust ( $\delta_T$ ): Thrust is modeled as % of available thrust and a positive  $\delta_T$  calls for an increase in thrust.

Body Axis System This thesis uses the body axis system shown in Figure 1. It should be noted that Appendix A takes the nondimensional stability axis derivatives found in Reference 13 and converts them to dimensional body axis values.

### Summary

This chapter presents a physical description of the KC-135A aircraft. The system models, as developed in Appendix A, are overviewed. Also, sign conventions and the axis system used in this thesis are defined. Chapter IV, the next chapter, presents a computational time delay modification made to the computer program MULTI by this author.

#### IV. TIME DELAY MODIFICATION TO COMPUTER PROGRAM MULTI

##### Introduction

The core of this thesis is developed around the use of a computer program MULTI (Ref. 4) which was developed to design and simulate the techniques of Professor Brain Porter discussed in Chapter II. MULTI is a highly interactive program designed to give the user the opportunity to both design a multivariable controller and simulate it with the help of a computer. The computer provides a means for multiple iterations of the design and simulation to allow the user to achieve a suitable design. For an understanding of the program's development and structure, as well as the basic User and Programmer Manual, the reader is referred to Reference 4. This reference provides the reader with a basic setup of the program. However, MULTI has gone through several revisions and to find information on the most current status of MULTI the reader should contact Professor John J. D'Azzo, Deputy Department Head, Department of Electrical Engineering, Air Force Institute of Technology, Wright-Patterson Air Force Base, Ohio, 45433.

The remainder of this chapter presents a discussion of the time delay modification made to MULTI by this author.

##### Theory of Computational Time Delay (Ref. 14)

The simulation portion of the computer program MULTI

provides the designer with a method of determining how well his design will perform. The simulation, up until the time of this author's modification, made the assumption that there is no computational time delay for generation of the inputs to the plant. In some cases this assumption may not be valid. Therefore it became necessary to provide the user an option which includes a computational delay in the simulation if desired. At the same time that the computational time delay was added to MULTI, a compensator of the form presented in Reference 14 was also added. Indeed, if no such compensation is provided the resulting tracking system may have either very poor performance or even be unstable.

The controller of Chapter II generates a signal of the form:

$$s(kT) = f[K_0 e(kT) + K_1 z(kT)] \quad (4-1)$$

where  $f$  is the sampling frequency,  $e(kT)$  is the error vector,  $z(kT)$  is the integral of the error vector, and  $K_0$  and  $K_1$  are controller matrices of the form discussed in Chapter II. Reference 14 proposes a computational time delay equation of the form:

$$r(kT) = s(kT) - r[(k-1)T] \quad (4-2)$$

Thus, with a computational time delay of one sampling period, the digital controller is required to generate the

input vector

$$u(kT) = r[(k-1)T] \quad (4-3)$$

For computational time delays of more than one sampling period Equation (4-2) becomes

$$r(kT) = s(kT) - r[(k-1)T] - r[(k-2)T] - \dots - r[(k-x)T] \quad (4-4)$$

and the new input vector is now given by

$$u(kT) = r[(k-x)T] \quad (4-5)$$

where  $x$  is the number of sampling periods equal to the computational delay. Figure 4-1 gives a generalized block diagram for this computational time delay and compensation.

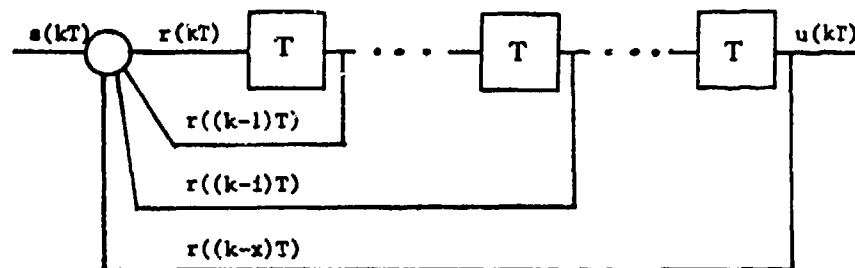


FIGURE 4-1: Computational Time Delay With Compensation

Reference 14 develops the theory for the new system with this computational time delay and the compensation represented by Equations (4-3) and (4-2) respectively. This

theory shows that the time delay has no affect on the "slow" modes as  $f$  approaches infinity but the "fast" modes are affected. In fact, it can be shown, Reference 14, that as  $f$  approaches infinity, if no time delay compensation is used, at least some of the "fast" modes become unstable. For the complete analysis of this system the reader is referred to Reference 14.

#### Summary of MULTI Code Changes

To accommodate this time delay a few simple modifications were made to the existing Fortran code for MULTI. First, under OPTION #23 the user is given the opportunity to set the amount of computational delay desired. Computational delay is limited to an integer multiple from 1 to 5 of the sampling time used. This integer is passed throughout the program as "NCD" and is now entered along with the sampling time in OPTION #23. The program still allows for no computational delay if NCD is set to zero. The code under OPTION 23 reads as follows:

```

200=C *****
210=C OPTION #23
220= 2023 PRINT*, 'THIS OPTION SETS THE SAMPLING TIME AND'
230=     PRINT*(A/), ' COMPUTATIONAL DELAY TIME'
240=     PRINT*, 'ENTER THE SAMPLING TIME >'
250=     READ*, SAMPT
260=     PRINT*, ' '
270=     PRINT*, 'COMPUTATIONAL DELAY IS AN INTEGER MULTIPLE'
280=     PRINT*, 'FROM 1 TO 5 OF THE SAMPLING TIME. USE ZERO IF'
290=     PRINT*(A/), ' NO DELAY IS DESIRED'
300= 1051 PRINT*, 'ENTER THAT INTEGER >'

```

```

310= READ*,NCD
320= IF (NCD.LE.5) GO TO 1852
330= PRINT*, ' '
340= PRINT*, 'COMPUTATIONAL DELAY MUST BE AN INTEGER MULTIPLE'
350= PRINT*, 'FROM 1 TO 5 OF THE SAMPLING TIME. USE ZERO IF'
360= PRINT*(A/)', ' NO DELAY IS DESIRED'
370= GO TO 1851
380= 1852 IFLAG(23)=1
390= GO TO 8007

```

When OPTION 23 is executed lines 220 thru 250 prompt the user with the following statements:

THIS OPTION SETS THE SAMPLING TIME AND  
COMPUTATIONAL DELAY TIME.

ENTER THE SAMPLING TIME>

Here SAMPT is entered and the program continues with lines 270 thru 300 and the user is prompted with:

COMPUTATIONAL DELAY IS AN INTEGER MULTIPLE  
FROM 1 TO 5 OF THE SAMPLING TIME. USE ZERO IF  
NO DELAY IS DESIRED.

ENTER THAT INTEGER>

The integer entered here is stored as NCD and is passed to various portions of the program by the common statement:

COMMON /B i2B/ ST,TT,SAMPT,NCD

Lines 320 thru 370 of the code under OPTION #23 prevent the user from entering a value for NCD which is out of the range from 0 to 5. This is necessary to prevent overflow of the set aside storage space under OPTION #26, which is explained later.

Code also was also added to OPTION #29 to allow NCD to be read in from a memory file and to OVERLAY (14,0) to write NCD to a memory file when OPTION #99 is executed. The read statement;

```
READ (DAT3,*) NCD
```

was added to OPTION #29 and the write statement;

```
WRITE (DAT3,*) NCD
```

was added to OVERLAY (14,0). Under OPTION #123 TO #126 the code was changed to read as follows.

```
400=C *****
410=C OPTIONS #123 TO #125
420= 2123 PRINT '(A,19X,F10.5)', ' SAMPLING TIME...',SAMPT
430=    CD=NCD*SAMPT
440=    PRINT '(A,13X,F10.5)', ' COMPUTATIONAL DELAY...',CD
450=    PRINT '(A,17X,F10.5)', ' SIMULATION TIME...',TT
460=    PRINT '(A,11X,F10.5)', ' CALCULATION STEP SIZE...',ST
470=    GO TO 8015
```

Line 430 computes the computational delay time using the equation  $CD = (NCD) * (SAMPT)$ . Line 440 adds the print out of CD to this option so that the user sees the following example print out for one delay period and  $T = 0.050$  seconds whenever OPTION #123 TO #126 is called:

```
SAMPLING TIME ...           .050
COMPUTATIONAL DELAY ...     .050
SIMULATION TIME ...        20.000
CALCULATION STEP SIZE ...   .050
```

When the simulation OPTION #26 is executed several



additional steps occur if the user has selected a computational delay under OPTION #23. First a storage matrix UD is dimensioned as 10 by 6. This matrix accommodates a delay of up to 5 sampling periods, thus the restriction set in OPTION #23 on the size of NCD. The matrix UD is then initialized to zero and the user is reminded that a computational delay is being included in the simulation.

The code that accounts for the computational delay is added immediately following the formation of the control law in the existing program. As mentioned earlier, this code can accommodate up to 5 periods of delay and provide for the compensation given by Equation (4-4). This code as it now appears in MULTI is listed below and resides in the main loop which is executed for each sampling period.

```

520=C-----DELAY OF U BY NCD TIMES-----
530=    IF (NCD.EQ.0) GO TO 1211
540=    DO 1201 J=1,NCD
550=    DO 1202 I=1,M
560=    U(I)=U(I)-UD(I,J)
570= 1202 CONTINUE
580= 1201 CONTINUE
590=    DO 1206 I=1,M
600= 1206 UD(I,NCD+1)=U(I)
610=    DO 1207 I=1,M
620= 1207 U(I)=UD(I,1)
630=    DO 1208 J=1,NCD
640=    DO 1209 I=1,M
650=    UD(I,J)=UD(I,J+1)
660= 1209 CONTINUE
670= 1208 CONTINUE

```

Line 530 is an IF statement that checks to see if the integer NCD equals zero, which would represent a

computational delay of zero. If this is true the program skips the next fourteen lines of code and no delay is encountered. Investigation of the remaining list of code reveals the following fact about the matrix UD. This matrix is used to store the input vectors that are generated by Equation (4-2) and thus acts as the delay mechanism. The easiest way to understand this code is to take a simple example where NCD equals one and to walk through the process. The first time through the main loop a vector  $s(kT)$  is formed as given by Equation (4-1). Since NCD equals one, lines 540 thru 580 subtract from  $s(kT)$  the vector that resides in the first column of UD to form  $r(kT)$  in accordance with Equation (4-2). The first column of UD always contains the vector  $r[(k-1)T]$ . Next, lines 590 and 600 store  $r(kT)$ , given by Equation (4-2), in the  $NCD+1$  column of UD. Lines 610 and 620 assign the input vector  $u(kT)$  from the first column of UD which corresponds to performing Equation (4-3) and thus a time delay of one sampling period is encountered. Finally, lines 620 thru 670 move the second column of UD into the first column so that the program is ready for the next time the main loop is executed. It is important to note that the computer code does not use the symbols  $s(.)$  and  $r(.)$  in order to save storage space.

If NCD equals 3 it can be shown that the matrix UD is composed of the following:

$$UD = \begin{bmatrix} r[(k-3)T] & r[(k-2)T] & r[(k-1)T] & r[kT] \\ \vdots & \vdots & \vdots & \vdots \\ \vdots & \vdots & \vdots & \vdots \\ \vdots & \vdots & \vdots & \vdots \end{bmatrix}$$

from this it is easy to see how UD is used in execution of Equations (4-4) and (4-5) and that UD indeed acts as the delay mechanism.

### Summary

Fortran code changes, as discussed in this chapter, were made to the computer program MULTI to incorporate a computational time delay. Debugging of the code became necessary because unexpected results were initially obtained when example problems were worked. An error was found in the existing code and, once corrected, favorable results are obtained both with and without computational time delay.

## V. MULTIVARIABLE CONTROL LAW DESIGN

### Introduction

This chapter presents the procedures used in the development of multivariable tracker control laws for the KC-135A. Controllers are designed for each of the three flight conditions discussed in chapter III. This chapter begins with a listing of the requirements for the design method, followed by a detailed discussion of the maneuvers to be performed and the inputs and outputs needed to perform those maneuvers. Next, the procedures used to arrive at a final design are presented followed by the control laws developed using those procedures. A computational time delay of one sampling period is added and a detailed comparison of the delayed results with the undelayed is given. The computational time delay results in some undesirable effects such as overshoot in the outputs and/or oscillations in control surfaces. The controllers are redesigned so as to minimize these undesirable effects. In order to reduce the number of amplifiers required to implement the designs, the controller matrices  $K_0$  and  $K_1$  are studied. Justification for setting some of the elements of  $K_0$  and  $K_1$  to zero is given along with the result of these reduced controllers. Finally robustness is tested by applying the control laws developed for flight condition #3 with computational time delay and minimum  $K_0$  and  $K_1$  to each of the other two flight conditions.

## Requirements

The following requirements must be satisfied in applying the design method.

1. The number of inputs must equal the number of outputs.
2. The system must be controllable and observable.
3. All transmission zeros must be in the left hand s-plane.

4.  $\text{Rank} \begin{bmatrix} A & B \\ -C & 0 \end{bmatrix} = n+p$

Appendix A gives a state space model for each of the three flight conditions studied. Controllability and observability of each of the models can be checked by using the controllability matrix  $M$  and the observability matrix  $M$  respectively. Where

$$\text{Rank } M_C = \text{Rank} [B \ AB \ \dots \ A^{n-1}B] = n \quad (5-1)$$

must be true if the system is controllable and

$$\text{Rank } M_O = \text{Rank} [C^T \ A^T C^T \ \dots \ A^{T(n-1)} C^T] = n \quad (5-2)$$

must be true if the system is observable.

Transmission zeros can be checked using a computer program given by Reference 7. Since the three conditions studied all involved irregular designs, the matrix  $F = [F_1 \ F_2]$  must be used in place of  $C = [C_1 \ C_2]$  in checking for the transmission zeros.

Condition one above requires that the number of outputs

equal the number of inputs. This is also true for the three flight conditions studied and a discussion of the inputs and outputs is given later in this chapter.

### Maneuvers

Maneuvers to be performed need to meet two requirements. They must be useful to the pilot and they must be feasible for the aircraft to perform. Remember that this is a heavy transport aircraft not a small highly maneuverable fighter. In order to illustrate the performance of this design method, four maneuvers, two lateral and two longitudinal, are chosen. The four maneuvers are:

1. Coordinated turn ( $\phi \leq 30$ ,  $\beta = 0$ )
2. Sideslip ( $\beta \leq 5$ ,  $\phi = 0$ )
3. Constant airspeed climb ( $\gamma > 0$ ,  $u = 0$ )
4. Pitch pointing ( $\theta < 5$ ,  $h = 0$ ,  $u = 0$ )

The first two maneuvers are intended to demonstrate the performance of lateral controllers while the next two demonstrate longitudinal controller performance.

The coordinated turn and constant airspeed climb (normal climb) are basic flight maneuvers that are performed in every operational mission of the KC-135A. Since it is desirable to have a minimum of four maneuvers to demonstrate the design method, two more maneuvers listed above are included.

When flying an approach to landing, under crosswind conditions, the KC-135A aircraft flies with a crab into the wind. Due to side forces on the landing gear the aircraft cannot land in this crab. Thus the pilot is required to use a wing low technique to eliminate the crab just prior to landing. To perform this the pilot must use an appropriate amount of rudder to align the aircraft with the runway, and at the same time bank the aircraft enough to prevent a side velocity from developing. This maneuver would be very useful, but it cannot be simulated with MULTI since it requires nonlinear sines of angles in the output matrix C. Until nonlinear terms are allowed in MULTI a compromise had to be made. Thus the choice of the sideslip maneuver. Although the sideslip would have limited use in the aircraft, it does allow for demonstration of the design method. Finally, during a landing in which a minimum flap setting is used, the KC-135A aircraft attitude is such that there is the possibility of dragging the tail. Thus the pitch pointing is chosen in order to alleviate this occurrence.

#### Input/Output Models

The "inputs" of the system refers to the control surfaces of the aircraft. Control surfaces for the KC-135A include two lateral controls, the rudder ( $\delta_r$ ) and the ailerons and spoilers ( $\delta_w$ ) along with three longitudinal

controls, the elevator ( $\delta_e$ ), the thrust ( $\delta_T$ ), and speed brakes ( $\delta_{sb}$ ). These control surfaces are discussed in detail in Chapter III. The designs developed in this chapter include the control surface limitations discussed in Chapter III and listed below.

$$-17 \text{ deg} \leq \delta_r \leq 17 \text{ deg} \quad (5-3)$$

$$-90 \text{ deg} \leq \delta_w \leq 90 \text{ deg} \quad (5-4)$$

$$-25 \text{ deg} \leq \delta_e \leq 25 \text{ deg} \quad (5-5)$$

$$0 \text{ deg} \leq \delta_{sb} \leq 60 \text{ deg} \quad (5-6)$$

$\delta_T$  is dependent upon thrust available and varies for each flight condition. In general, the thrust required for each of the three trimmed flight conditions does not exceed 50% of available thrust. Thus a subjective limit of  $\pm 50\%$  is placed on  $\delta_T$ .

The "outputs" are the variables contained in the vector  $y$  and as such represent the responses which are to be controlled. The outputs can be states of the system or linear combinations of the states. For this study, the lateral directional outputs are chosen to be the sideslip angle ( $\beta$ ) and the roll angle ( $\phi$ ). Due to distinct differences in the two longitudinal maneuvers being performed, two sets of longitudinal outputs are chosen. The first, used to perform the constant airspeed climb, is the flight path angle ( $\gamma$ ), where  $\gamma = \theta - \alpha$ , and ( $u$ ), the perturbation velocity in the x-direction. The second set,



used to perform pitch pointing, is the pitch angle ( $\theta$ ), the perturbation velocity in the x-direction, ( $u$ ), and the altitude ( $h$ ) where, for small angle approximations,  $h = U (\theta - \alpha)$ . Thus for the design of the lateral controllers the state, input, and output vectors are:

$$x = \begin{bmatrix} \phi \\ \beta \\ p \\ r \end{bmatrix} \quad u = \begin{bmatrix} \delta_r \\ \delta_w \end{bmatrix} \quad y = \begin{bmatrix} \phi \\ \beta \end{bmatrix} \quad (5-7)$$

For the longitudinal case of the constant airspeed climb:

$$x = \begin{bmatrix} h \\ \theta \\ u \\ \alpha \\ q \\ e \\ \dot{e} \end{bmatrix} \quad u = \begin{bmatrix} \delta_e \\ \delta_T \end{bmatrix} \quad y = \begin{bmatrix} \gamma \\ u \end{bmatrix} \quad (5-8)$$

and for pitch pointing:

$$x = \begin{bmatrix} h \\ \theta \\ u \\ \alpha \\ q \\ e \\ \dot{e} \end{bmatrix} \quad u = \begin{bmatrix} \delta_e \\ \delta_{sb} \\ \delta_T \end{bmatrix} \quad y = \begin{bmatrix} h \\ \theta \\ u \end{bmatrix} \quad (5-9)$$

Where  $e$  represents the body bending at the crew station as discussed in Appendix A.

### Design Procedures

What follows is a brief discussion of the steps used in finding digital controllers which achieve "good" performance

characteristics. Before describing this it is necessary to first define the guide lines used by this author in determining what "good" performance is. All command inputs greater than zero are ramped up to their steady-state values. This usually results in some overshoot of the output before it reaches steady-state. In determining "good" responses it is first desired to keep as many outputs as possible from overshooting their steady-state values by more than 2%. It is also desired to keep control surface deflections to a minimum and to prevent any unnecessary oscillations in the control surfaces.

The steps used by this author in development of the digital controllers presented in this chapter are listed below. A discussion of each step follows:

1. For each of the state space models given in Appendix A, determine the design method of Chapter II that is to be used.
2. If the design method selected is irregular, which requires a 'M' matrix, determine the minimum number of M matrix elements required.
3. Check controllability and observability of the system.
4. Determine the location of the transmission zeros.
5. Select a sampling time for discrete controllers.
6. Vary  $\sigma$ ,  $\alpha$ , and elements of M and  $\Sigma$  to achieve a "good" design.

The first step in the design is to determine which of the design methods discussed in Chapter II is to be used. Since the matrices A, B, C, and D of Equations (2-1) and

(2-2) are known, the choice is narrowed to the Known/Regular or Known/Irregular methods. However, the first Markov parameter, CB, does not have full rank, thus the Known/Irregular design method must be used.

Since the design method requires a measurement matrix 'M', the next step is to determine which elements of the 'M' matrix are to be used. Three measurement matrices are selected, one for the lateral-direction case, and one each for the two maneuvers in the longitudinal case. Each of these 'M' matrices are chosen based on the requirements outlined in Chapter II and given in Reference 8.

Next, controllability and observability are checked using the matrices  $M_c$  and  $M_o$  as discussed earlier. Also the transmission zeros are determined using a computer program given by Reference 7.

For the discrete systems studied, a sampling time,  $T$ , must also be selected. The sampling time of 0.05 seconds (20 hertz) is chosen since this represents a reasonable sampling rate for aircraft computers.

The final step is to vary the design parameters in order to achieve a "good" design. Initial design are accomplished using no actuators or sensors. Using Options 11, 13, 12, and 16 of the MULTI program the following values are entered:  $\alpha=1$ ,  $\epsilon=1$ , all diagonal elements of  $\Sigma=1$ , and all necessary elements of  $M=0.25$ . Next, the matrices  $K_0$  and  $K_1$  are examined for magnitude. Generally, in order to achieve

stable responses the relative magnitudes of each element in these matrices should be on the order of 10 or 100. If the magnitudes are found to be too large, the value of epsilon, under Option #13, needs to be reduced. After achieving stability, individual parameters are varied in order to observe its effect on system performance. The following generalizations are found to hold true under most conditions. Epsilon, the sigma matrix multiplier, affects output overshoot. Reducing epsilon reduces overshoot. Reductions in epsilon usually require an increase in alpha, which controls the proportion of integral feedback, in order to keep rise time of the outputs from increasing. Changes of individual sigma elements affect certain inputs and outputs. Increasing sigma would in general result in an increase in its respective control surface deflections and a reduction in rise time of the outputs. Increasing some M matrix elements greatly reduced control surface deflections, but also slowed responses. In all design cases, notes are taken on the effects of vary each of the design parameters. These notes proved helpful when actuators are added, time delays are considered, and when designing for other maneuvers and/or other flight conditions.

After a design is found to work with no actuators, the next step is to include them. Using guidelines found in Reference 12 all control surface actuators are entered as  $10/(s+10)$  using Option #4. In order to simulate engine

dynamics a transfer function of  $2/(s+2)$  is added for the thrust. In all cases, controllers developed with no actuators produced unstable responses when actuators are added. Thus, it became necessary to again trim the design parameters.

Next, the addition of a computational time delay of one sample period is considered. In general, the addition of this time delay results in two noticeable differences. These differences are discussed later with examples being presented. The final design is then developed reducing any ill effects caused by introduction of the time delay.

### Tracker Control Laws For Flight Condition #3

Using the above design procedure controllers are developed for each of the three flight conditions being studied. A detailed discussion of the results obtained for flight condition #3 follows. This includes tabular listings of Peak Value, Final Value,  $t_s$  and  $t_p$  for the outputs being controlled along with Peak Values for each of the control surfaces used. Also included are Calcomp plots showing simulation results.

Coordinated Turn, Flight Condition #3 To accomplish a coordinated turn, the bank angle,  $\phi$ , is commanded to 30 degrees in 4 seconds while sideslip,  $\beta$ , is commanded to zero. The control law selected for this maneuver is defined by the following parameters:

$$T = 0.05 \text{ seconds (20 hertz)} \quad (5-10)$$

$$\alpha = 4.25 \quad (5-11)$$

$$\epsilon = 0.045 \quad (5-12)$$

$$\Sigma = \text{diagonal [1.5 \quad 2.0]} \quad (5-13)$$

$$M = \begin{bmatrix} 0.75 & 0.0 \\ 0.0 & 0.4 \end{bmatrix} \quad (5-14)$$

which yield

$$K_0 = \begin{bmatrix} 0.02204 & 1.68 \\ 0.9891 & -1.486 \end{bmatrix} \quad (5-15)$$

$$K_1 = \begin{bmatrix} 0.005186 & 0.3953 \\ 0.2327 & -0.3496 \end{bmatrix} \quad (5-16)$$

Figures 5-1a thru 5-1f show the simulation for this controller for a commanded 30 degree coordinated turn.

The command input vector is given by Figure 5-1a. Figure 5-2b shows the roll angle,  $\phi$ . The peak value 30.478 degrees occurs at 7 seconds. This is 3 seconds after the commanded input reaches steady-state. Settling time for  $\phi$  is 5.2 seconds and is based on 2% of the final value. Sideslip, shown in Figure 5-1c, is almost negligible with peak values of +0.015 and -0.04. Figures 5-1e and 5-1d show control wheel and rudder deflections respectively. The control wheel proved to be a big factor in performing this maneuver. Settling time for  $\phi$  had to be compromised in order to keep maximum deflections of the control wheel

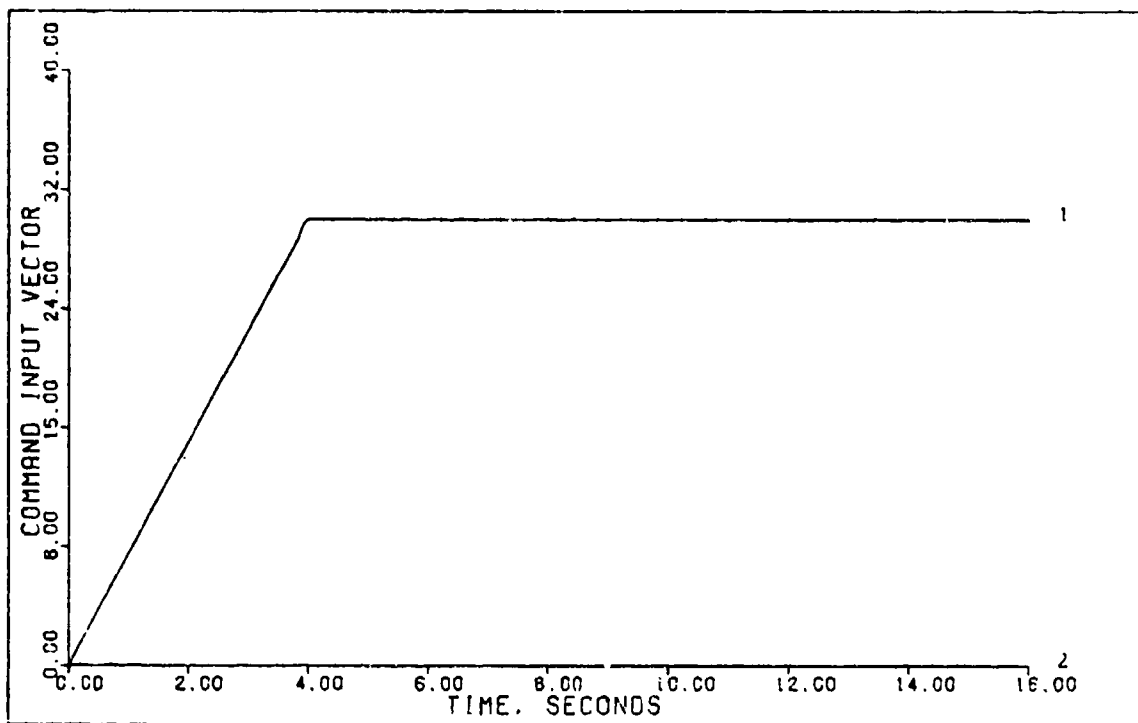


FIGURE 5-1a: Flight Condition #3, Coordinated Turn  
(Command Input Vector)

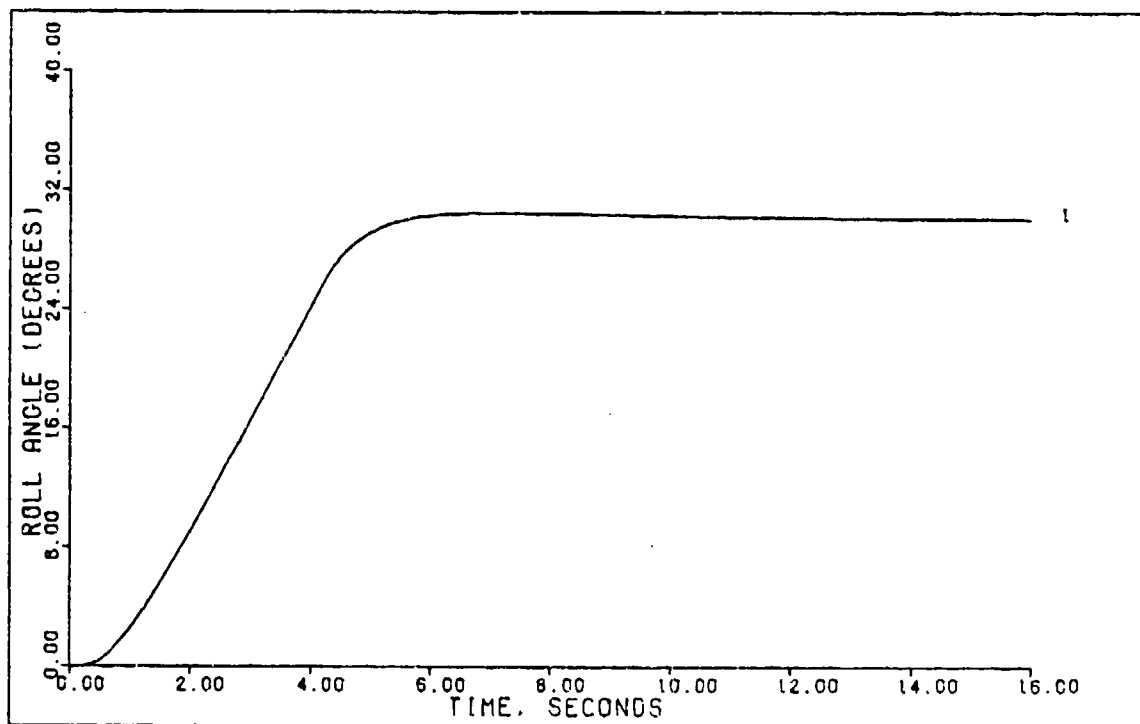


FIGURE 5-1b: Flight Condition #3, Coordinated Turn  
(Output 1: Roll Angle)

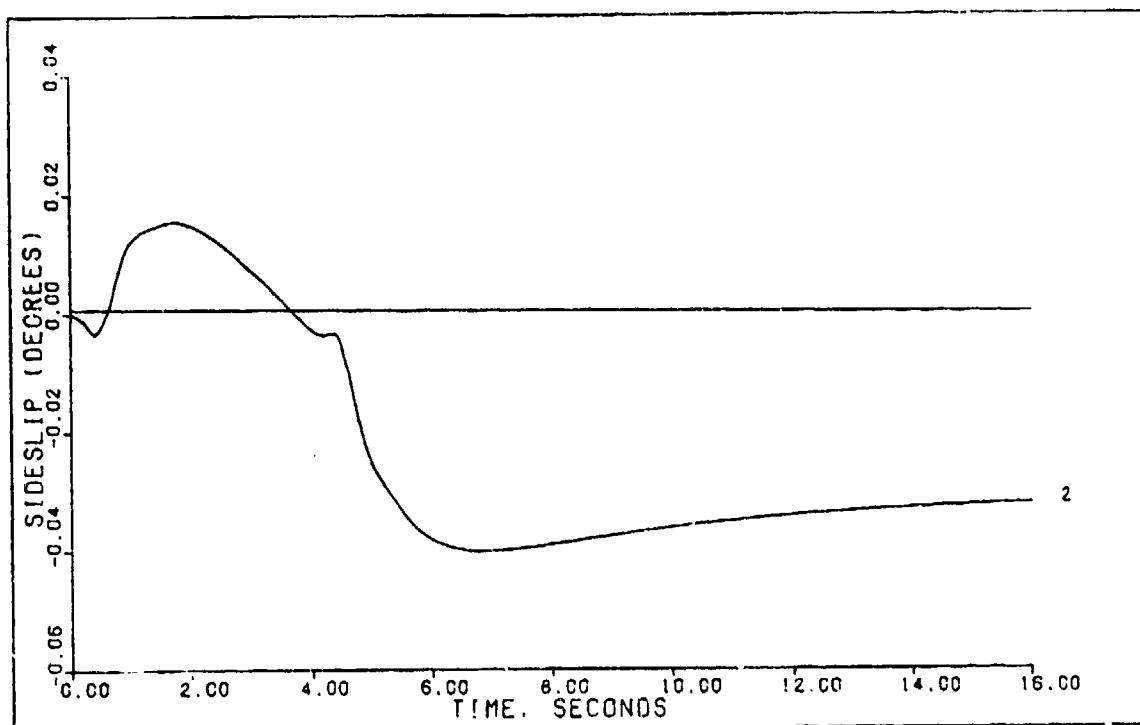


FIGURE 5-1c: Flight Condition #3, Coordinated Turn  
(Output 2: Sideslip)

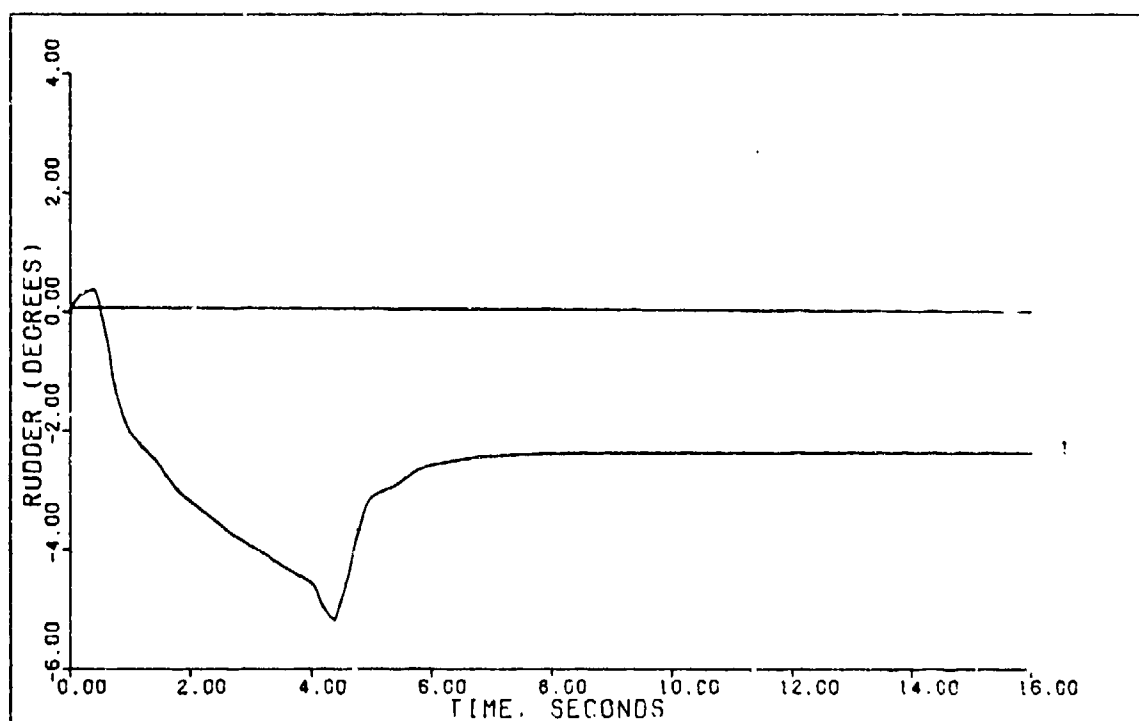


FIGURE 5-1d: Flight Condition #3, Coordinated Turn  
(Control 1: Rudder)



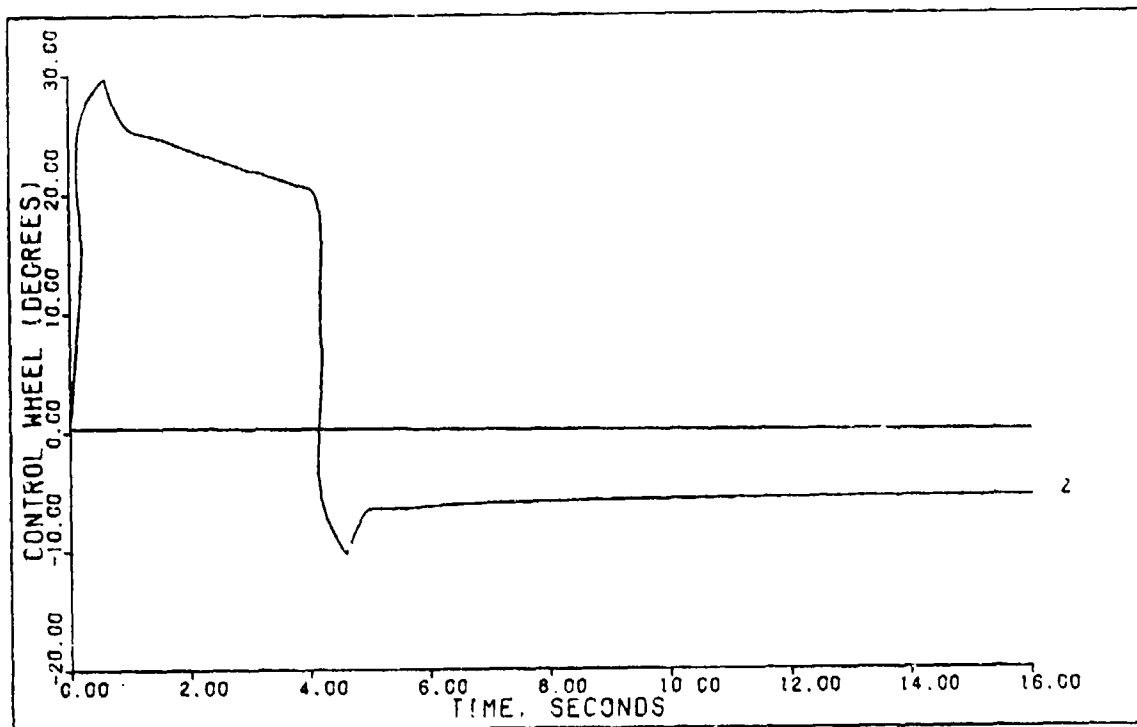


FIGURE 5-1e: Flight Condition #3, Coordinated Turn  
(Control 2: Control Wheel)

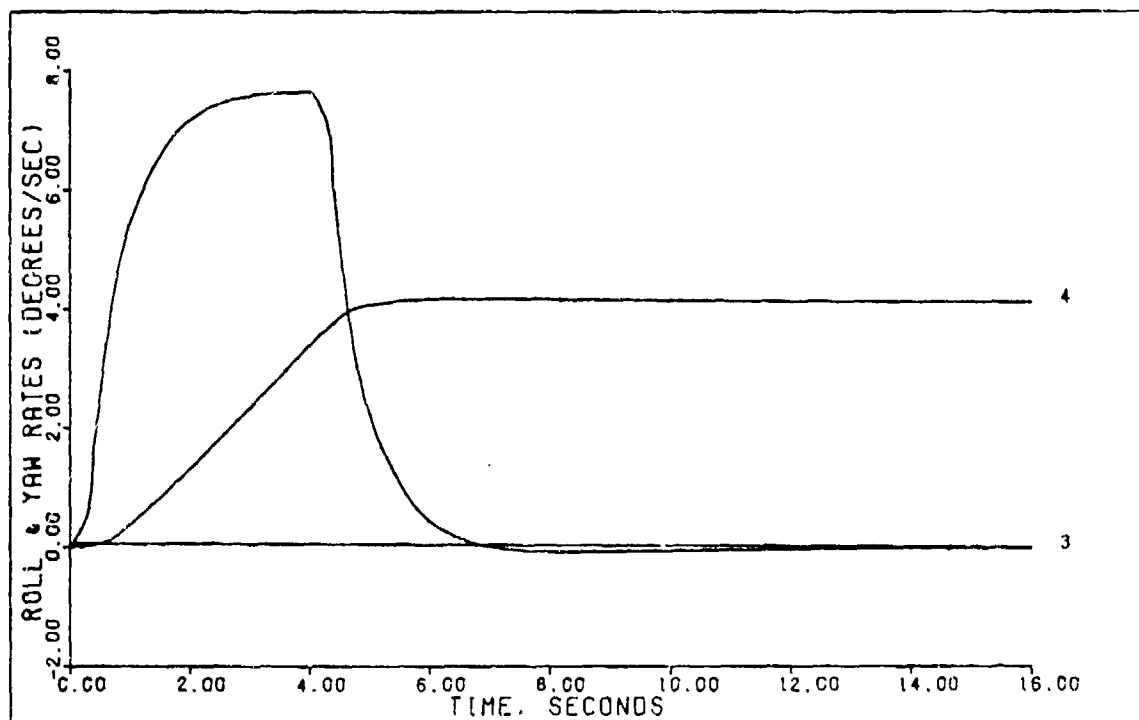


FIGURE 5-1f: Flight Condition #3, Coordinated Turn  
(State 3: Roll Rate; State 4: Yaw Rate)

within acceptable limits. A reminder of what the control wheel represents is needed at this time for clarification of what Figure 5-1d represents. The peak value of approximately 30 degrees, in Figure 5-1d, represents 1/3 of total control wheel deflection. Assuming a linear representation between the control wheel and aileron movement, this would represent approximately 7 degrees of aileron deflection. This 7 degrees of movement occurs in 0.3 seconds, which equates to a rate of 23.3 deg/sec--well within the capability of the actuator. Likewise, a rudder deflection of 6 degrees in 3.8 seconds, as shown in Figure 5-1e, equates to a deflection rate of 1.57 deg/sec. Again, well within the limits of the actuator.

Additionally, based on the assumptions used in Appendix A, Blakelock (Ref. 12) requires that a constant yaw rate,  $r$ , be achieved in a coordinated turn. This yaw rate is defined by:

$$r = 57.3[g/U_0]\sin\phi \quad \text{deg/sec} \quad (5-17)$$

Figure 5-1f shows that the state  $r$  does, in fact, reach the steady-state value of 3.925 deg/sec as computed from Equation (5-17). Table 5-1 summarizes the results of the simulation represented by Figures 5-1a thru 5-1f.

TABLE 5-1  
Simulation Results For  
Coordinated Turn Flight Condition #3.

Input/ Output	Peak Value	Final Value	$t_p$ (sec)	$t_s$ (sec)
$\phi$ (deg)	30.478	30.0	7	5.2
$\beta$ (deg)	-0.04	-0.032	7	14.4
$r$ (deg/sec)	3.93	3.93	5.2	5.2
$\delta_r$ (deg)	-5.5	--	--	--
$\delta_w$ (deg)	32.0	--	--	--

Sideslip, Flight Condition #3. The control laws defined by Equations (5-10) thru (5-16) are used to simulate the sideslip maneuver. This maneuver is accomplished by commanding sideslip to 5 degrees in 8 seconds while commanding bank angle to zero. When this maneuver is performed, the bank angle exceeds two degrees. In order to improve this result a new controller is designed. A constraint imposed on this new controller is to keep the number of gain changes in  $M$ ,  $K$ , and  $K$  given by Equations (5-14), (5-15), and (5-16) to a minimum. Thus, the following parameters are used in design of the new controller:

$$T = 0.05 \text{ seconds (20 hertz)} \quad (5-18)$$

$$\alpha = 4.25 \quad (5-19)$$

$$\epsilon = 0.045 \quad (5-20)$$

$$\Sigma = \text{diag}[1.5 \quad 2.0] \quad (5-21)$$

$$M = \begin{bmatrix} 0.25 & 0.0 \\ 0.0 & 0.4 \end{bmatrix} \quad (5-22)$$

which yields

$$K_0 = \begin{bmatrix} 0.06612 & 1.680 \\ 2.967 & -1.486 \end{bmatrix} \quad (5-23)$$

$$K_1 = \begin{bmatrix} 0.01556 & 0.3953 \\ 0.6982 & -0.3496 \end{bmatrix} \quad (5-24)$$

Notice that this new controller involves only changes in the first columns of  $M$ ,  $K_0$ , and  $K_1$ . Using this controller design the sideslip maneuver is accomplished with the results of the simulation shown in Figures 5-2a thru 5-2d.

The outputs for this maneuver are shown in Figure 5-2b for the inputs of Figure 5-2a. The sideslip angle peaked at 5.076 degrees at 10 seconds and settles to within 2% of the final value of 5 degrees by 8.4 seconds, 0.4 seconds after the input reaches steady-state. Roll angle is negligible with a peak of only -0.2426 occurring at 8.2 seconds.

The control surfaces are shown in Figure 5-2c. Both have initial transients and transients at 8 seconds corresponding to slope changes in the command input. These transients are considered minimal. The transients occurring at 8 seconds can be reduced, but at the expense of increasing settling time. Therefore a compromise must be

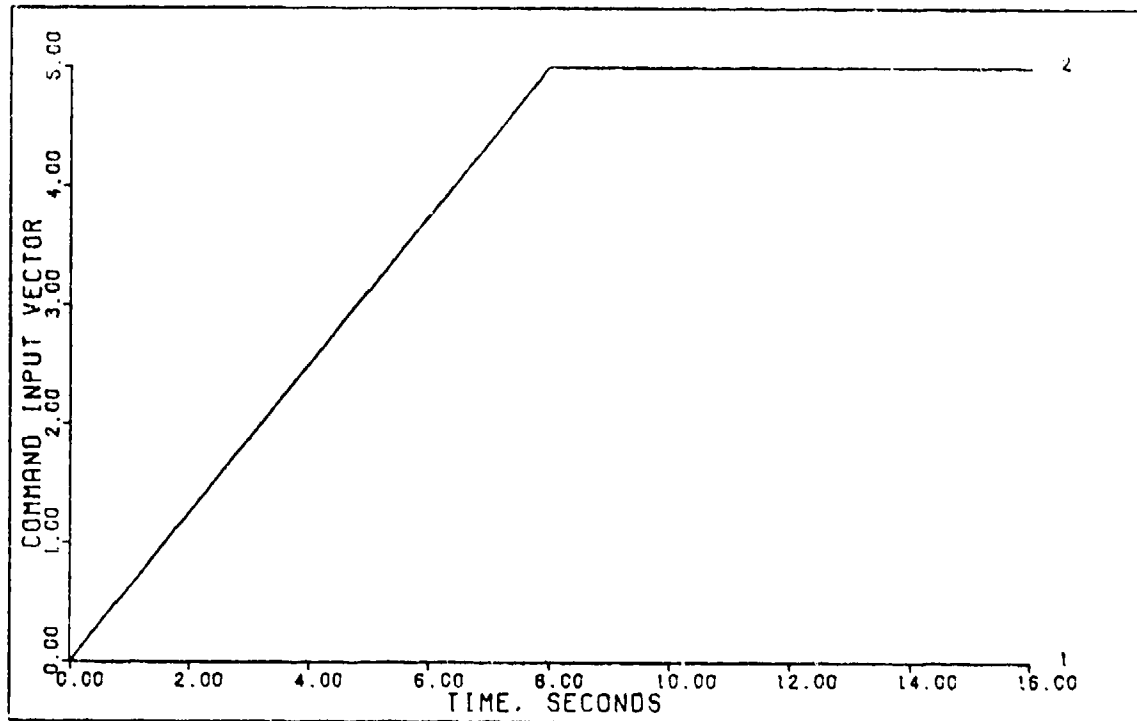


FIGURE 5-2a: Flight Condition #3, Sideslip  
(Command Input Vector)

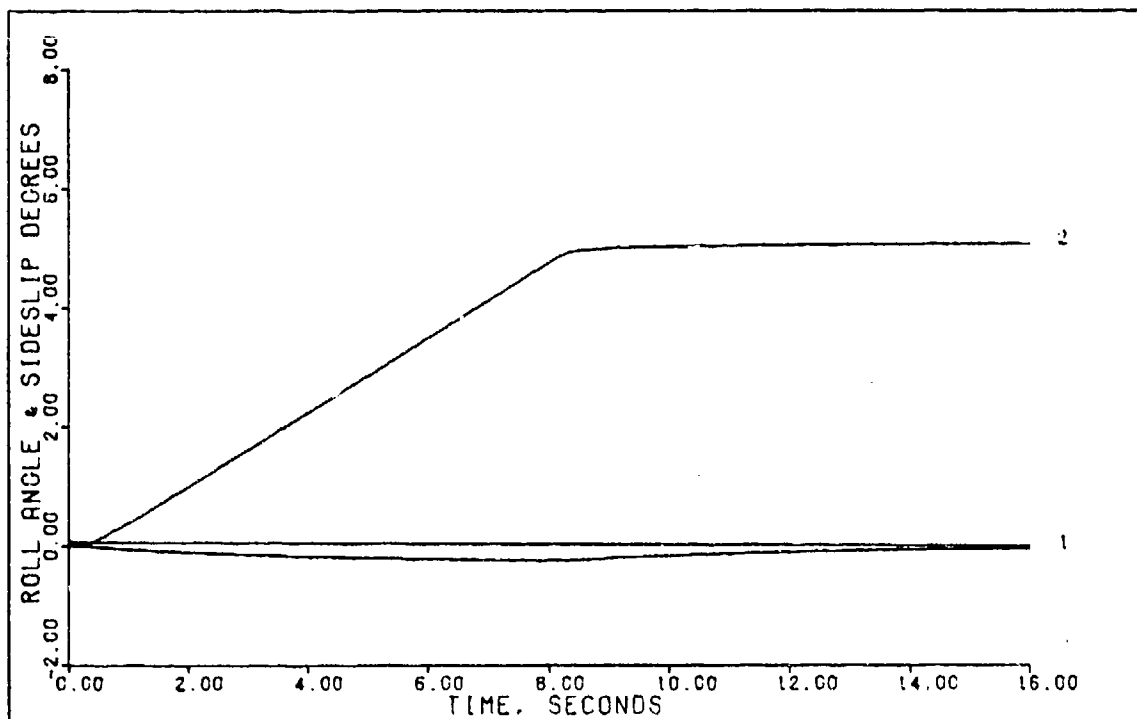


FIGURE 5-2b: Flight Condition #3, Sideslip  
(Output 1: Roll Angle; Output 2: Sideslip)

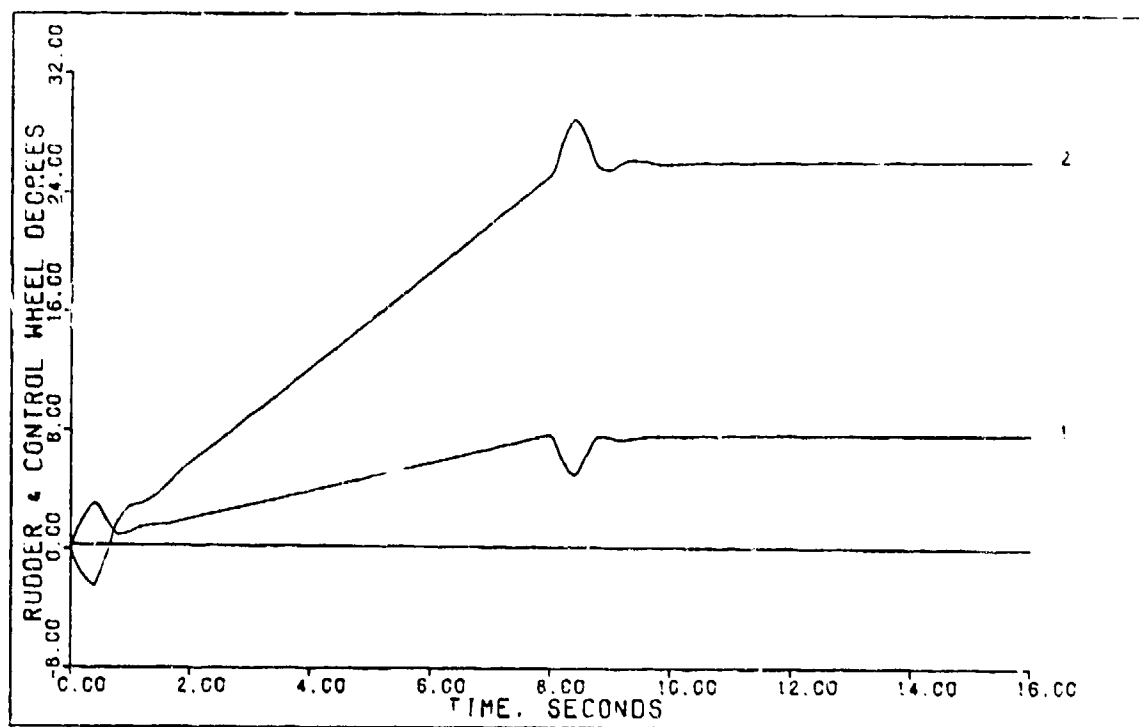


FIGURE 5-2c: Flight Condition #3, Sideslip  
(Control 1: Rudder; Control 2: Control Wheel)

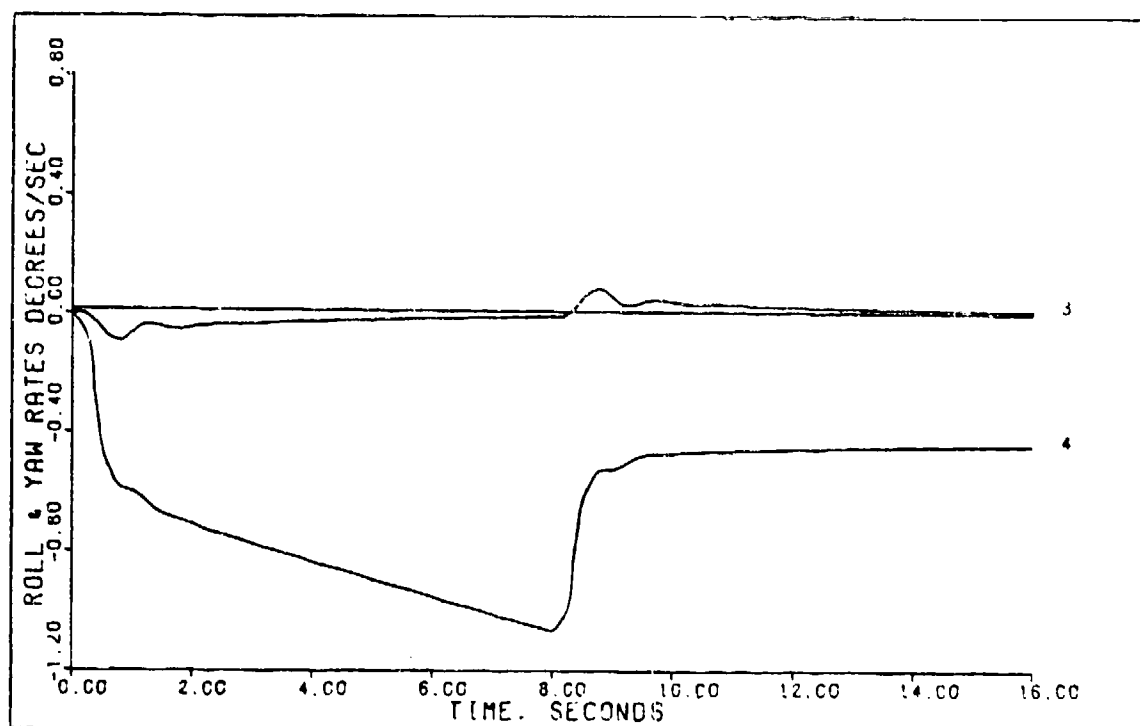


FIGURE 5-2d: Flight Condition #3, Sideslip  
(State 3: Roll Rate; State 4: Yaw Rate)

made here. The results of this simulation are summarized in Table 5-2.

Table 5-2  
Simulation Results For  
Sideslip Flight Condition #3.

Input/ Output	Peak Value	Final Value	$t_p$ (sec)	$t_s$ (sec)
$\phi$ (deg)	-0.242	0.0	8.2	--
$\beta$ (deg)	5.076	5.0	10.0	8.4
$\delta_r$ (deg)	7.8	--	--	--
$\delta_w$ (deg)	28.0	--	--	--

Normal Climb, Flight Condition #3. Using the design procedures discussed earlier, a longitudinal controller is designed to accomplish a 1200 fpm climb. To accomplish this flight path angle, gamma, is commanded to a value of 4.86 degrees in 6 seconds and at the same time perturbation velocity in the x-direction is commanded to zero. The control law selected for this maneuver is defined by the parameters:

$$T = 0.05 \text{ seconds (20 hertz)} \quad (5-25)$$

$$\alpha = 2.5 \quad (5-26)$$

$$\epsilon = 0.5 \quad (5-27)$$

$$Z = \text{diag}[0.5 \quad 0.3] \quad (5-28)$$

$$M = \begin{bmatrix} 0.0 & 0.75 & 0.0 \\ 0.0 & 0.0 & 0.0 \end{bmatrix} \quad (5-29)$$

which yields

$$K_0 = \begin{bmatrix} -0.9558 & 0.0 \\ 0.04861 & 2.957 \end{bmatrix} \quad (5-30)$$

$$K_1 = \begin{bmatrix} -0.3823 & 0.0 \\ 0.01944 & 1.183 \end{bmatrix} \quad (5-31)$$

Figures 5-3a thru 5-3h show the simulation results for this controller. The command input vector is given by Figure 5-3a. Figure 5-3b shows flight path angle and velocity. Flight path angle has a peak value of 5.32 occurring at 8.1 seconds which is 2.1 seconds after the input reaches steady-state. Settling time for the flight path angle is 12.3 seconds, 6.3 seconds after the input reaches steady-state. At first this may appear to be a rather large settling time. But when the size of the aircraft and the slow responding engines are considered, 12.3 seconds to stabilize in a 1200 rpm constant airspeed climb isn't unreasonable. Perturbation velocity,  $u$ , peaked at -0.1476 ft/sec in 4.8 seconds, then slowly returns to zero.

The flight controls needed for this maneuver are shown in Figure 5-3c. Thrust peaks at 24% in 7 seconds. This should be easily attainable by the engines on the KC-135A. Remember that this represents an increase in thrust above that used for level flight. The elevator averages a 3



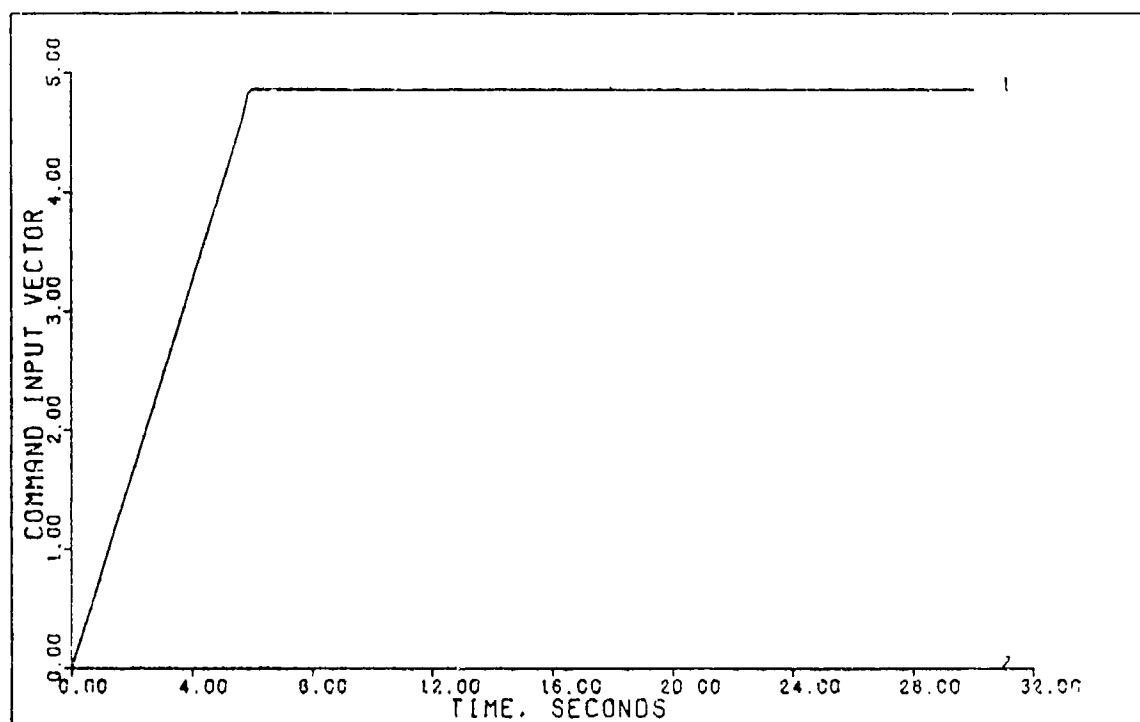


FIGURE 5-3a: Flight Condition #3, Normal Climb  
(Command Input Vector)

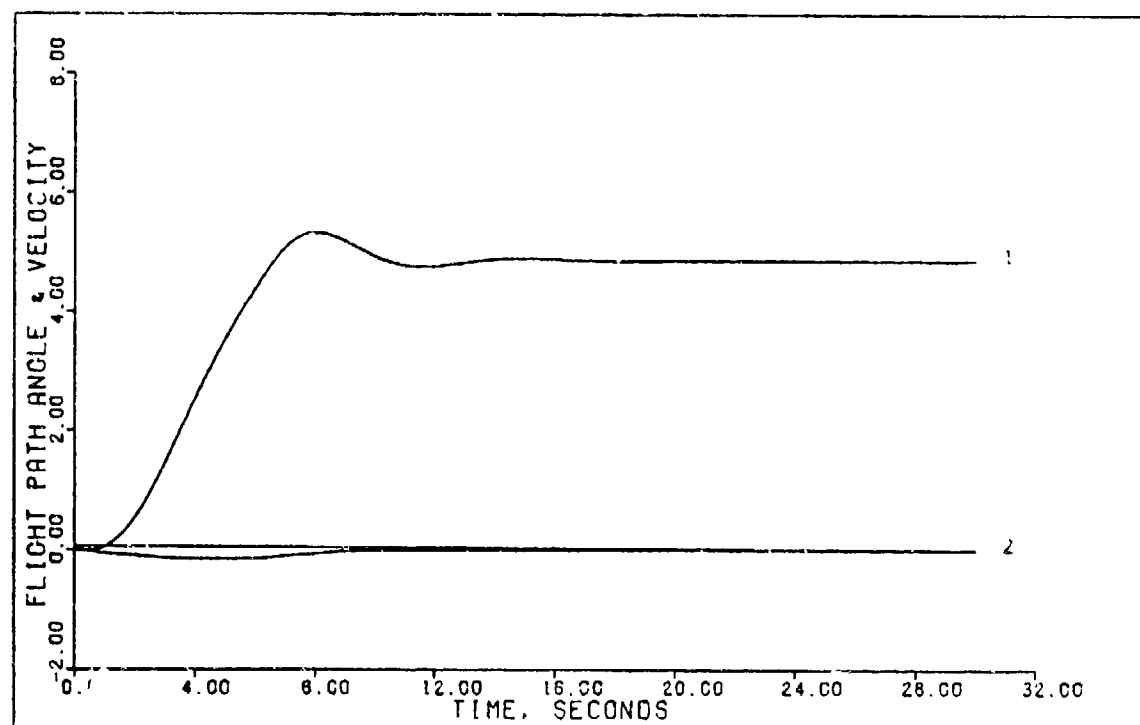


FIGURE 5-3b: Flight Condition #3, Normal Climb  
(Output 1: Flight Path Angle; Output 2: Velocity)

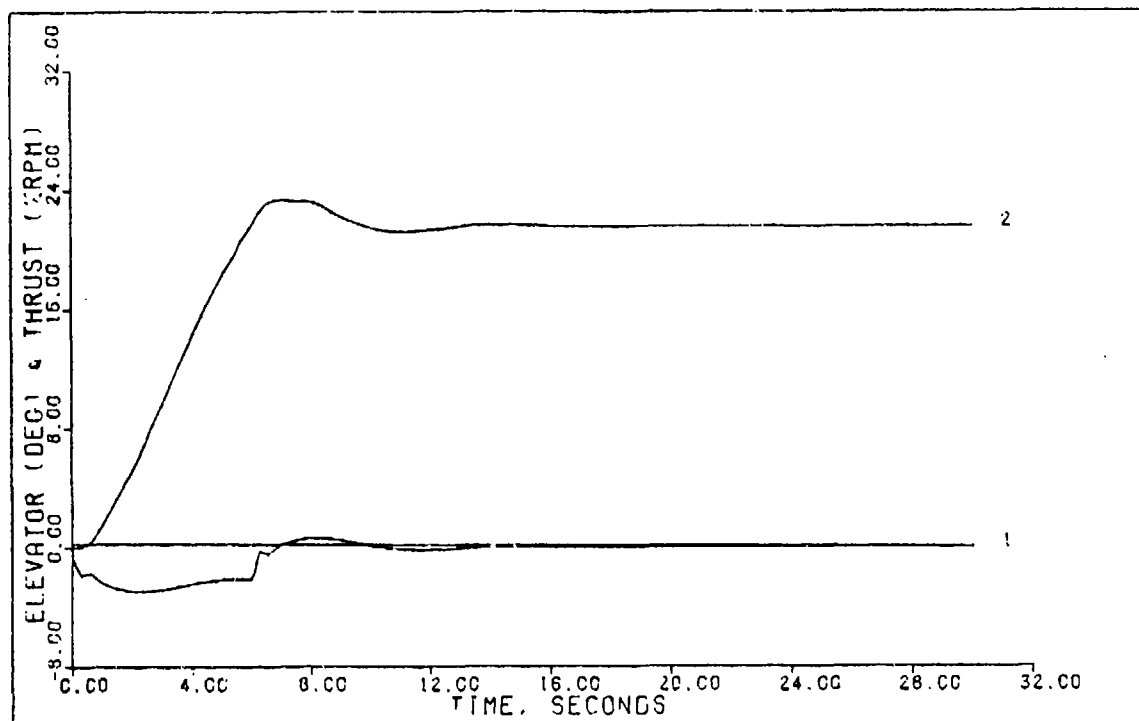


FIGURE 5-3c: Flight Condition #3, Normal Climb  
(Control 1: Elevator; Control 2: Thrust)

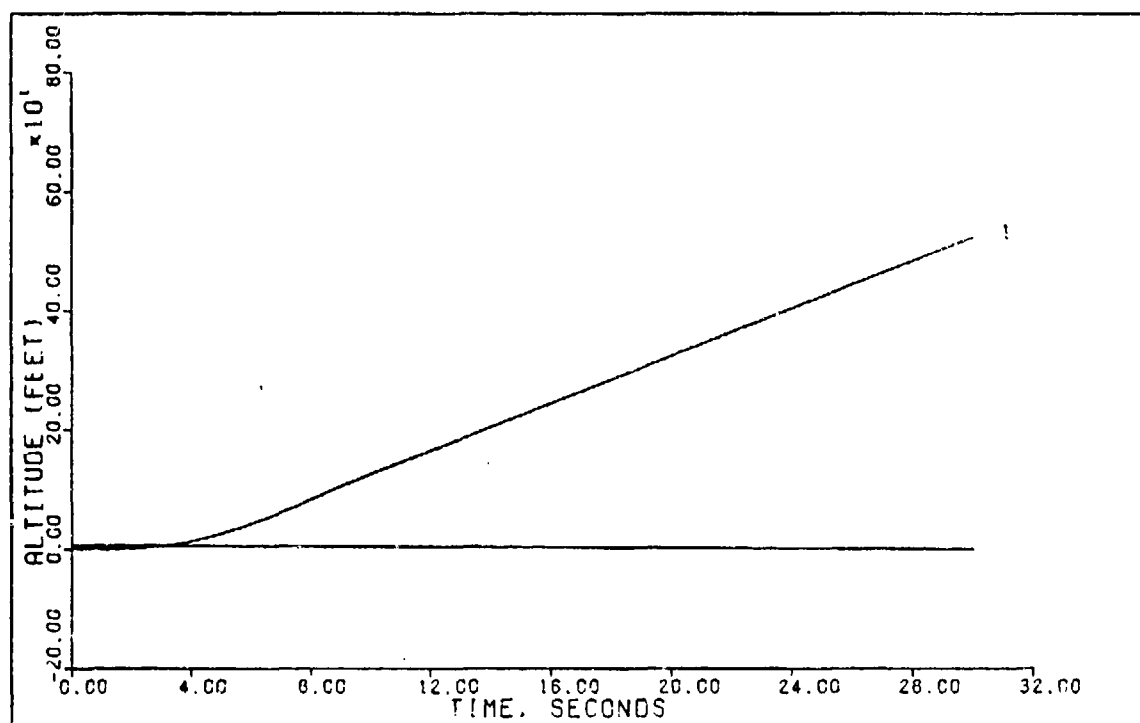


FIGURE 5-3d: Flight Condition #3, Normal Climb  
(State 1: Altitude)

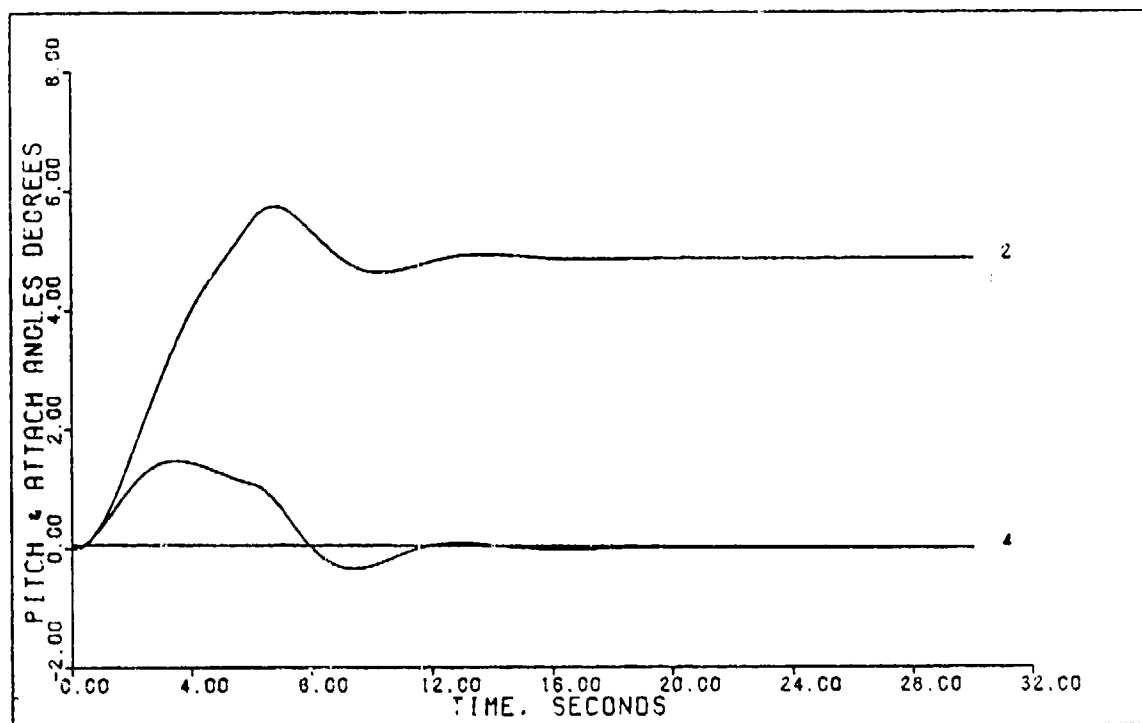


FIGURE 5-3e: Flight Condition #3, Normal Climb  
(State 2: Pitch Angle; State 4: Attack Angle)

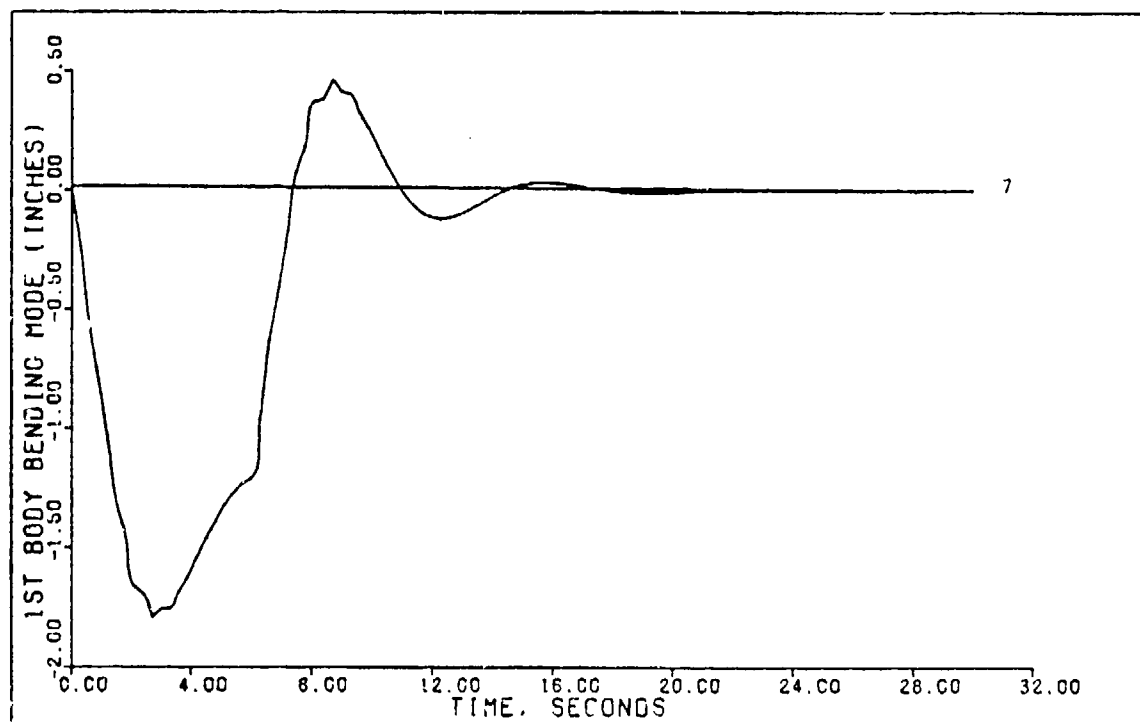


FIGURE 5-3f: Flight Condition #3, Normal Climb  
(State 7: 1st Body Bending Mode)

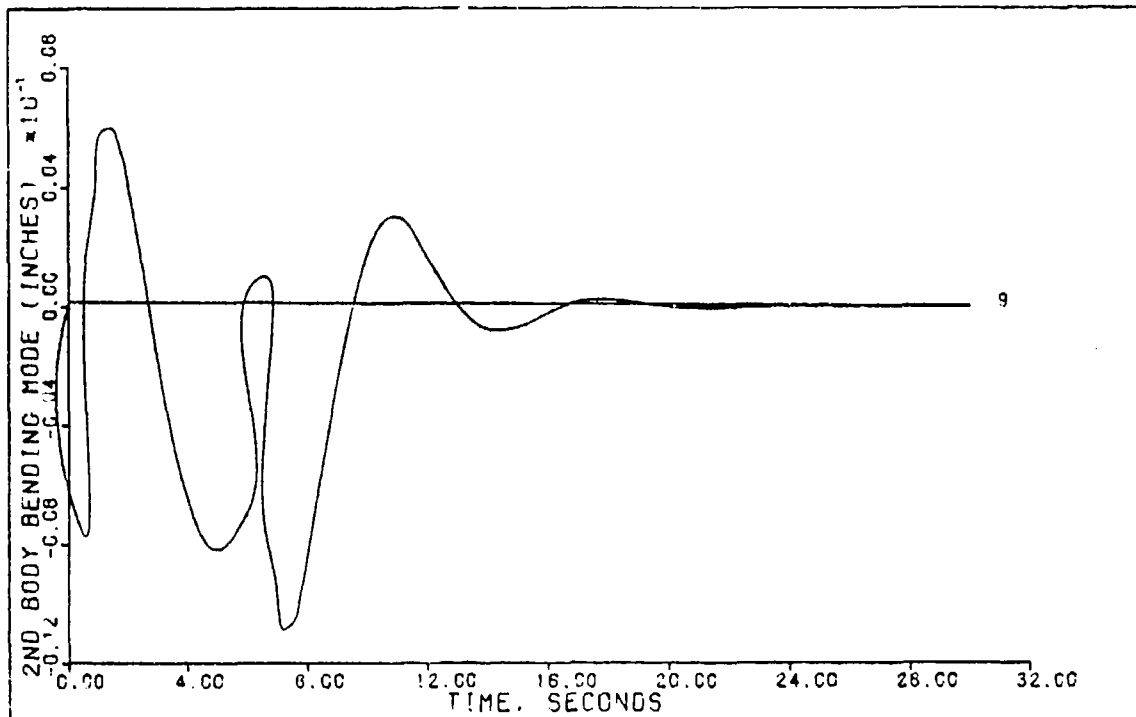


FIGURE 5-3g: Flight Condition #3, Normal Climb  
(State 9: 2nd Body Bending Mode)

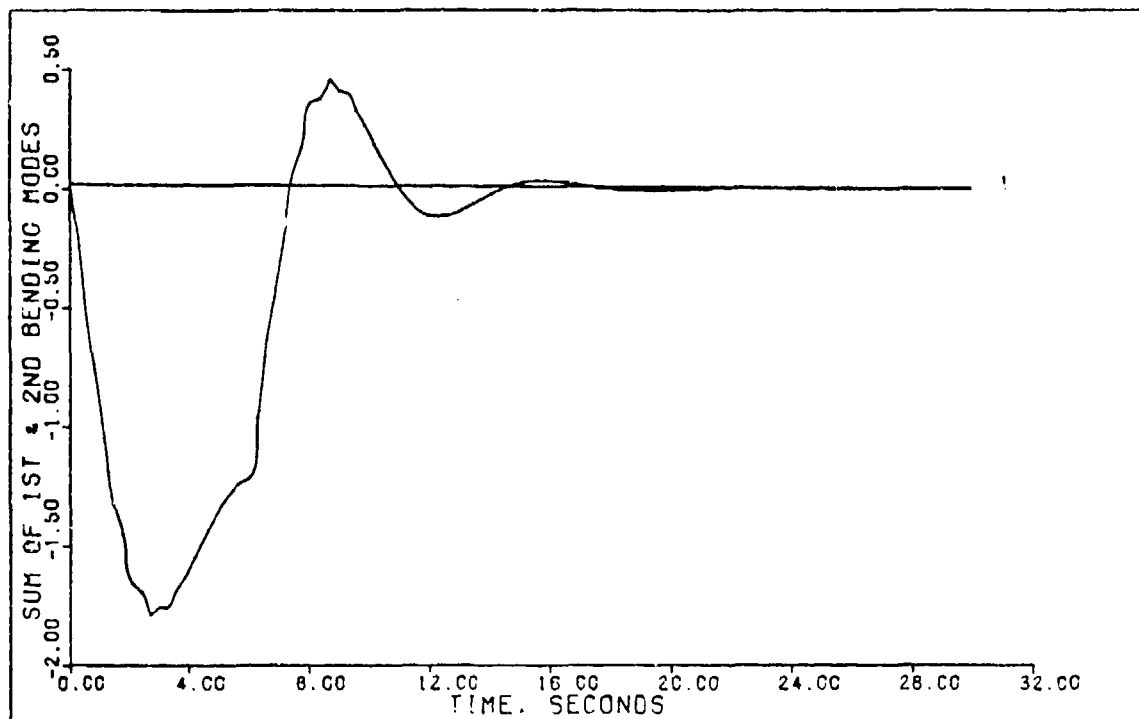


FIGURE 5-3h: Flight Condition #3, Normal Climb  
(Sum of 1st & 2nd Bending Modes)

degree deflection over a 5 second duration and the rates of deflection are approximately 20 deg/sec. Again, an easily attainable limit.

Figure 5-3d shows the altitude  $h$  as a function of time. The slope of this curve represents the desired 1200 fpm climb. Figures 5-3f thru 5-3h represent the body bending mode. This body bending is measured at the crew station. Figure 5-3f shows the first bending mode, Figure 5-3g shows the second and Figure 5-3h shows the sum of the two. Comparison of Figure 5-3f and Figure 5-3h shows that the 1st bending mode accurately represents the total bending of the aircraft and that future studies involving aircraft bending need only consider this mode. This by no means represents any new discovery but merely supports what has already been known. It should also be noted that body bending is only observed here and that its effects on sensors, etc. are not included in the model. See Appendix A and Reference 10 for the equations used to model the aircraft bending. Table 5-3 gives a summary of the results of this simulation.

Table 5-3  
Simulation Results For  
Normal Climb Flight Condition #3.

Input/ Output	Peak Value	Final Value	$t_p$ (sec)	$t_s$ (sec)
$\gamma$ (deg)	5.322	4.86	8.1	12.3
$u$ (ft/sec)	-0.1476	0.0	4.8	0.0
$\delta_e$ (deg)	-3.8	--	--	--
$\delta_T$ (%RPM)	24.0	--	--	--

Pitch Pointing, Flight Condition #3. The longitudinal controller used to perform the normal climb uses only elevator and thrust as inputs. Speed Brakes are left out of the model since they would contribute nothing to this maneuver. For pitch pointing, speed brakes need to be included since there are now three outputs to control and thus three inputs are needed. Therefore, a second longitudinal controller is designed using three inputs. This controller is defined by the parameters:

$$T = 0.05 \text{ seconds (20 hertz)} \quad (5-32)$$

$$\alpha = 2.5 \quad (5-33)$$

$$\epsilon = 0.3 \quad (5-34)$$

$$\Sigma = \text{diag}[1.0 \quad 0.75 \quad 0.1] \quad (5-35)$$

$$M = \begin{bmatrix} 0.75 & 0.0 \\ 0.0 & 0.25 \\ 0.0 & 0.0 \end{bmatrix} \quad (5-36)$$

$$K_0 = \begin{bmatrix} -0.4157 & -2.597 & 0.0 \\ -4.017 & -1.508 & 0.0 \\ -1.978 & -0.6188 & 0.5915 \end{bmatrix} \quad (5-37)$$

$$K_1 = \begin{bmatrix} -0.1663 & -1.039 & 0.0 \\ -1.607 & -0.6033 & 0.0 \\ -0.7914 & -0.2475 & 0.2366 \end{bmatrix} \quad (5-38)$$

To perform pitch pointing, pitch angle is commanded to 4 degrees in 4 seconds while at the same time altitude and perturbation velocity are commanded to zero. Figures 5-4a thru 5-4h represent the simulation results for this maneuver using the controller defined by Equations (5-32) thru (5-38). The command input vector is given in Figure 5-4a. Figure 5-4b shows two of the outputs, altitude and perturbation velocity. Both of these remain negligible since altitude peaks at 0.299 feet in 4.4 seconds and  $u$  peaks at -0.479 in 1.6 seconds. Figure 5-4c shows pitch and attack angles. Pitch angle closely follows the input and reaches a peak of 4 degrees in 16 seconds. Settling time for pitch angle is 4.4 seconds. Elevator and thrust are shown in Figure 5-4d. Thrust peaks at 32 %rpm in approximately 4.5 seconds. The elevator is somewhat shaky and thus decreases the effectiveness of this maneuver. Figure 5-4e shows speed brake deflections which peak at 52 degrees in 4.25 seconds. This in itself says something about the maneuver since 52 degrees of speed brakes to produce 4 degrees of pitch pointing doesn't seem like much of a trade off. Figures 5-4f thru 5-4h show the body

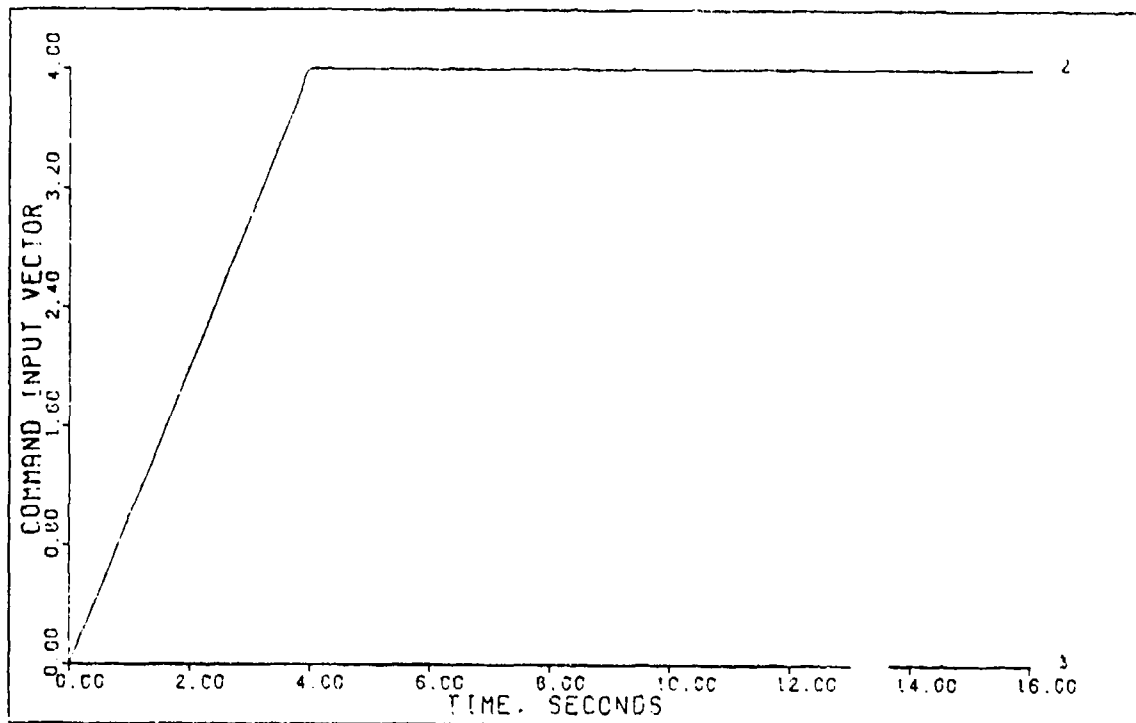


FIGURE 5-4a: Flight Condition #3, Pitch Pointing  
(Command Input Vector)

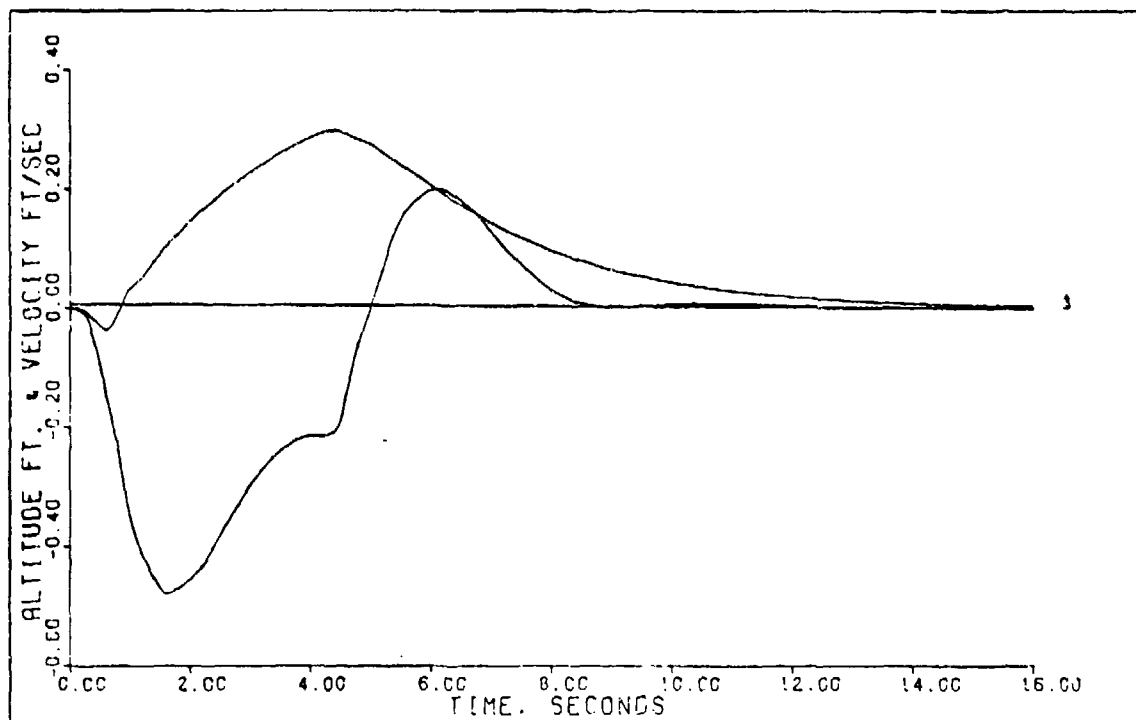


FIGURE 5-4b: Flight Condition #3, Pitch Pointing  
(Output 1: Altitude; Output 2: Velocity)



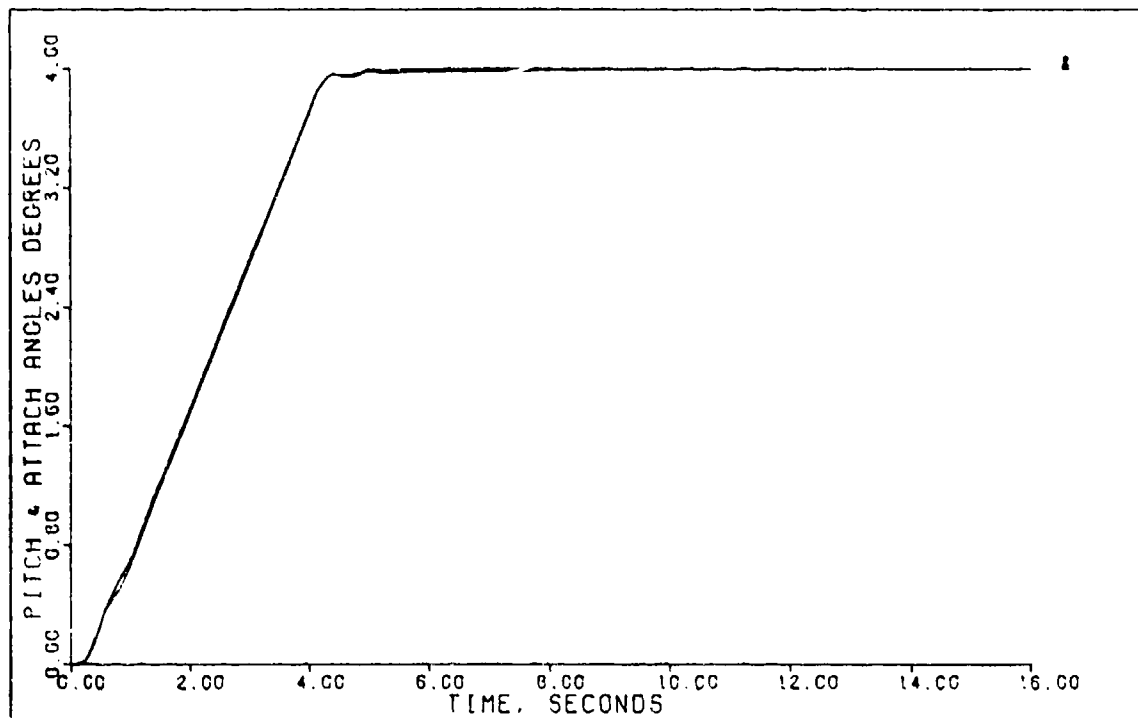


FIGURE 5-4c: Flight Condition #3, Pitch Pointing  
(State 2: Pitch Angle; State 4: Attack Angle)

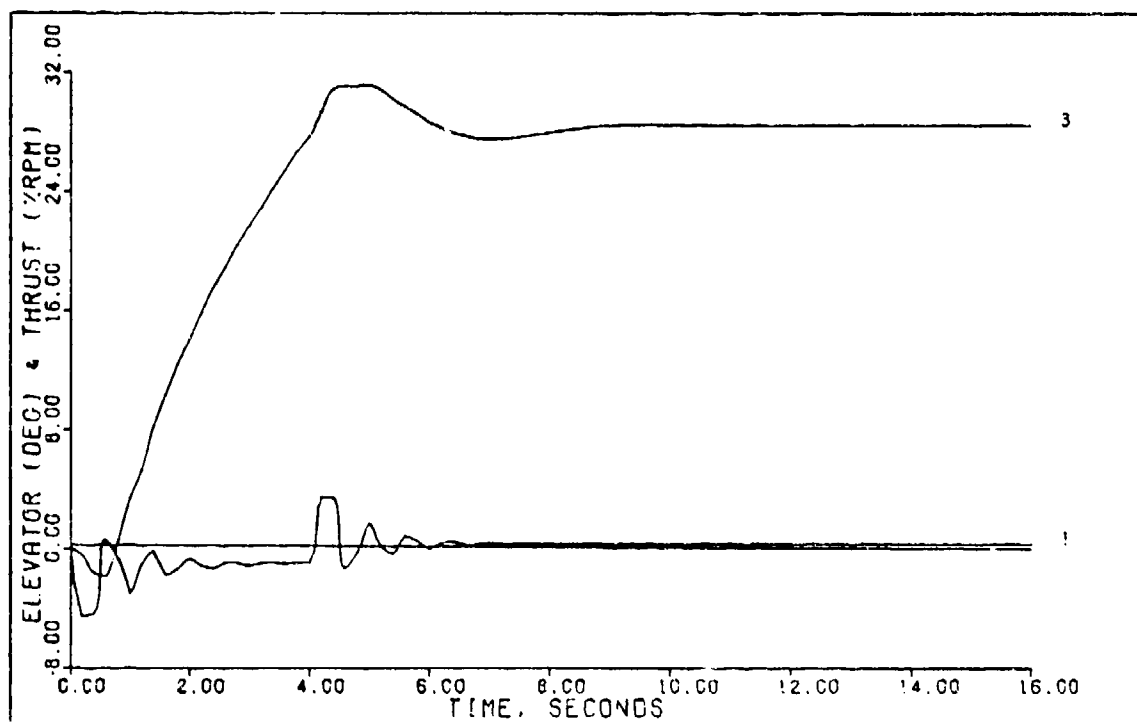


FIGURE 5-4d: Flight Condition #3, Pitch Pointing  
(Control 1: Elevator; Control 2: Thrust)

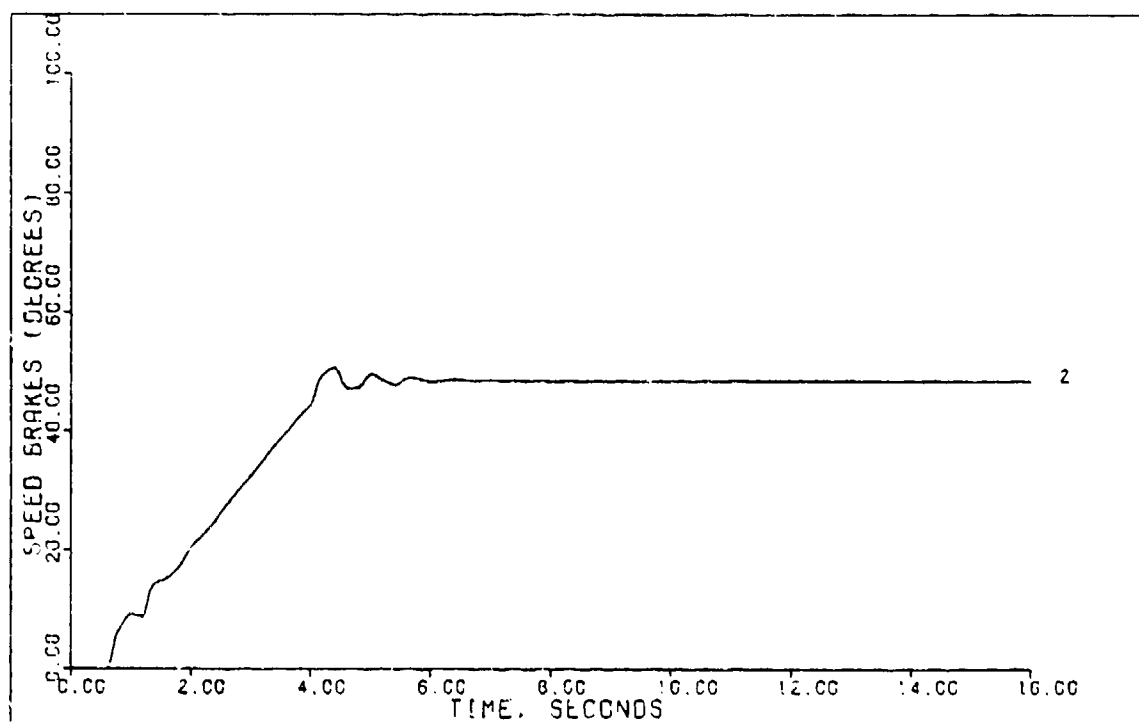


FIGURE 5-4e: Flight Condition #3, Pitch Pointing  
(Control 3: Speed Brakes)

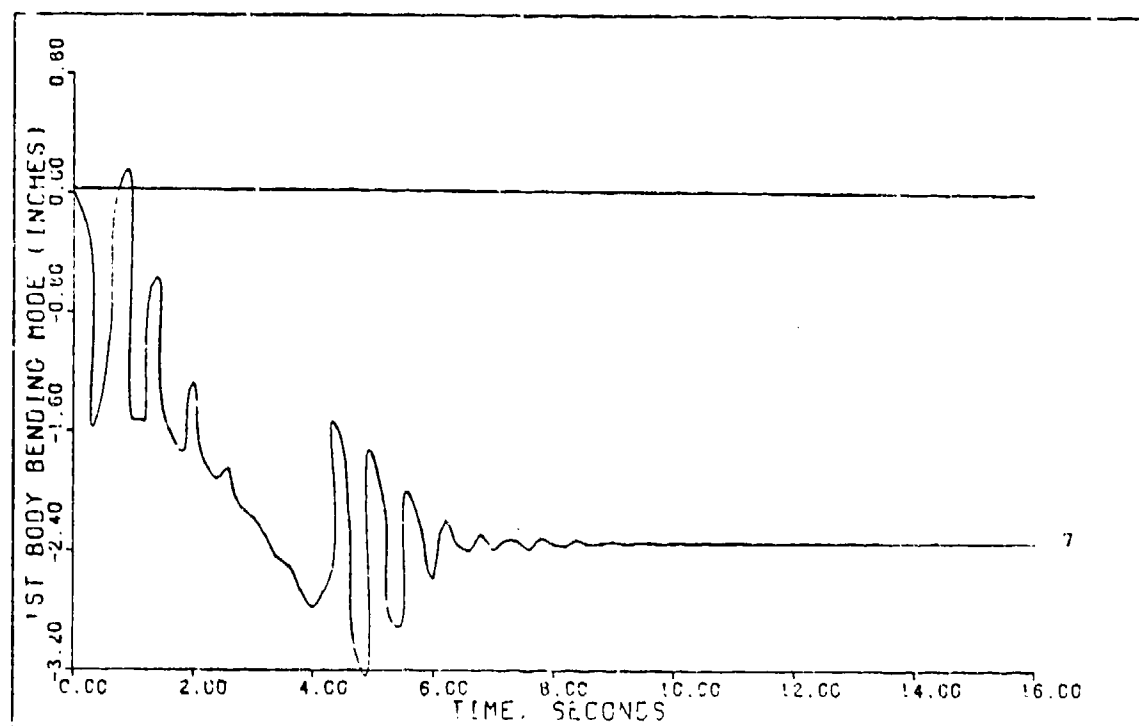


FIGURE 5-4f: Flight Condition #3, Pitch Pointing  
(State 7: 1st Body Bending Mode)

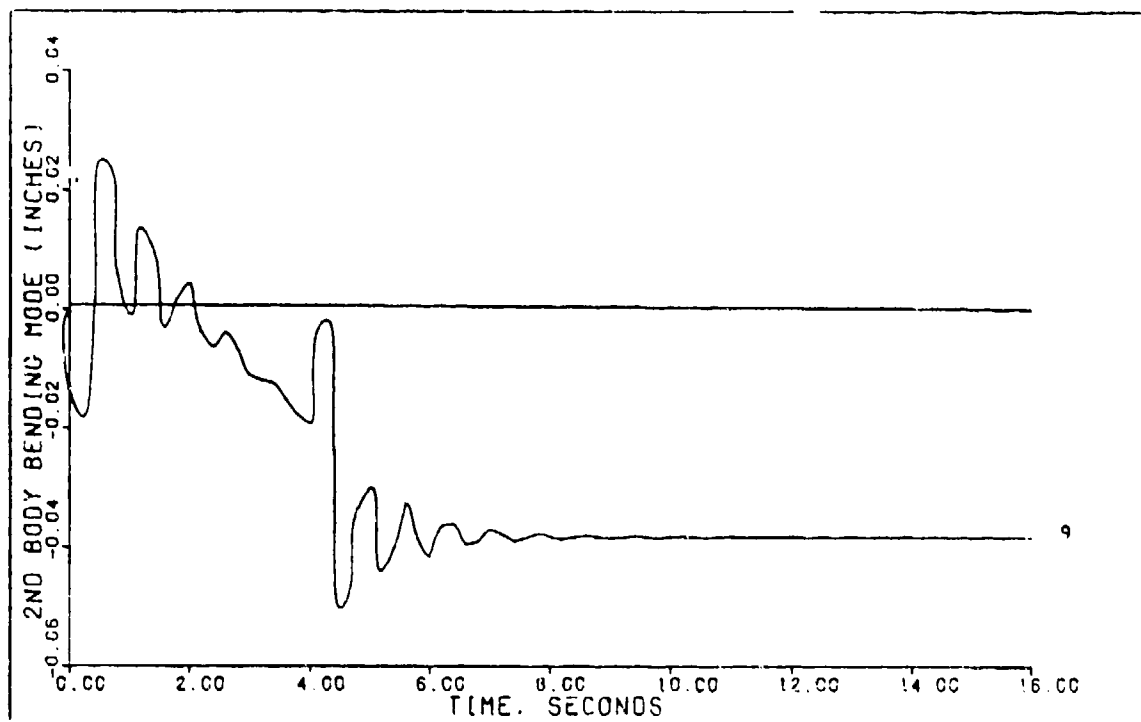


FIGURE 5-4g: Flight Condition #3, Pitch Pointing  
(State 9: 2nd Body Bending Mode)

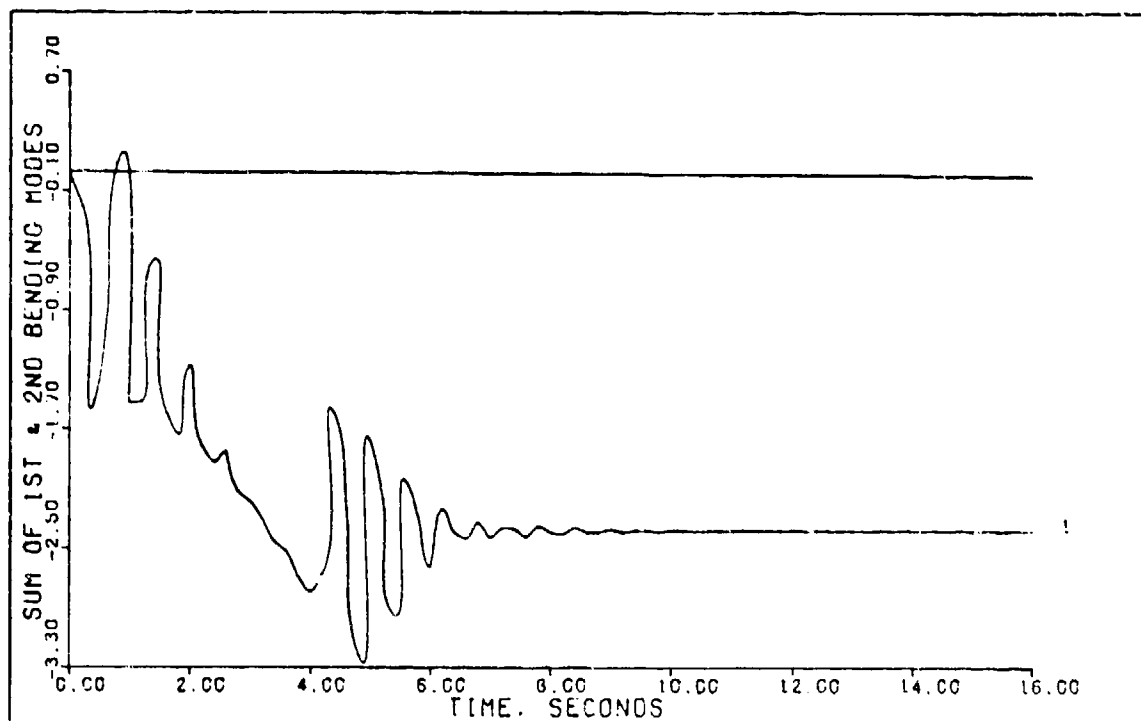


FIGURE 5-4h: Flight Condition #3, Pitch Pointing  
(Sum of 1st & 2nd Bending Modes)

bending modeled at the crew station. Table 5-4 summarizes the results of this maneuver.

Table 5-4  
Simulation Results For  
Pitch Pointing Flight Condition #3

Input/ Output	Peak Value	Final Value	$t_p$ (sec)	$t_s$ (sec)
h (ft)	0.299	0.0	4.4	--
$\theta$ (deg)	4.0	4.0	16.0	--
u (ft/sec)	-0.479	0.0	1.6	--
$\delta_e$ (deg)	4.0	--	--	--
$\delta_{sb}$ (deg)	52.0	--	--	--
$\delta_T$ (%RPM)	32.0	--	--	--

#### Tracker Control Laws For Flight Condition #2 and #1

Using the same procedures, controllers are developed for each of the two remaining flight conditions. What follows is a list of the parameters used to define each of the controllers used. Simulations are accomplished for each of these controllers. Rather than discuss these simulations in detail, their results are simply compiled in Appendix C for observation.

Coordinated Turn, Flight Condition #2 The control law developed for this maneuver is defined by the following parameters:

$$T = 0.05 \text{ seconds (20 hertz)} \quad (5-39)$$

$$\alpha = 4.0 \quad (5-40)$$

$$\epsilon = 0.03 \quad (5-41)$$

$$\Sigma = \text{diagonal } [1.5 \quad 5] \quad (5-42)$$

$$M = \begin{bmatrix} 0.75 & 0.0 \\ 0.0 & 0.4 \end{bmatrix} \quad (5-43)$$

$$K_0 = \begin{bmatrix} 0.003759 & 1.151 \\ 0.511 & -2.415 \end{bmatrix} \quad (5-44)$$

$$K_1 = \begin{bmatrix} 0.0009397 & 0.2877 \\ 0.1277 & -0.6037 \end{bmatrix} \quad (5-45)$$

Figures C-1a thru C-1f and Table C-1 given in Appendix C show the simulation results for this controller.

Sideslip, Flight Condition #2 The control law developed for this maneuver is defined by the following parameters:

$$T = 0.05 \text{ seconds (20 hertz)} \quad (5-46)$$

$$\alpha = 4.0 \quad (5-47)$$

$$\epsilon = 0.03 \quad (5-48)$$

$$\Sigma = \text{diagonal } [1.5 \quad 5] \quad (5-49)$$

$$M = \begin{bmatrix} 0.25 & 0.0 \\ 0.0 & 0.4 \end{bmatrix} \quad (5-50)$$

$$K_0 = \begin{bmatrix} 0.01031 & 1.151 \\ 0.01535 & -2.415 \end{bmatrix} \quad (5-51)$$

$$K_1 = \begin{bmatrix} 0.002579 & 0.2877 \\ 0.3838 & -0.6037 \end{bmatrix} \quad (5-52)$$

Figures C-2a thru C-2d and Table C-2 given in Appendix C show the simulation results for this controller.

Normal Climb, Flight Condition #2 The control law developed for this maneuver is defined by the following parameters:

$$T = 0.05 \text{ seconds (20 hertz)} \quad (5-53)$$

$$\alpha = 2.5 \quad (5-54)$$

$$\epsilon = 0.3 \quad (5-55)$$

$$\Sigma = \text{diagonal } [1.75 \quad .1] \quad (5-56)$$

$$M = \begin{bmatrix} 0.0 & 0.75 & 0.0 \\ 0.0 & 0.0 & 0.0 \end{bmatrix} \quad (5-57)$$

$$K_0 = \begin{bmatrix} -1.01 & 0.0 \\ 0.3118 & 2.206 \end{bmatrix} \quad (5-58)$$

$$K_1 = \begin{bmatrix} -0.4039 & 0.0 \\ 0.1247 & 0.8824 \end{bmatrix} \quad (5-59)$$

Figures C-3a thru C-3h and Table C-3 given in Appendix C show the simulation results for this controller.

Pitch Pointing, Flight Condition #2 The control law designed for this maneuver is defined by the following parameters:

$$T = 0.05 \text{ seconds (20 hertz)} \quad (5-60)$$

$$\alpha = 2.5 \quad (5-61)$$

$$\epsilon = 0.3 \quad (5-62)$$

$$\Sigma = \text{diagonal } [1 \quad 0.75 \quad 0.1] \quad (5-63)$$

$$M = \begin{bmatrix} 0.75 & 0.0 \\ 0.0 & 0.25 \\ 0.0 & 0.0 \end{bmatrix} \quad (5-64)$$

$$K_0 = \begin{bmatrix} -0.3687 & -1.398 & 0.0 \\ -2.973 & -0.9532 & 0.0 \\ -6.865 & -1.806 & 2.206 \end{bmatrix} \quad (5-65)$$

$$K_1 = \begin{bmatrix} -0.1475 & -0.5592 & 0.0 \\ -1.189 & -0.3813 & 0.0 \\ -2.746 & -0.7222 & 0.8824 \end{bmatrix} \quad (5-66)$$

Figures C-4a thru C-4h and Table C-4 given in Appendix C show the simulation results for this controller.

Coordinated Turn, Flight Condition #1 The control law developed for this maneuver is defined by the following parameters:

$$T = 0.05 \text{ seconds (20 hertz)} \quad (5-67)$$

$$\alpha = 4.0 \quad (5-68)$$

$$\epsilon = 0.03 \quad (5-69)$$

$$\Sigma = \text{diagonal } [1.5 \quad 5.0] \quad (5-70)$$

$$M = \begin{bmatrix} 0.75 & 0.0 \\ 0.0 & 0.4 \end{bmatrix} \quad (5-71)$$

$$K_0 = \begin{bmatrix} 0.00525 & 1.488 \\ 0.6493 & -2.527 \end{bmatrix} \quad (5-72)$$

$$K_1 = \begin{bmatrix} 0.001312 & 0.3721 \\ 0.1623 & -0.6317 \end{bmatrix} \quad (5-73)$$

Figures C-5a thru C-5f and Table C-5 given in Appendix C show the simulation results for this controller.

Sideslip, Flight Condition #1 The control law developed for this maneuver is defined by the following parameters:

$$T = 0.05 \text{ seconds (20 hertz)} \quad (5-74)$$

$$\alpha = 4.0 \quad (5-75)$$

$$\epsilon = 0.03 \quad (5-76)$$

$$\Sigma = \text{diagonal [1.5 5]} \quad (5-77)$$

$$M = \begin{bmatrix} 0.25 & 0.0 \\ 0.0 & 0.4 \end{bmatrix} \quad (5-78)$$

$$K_0 = \begin{bmatrix} 0.01575 & 1.488 \\ 1.948 & -2.527 \end{bmatrix} \quad (5-79)$$

$$K_1 = \begin{bmatrix} 0.003937 & 0.3721 \\ 0.487 & -0.6317 \end{bmatrix} \quad (5-80)$$

Figures C-6a thru C-6d and Table C-6 given in Appendix C show the simulation results for this controller.

Normal Climb, Flight Condition #1 The control law developed for this maneuver is defined by the following parameters:

$$T = 0.05 \text{ seconds (20 hertz)} \quad (5-81)$$

$$\alpha = 2.5 \quad (5-82)$$

$$\epsilon = 0.3 \quad (5-83)$$

$$\Sigma = \text{diagonal [1.5 0.2]} \quad (5-84)$$

$$M = \begin{bmatrix} 0.0 & 0.75 & 0.0 \\ 0.0 & 0.0 & 0.0 \end{bmatrix} \quad (5-85)$$

$$K_0 = \begin{bmatrix} -0.9256 & 0.0 \\ 0.2171 & 3.028 \end{bmatrix} \quad (5-86)$$



$$K_1 = \begin{bmatrix} -0.3702 & 0.0 \\ 0.08682 & 1.211 \end{bmatrix} \quad (5-87)$$

Figures C-7a thru C-7h and Table C-7 given in Appendix C show the simulation results for this controller.

Pitch Pointing, Flight Condition #1 The control law developed for this maneuver is defined by the following parameters:

$$T = 0.05 \text{ seconds (20 hertz)} \quad (5-88)$$

$$\alpha = 4.5 \quad (5-89)$$

$$\epsilon = 0.3 \quad (5-90)$$

$$= \text{diagonal } [1 \quad 0.75 \quad 0.1] \quad (5-91)$$

$$M = \begin{bmatrix} 0.75 & 0.0 \\ 0.0 & 0.25 \\ 0.0 & 0.0 \end{bmatrix} \quad (5-92)$$

$$K_0 = \begin{bmatrix} -0.272 & -1.467 & 0.0 \\ -2.588 & -0.9788 & 0.0 \\ -4.257 & -1.29 & 1.514 \end{bmatrix} \quad (5-93)$$

$$K_1 = \begin{bmatrix} -0.1088 & -0.5869 & 0.0 \\ -1.035 & -0.3915 & 0.0 \\ -1.703 & -0.516 & 0.6056 \end{bmatrix} \quad (5-94)$$

Figures C-8a thru C-8h and Table C-8 given in Appendix C show the simulation results for this controller.

### Time Delay

Once the control laws are developed for each of the maneuvers the next step in achieving a final design is to consider a computational time delay of one sampling period. Computational time delay represents the aircraft computer

computation time needed to generate the input to the actuators, based on the current error vector. No delay would mean that the computer performs instantaneous calculations of the control law. A delay of one sampling period means that the time it takes the computer to perform these calculations is less than one sampling time. This time delay is entered under Option #23 in MULTI. What follows is a discussion of the effect of the time delay for each of the previously designed controllers of flight condition #3.

Coordinated Turn, Flight Condition #3 With Time Delay.

Using the control law given by Equations (5-10) thru (5-16) the coordinated turn is performed again, this time including a computational time delay of one sampling period. Figures 5-5a thru 5-5f shows the simulation results for this condition. Comparison of Figures 5-5a thru 5-5f with Figures 5-1a thru 5-1f show the effects of the computational time delay. At first glance there appears to be very little difference, but a comparison of the figures of merit and the maximum control deflections shows that there are indeed some differences. Table 5-5 gives a summary of the results of the computational time delay simulation.

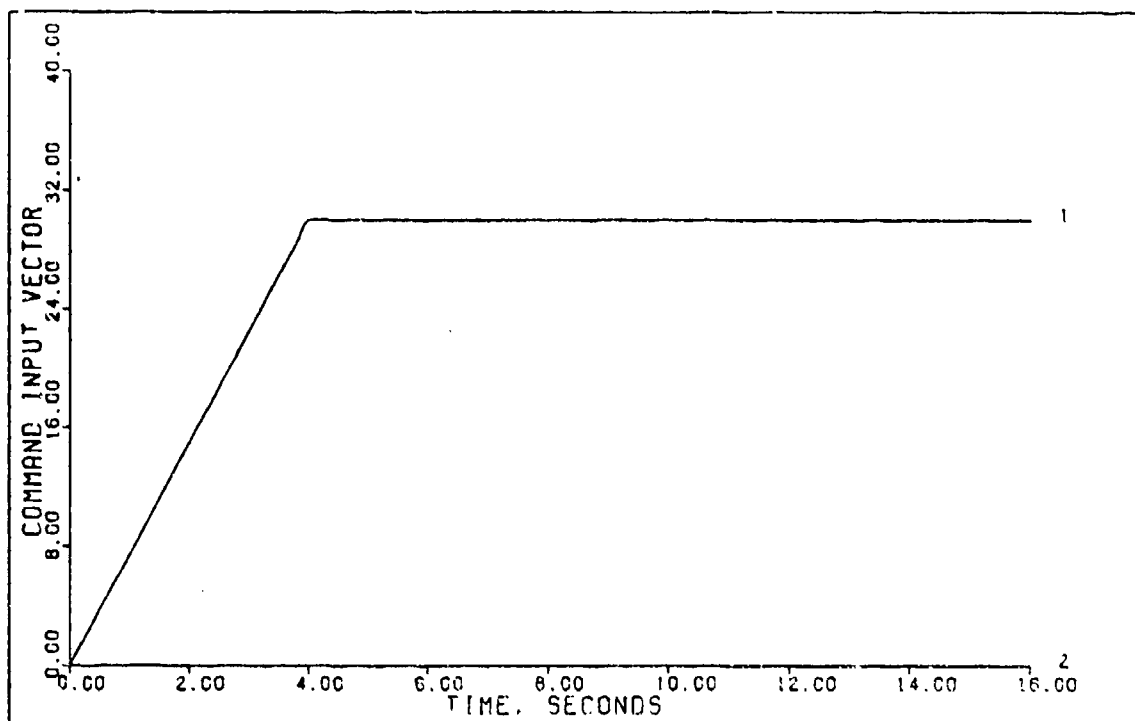


FIGURE 5-5a: Flight Condition #3, Coordinated Turn With Time Delay (Command Input Vector)

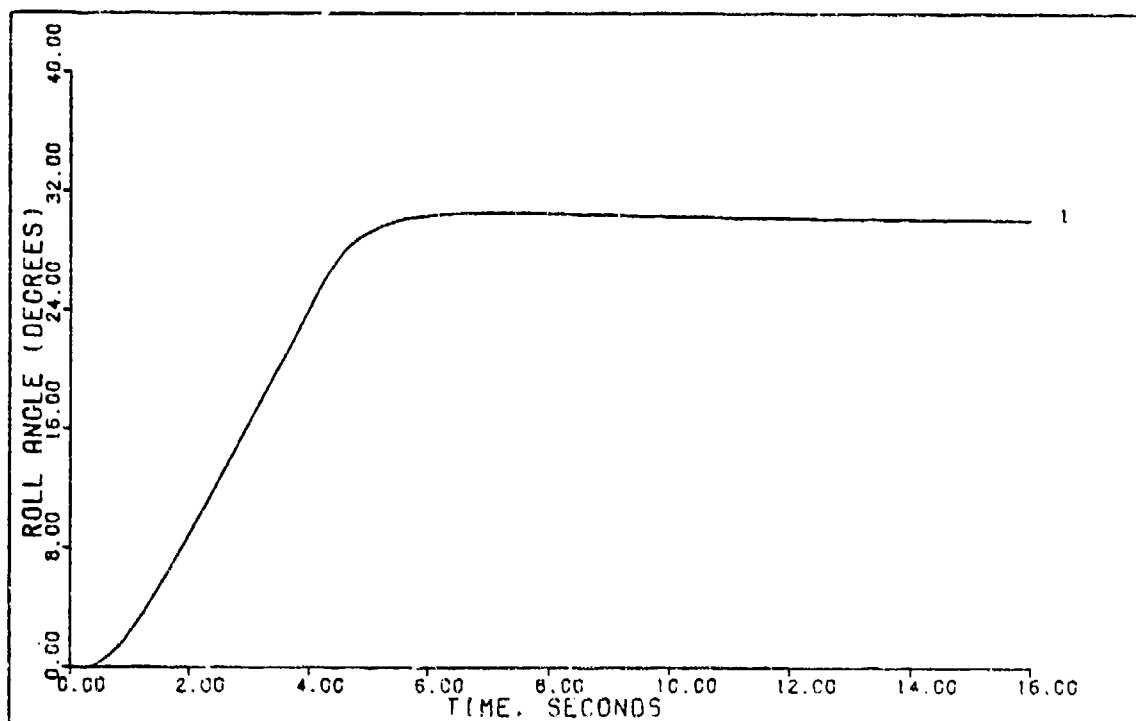


FIGURE 5-5b: Flight Condition #3, Coordinated Turn With Time Delay (Output 1: Roll Angle)

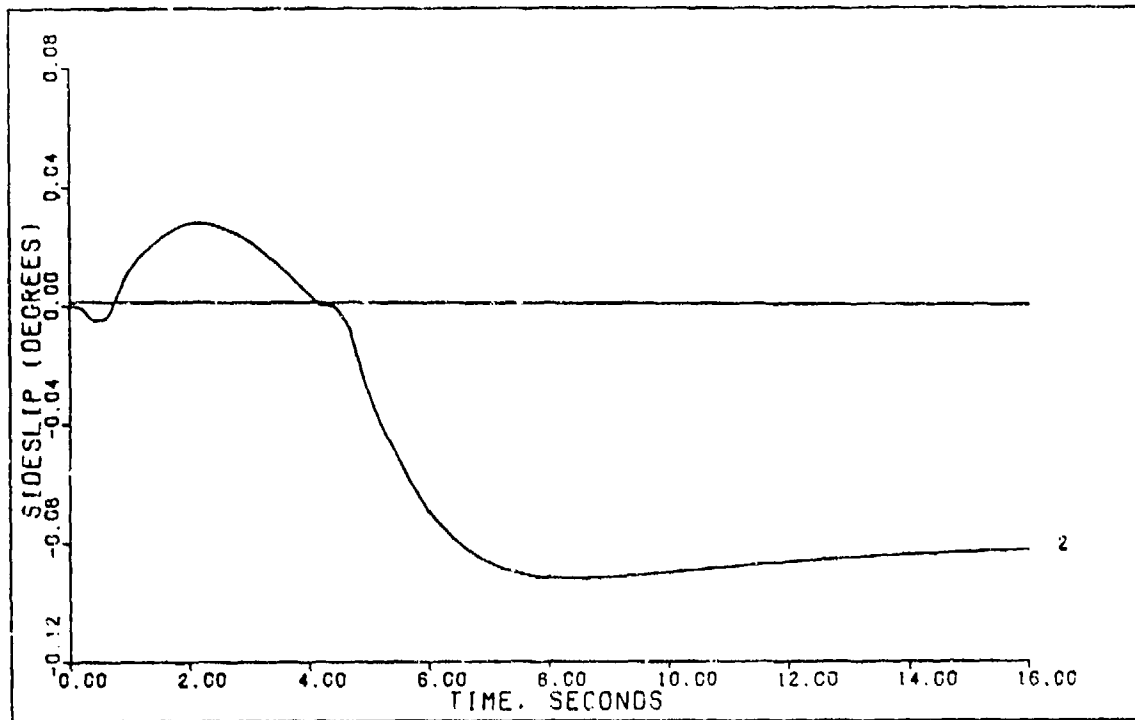


FIGURE 5-5c: Flight Condition #3, Coordinated Turn With Time Delay (Output 2: Sideslip)

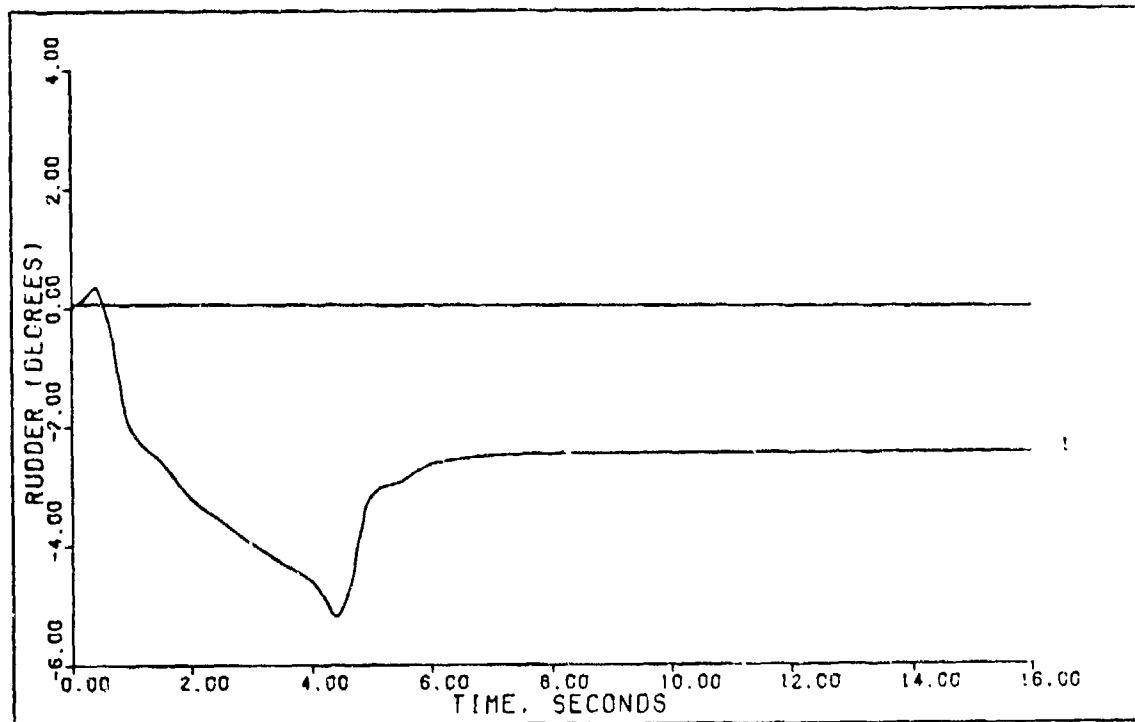


FIGURE 5-5d: Flight Condition #3, Coordinated Turn With Time Delay (Control 1: Rudder)

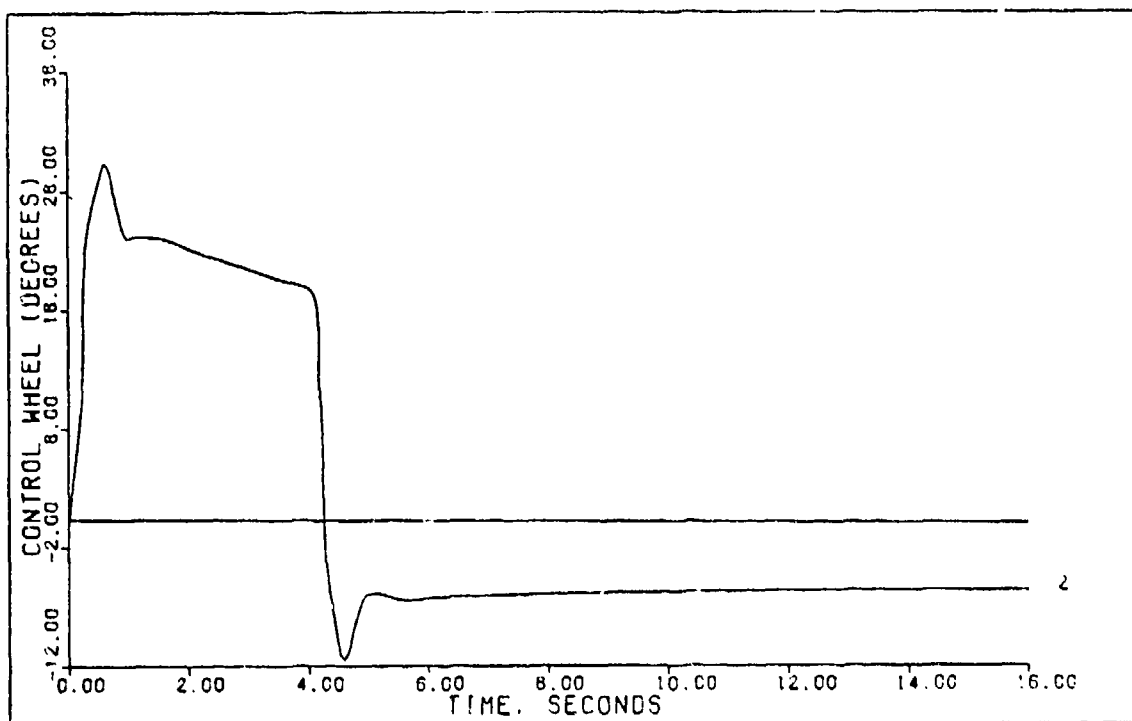


FIGURE 5-5e: Flight Condition #3, Coordinated Turn  
With Time Delay (Control 2: Control Wheel)

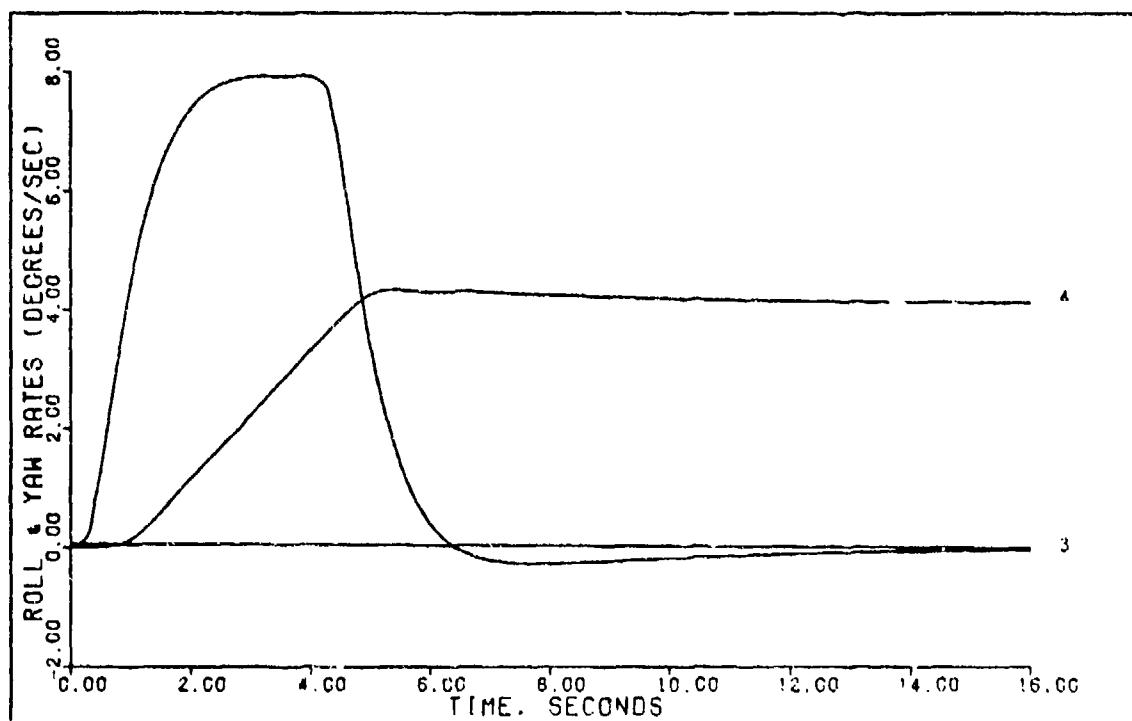


FIGURE 5-5f: Flight Condition #3, Coordinated Turn  
With Time Delay (State 3: Roll Rate;  
State 4: Yaw Rate)

Table 5-5  
Simulation Results For  
Coordinated Turn With Time Delay Flight Condition #3.

Input/ Output	Peak Value	Final Value	$t_p$ (sec)	$t_s$ (sec)
$\phi$ (deg)	31.229	30.0	6.6	10.0
$\beta$ (deg)	0.099	-0.03	2.2	15.2
$r$ (deg/sec)	4.10	3.925	5.2	10.0
$\delta_r$ (deg)	-5.5	--	--	--
$\delta_w$ (deg)	32.0	--	--	--

By comparison of Table 5-5 with Table 5-1 the effects of the time delay become more noticeable. From this it is seen that the bank angle has an overshoot of 1.229 degrees and that settling time has increased to 10 seconds. Control deflections remain about the same and sideslip is still negligible. These effects appear to be acceptable and nothing more needs to be done, but if they are not, then, it is necessary to redesign the controller to reduce or eliminate any of the undesired time delay effects. Either way, the overshoot of the bank angle can be controlled with the development of a new controller. To demonstrate that this is possible, using the same guidelines as before a new controller is designed using the following parameters:

$$T = 0.05 \text{ seconds (20hertz)} \quad (5-95)$$

$$\alpha = 4.25 \quad (5-96)$$

$$\epsilon = 0.08 \quad (5-97)$$

$$\Sigma = \text{diagonal } [1.5 \quad 2.0] \quad (5-98)$$

$$M = \begin{bmatrix} 0.75 & 0.0 \\ 0.0 & 1.0 \end{bmatrix} \quad (5-99)$$

$$K_0 = \begin{bmatrix} 0.03104 & 1.337 \\ 1.766 & -1.182 \end{bmatrix} \quad (5-100)$$

$$K_1 = \begin{bmatrix} 0.007304 & 0.3145 \\ 0.4154 & -0.2782 \end{bmatrix} \quad (5-101)$$

Figures 5-6 thru 5-6f show the simulation results for this new controller. The biggest problem encountered in trying to reduce the bank angle overshoot caused by the computational time delay is keeping control surfaces from oscillating. Table 5-6 summarizes the results of the redesigned controller given by Equations (5-95) thru (5-101).

Table 5-6  
Simulation Results For Coordinated Turn With  
Time Delay Flight Condition #3 (Redesigned)

Input/ Output	Peak Value	Final Value	$t_p$ (sec)	$t_s$ (sec)
$\phi$ (deg)	30.563	30.0	7.0	5.2
$\beta$ (deg)	-0.09	-0.082	8.4	14.0
$r$ (deg/sec)	4.17	3.93	5.0	7.2
$\delta_r$ (deg)	-5.5	--	--	--
$\delta_w$ (deg)	32.0	--	--	--

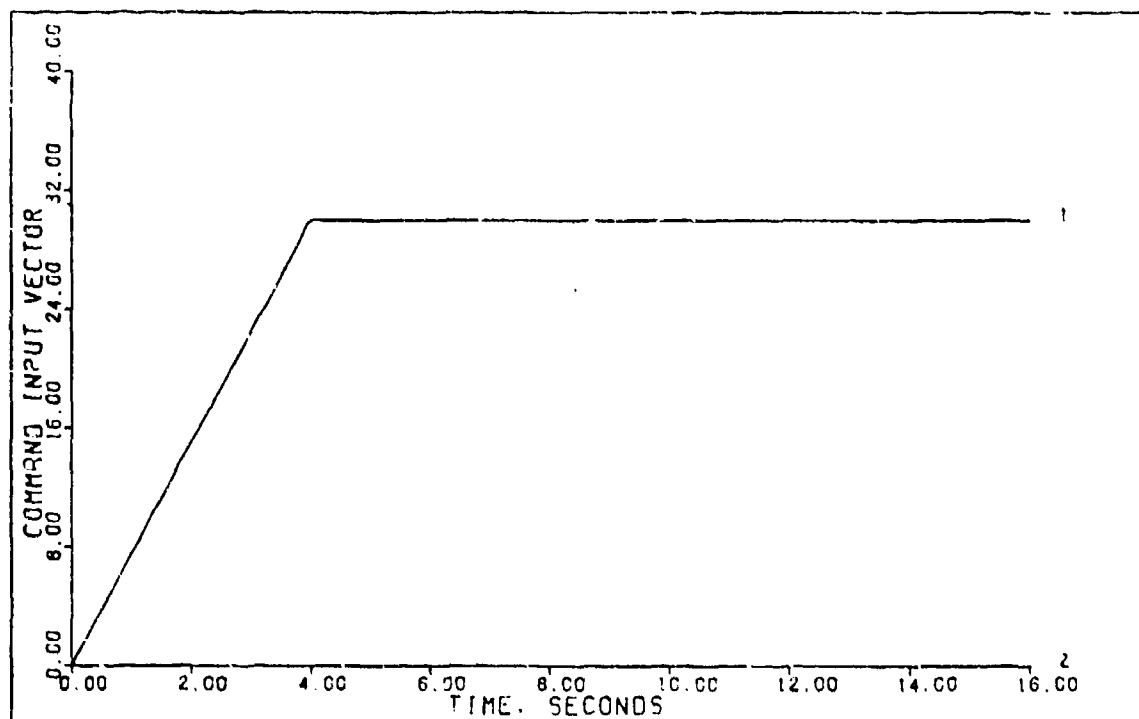


FIGURE 5-6a: Flight Condition #3, Coordinated Turn  
With Time Delay, Redesigned  
(Command Input Vector)

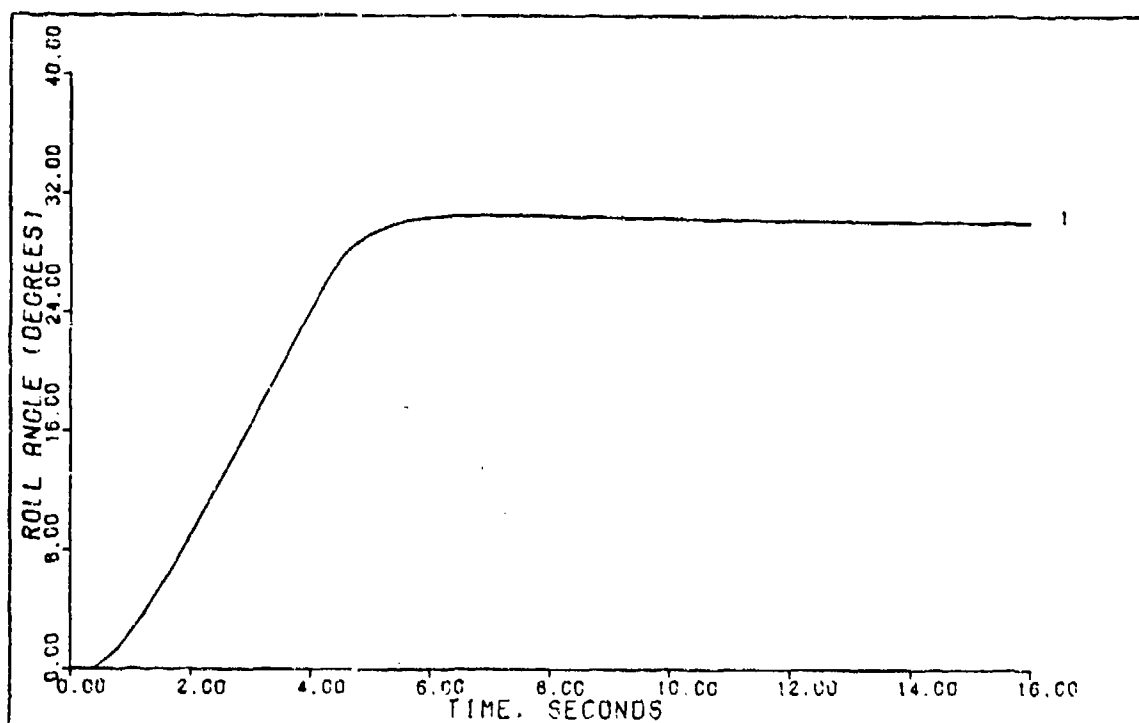


FIGURE 5-6b: Flight Condition #3, Coordinated Turn  
With Time Delay, Redesigned  
(Output 1: Roll Angle)



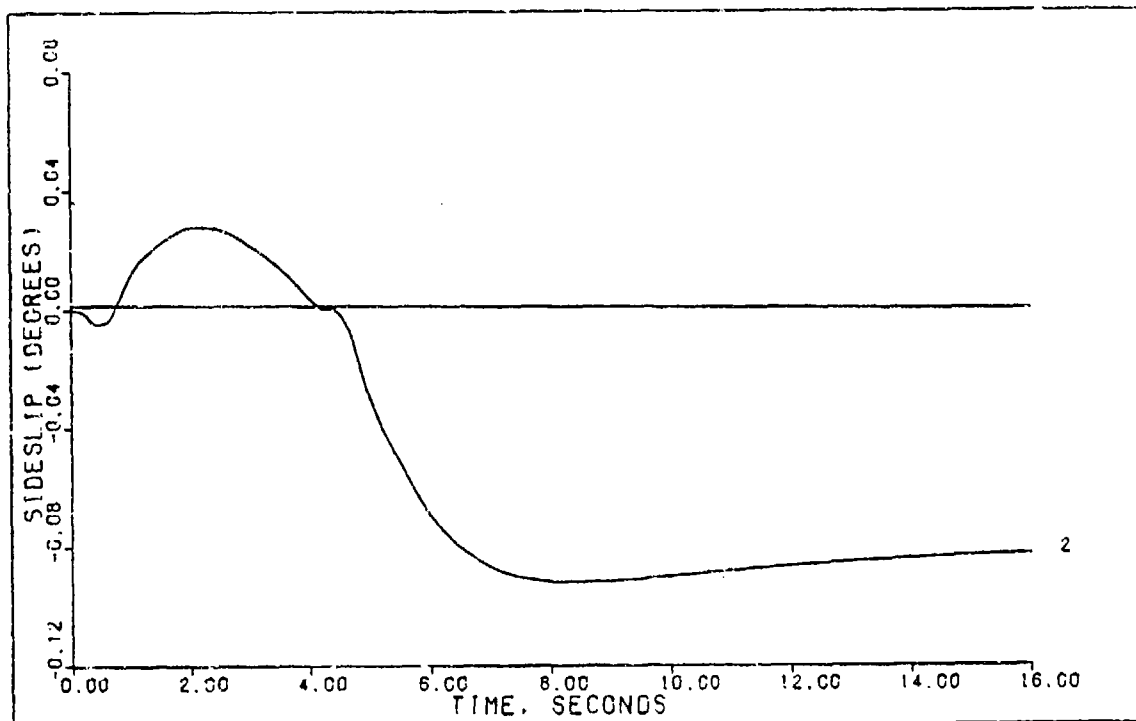


FIGURE 5-6c: Flight Condition #3, Coordinated Turn  
With Time Delay, Redesigned  
(Output 2: Sideslip)

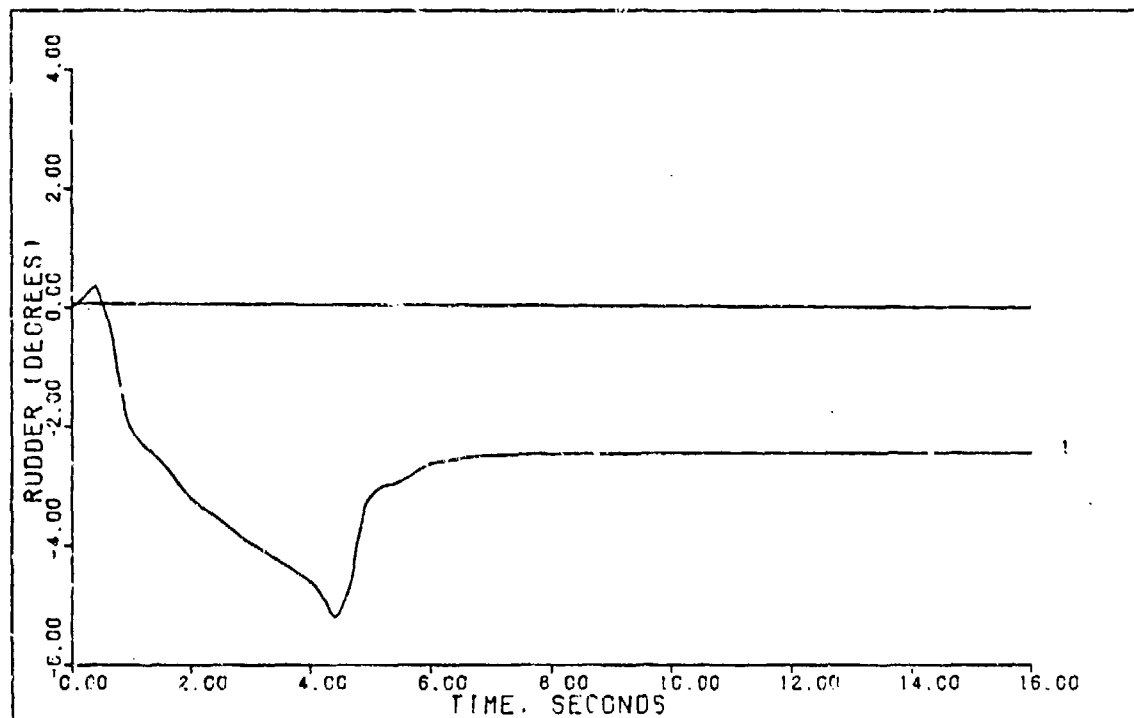


FIGURE 5-6d: Flight Condition #3, Coordinated Turn  
With Time Delay, Redesigned  
(Control 1: Rudder)

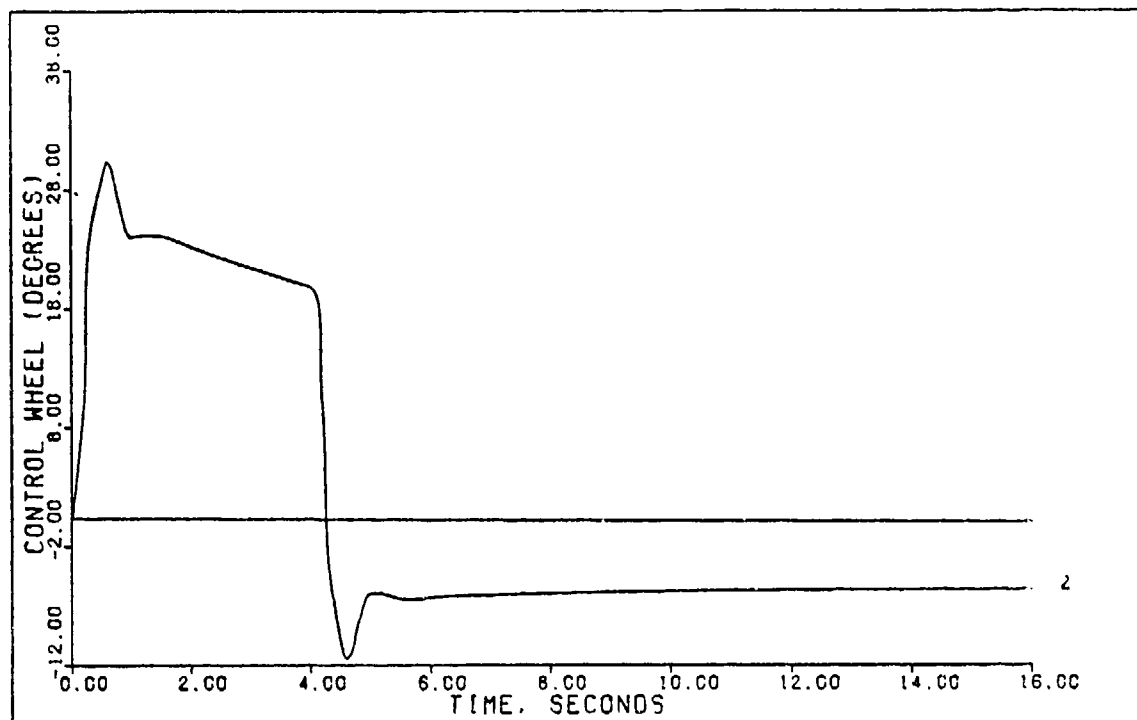


FIGURE 5-6e: Flight Condition #3, Coordinated Turn  
With Time Delay, Redesigned  
(Control 2: Control Wheel)

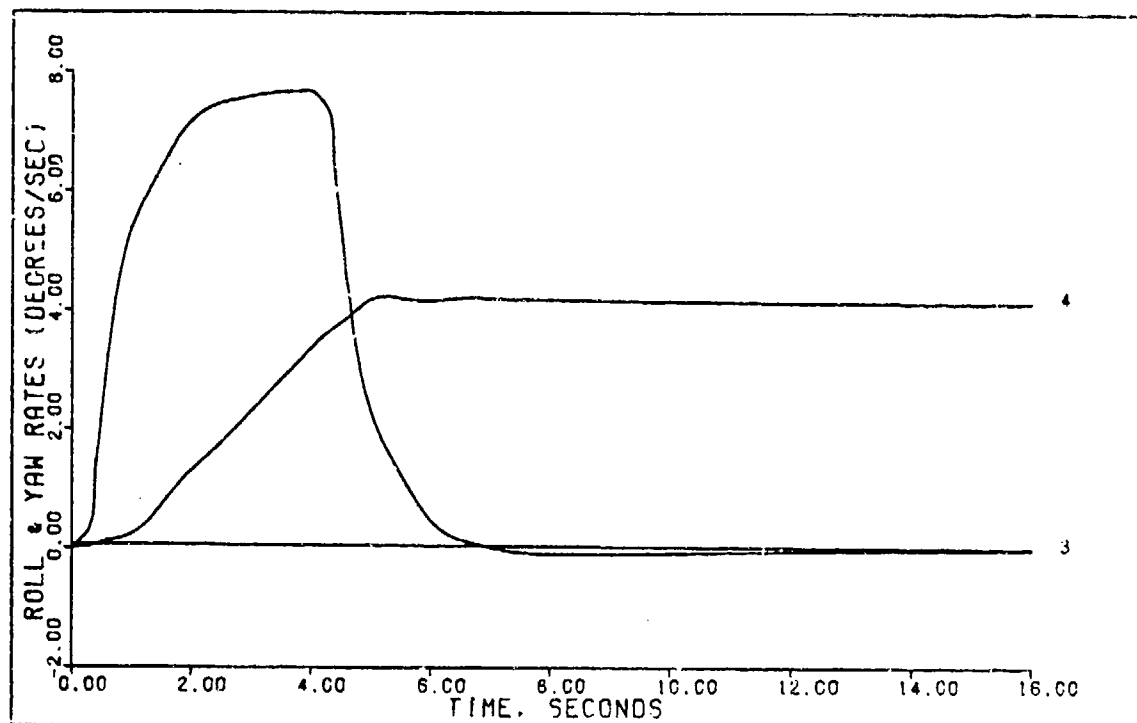


FIGURE 5-6f: Flight Condition #3, Coordinated Turn  
With Time Delay, Redesigned  
(State 3: Roll Rate; State 4: Yaw Rate)

A Comparison of Table 5-1 with 5-5, and 5-6 show that with the new controller the time delayed system's performance compares vary favorably with the undelayed system, thus showing that any ill effects caused by the introduction of the computational time delay can be eliminated.

Sideslip, Flight Condition #3 With Time Delay Using the control law given by Equations (5-18) thru (5-24) the sideslip maneuver is performed with a controller computational time delay of one sampling period. Figures 5-7a thru 5-7d show the results of this simulation. Also, Table 5-7 summarizes these results.

Table 5-7  
Simulation Results For  
Sideslip With Time Delay Flight Condition #3

Input/ Output	Peak Value	Final Value	$t_p$ (sec)	$t_s$ (sec)
$\phi$ (deg)	-0.4879	0.0	8.4	--
$\beta$ (deg)	5.0359	5.0	16.0	8.4
$\delta_r$ (deg)	8.0	--	--	--
$\delta_w$ (deg)	30.0	--	--	--

In this case a comparison of Tables 5-2 with 5-7 shows that performance is not lost when the time delay is included. However, by looking at Figure 5-2c and 5-7c it is seen that the control surfaces tend to be more oscillatory

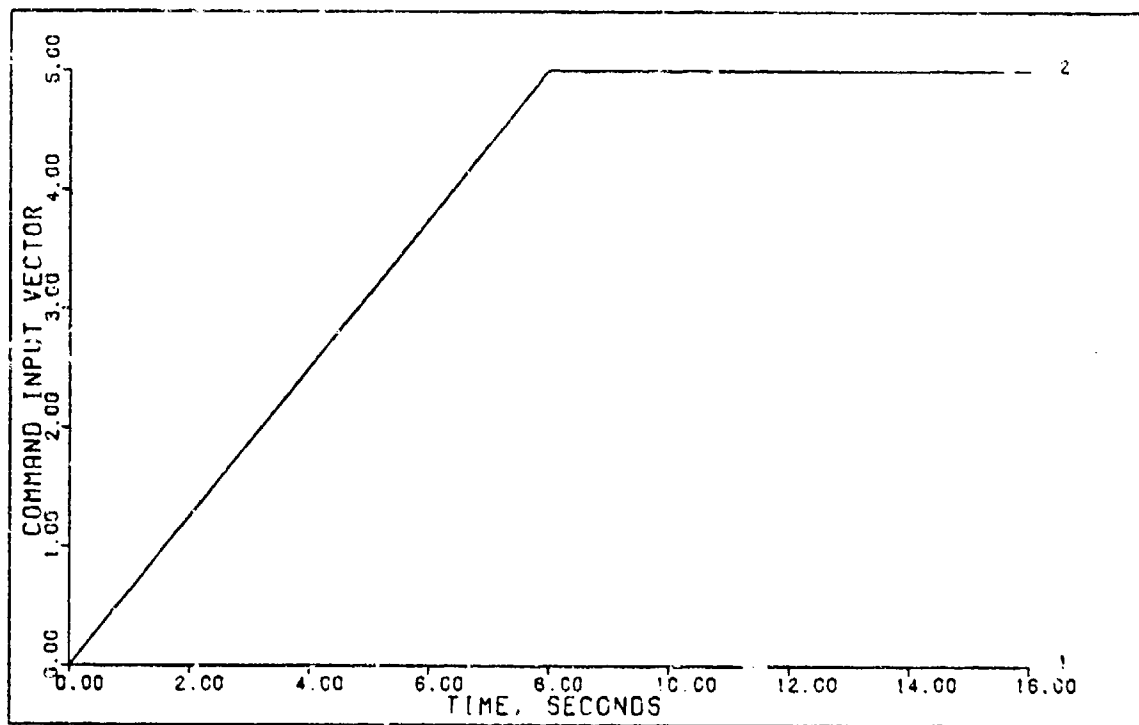


FIGURE 5-7a: Flight Condition #3, Sideslip With Time Delay (Command Input Vector)

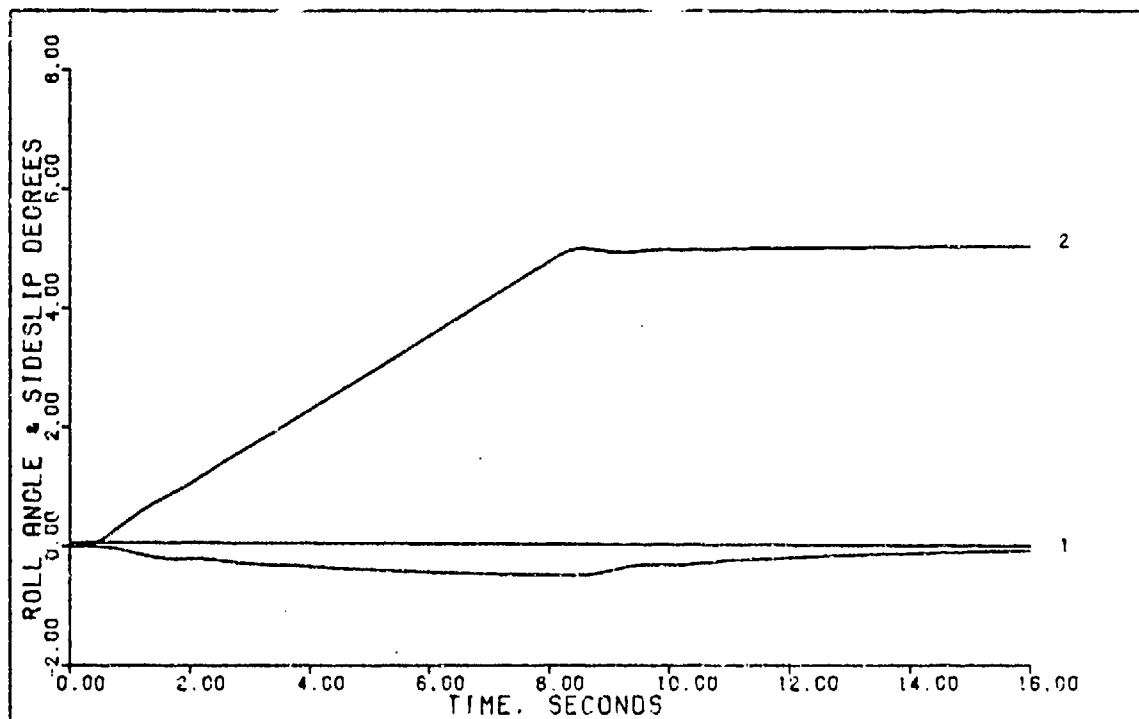


FIGURE 5-7b: Flight Condition #3, Sideslip With Time Delay (Output 1: Roll Angle; Output 2: Sideslip)

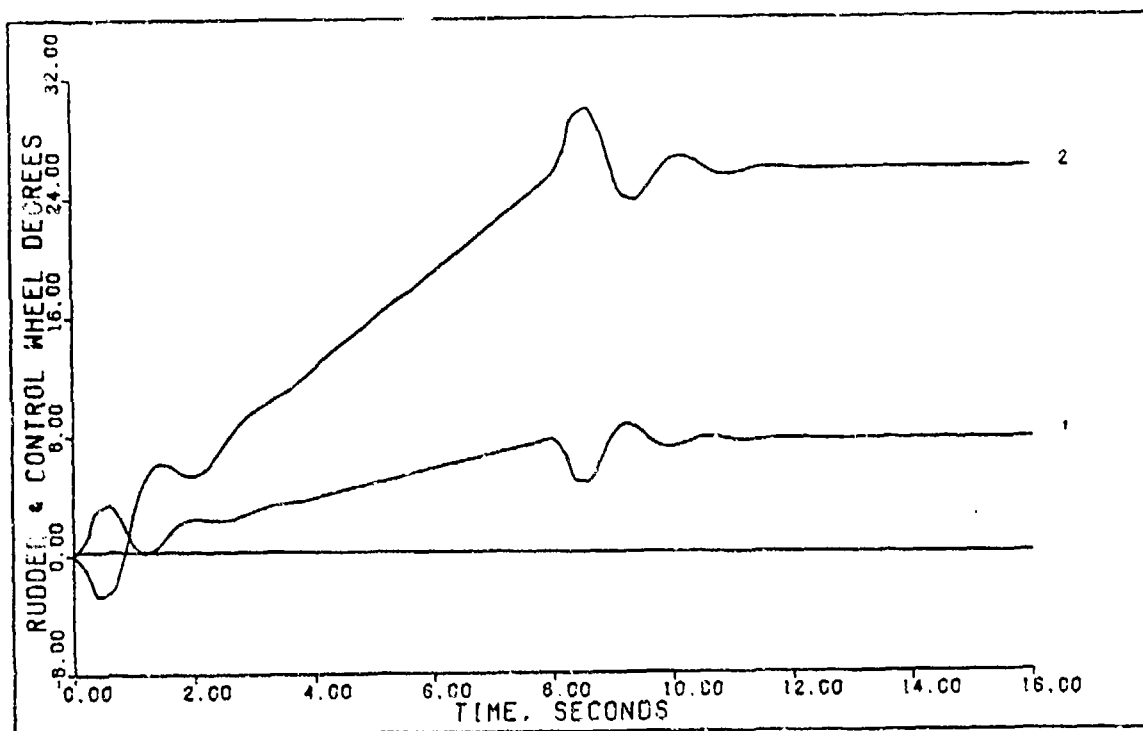


FIGURE 5-7c: Flight Condition #3, Sideslip With Time Delay  
(Control 1: Rudder; Control 2: Control Wheel)

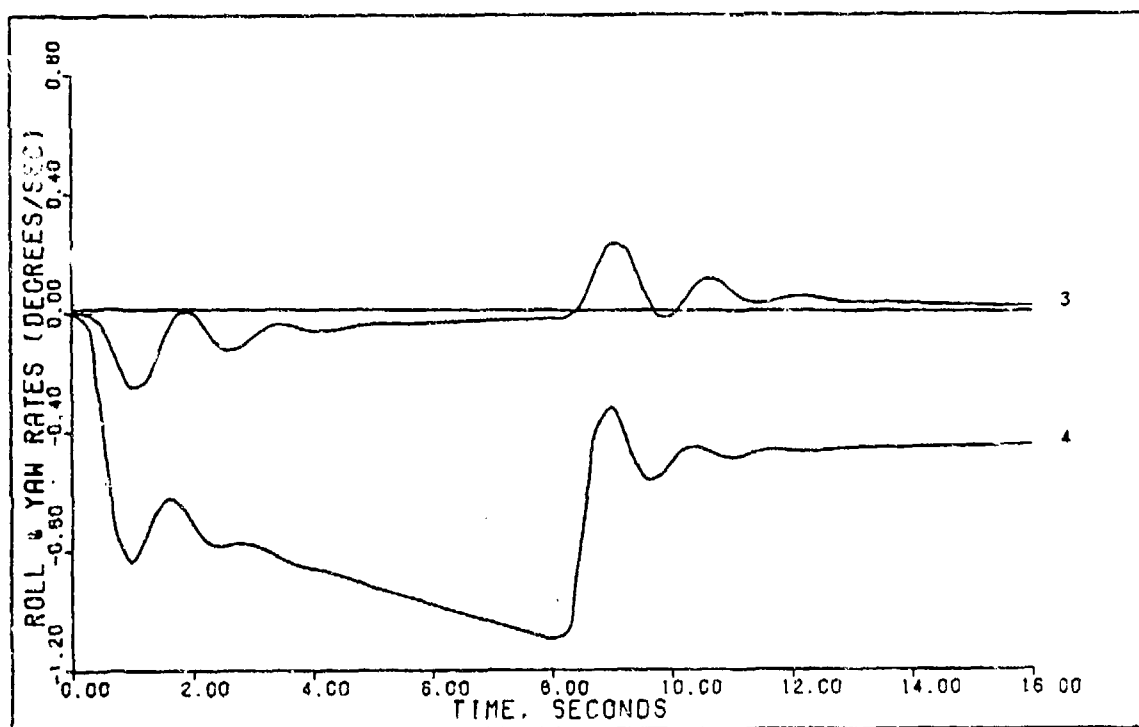


FIGURE 5-7d: Flight Condition #3, Sideslip With Time Delay  
(State 3: Roll Rate; State 4: Yaw Rate)

when the time delay is introduced. Thus a new controller is designed with these oscillations in mind. The new controller is defined by the parameters:

$$T = 0.05 \text{ seconds (20 hertz)} \quad (5-102)$$

$$\alpha = 3.0 \quad (5-103)$$

$$\epsilon = 0.08 \quad (5-104)$$

$$\Sigma = \text{diagonal } [1 \quad 1.2] \quad (5-105)$$

$$M = \begin{bmatrix} 0.25 & 0.0 \\ 0.0 & 0.5 \end{bmatrix} \quad (5-106)$$

$$K_0 = \begin{bmatrix} 0.05176 & 1.049 \\ 2.486 & -0.9278 \end{bmatrix} \quad (5-107)$$

$$K_1 = \begin{bmatrix} 0.01725 & 0.3497 \\ 0.8285 & -0.3093 \end{bmatrix} \quad (5-108)$$

Figures 5-8a thru 5-8d show the simulation results of this new controller. A comparison of Figure 5-7c and 5-8c shows that it is possible to reduce the oscillations to some degree. Table 5-8 summarizes the results for this new controller. This table shows that the reduction of the control surface oscillations is at the expense of a slight increase in settling time. These oscillations may be reduced more, however, settling time will increase.

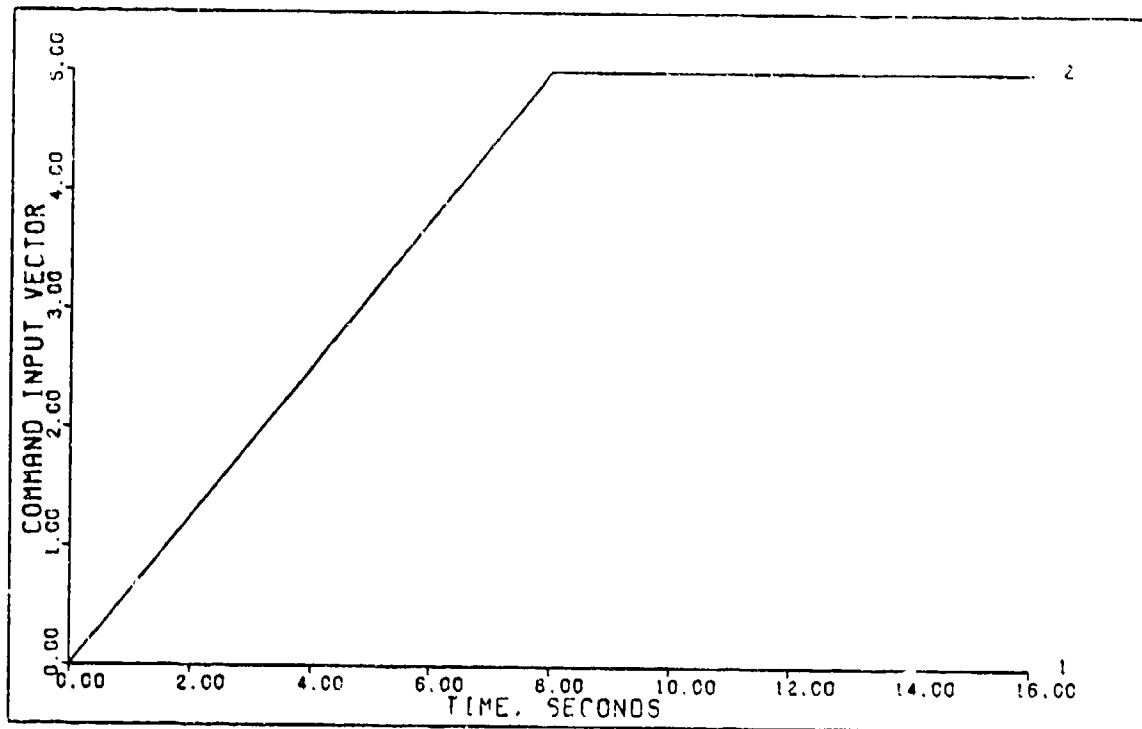


FIGURE 5-8a: Flight Condition #3, Sideslip With Time Delay, Redesigned (Command Input Vector)

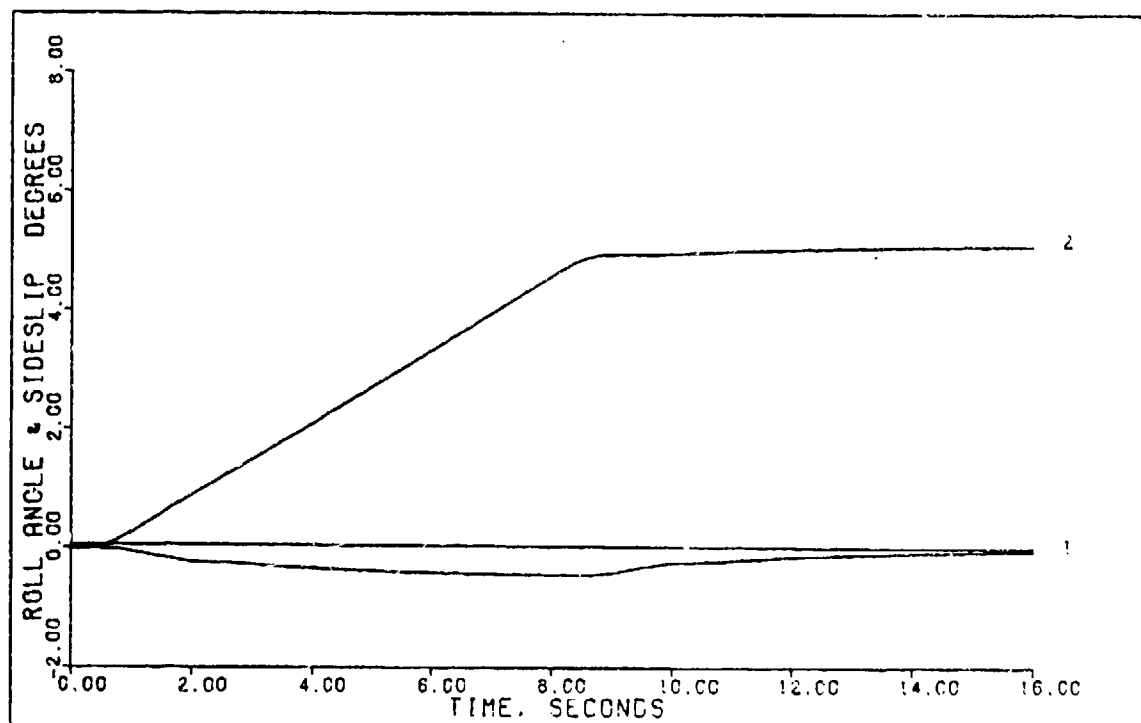


FIGURE 5-8b: Flight Condition #3, Sideslip With Time Delay, Redesigned (Output 1: Roll Angle; Output 2: Sideslip)

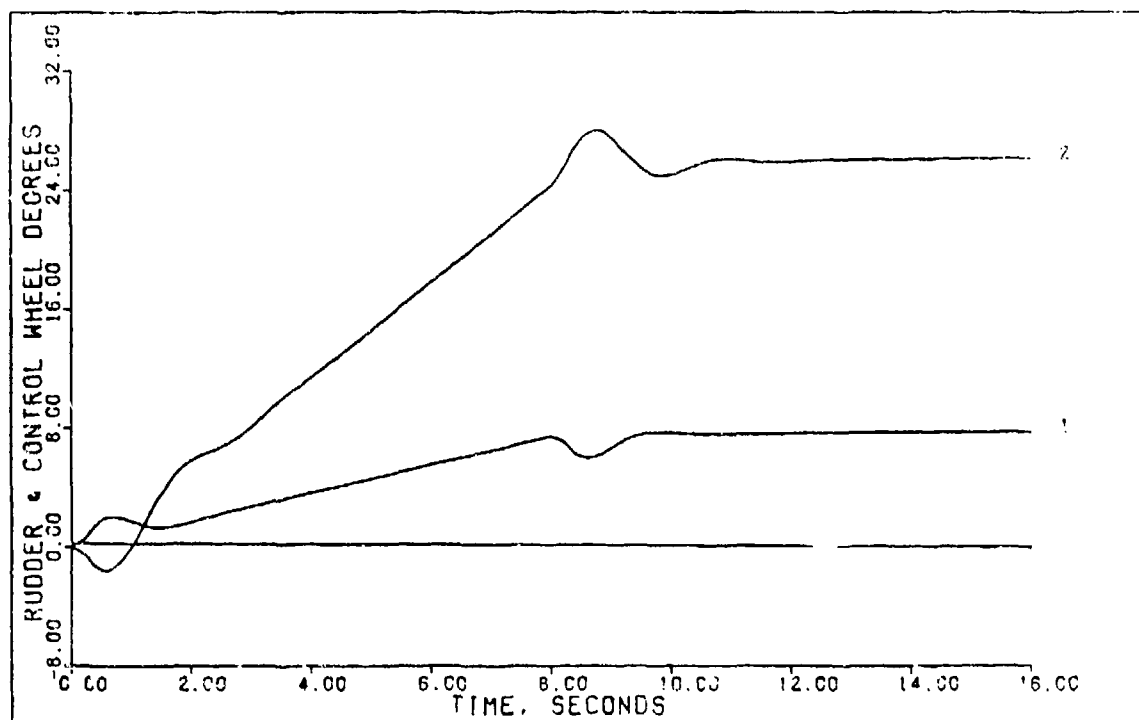


FIGURE 5-8c: Flight Condition #3, Sideslip With Time Delay, Redesigned (Control 1: Rudder; Control 2: Control Wheel)

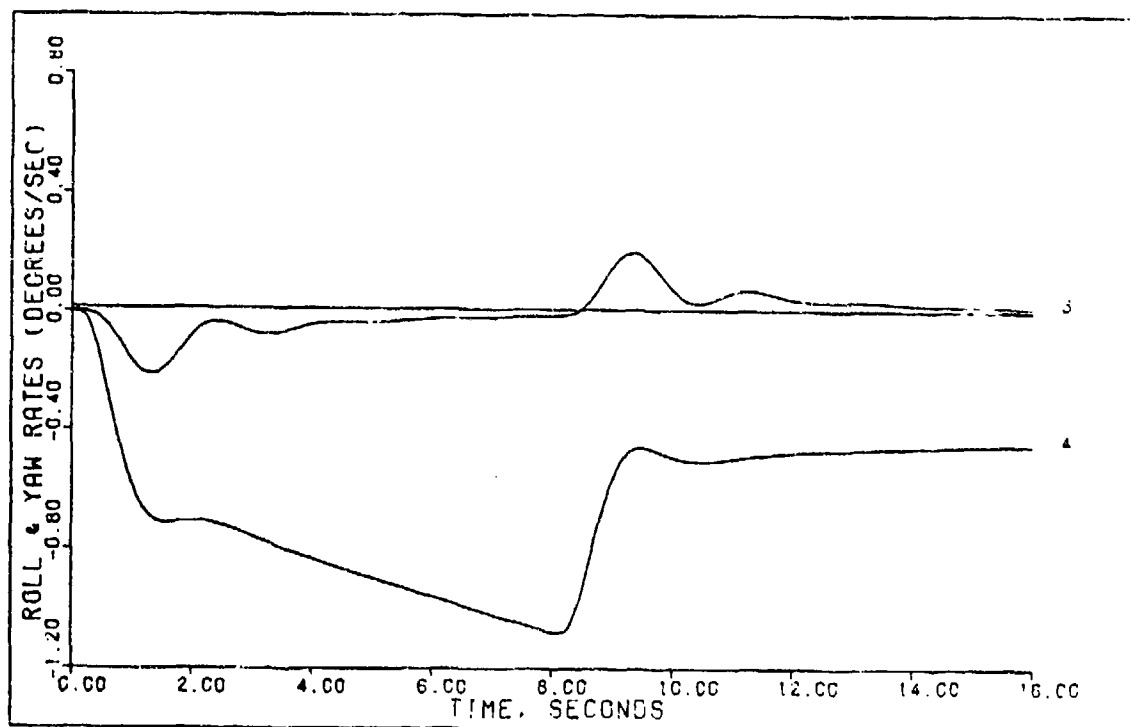


FIGURE 5-8d: Flight Condition #3, Sideslip With Time Delay, Pedesigned (State 3: Roll Rate; State 4: Yaw Rate)



Table 5-8  
Simulation Results For Sideslip With  
Time Delay Flight Condition #3 (Redesigned)

Input/ Output	Peak Value	Final Value	$t_p$ (sec)	$t_s$ (sec)
$\phi$ (deg)	-0.4475	0.0	8.4	--
$\beta$ (deg)	5.088	5.0	16.0	8.8
$\delta_r$ (deg)	6.0	--	--	--
$\delta_w$ (deg)	28.0	--	--	--

Normal Climb, Flight Condition #3 With Time Delay

Using the control law defined by Equations (5-25) thru (5-31) the normal climb with a computational time delay of one sampling period is simulated. Figures 5-9a thru 5-9h show the results of this simulation and Table 5-9 summarizes the results.

Table 5-9  
Simulation Results For Normal Climb  
With Time Delay Flight Condition #3

Input/ Output	Peak Value	Final Value	$t_p$ (sec)	$t_s$ (sec)
$\gamma$ (deg)	5.434	4.86	8.1	12.9
$u$ (ft/sec)	-0.3108	0.0	4.8	--
$\delta_e$ (deg)	-3.5	--	--	--
$\delta_T$ (%RPM)	24.0	--	--	--

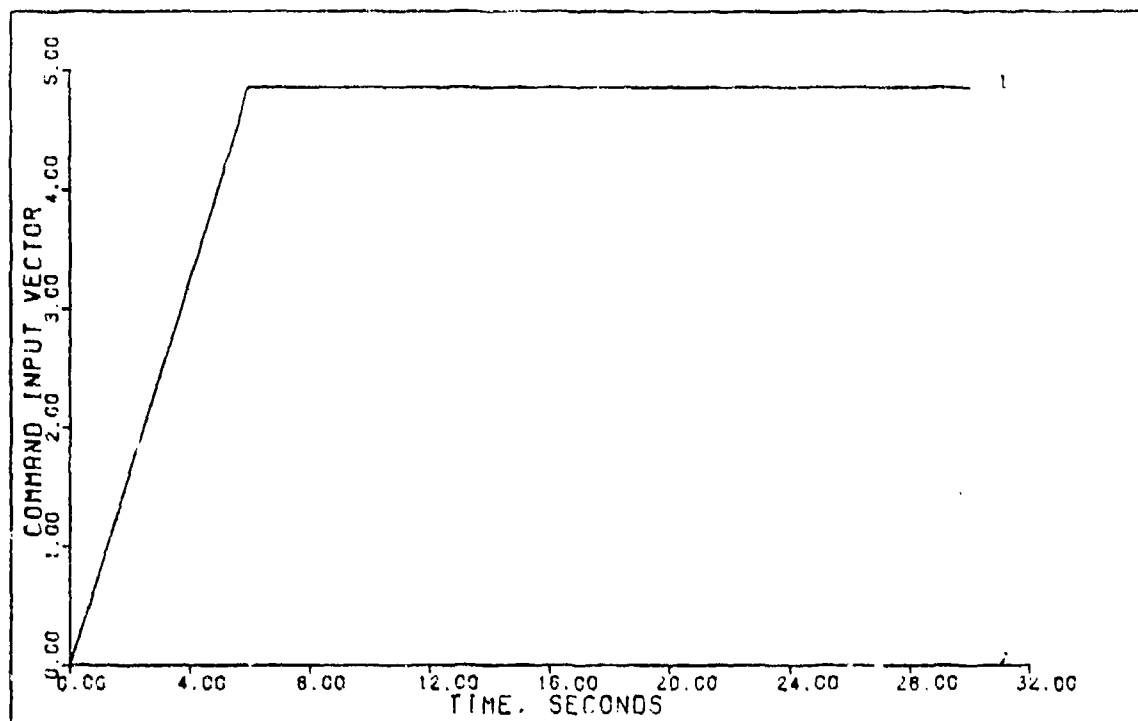


FIGURE 5-9a: Flight Condition #3, Normal Climb With Time Delay, (Command Input Vector)

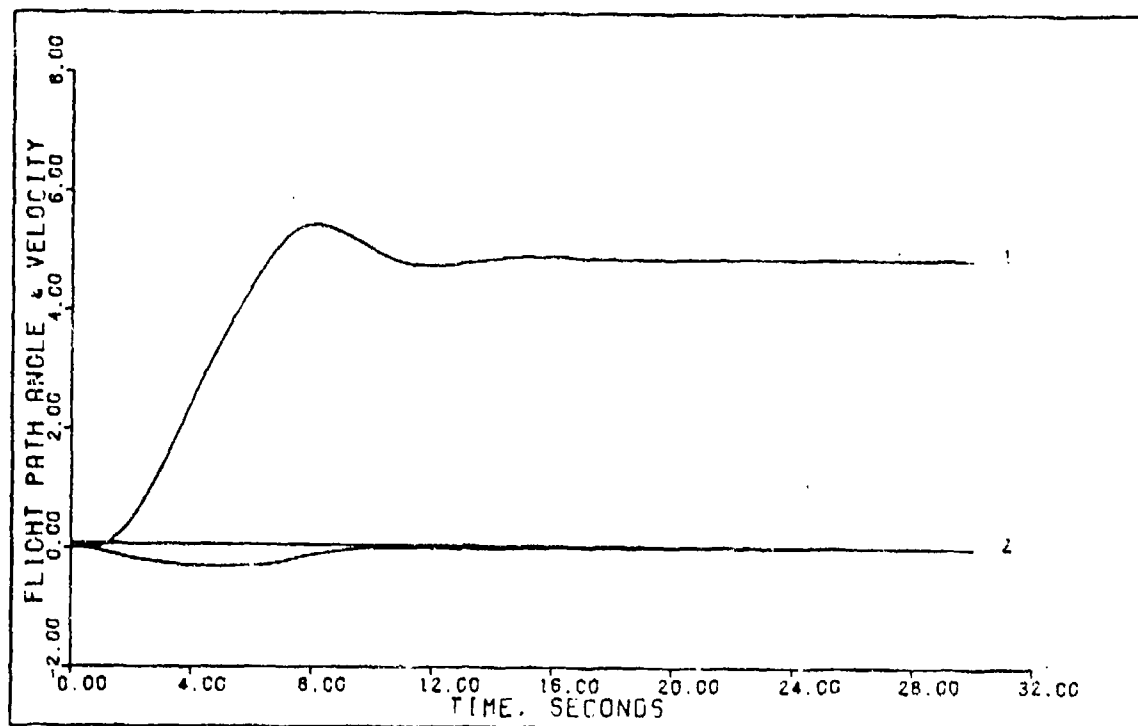


FIGURE 5-9b: Flight Condition #3, Normal Climb With Time Delay, (Output 1: Flight Path Angle; Output 2: Velocity)

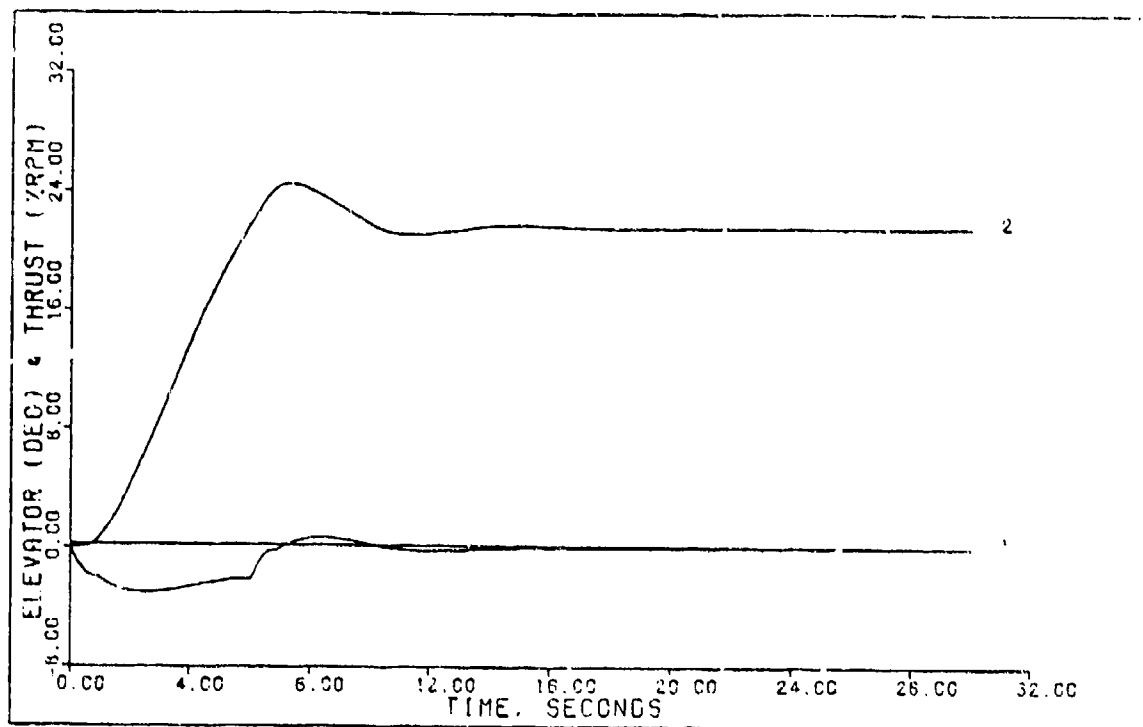


FIGURE 5-9c: Flight Condition #3, Normal Climb With Time Delay, (Control 1: Elevator; Control 2: Thrust)

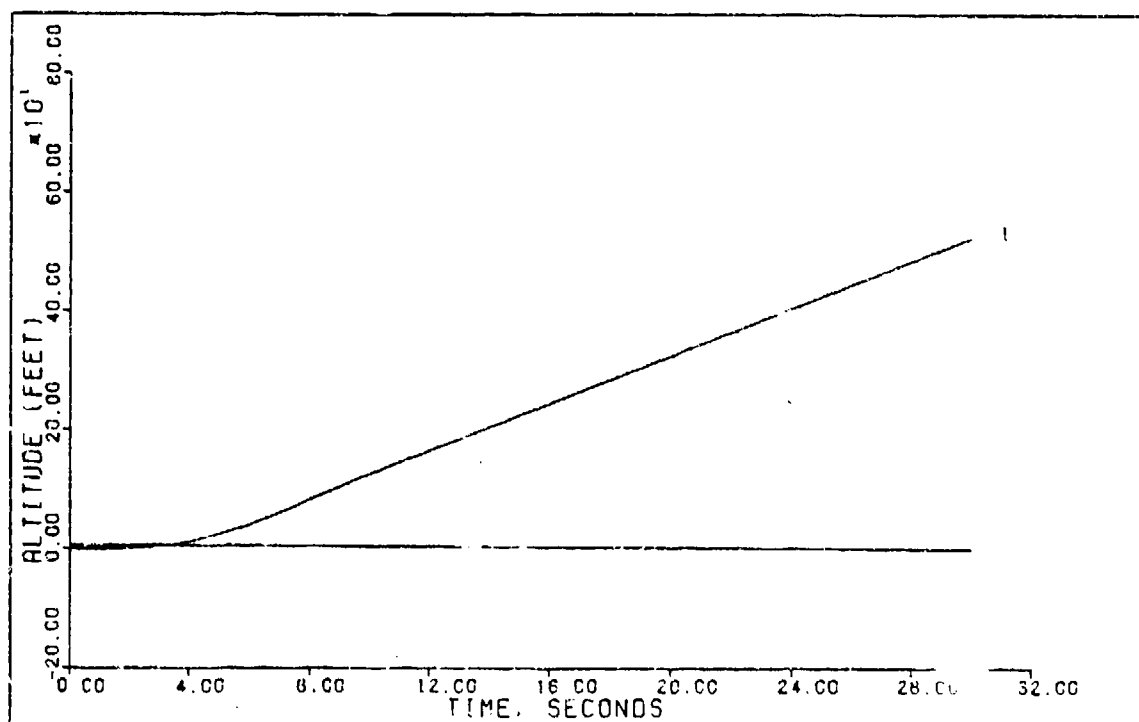


FIGURE 5-9d: Flight Condition #3, Normal Climb With Time Delay, (State 1: Altitude)

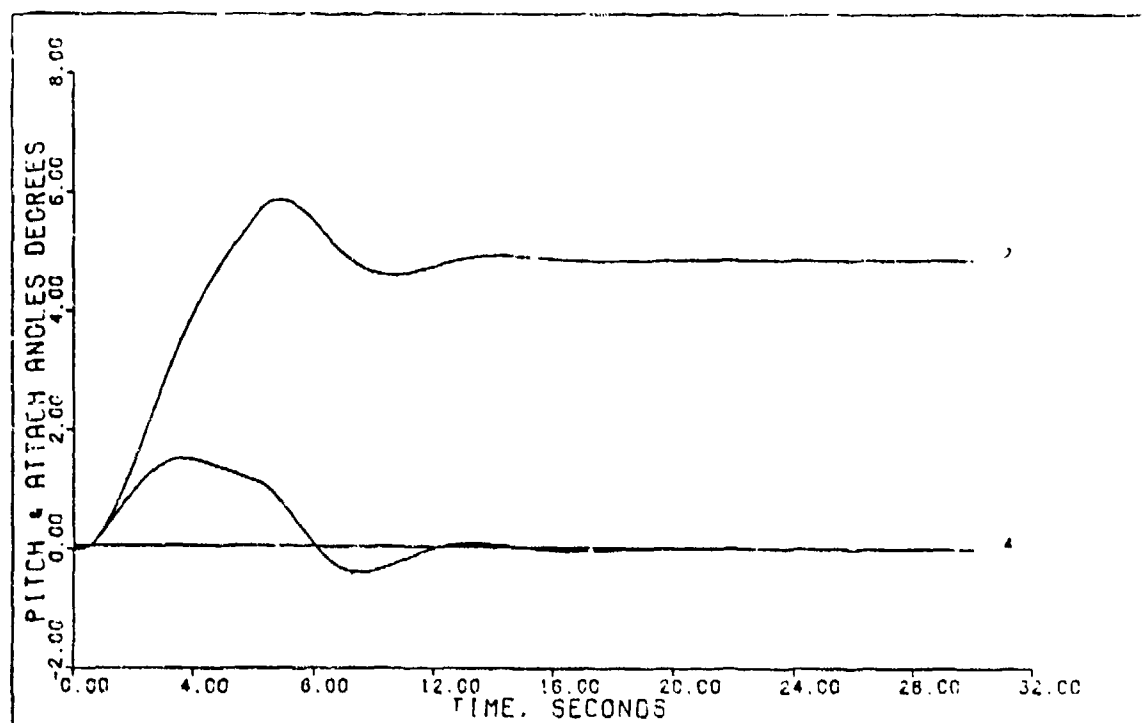


FIGURE 5-9e: Flight Condition #3, Normal Climb With Time Delay, (State 2: Pitch Angle; State 4: Attack Angle)

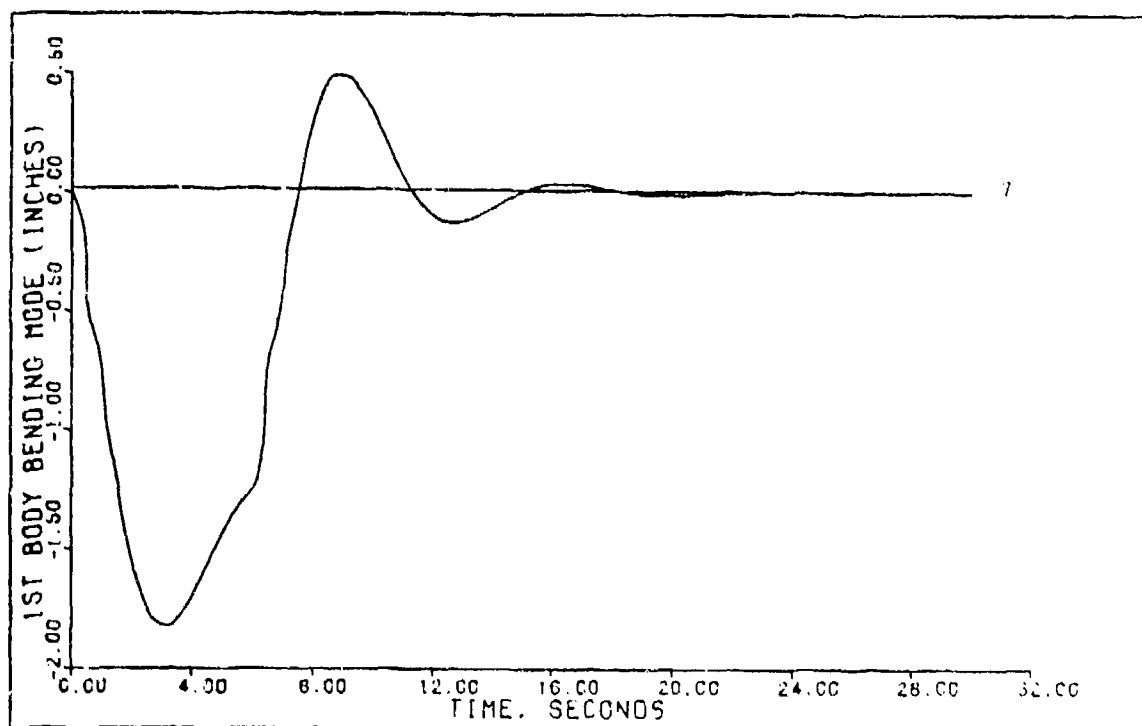


FIGURE 5-9f: Flight Condition #3, Normal Climb With Time Delay, (State 7: 1st Body Bending Mode)

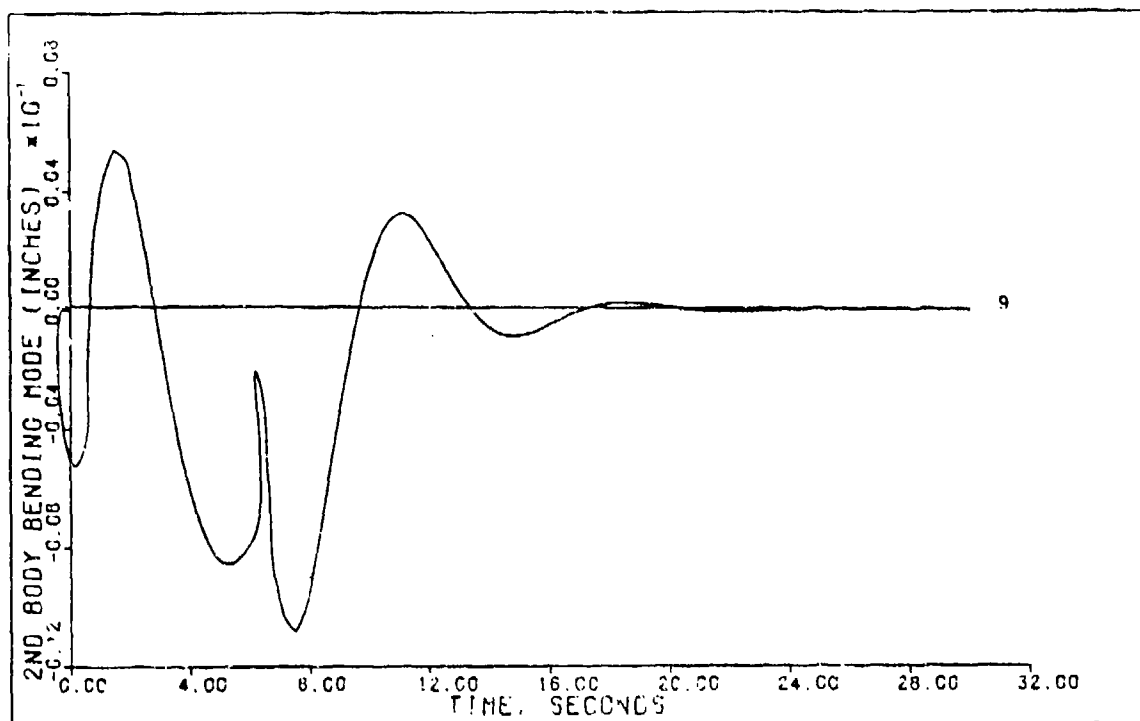


FIGURE 5-9g: Flight Condition #3, Normal Climb With Time Delay, (State 9: 2nd Body Bending Mode)

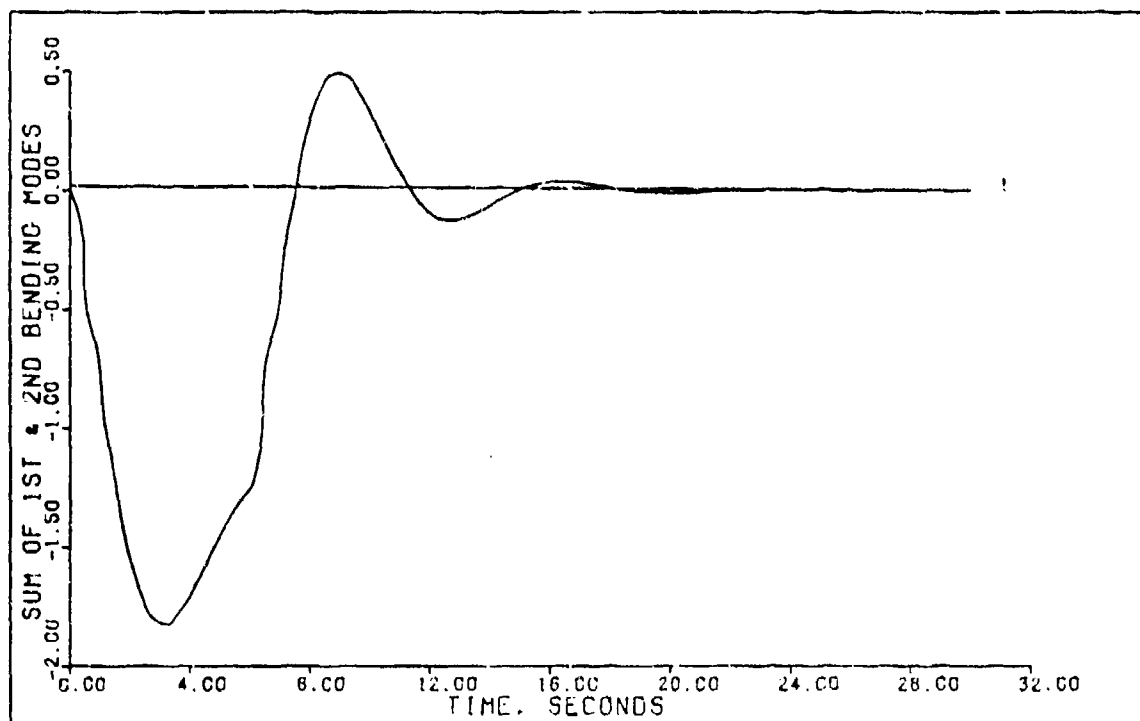


FIGURE 5-9h: Flight Condition #3, Normal Climb With Time Delay, (Sum of 1st & 2nd Bending Mode)

Comparison of Table 5-9 with Table 5-3 and Figures 5-9a thru 5-9h with Figures 5-3a thru 5-3h show that only minor changes occur when introducing the time delay. Since these changes are minor in nature there is no need to redesign the controller.

Pitch Pointing, Flight Condition #3 With Time Delay

Using the control law defined by Equations (5-32) thru (5-38) the pitch pointing maneuver including a computational time delay is performed. Figures 5-10a thru 5-10h and Table 5-10 show the results of this simulation.

Comparison of Table 5-10 with Table 5-4 and Figures 5-10a thru 5-10h with Figures 5-4a thru 5-4h shows the effect of the computational time delay on this maneuver. The only substantial difference is in the settling time for the pitch angle which increases by 0.8 seconds.

Table 5-10  
Simulation Results For  
Pitch Pointing With Time Delay Flight Condition #3

Input/ Output	Peak Value	Final Value	$t_p$ (sec)	$t_s$ (sec)
h (ft)	0.598	0.0	4.6	--
$\theta$ (deg)	4.0	4.0	16.0	5.2
u (ft/sec)	-0.899	0.0	3.0	--
$\delta_e$ (deg)	5.0	--	--	--
$\delta_{sb}$ (deg)	52.0	--	--	--
$\delta_T$ (%RPM)	32.0	--	--	--

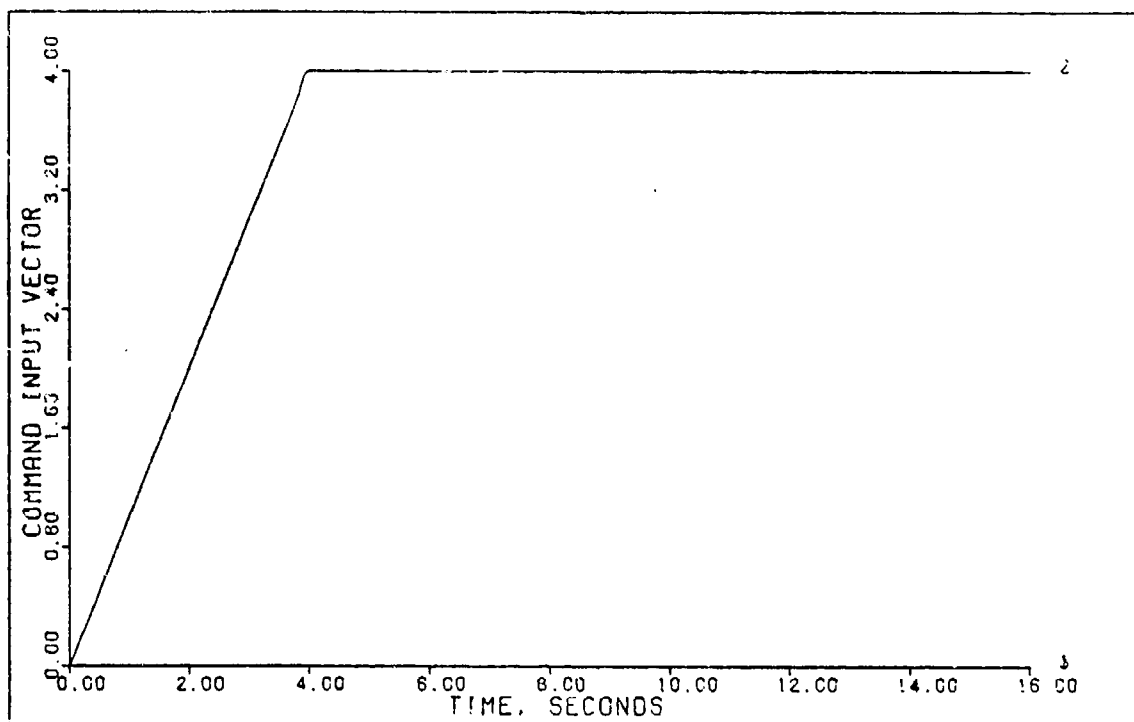


FIGURE 5-10a: Flight Condition #3, Pitch Pointing With Time Delay (Command Input Vector)

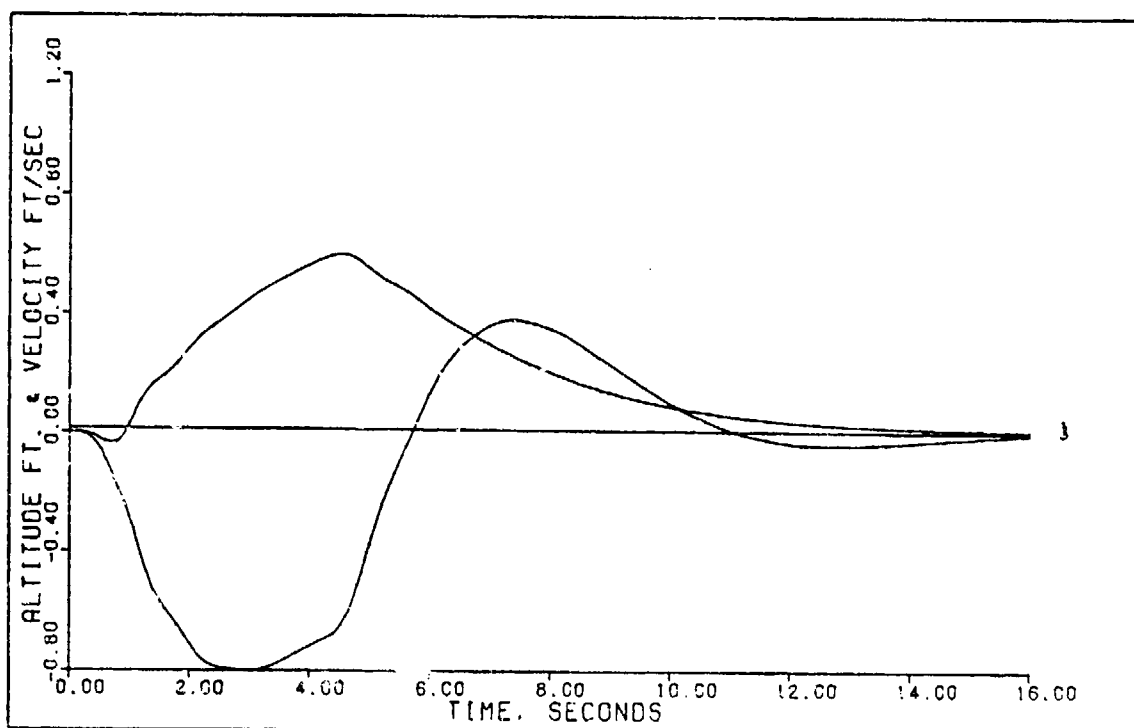


FIGURE 5-10b: Flight Condition #3, Pitch Pointing With Time Delay (Output 1: Altitude; Output 2: Velocity)

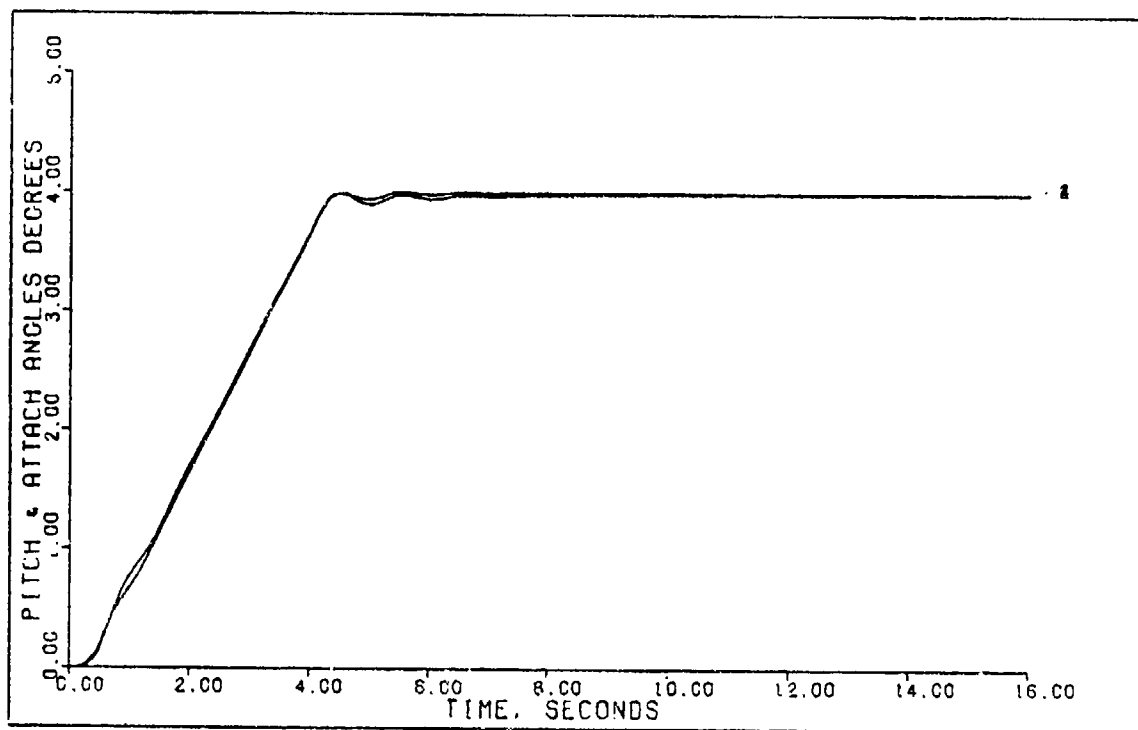


FIGURE 5-10c: Flight Condition #3, Pitch Pointing With Time Delay (State 2: Pitch Angle; State 4: Attack Angle)

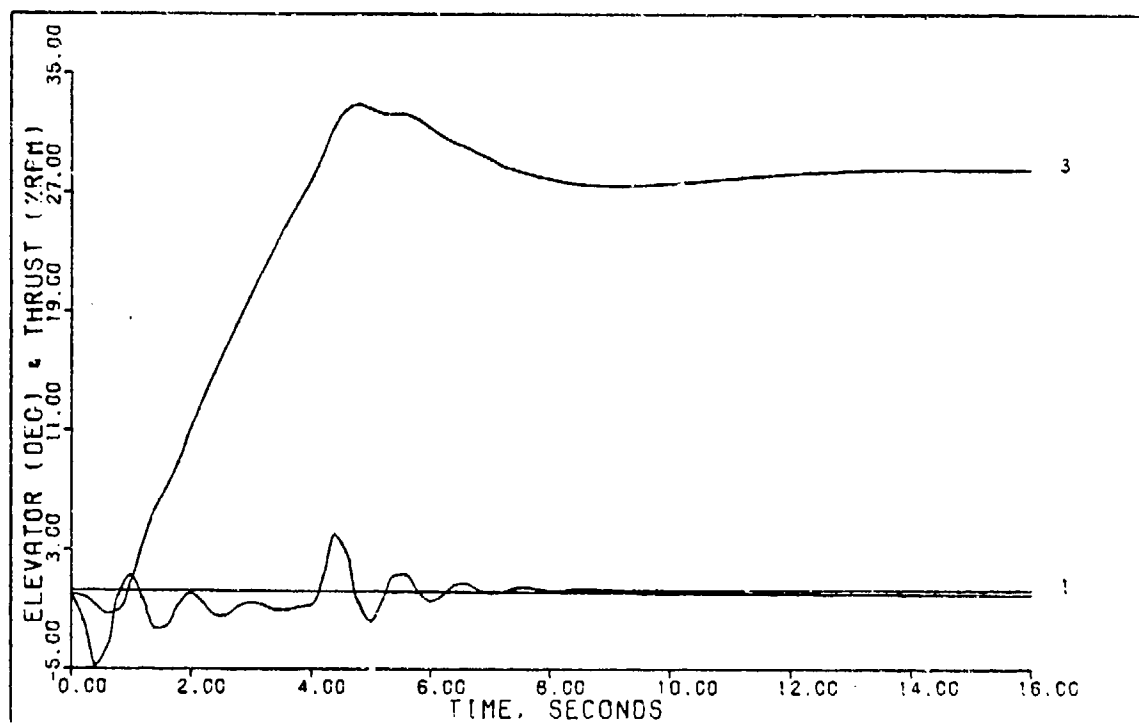


FIGURE 5-10d: Flight Condition #3, Pitch Pointing With Time Delay (Control 1: Elevator; Control 2: Thrust)



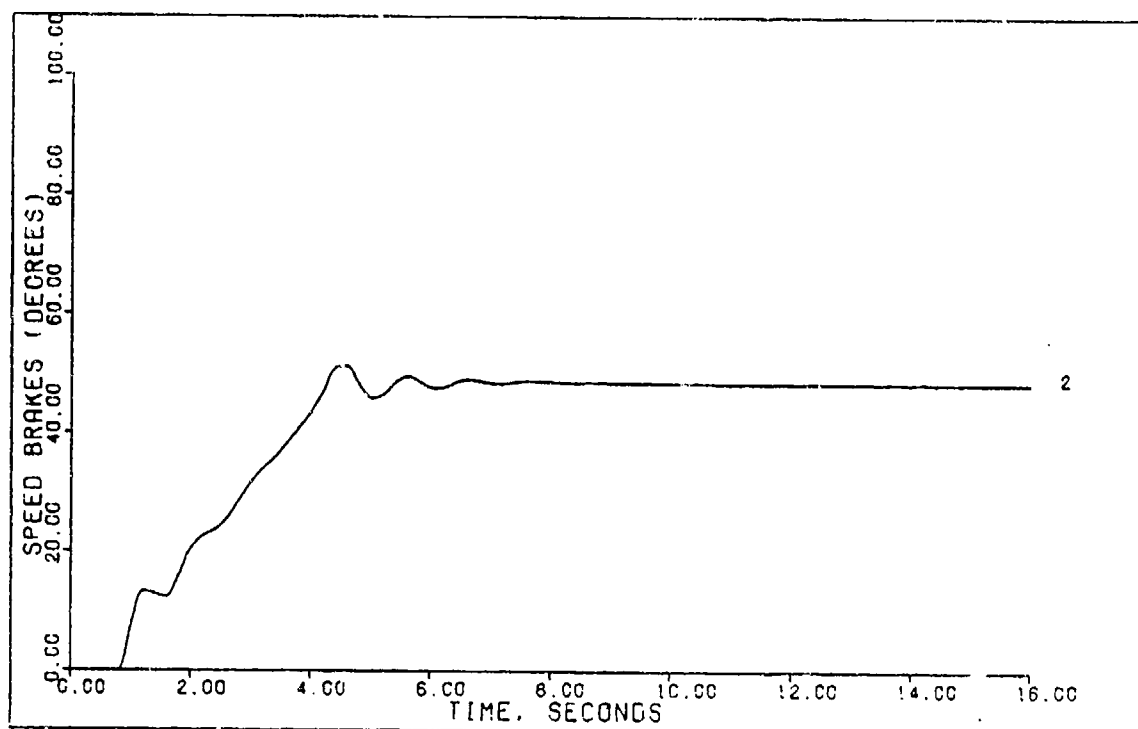


FIGURE 5-10e: Flight Condition #3, Pitch Pointing  
With Time Delay (Control 3: Speed Brakes)

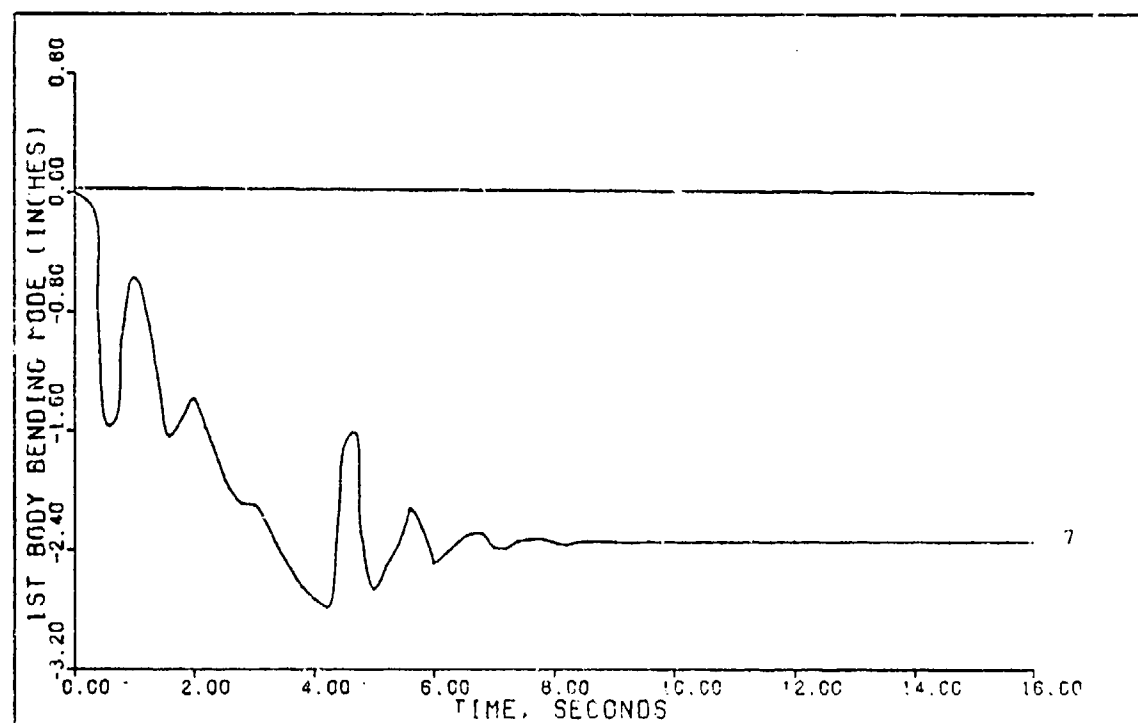


FIGURE 5-10f: Flight Condition #3, Pitch Pointing  
With Time Delay (State 7: 1st Body  
Bending Mode)

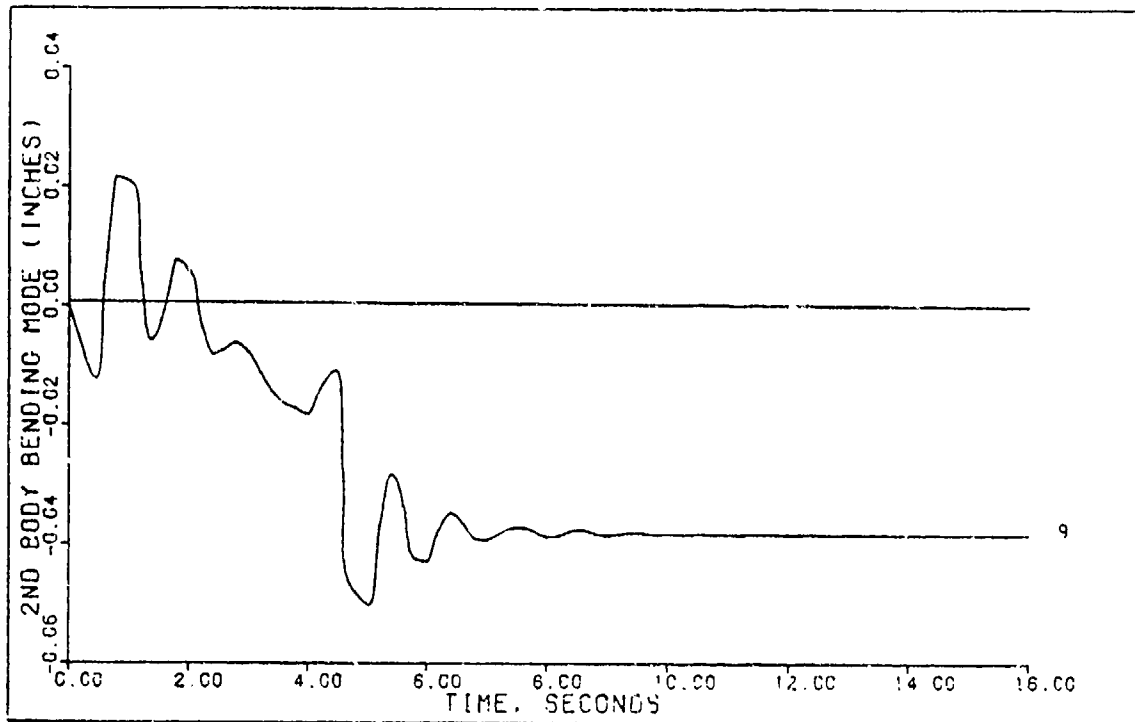


FIGURE 5-10g: Flight Condition #3, Pitch Pointing With Time Delay (State 9: 2nd Body Bending Mode)

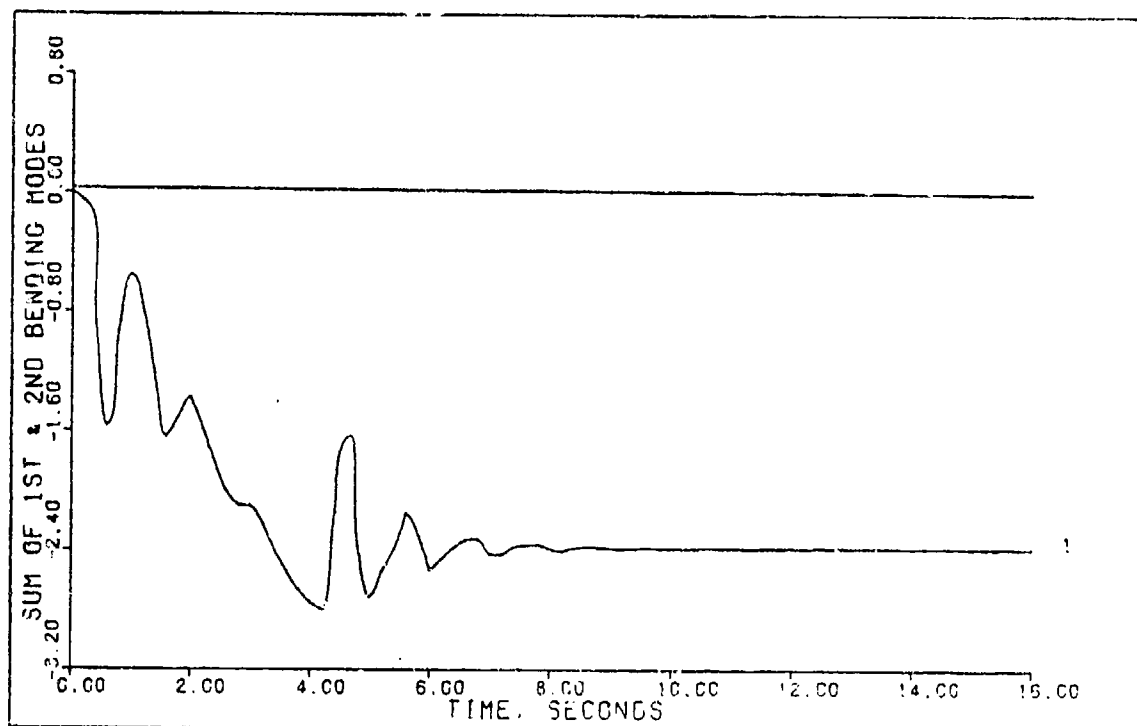


FIGURE 5-10h: Flight Condition #3, Pitch Pointing With Time Delay (Sum of 1st & 2nd Bending Modes)

A new controller is designed attempting to reduce this settling time. As in the other maneuvers, when trying to redesign the controller to reduce the effects of the time delay the control surfaces prove to be very sensitive. A small change in design parameters would in this case cause unacceptable elevator and speed brake oscillations. Thus a compromise between the settling time and control surface movement is needed. If settling time is allowed to increase slightly, elevator and speed brake oscillations are reduced. A new controller is designed to show this effect. This controller is defined by the following parameters:

$$T = 0.05 \text{ seconds (20 hertz)} \quad (5-109)$$

$$\alpha = 2.5 \quad (5-110)$$

$$\epsilon = 0.5 \quad (5-111)$$

$$\Sigma = \text{diagonal [1.0 \quad 1.0 \quad 0.1]} \quad (5-112)$$

$$M = \begin{bmatrix} 0.75 & 0.0 \\ 0.0 & 0.5 \\ 0.0 & 0.0 \end{bmatrix} \quad (5-113)$$

$$K_0 = \begin{bmatrix} -0.6929 & -2.885 & 0.0 \\ -6.694 & -1.676 & 0.0 \\ -3.297 & -0.6876 & 0.9858 \end{bmatrix} \quad (5-114)$$

$$K_1 = \begin{bmatrix} -0.2272 & -1.154 & 0.0 \\ -2.678 & -0.6704 & 0.0 \\ -1.319 & -0.2750 & 0.3943 \end{bmatrix} \quad (5-115)$$

Figures 5-11a thru 5-11h and Table 5-11 show the results of this new controller.

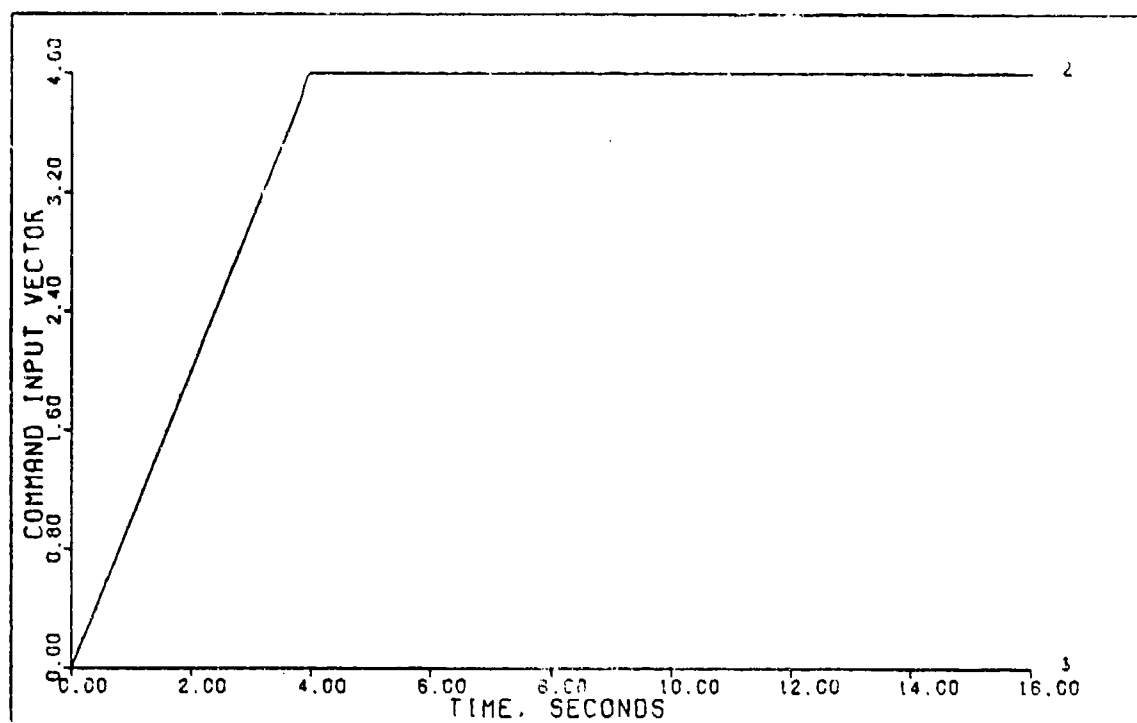


FIGURE 5-11a: Flight Condition #3, Pitch Pointing  
With Time Delay, Redesigned  
(Command Input Vector)

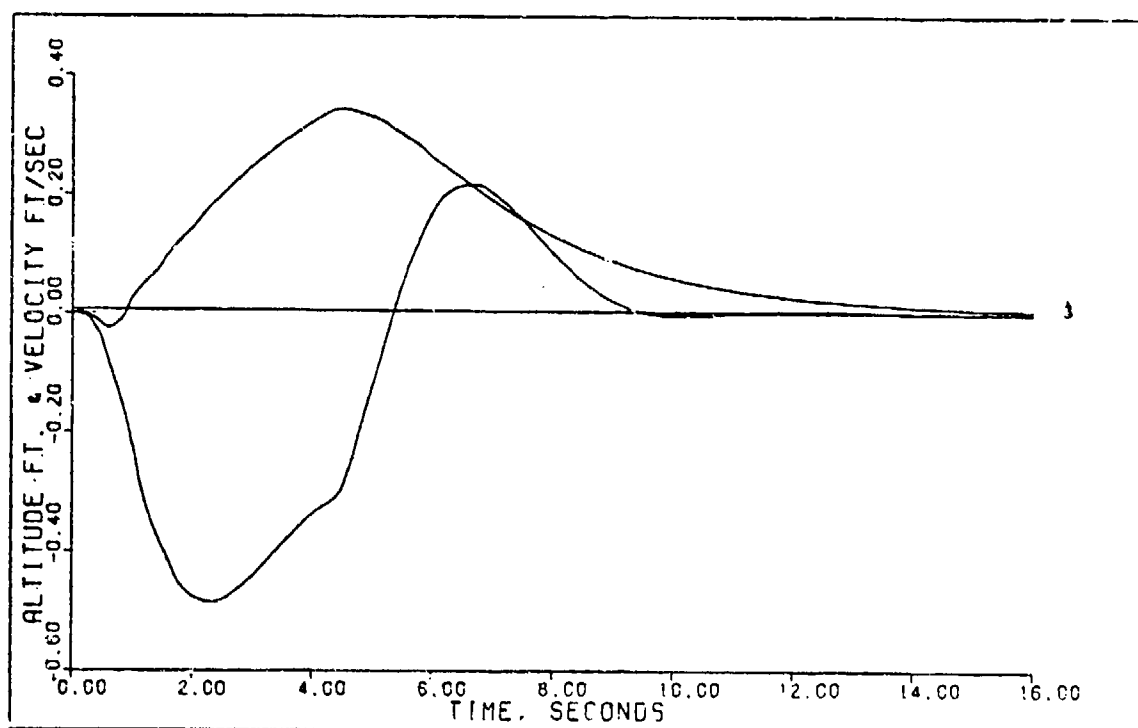


FIGURE 5-11b: Flight Condition #3, Pitch Pointing  
With Time Delay Redesigned  
(Output 1: Altitude; Output 2: Velocity)

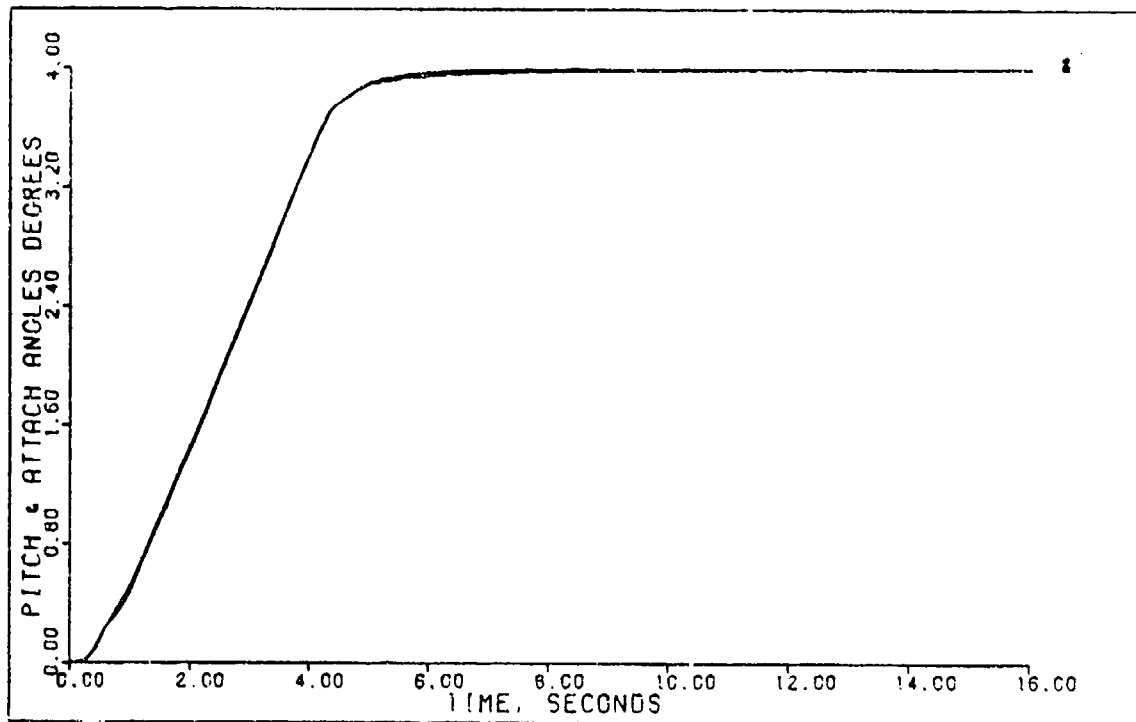


FIGURE 5-11c: Flight Condition #3, Pitch Pointing  
With Time Delay, Redesigned  
(State 2: Pitch Angle; State 4: Attack Angle)

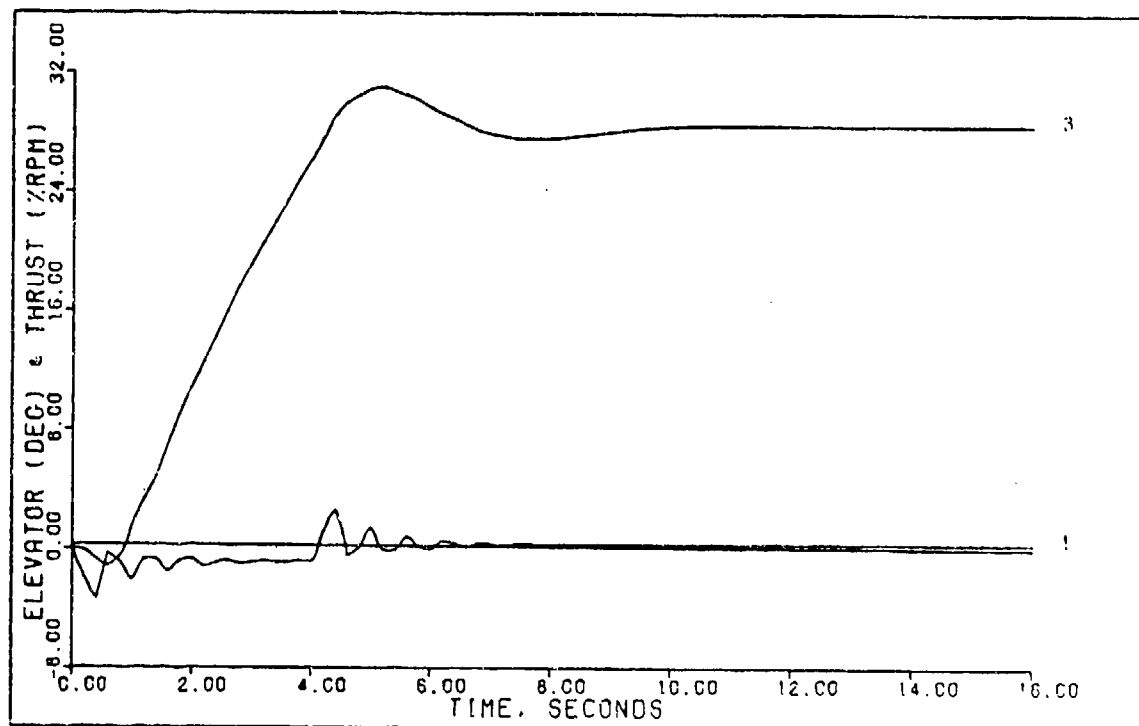


FIGURE 5-11d: Flight Condition #3, Pitch Pointing  
With Time Delay Redesigned  
(Control 1: Elevator; Control 2: Thrust)

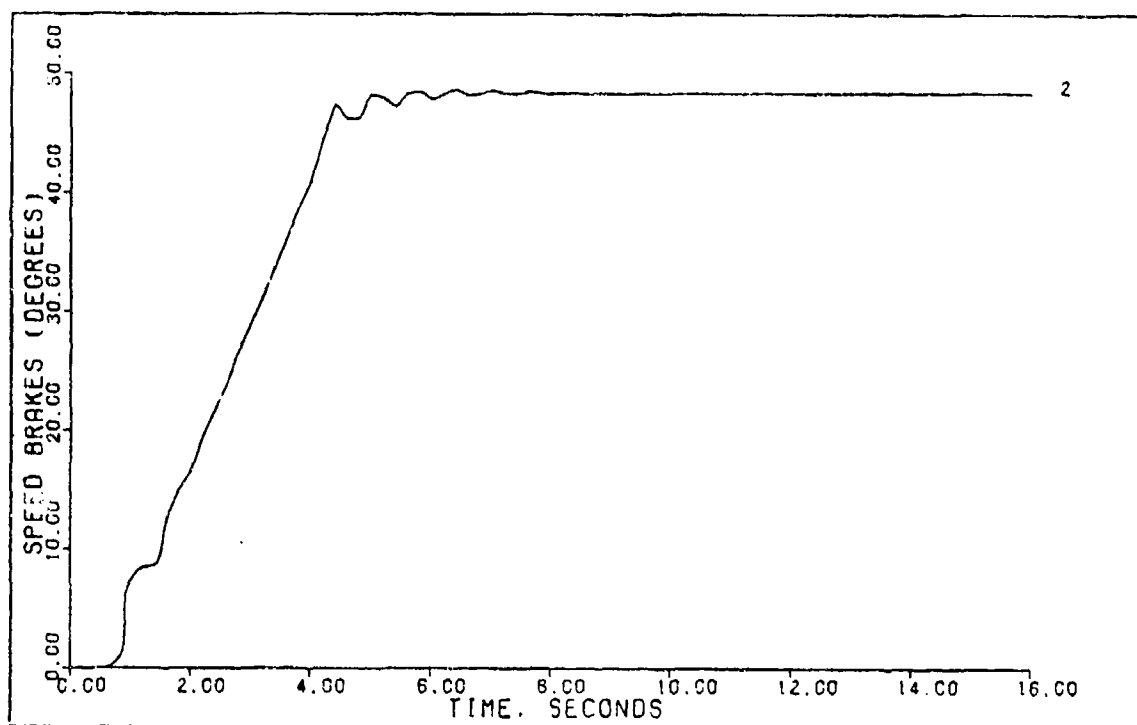


FIGURE 5-11e: Flight Condition #3, Pitch Pointing  
With Time Delay, Redesigned  
(Control 3: Speed Brakes)

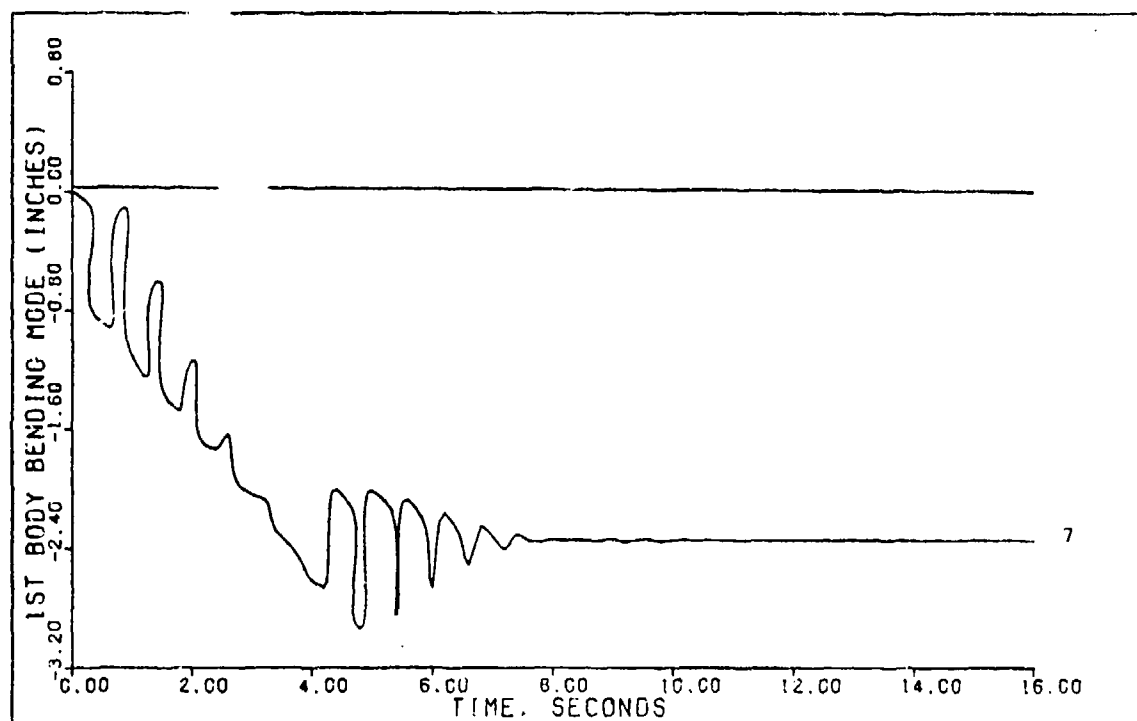


FIGURE 5-11f: Flight Condition #3, Pitch Pointing  
With Time Delay, Redesigned  
(State 7: 1st Body Bending Mode)

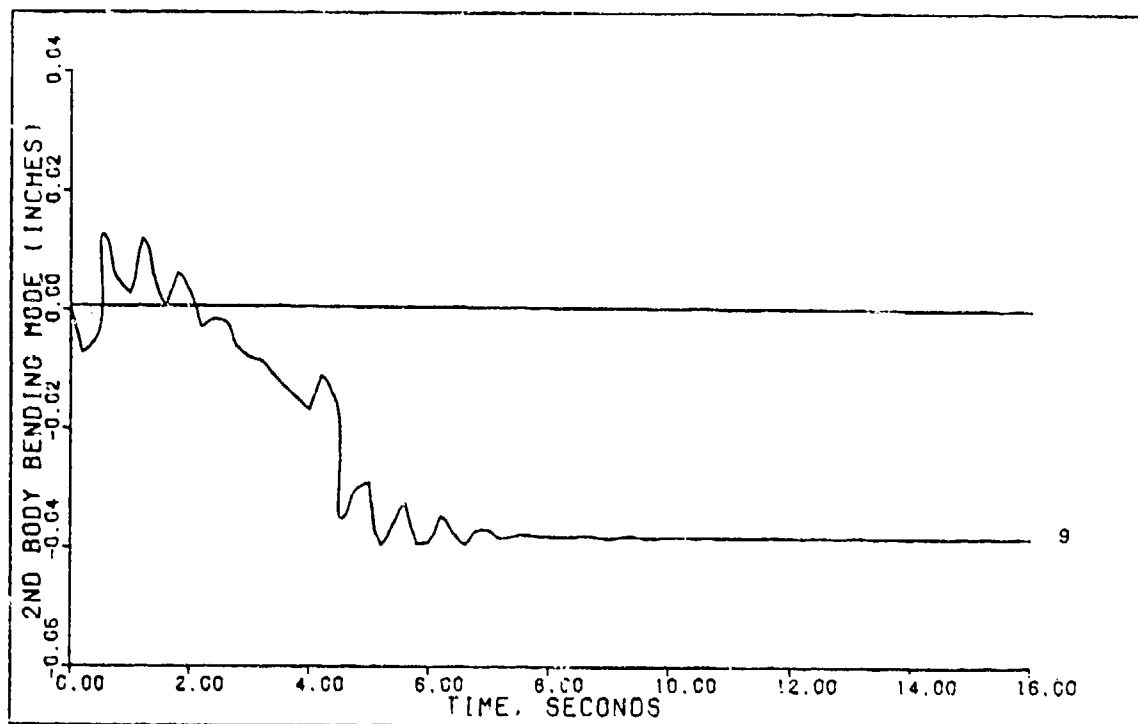


FIGURE 5-11g: Flight Condition #3, Pitch Pointing  
With Time Delay, Redesigned  
(State 9: 2nd Body Bending Mode)

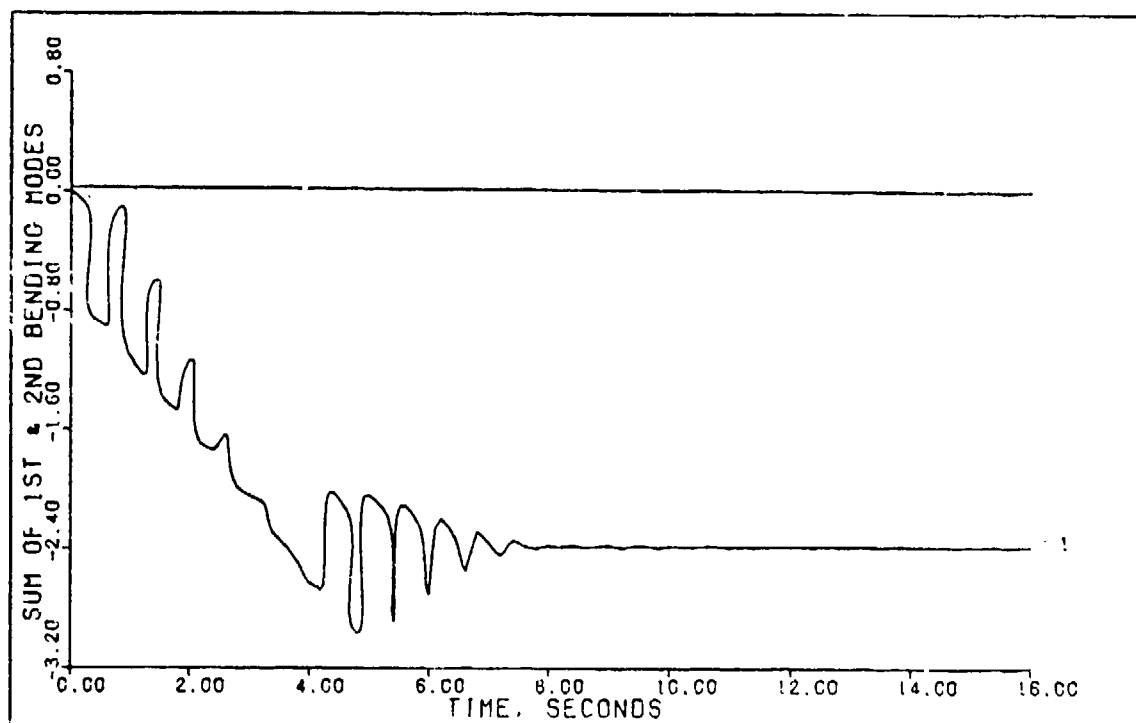


FIGURE 5-11h: Flight Condition #3, Pitch Pointing  
With Time Delay, Redesigned  
(Sum of 1st & 2nd Bending Modes)

Table 5-11  
Simulation Results For Pitch Pointing  
With Time Delay Flight Condition #3 Redesigned

Input/ Output	Peak Value	Final Value	$t_p$ (sec)	$t_s$ (sec)
h (ft)	0.343	0.0	4.6	--
$\theta$ (deg)	4.0	4.0	16.0	5.4
u (ft/sec)	-0.485	0.0	2.4	--
$\delta_e$ (deg)	3.0	--	--	--
$\delta_{sb}$ (deg)	48.0	--	--	--
$\delta_T$ (%RPM)	31.0	--	--	--

Comparison of Table 5-11 with 5-10 and Figures 5-11a thru 5-11h with 5-10a thru 5-11h demonstrates that a small increase in settling time, 0.2 seconds to be exact, can reduce control surface deflections. Further increase in the settling time, to 6.5 seconds, reduces the elevator deflections shown in Figure 5-11d even further. When settling time is allowed to increase to 6.5 seconds, the elevator has just two spikes and the transients that appear after the two spikes shown in Figure 5-11d disappear completely. Thus a trade off between control surface movement and maneuver performance is required. This in general is found to hold true for all the designs performed in this thesis.



### Modifications to $K_0$ and $K_1$

MULTI has been modified recently to allow changing of any element in any matrix at any time without having to reenter the entire matrix. This was originally added to avoid the inconvenience involved in making an error when entering the A, B, and C matrices in Option #3. However, this modification also added an interesting sidelight. The matrices  $K_0$  and  $K_1$  are stored in MULTI and can be viewed by selecting Option #114. Allowing the user the option of changing the elements of these matrices in Option #114, the effect of each element on the simulation results can be tested. In fact, a reduction in amplifiers needed to implement the controller would result if some of these elements could be set to zero, without affecting the results significantly.

Examination of the theoretical basis of the elements of  $K_0$  and  $K_1$  gives some interesting insight into selecting elements to be set to zero. To demonstrate this, take the case of Equations (5-100) and (5-101) which are repeated here for convenience.

$$K_0 = \begin{bmatrix} 0.03104 & 1.337 \\ 1.766 & -1.182 \end{bmatrix} \quad (5-116)$$

$$K_1 = \begin{bmatrix} 0.007304 & 0.3145 \\ 0.4154 & -0.2782 \end{bmatrix} \quad (5-117)$$

Remember that these represent the  $K_0$  and  $K_1$  matrices for the coordinated turn maneuver which was redesigned to

account for the time delay. The first column of  $K_0$  represents gains applied to the rudder, while the second column represents gains applied to the control wheel. The first row is associated with feedback from output one which is the bank angle and the second row is associated with sideslip feedback. Now, if it can be assumed that the control wheel contributes most of the control surface movements needed to control bank angle and that the rudder contributes what is needed to control sideslip, then it may be possible to zero the principle diagonal elements of the  $K$  matrices without affecting performance. This should be true since this just eliminates bank angle feedback to the rudder and sideslip feedback to the control wheel. If this is done Equations (5-116) and (5-117) become:

$$K_0 = \begin{bmatrix} 0.0 & 1.337 \\ 1.766 & 0.0 \end{bmatrix} \quad (5-118)$$

$$K_1 = \begin{bmatrix} 0.0 & 0.3145 \\ 0.4154 & 0.0 \end{bmatrix} \quad (5-119)$$

By no means will this eliminate the cross coupling that occurs between the control surfaces and the outputs in the state space model. What Equations (5-118) and (5-119) really say is that the system is not allowed to use bank angle feedback in determining how much rudder is needed or to use sideslip feedback in determining how much control wheel deflection is needed. The affect of using minimum  $K$  matrices of this type is given later since this is one of

the considerations used in determining the robust controllers of the next section.

#### Robustness of The Control Laws

Although control laws are designed at each flight condition, it is desirable that a single controller should result in satisfactory performance at all flight conditions. A robust controller, if feasible, would reduce the need for gain scheduling. Several schemes are tried in order to derive a robust controller. Gain elements of the  $K_0$  and  $K_1$  matrices for each maneuver are added together and averaged in an attempt to arrive at a robust controller for that maneuver. This, however, results in very poor performance of the controller when used in flight condition #3, the low altitude low airspeed case.

The method that proves to be the most successful is to use the controller designed for flight condition #3 and apply it to the other two flight conditions. In simulation of these robust controllers the  $K_0$  and  $K_1$  matrices are minimized using the techniques discussed earlier, and a computational time delay is included.

Robust Controller, Coordinated Turn. The controller used in performing the coordinated turn with computational time delay included is defined by Equations (5-95) thru (5-101). Using the guidelines discussed earlier, the  $K_0$  and  $K_1$  matrices of Equations (5-100) and (5-101) become:

$$K_0 = \begin{bmatrix} 0.0 & 1.337 \\ 1.766 & 0.0 \end{bmatrix} \quad (5-120)$$

$$K_1 = \begin{bmatrix} 0.0 & 0.3145 \\ 0.4154 & 0.0 \end{bmatrix} \quad (5-121)$$

Controller matrices of this form are referred to as minimum K. Figures 5-12a thru 5-12f show the results of this minimized controller for flight condition #3. These figures are titled "Robust Controller Cond #3 Coordinated Turn" since this is the controller used for a robustness check. Table 5-12 summarizes the results obtained from Figures 5-12a thru 5-12f.

Comparison of Table 5-12 with Table 5-6 and Figures 5-12a thru 5-12f with Figures 5-6a thru 5-6f shows the effect of minimizing the K matrices. From this it is seen that little has changed and definitely nothing is lost in reducing the K matrices.

The next step in determining robustness of this control law is to apply it to the other two flight conditions. This is done and the results for flight condition #2 are shown in Figures 5-13a thru 5-13f and summarized in Table 5-13. Results for flight condition #1 are shown in Figures 5-14a thru 5-14f and Table 5-14.

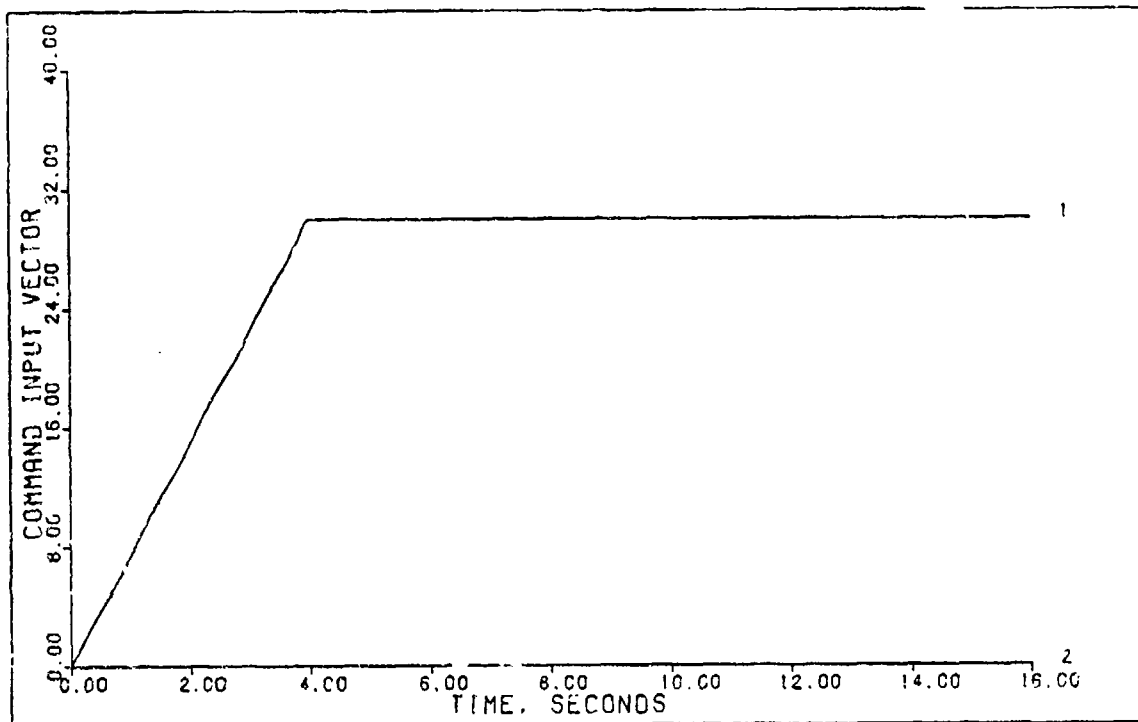


FIGURE 5-12a: Robust Controller Flight Condition #3, Coordinated Turn (Command Input Vector)

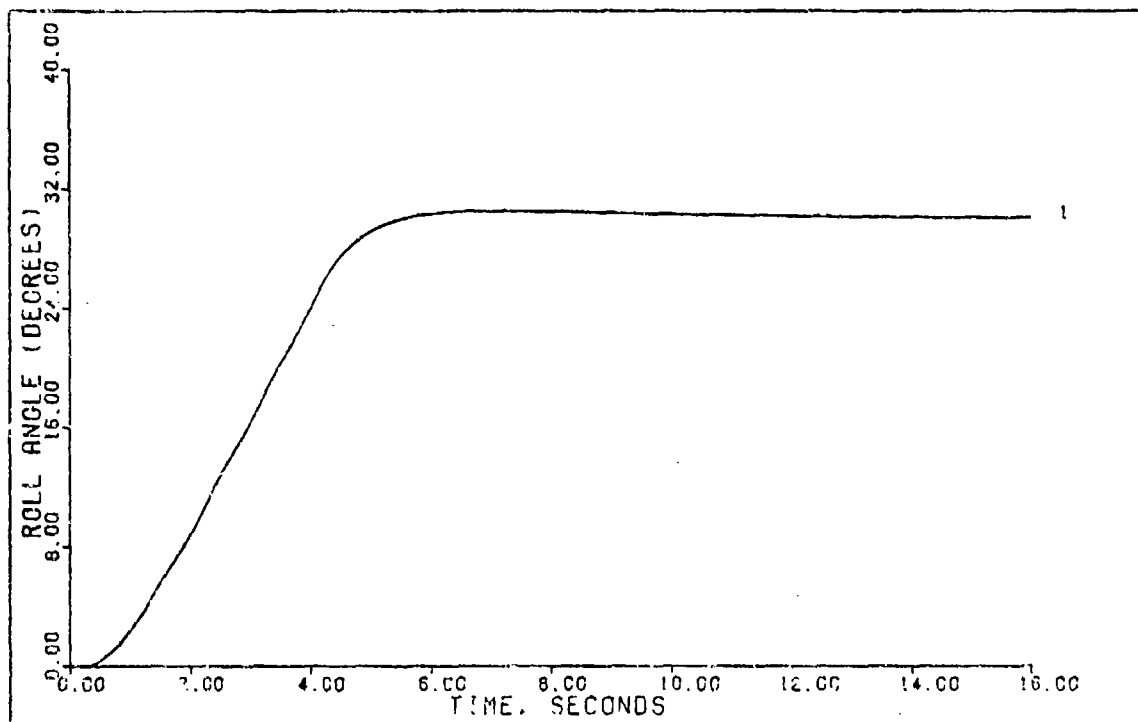


FIGURE 5-12b: Robust Controller Flight Condition #3, Coordinated Turn (Output 1: Roll Angle)

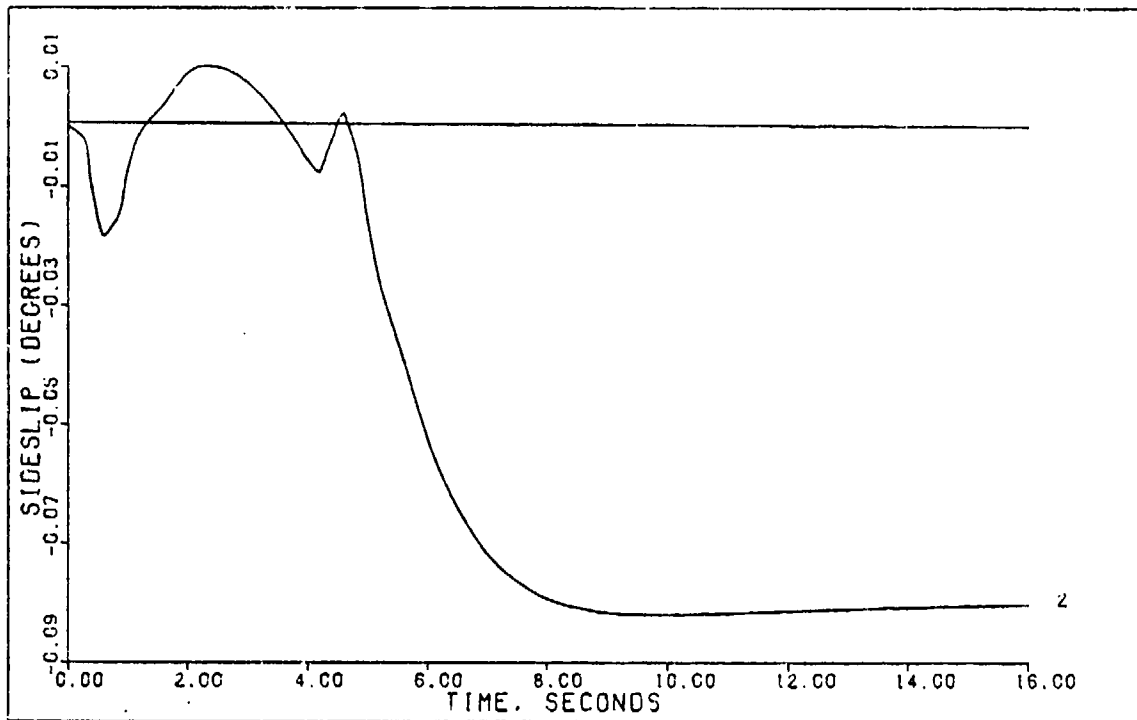


FIGURE 5-12c: Robust Controller Flight Condition #3, Coordinated Turn (Output 2: Sideslip)

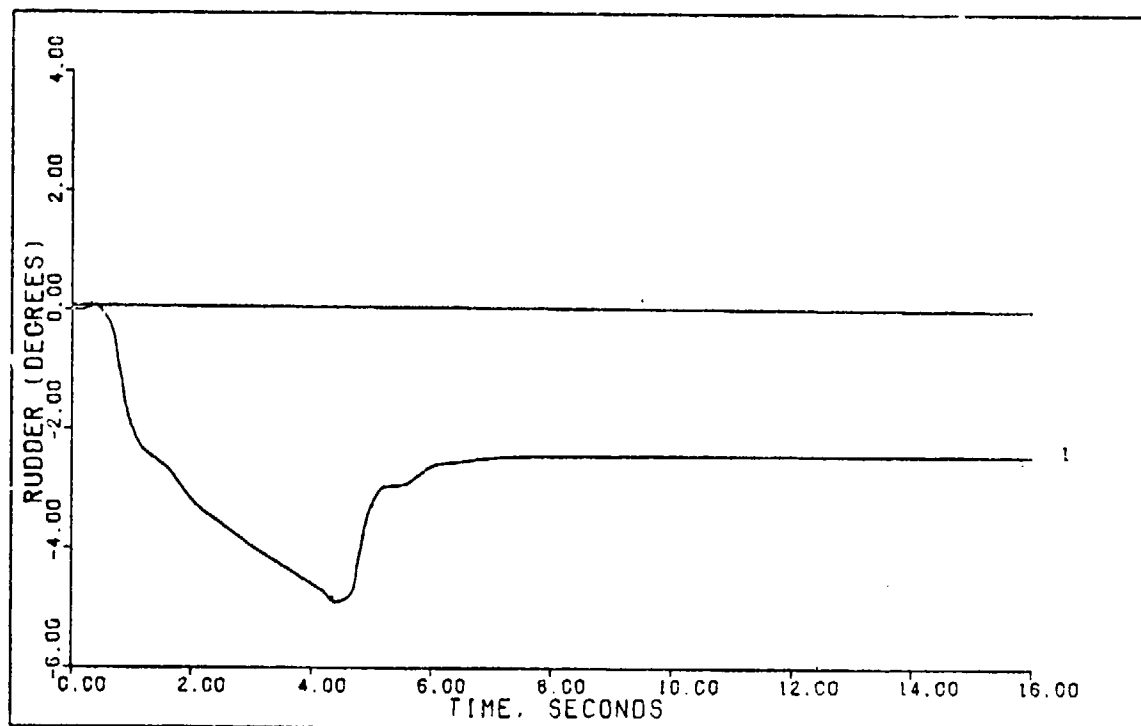


FIGURE 5-12d: Robust Controller Flight Condition #3, Coordinated Turn (Control 1: Rudder)

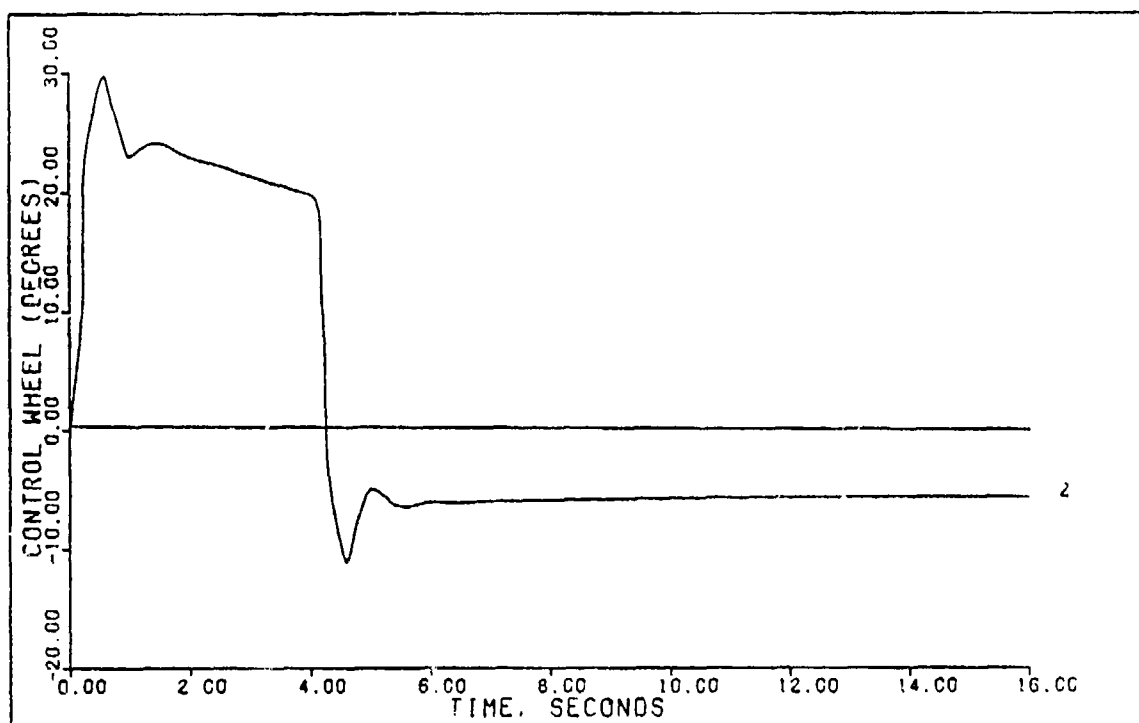


FIGURE 5-12e: Robust Controller Flight Condition #3, Coordinated Turn (Control 2: Control Wheel)

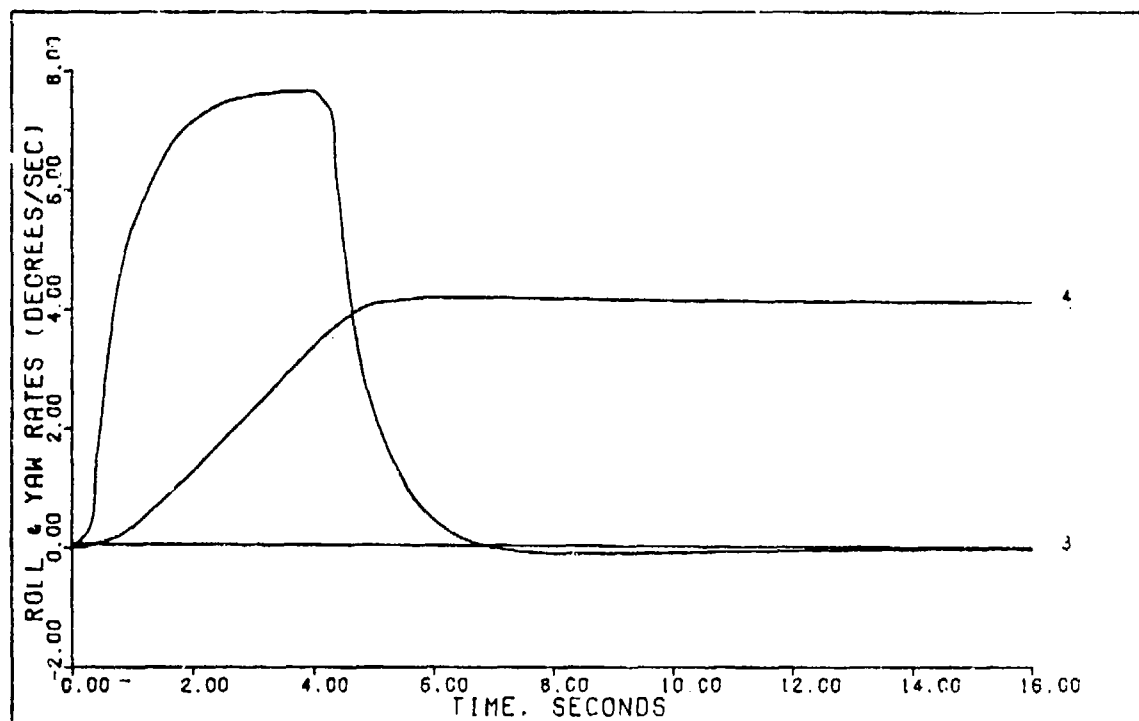


FIGURE 5-12f: Robust Controller Flight Condition #3, Coordinated Turn (State 3: Roll Rate; State 4: Yaw Rate)

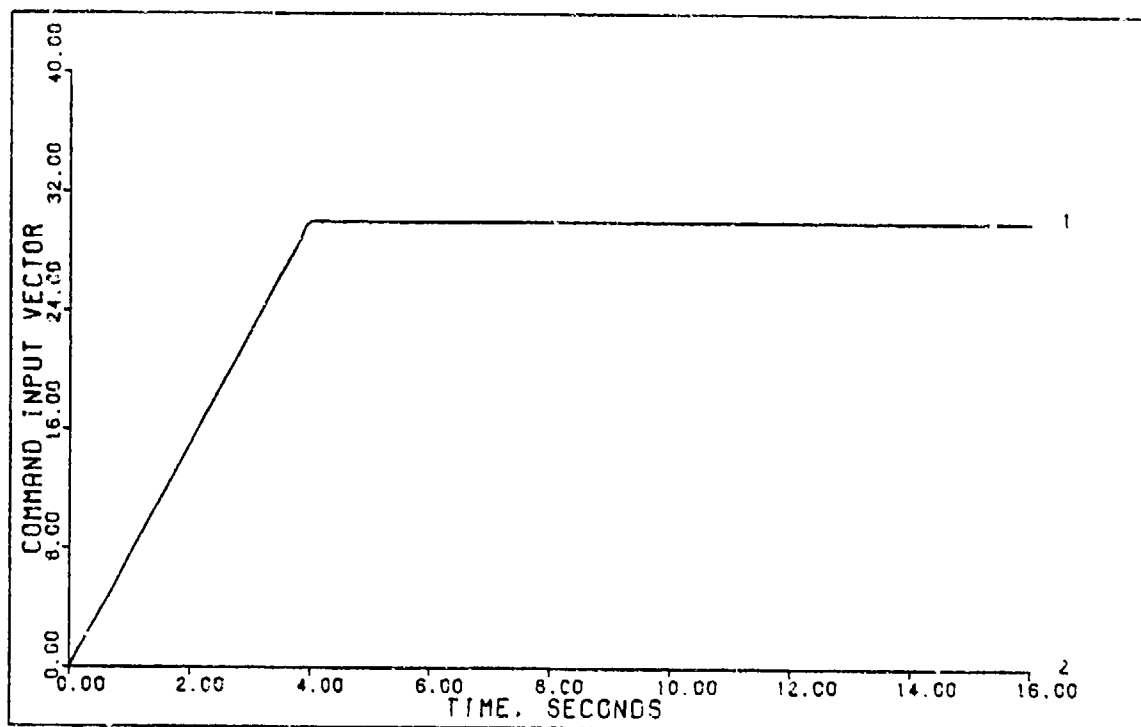


FIGURE 5-13a: Robust Controller Flight Condition #2, Coordinated Turn (Command Input Vector)

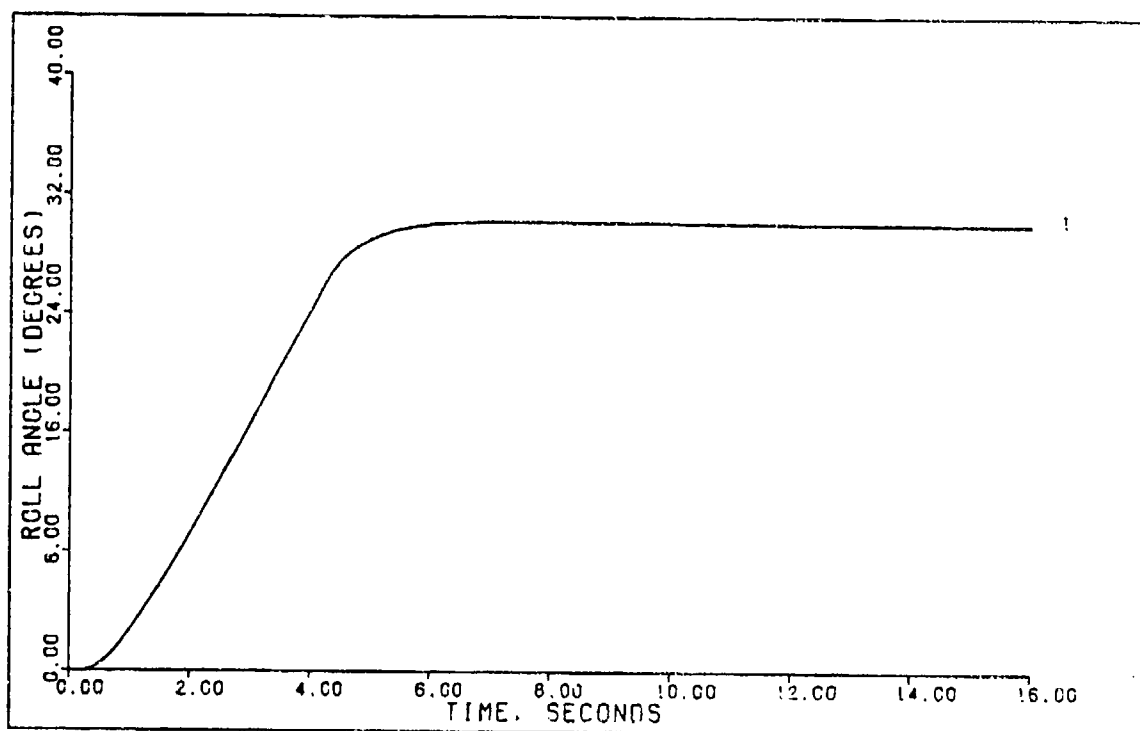


FIGURE 5-13b: Robust Controller Flight Condition #2, Coordinated Turn (Output 1: Roll Angle)



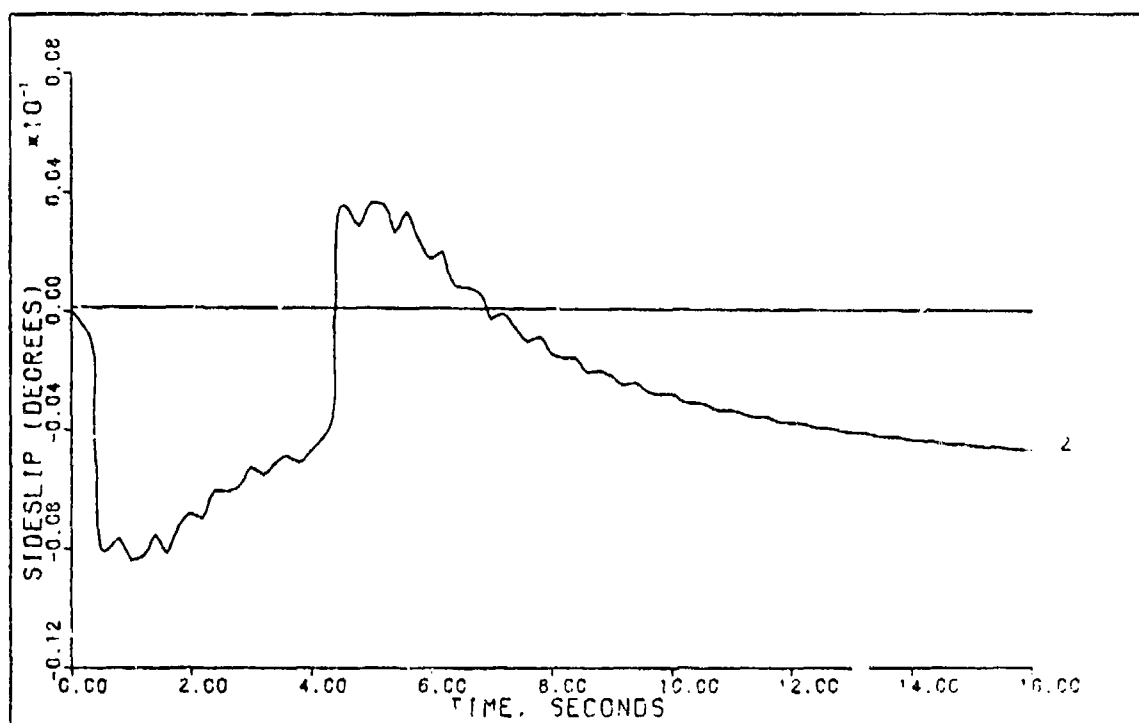


FIGURE 5-13c: Robust Controller Flight Condition #2,  
Coordinated Turn (Output 2: Sideslip)

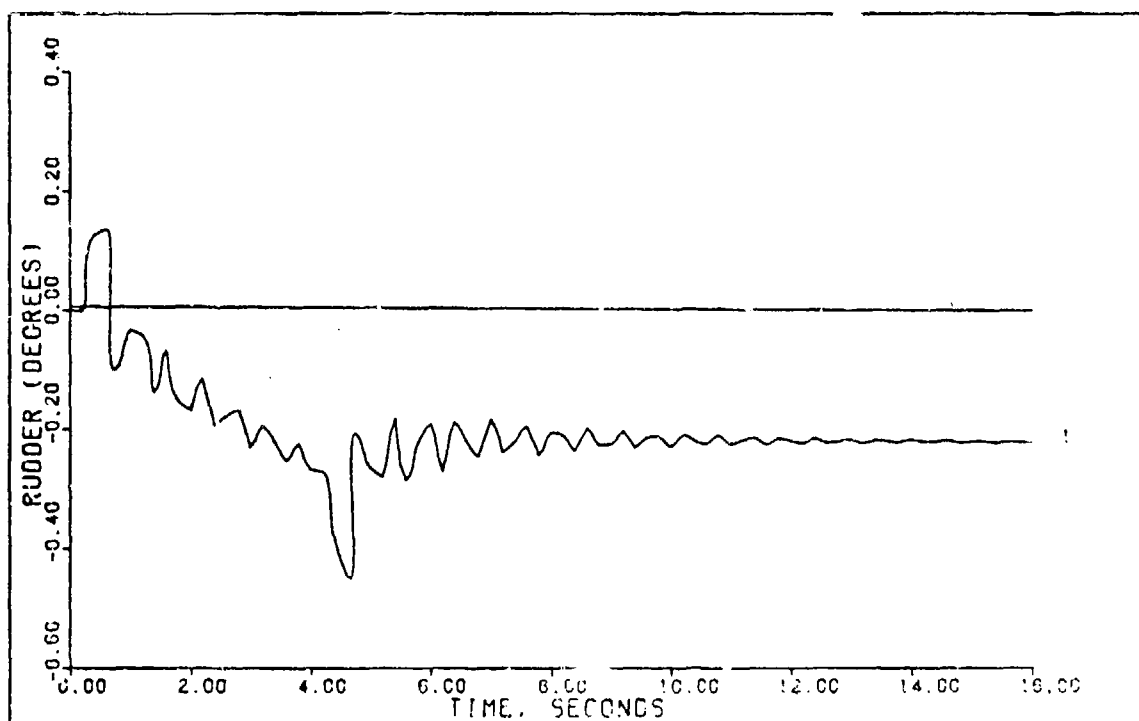


FIGURE 5-13d: Robust Controller Flight Condition #2,  
Coordinated Turn (Control 1: Rudder)

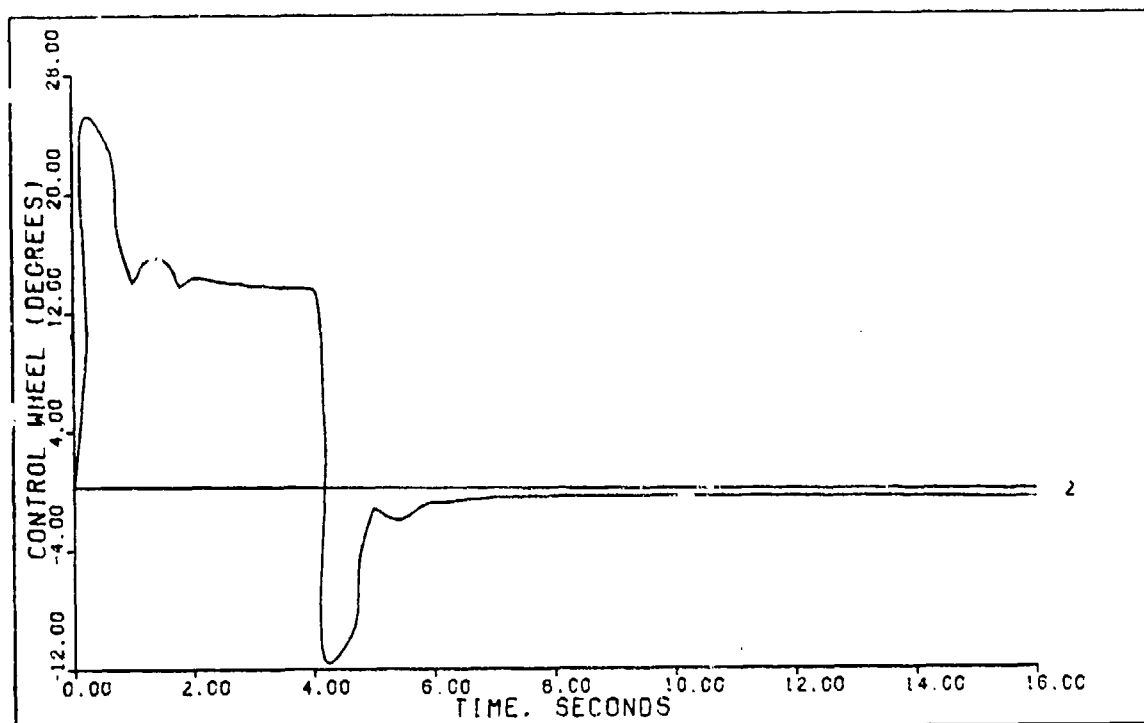


FIGURE 5-13e: Robust Controller Flight Condition #2, Coordinated Turn (Control 2: Control Wheel)

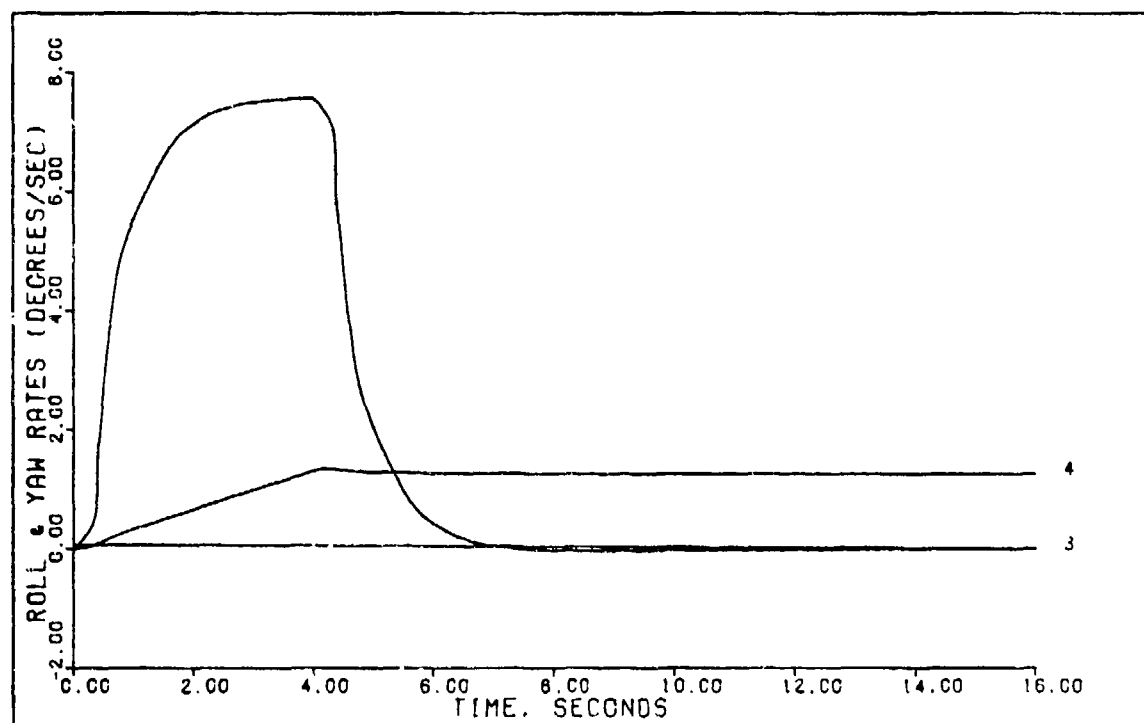


FIGURE 5-13f: Robust Controller Flight Condition #2, Coordinated Turn (State 3: Roll Rate; State 4: Yaw Rate)

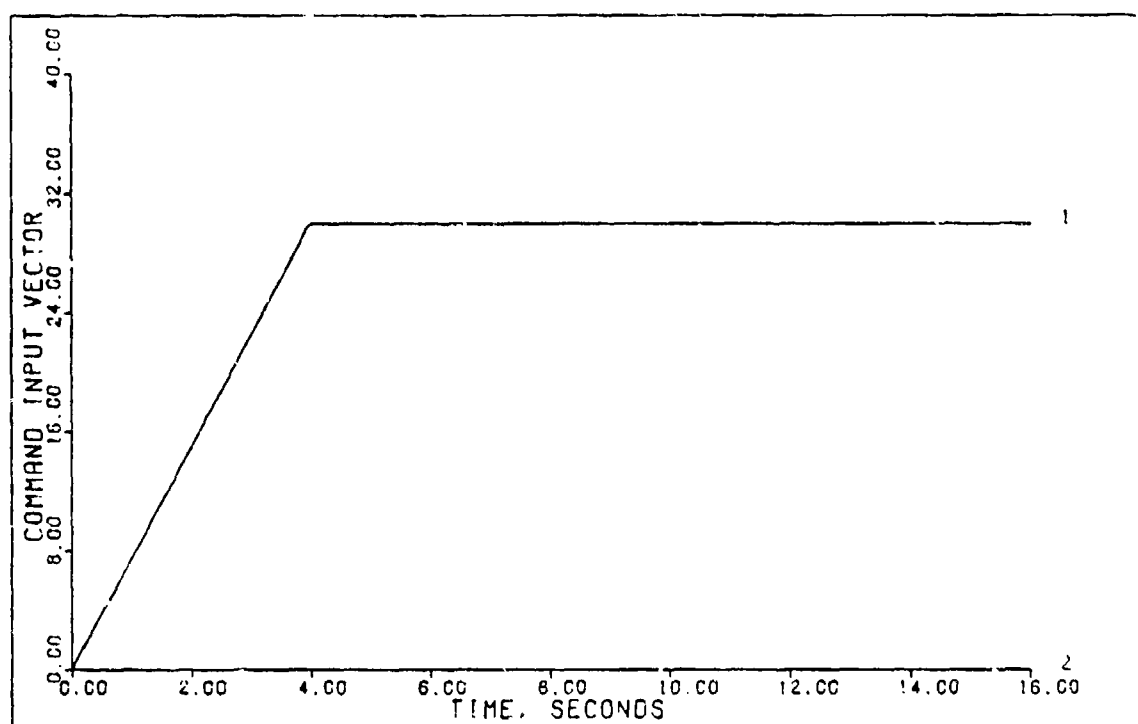


FIGURE 5-14a: Robust Controller Flight Condition #1, Coordinated Turn (Command Input Vector)

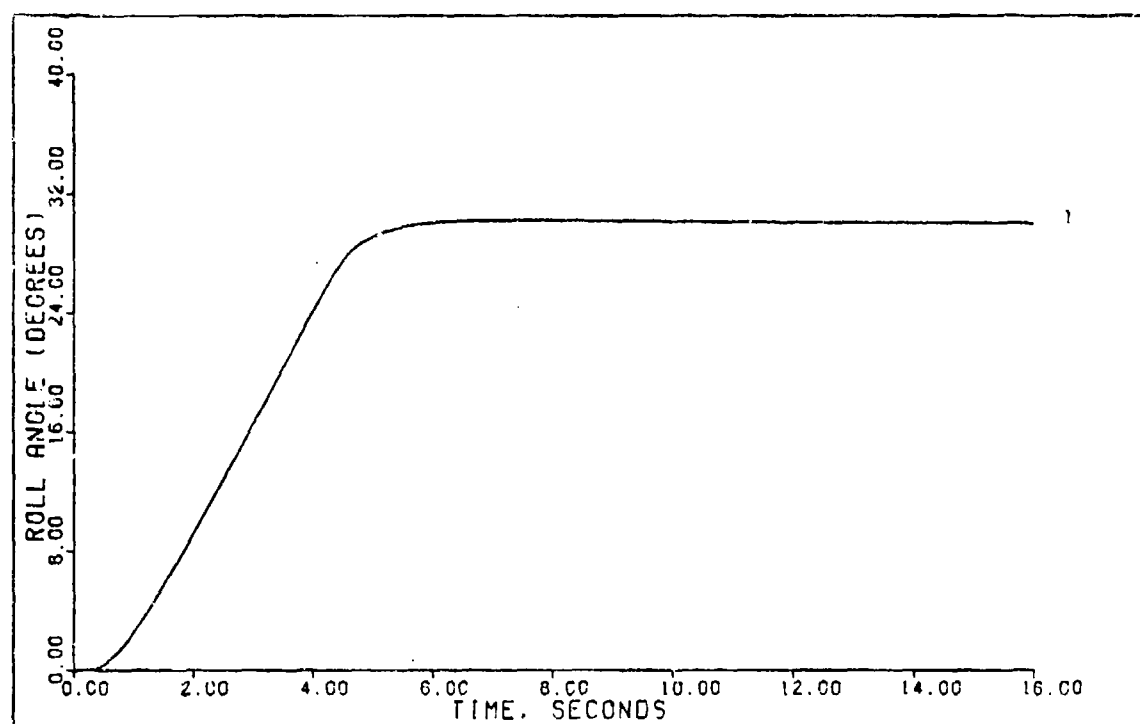


FIGURE 5-14b: Robust Controller Flight Condition #1, Coordinated Turn (Output 1: Roll Angle)

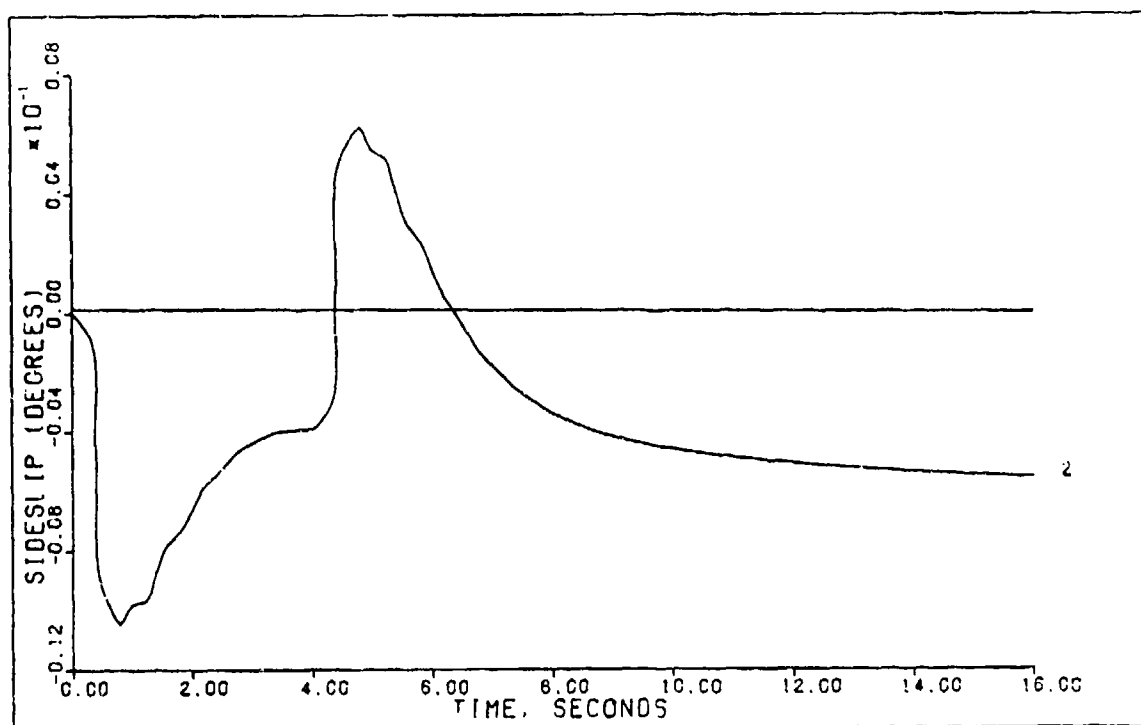


FIGURE 5-14c: Robust Controller Flight Condition #1,  
Coordinated Turn (Output 2: Sideslip)

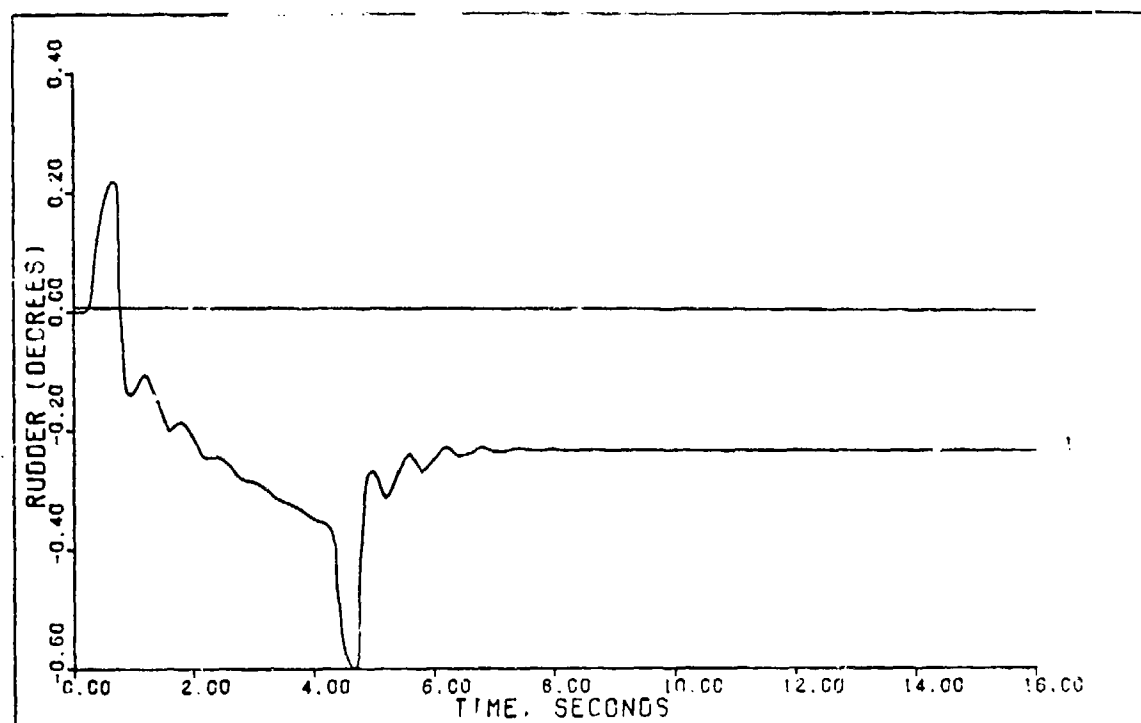


FIGURE 5-14d: Robust Controller Flight Condition #1,  
Coordinated Turn (Control 1: Rudder)

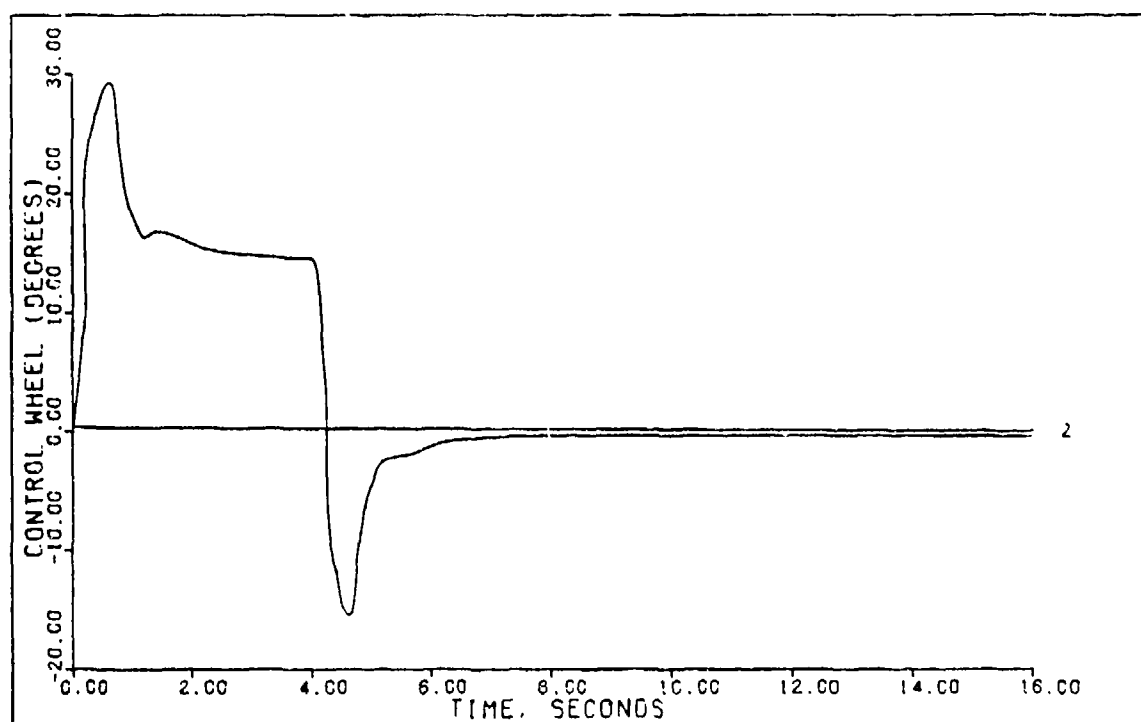


FIGURE 5-14e: Robust Controller Flight Condition #1, Coordinated Turn (Control 2: Control Wheel)

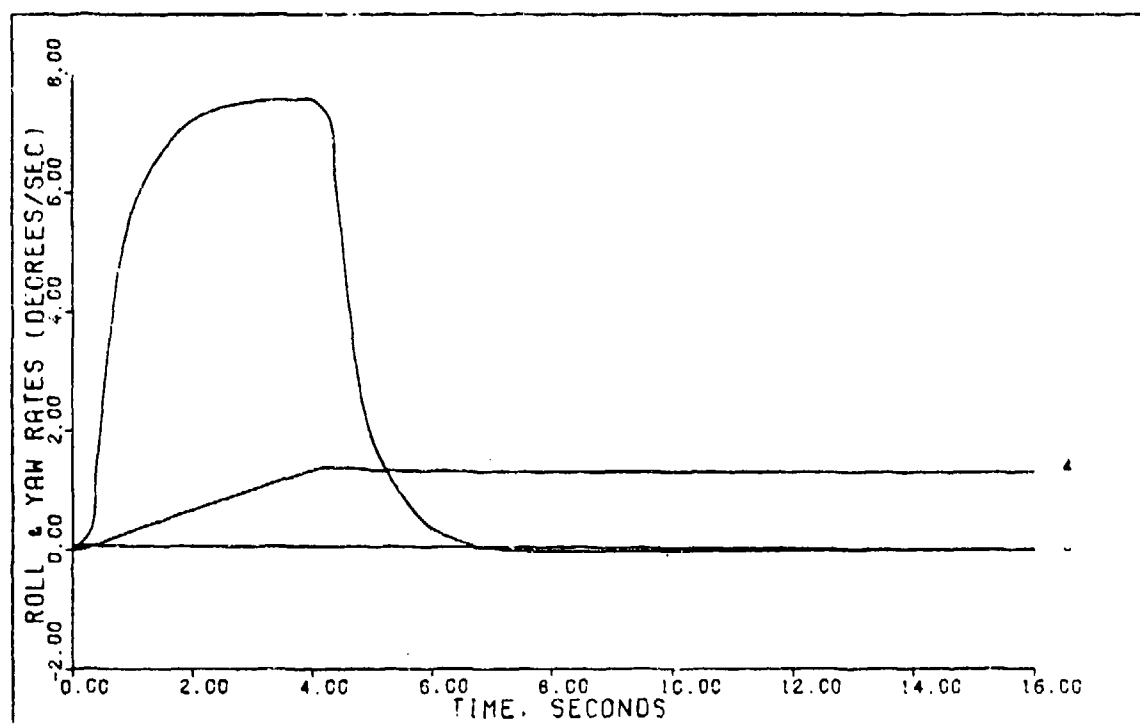


FIGURE 5-14f: Robust Controller Flight Condition #1, Coordinated Turn (State 3: Roll Rate; State 4: Yaw Rate)

Table 5-12  
Simulation Results For  
Robust Controller Condition #3 Coordinated Turn

Input/ Output	Peak Value	Final Value	$t_p$ (sec)	$t_s$ (sec)
$\phi$ (deg)	30.563	30.0	7.0	5.2
$\beta$ (deg)	-0.08	-0.08	10.0	10.6
$r$ (deg/sec)	4.20	3.93	5.5	8.0
$\delta_r$ (deg)	-5.0	--	--	--
$\delta_w$ (deg)	30.0	--	--	--

Table 5-13  
Simulation Results For  
Robust Controller Flight Condition #2 Coordinated Turn

Input/ Output	Peak Value	Final Value	$t_p$ (sec)	$t_s$ (sec)
$\phi$ (deg)	30.217	30.0	7.4	5.4
$\beta$ (deg)	-0.008	-0.005	1.0	15.6
$r$ (deg/sec)	1.38	1.19	4.2	6.0
$\delta_r$ (deg)	-0.46	--	--	--
$\delta_w$ (deg)	26.0	--	--	--

Overall, the robust controller is able to perform the coordinated turn with relatively good results. The only thing that might at first appear unacceptable is the rudder displacement for flight condition #2 shown in Figure 5-13d.

At first glance there appear to be large oscillations in the rudder while the maneuver is being performed. Closer examination shows these oscillations to be on the order of 0.1 degree. This small amount of rudder oscillation can hardly be considered unacceptable.

Table 5-14  
Simulation Results For  
Robust Controller Flight Condition #1 Coordinated Turn

Input/ Output	Peak Value	Final Value	$t_p$ (sec)	$t_s$ (sec)
$\phi$ (deg)	30.228	30.0	7.2	5.2
$\beta$ (deg)	-0.0104	-0.006	6.8	14.8
$r$ (deg/sec)	1.35	1.24	4.6	6.0
$\delta_r$ (deg)	-0.6	--	--	--
$\delta_w$ (deg)	29.0	--	--	--

Robust Controller, Sideslip Using the same approach as for the coordinated turn, a robust controller is tested for the sideslip maneuver. Equations (5-102) thru (5-108) define the controller used for flight condition #3 with time delay when performing the sideslip maneuver. The K matrices are again minimized and the simulation performed. This time, however, unacceptable oscillations of the control wheel occur. Thus in order to keep the effect of changing the K matrices to a minimum Equations, (5-107) and (5-108) are changed to

$$K_0 = \begin{bmatrix} 0.0 & 1.049 \\ 2.486 & -0.9278 \end{bmatrix} \quad (5-122)$$

$$K_1 = \begin{bmatrix} 0.0 & 0.3497 \\ 0.8285 & -0.3093 \end{bmatrix} \quad (5-123)$$

Therefore the robust controller for the sideslip maneuver is defined by Equations (5-102) thru (5-104) along with Equations (5-122) and (5-123).

Applying this robust controller to flight condition #3 produces the results shown in Figures 5-15a thru 5-15d and Table 5-15. Results for flight condition #2 are given in Figures 5-16a thru 5-16d along with Table 5-16 while results for flight condition #1 are shown in Figures 5-17a thru 5-17d and Table 5-17.

Table 5-15  
Simulation Results For  
Robust Controller Flight Condition #3 Sideslip

Input/ Output	Peak Value	Final Value	$t_p$ (sec)	$t_s$ (sec)
$\phi$ (deg)	-0.4774	0.0	8.4	--
$\beta$ (deg)	5.088	5.0	16.0	8.8
$\delta_r$ (deg)	6.0	--	--	--
$\delta_w$ (deg)	28.0	--	--	--

Again comparison of Table 5-15 with 5-8 along with Figures 5-15a thru 5-15d with Figures 5-8a thru 5-8d shows that there is little effect when minimizing the K matrices. Overall, the robust controller is able to perform the



sideslip maneuver with fair results. However some increases in settling time are noted.

Table 5-16  
Simulation Results For  
Robust Controller Flight Condition #2 Sideslip

Input/ Output	Peak Value	Final Value	$t_p$ (sec)	$t_s$ (sec)
$\phi$ (deg)	-0.7199	0.0	8.6	--
$\beta$ (deg)	5.06	5.0	16.0	11.6
$\delta_r$ (deg)	8.5	--	--	--
$\delta_w$ (deg)	50.0	--	--	--

Table 5-17  
Simulation Results For  
Robust Controller Flight Condition #1 Sideslip

Input/ Output	Peak Value	Final Value	$t_p$ (sec)	$t_s$ (sec)
$\phi$ (deg)	-0.37993	0.0	8.4	--
$\beta$ (deg)	5.025	5.0	16.0	8.8
$\delta_r$ (deg)	9.0	--	--	--
$\delta_w$ (deg)	47.0	--	--	--

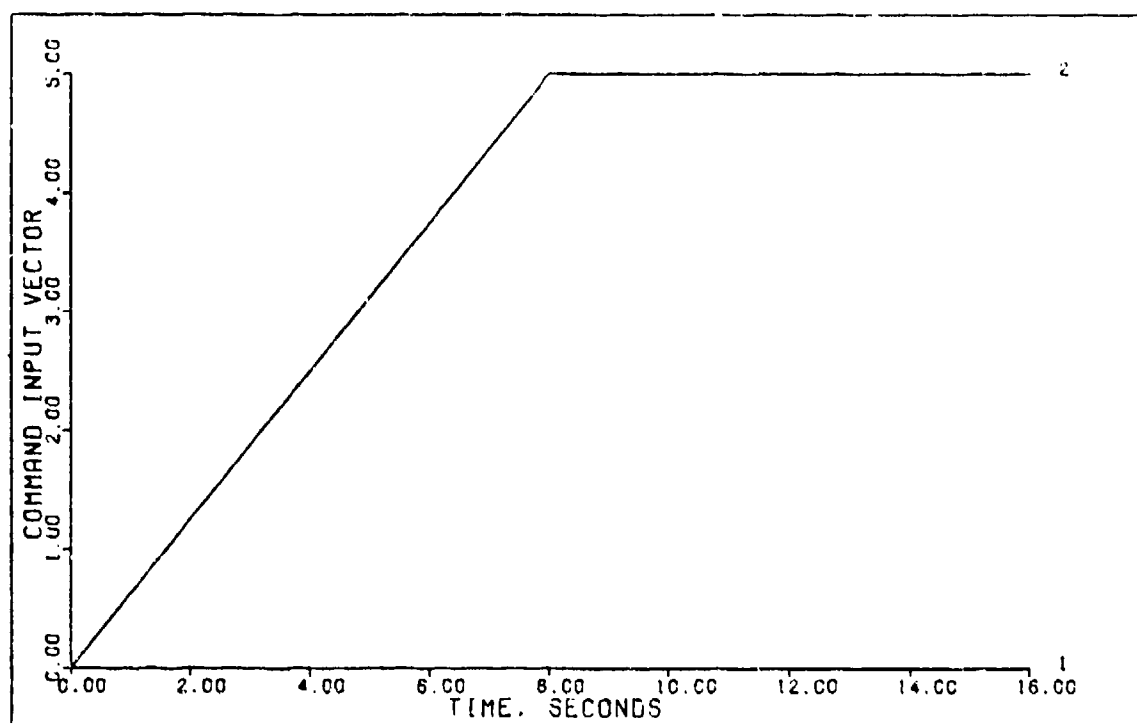


FIGURE 5-15a: Robust Controller Flight Condition #3, Sideslip (Command Input Vector)

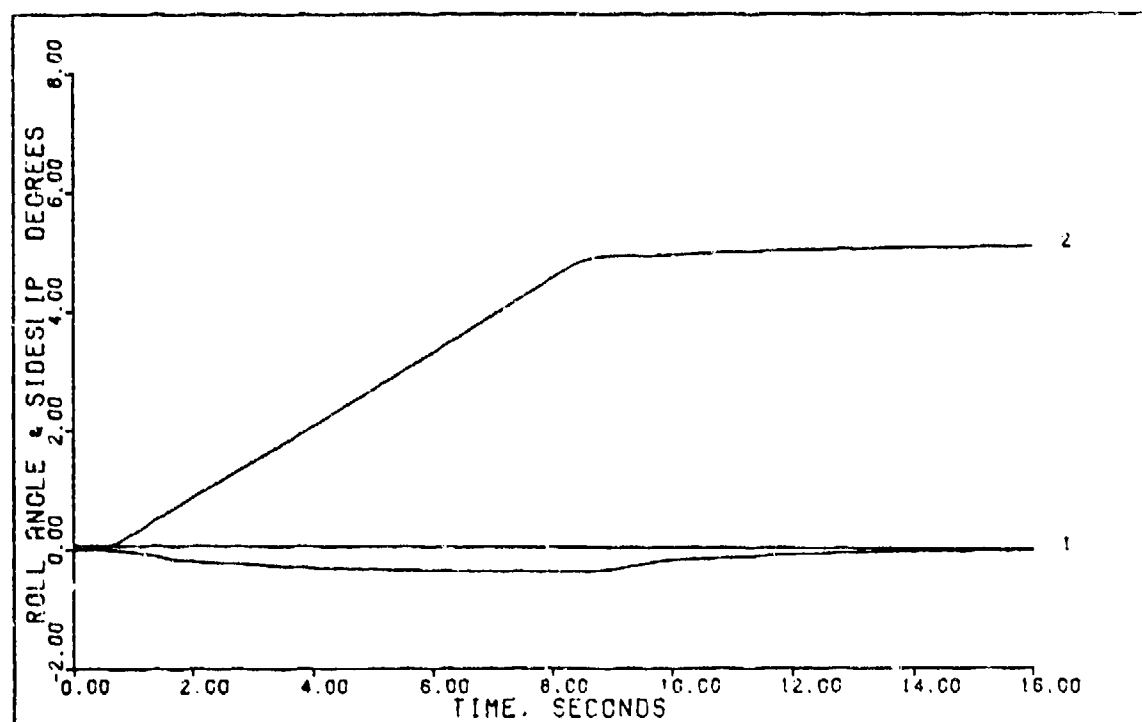


FIGURE 5-15b: Robust Controller Flight Condition #3, Sideslip (Output 1: Roll Angle; Output 2: Sideslip)

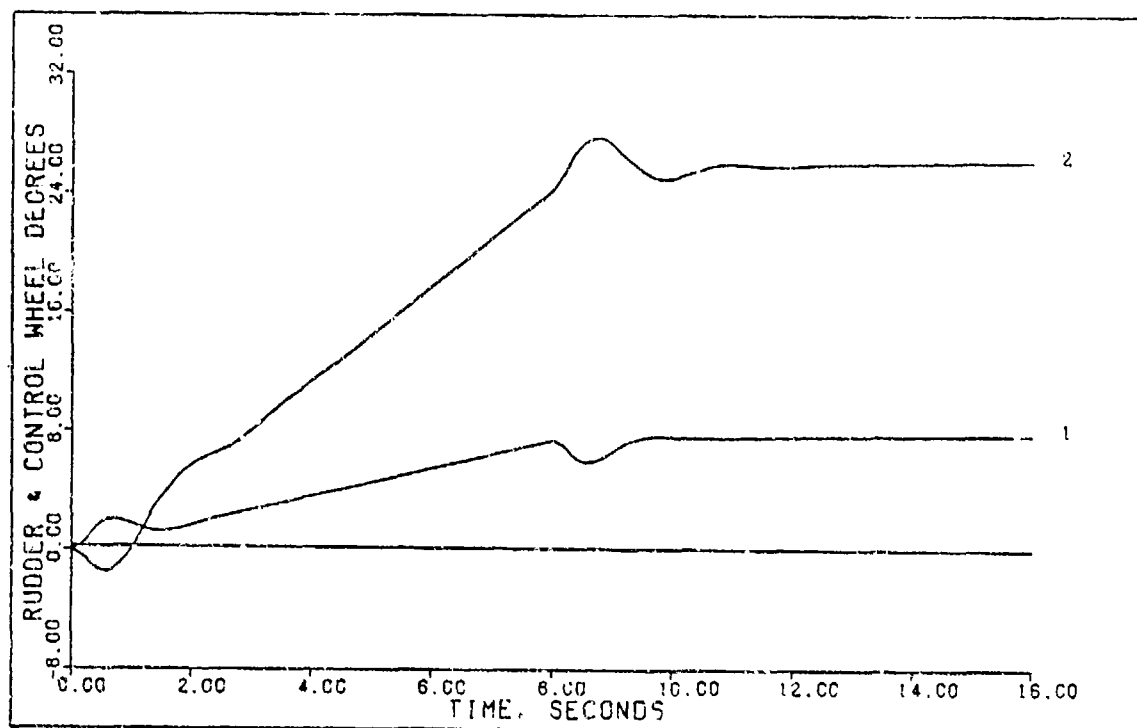


FIGURE 5-15c: Robust Controller Flight Condition #3, Sideslip (Control 1: Rudder; Control 2: Control Wheel)

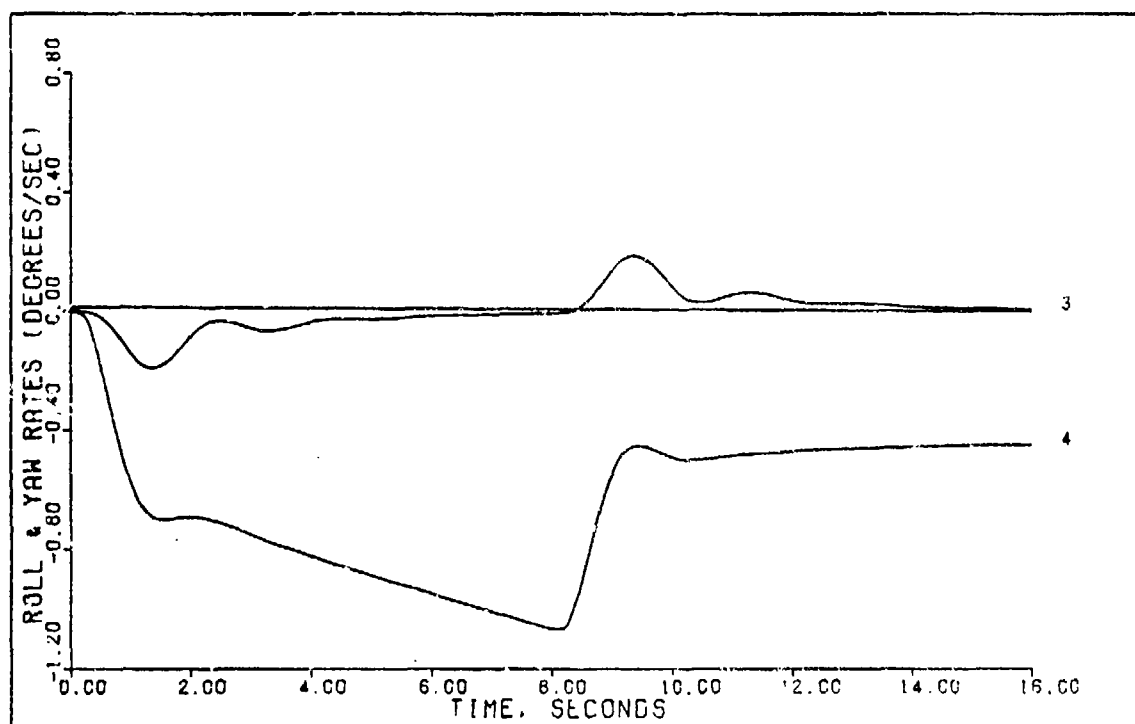


FIGURE 5-15d: Robust Controller Flight Condition #3, Sideslip (State 3: Roll Rate; State 4: Yaw Rate)

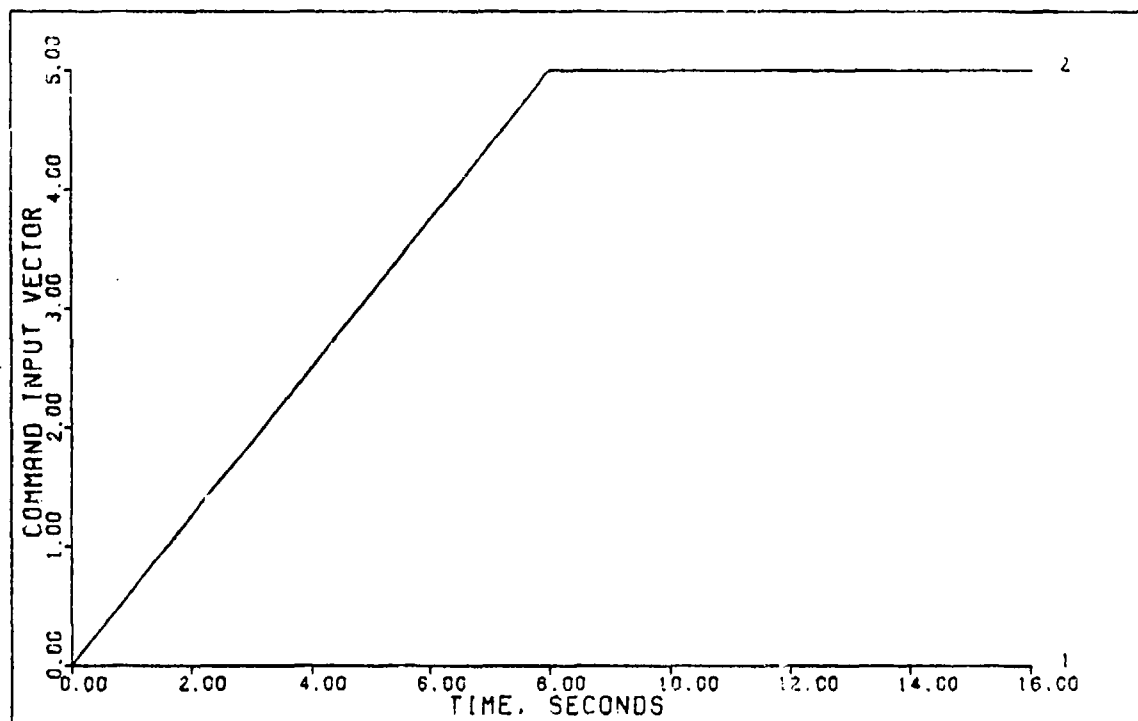


FIGURE 5-16a: Robust Controller Flight Condition #2, Sideslip (Command Input Vector)

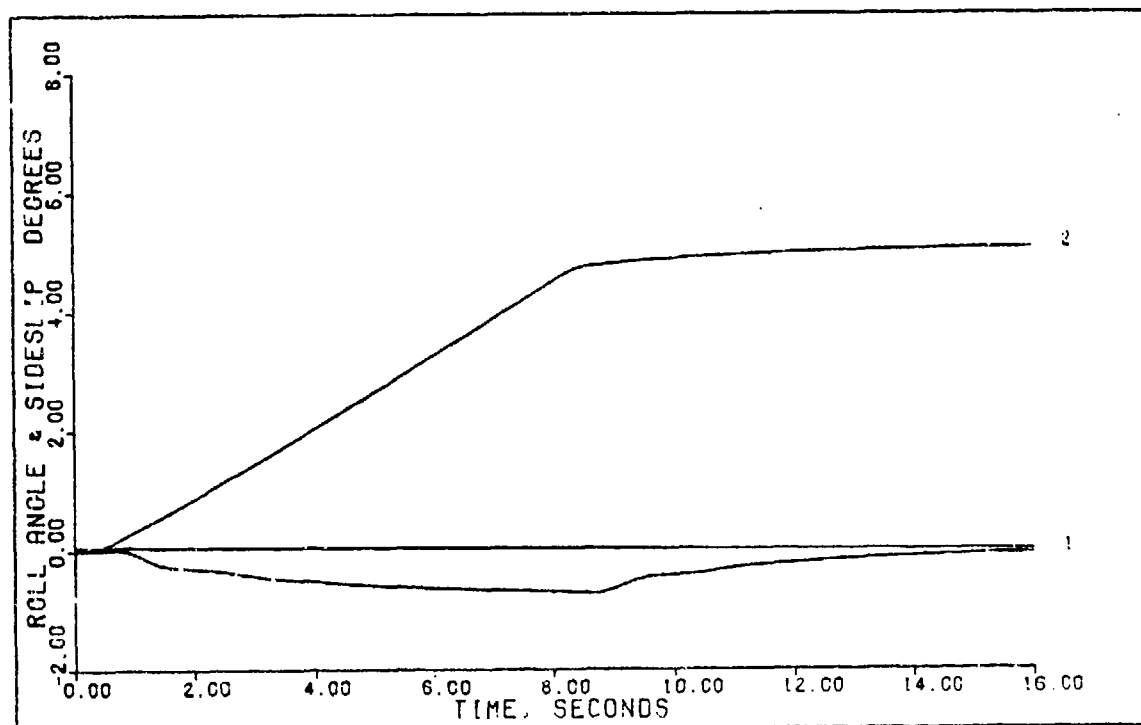


FIGURE 5-16b: Robust Controller Flight Condition #2, Sideslip (Output 1: Roll Angle; Output 2: Sideslip)

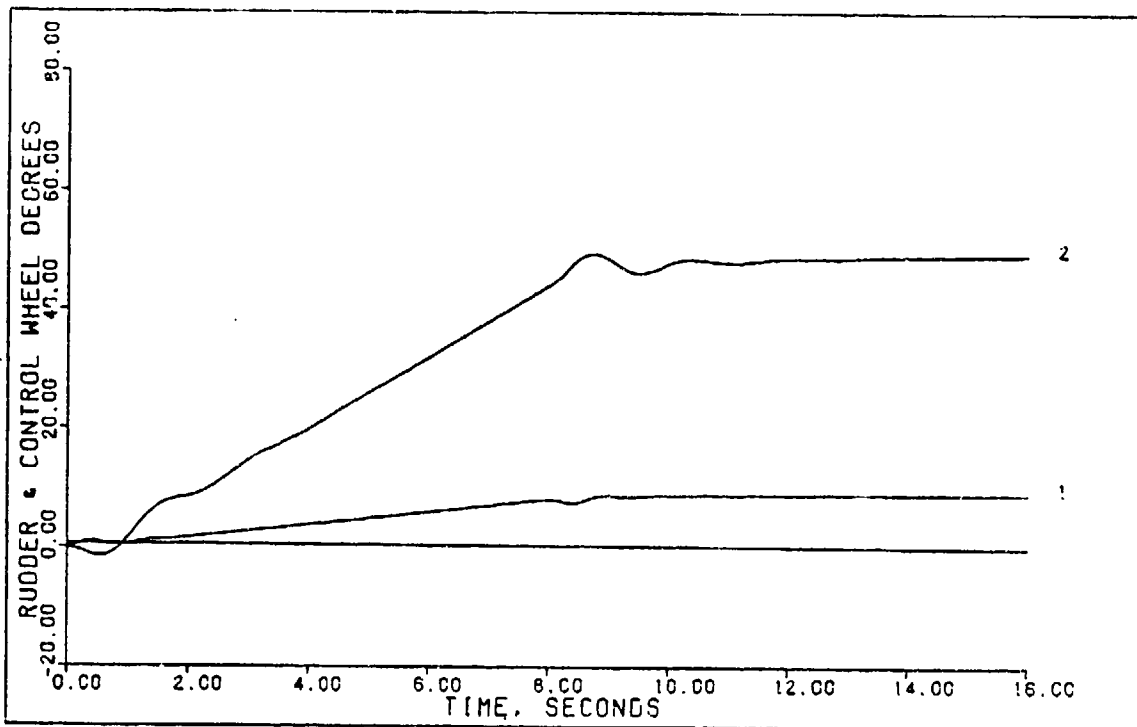


FIGURE 5-16c: Robust Controller Flight Condition #2, Sideslip (Control 1: Rudder; Control 2: Control Wheel)

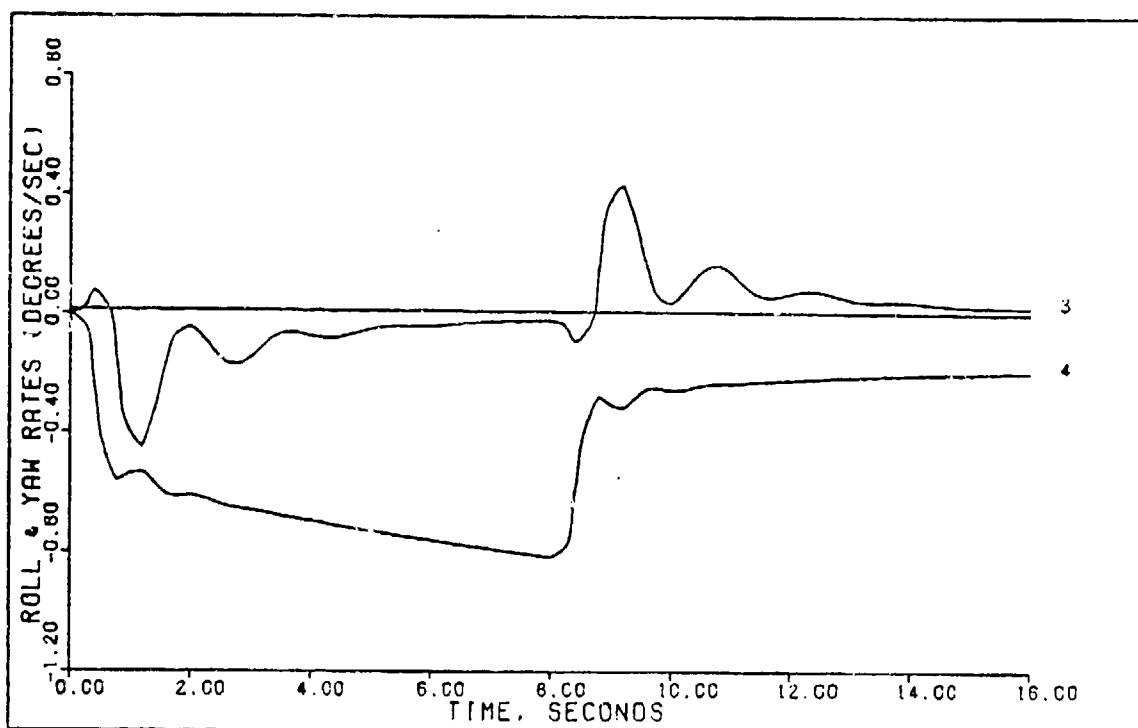


FIGURE 5-16d: Robust Controller Flight Condition #2, Sideslip (State 3: Roll Rate; State 4: Yaw Rate)

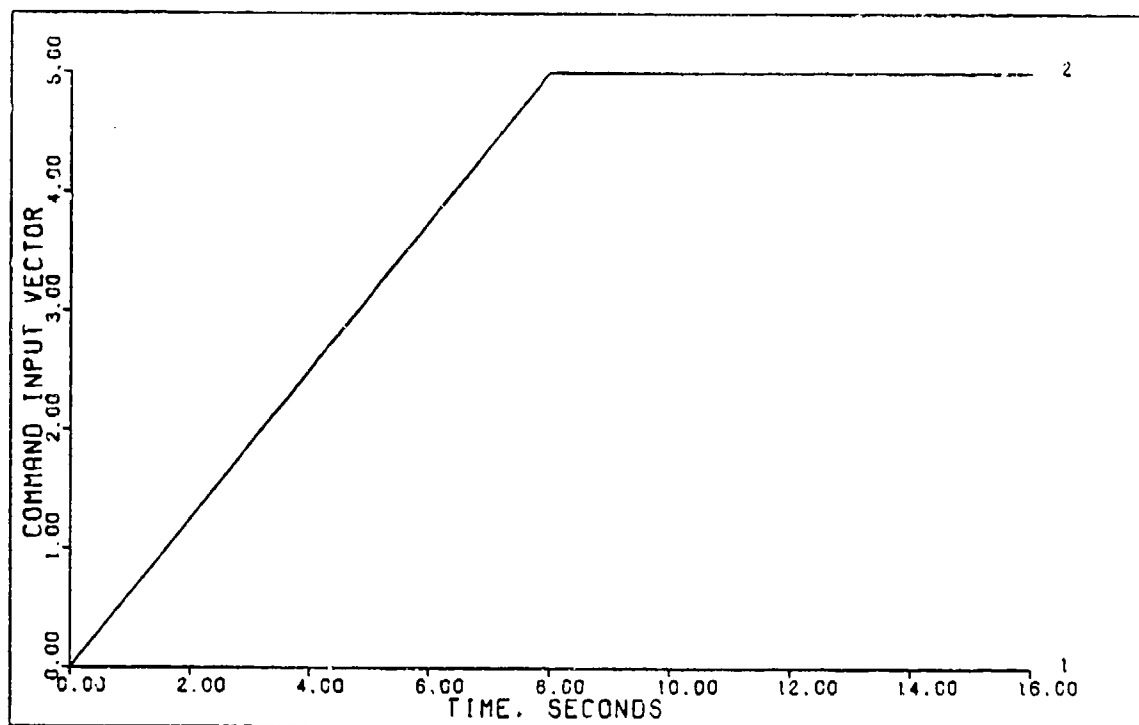


FIGURE 5-17a: Robust Controller Flight Condition #1, Sideslip (Command Input Vector)

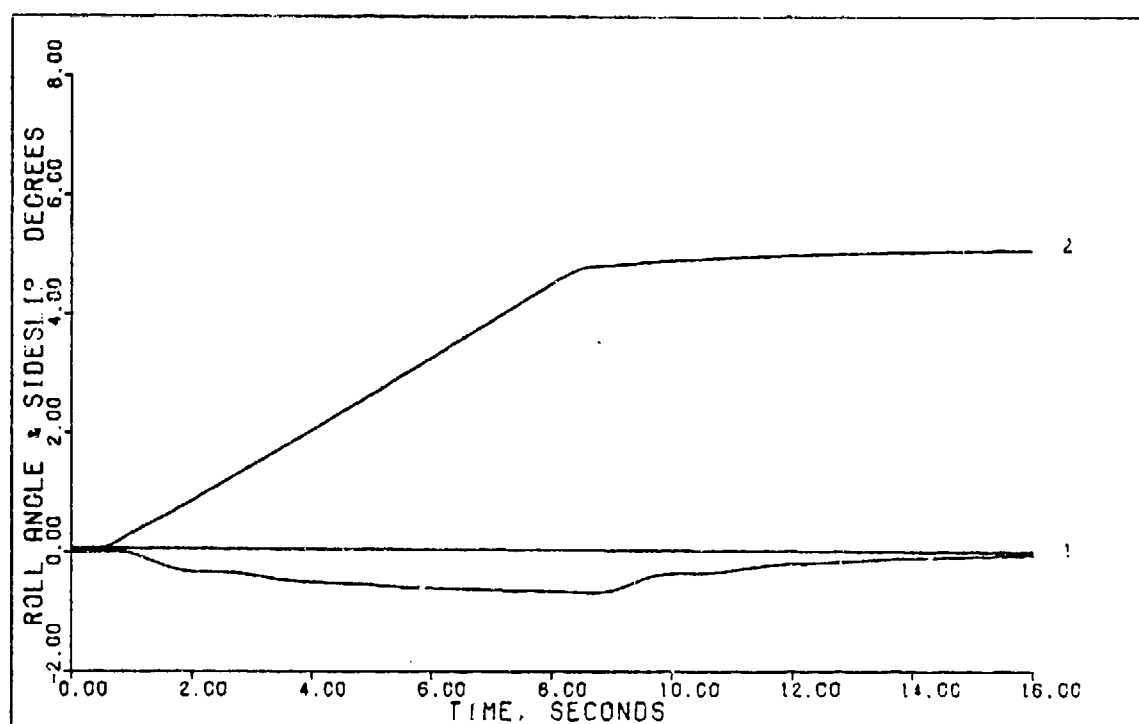


FIGURE 5-17b: Robust Controller Flight Condition #1, Sideslip (Output 1: Roll Angle; Output 2: Sideslip)

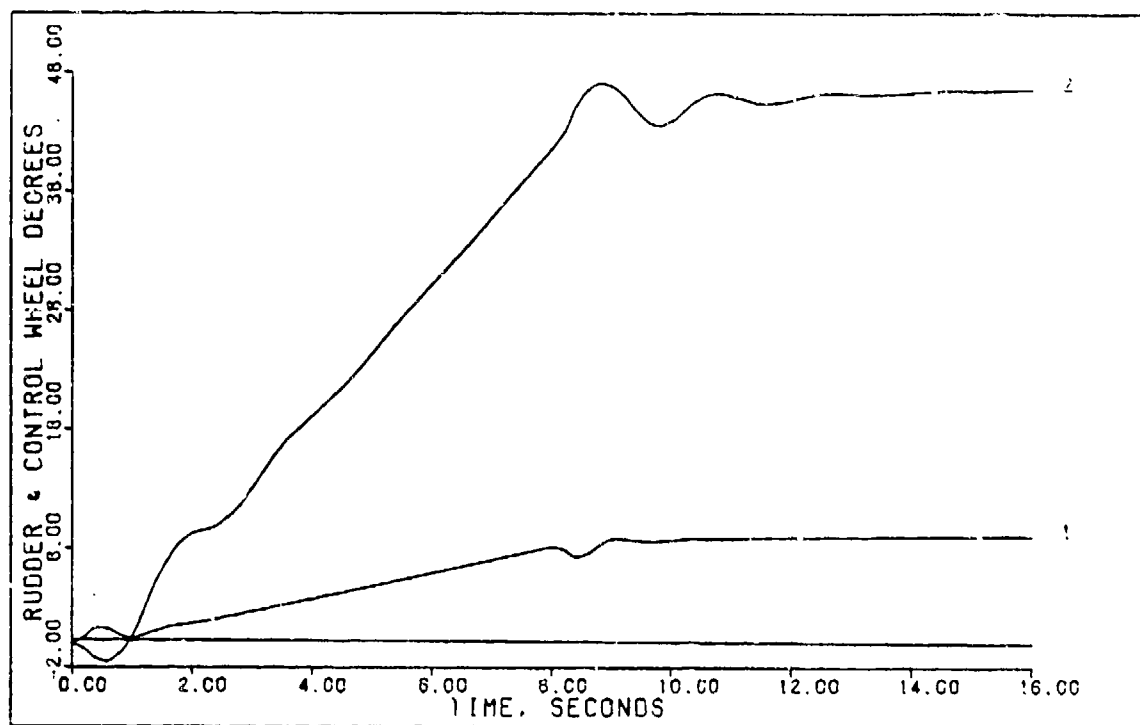


FIGURE 5-17c: Robust Controller Flight Condition #1, Sideslip (Control 1: Rudder; Control 2: Control Wheel)

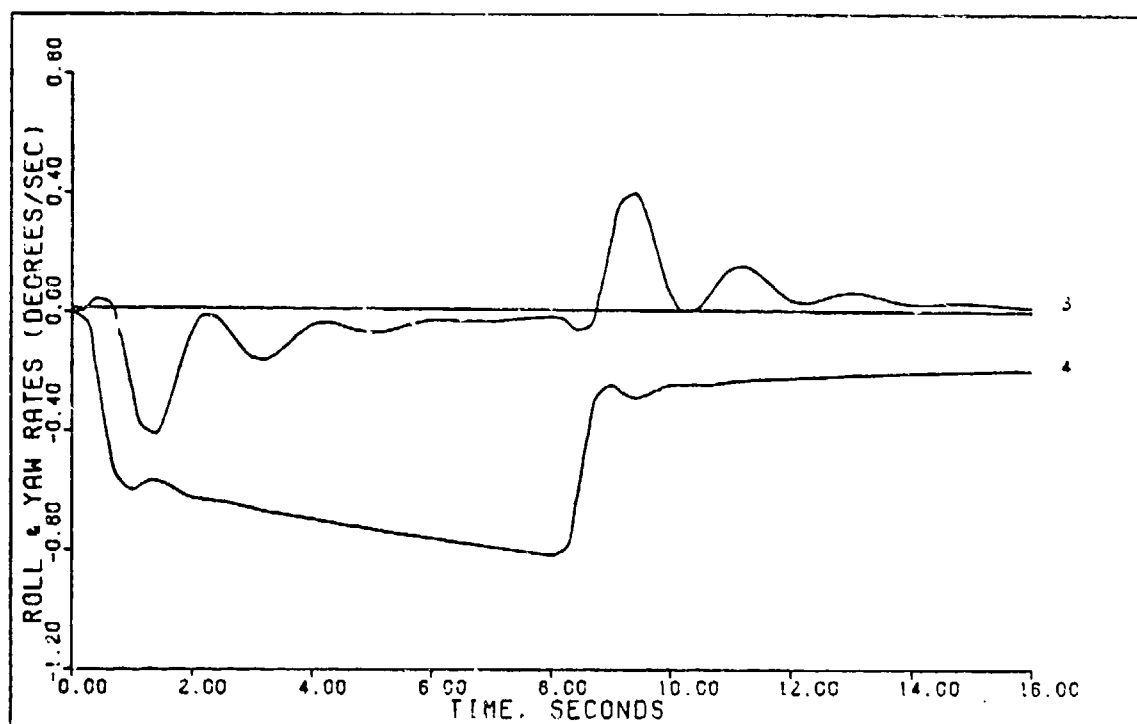


FIGURE 5-17d: Robust Controller Flight Condition #1, Sideslip (State 3: Roll Rate; State 4: Yaw Rate)

Robust Controller, Normal Climb The controller used to perform the normal climb for flight condition #3 with computational time delay is given by Equations (5-25) thru (5-31). The robust controller used to perform the climb maneuver for all flight conditions comes from this control law except  $K_0$  and  $K_1$  of Equations (5-30) and (5-31) are changed to

$$K_0 = \begin{bmatrix} -0.9558 & 0.0 \\ 0.0 & 2.957 \end{bmatrix} \quad (5-126)$$

$$K_1 = \begin{bmatrix} -0.3823 & 0.0 \\ 0.0 & 1.183 \end{bmatrix} \quad (5-125)$$

This represents the minimum form for the K matrices of this maneuver. Notice that the first element in the second row of both  $K_0$  and  $K_1$  have been set to zero. This eliminates the velocity feedback from affecting the elevator input. Thus the elevator only receives input from the feedback of the flight path angle.

Figures 5-18a thru 5-18h and Table 5-18 show the results of this robust controller when used to perform the normal climb for flight condition #3. Figures 5-19a thru 5-19h and Table 5-19 show the results for flight condition #2 while Figures 5-20a thru 5-20h and Table 5-20 show the results obtained for flight condition #1.

Comparisons of Figures 5-18a thru 5-18h with Figures 5-9a thru 5-9h and Table 5-18 with Table 5-9 shows the effect of reducing the  $K_0$  and  $K_1$  matrices to Equations



(5-70) and (5-71), respectively. Overall, the robust controller performs well over the three flight conditions if the settling times of flight condition #2 and flight condition #1 are not considered to be excessive.

Table 5-18  
Simulation Results For  
Robust Controller Flight Condition #3 Normal Climb

Input/ Output	Peak Value	Final Value	$t_p$ (sec)	$t_s$ (sec)
$\gamma$ (deg)	5.433	4.86	8.1	12.9
$u$ (ft/sec)	-0.31	0.0	4.8	--
$\delta_e$ (deg)	-3.5	--	--	--
$\delta_T$ (%RPM)	24.0	--	--	--

Table 5-19  
Simulation Results For  
Robust Controller Flight Condition #2 Normal Climb

Input/ Output	Peak Value	Final Value	$t_p$ (sec)	$t_s$ (sec)
$\gamma$ (deg)	1.759	1.49	8.4	15.3
$u$ (ft/sec)	-0.375	0.0	4.2	--
$\delta_e$ (deg)	-1.0	--	--	--
$\delta_T$ (%RPM)	30	--	--	--

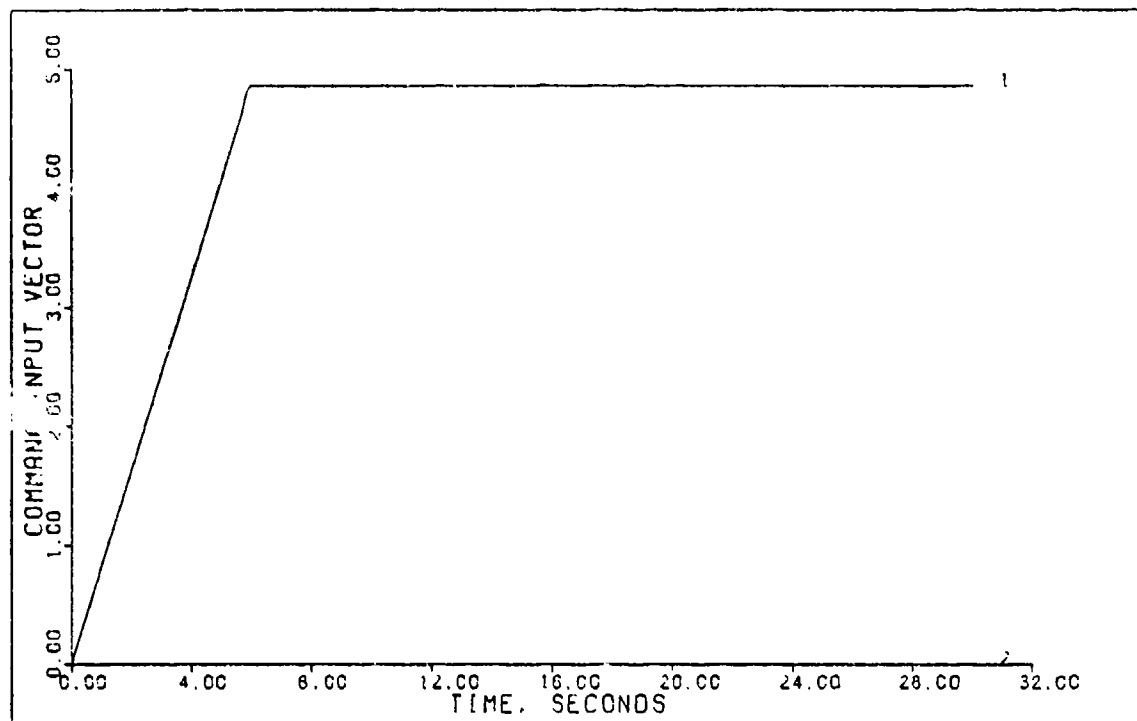


FIGURE 5-18a: Robust Controller Flight Condition #3, Normal Climb (Command Input Vector)

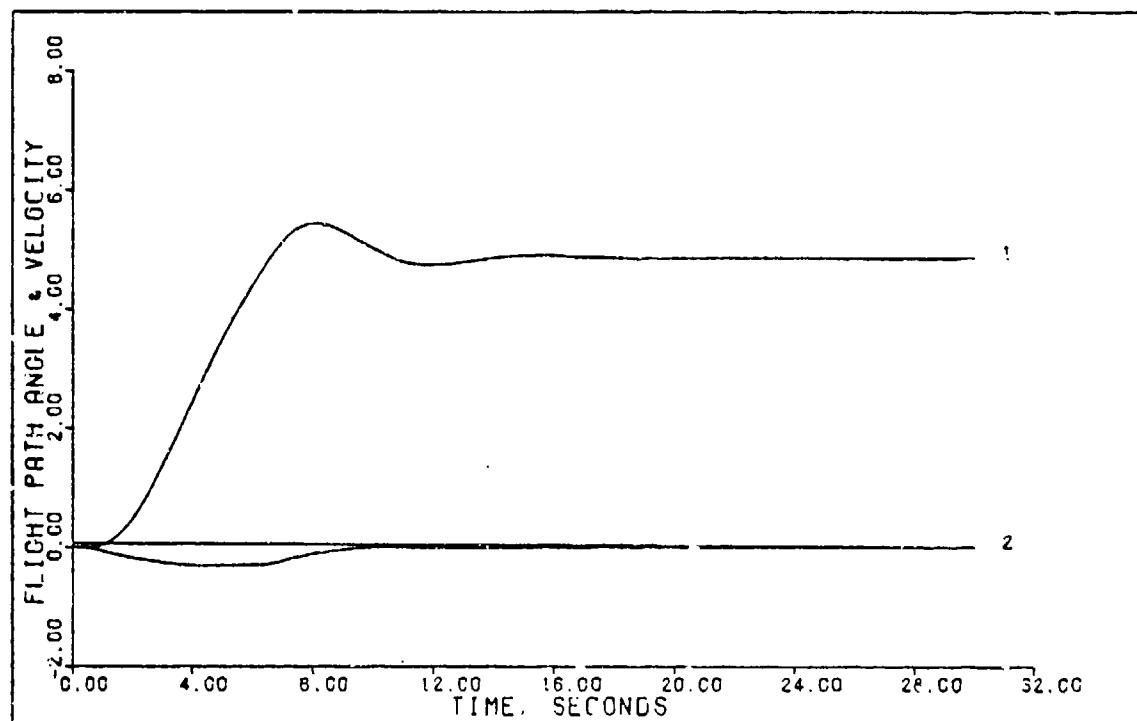


FIGURE 5-18b: Robust Controller Flight Condition #3, Normal Climb (Output 1: Flight Path Angle; Output 2: Velocity)

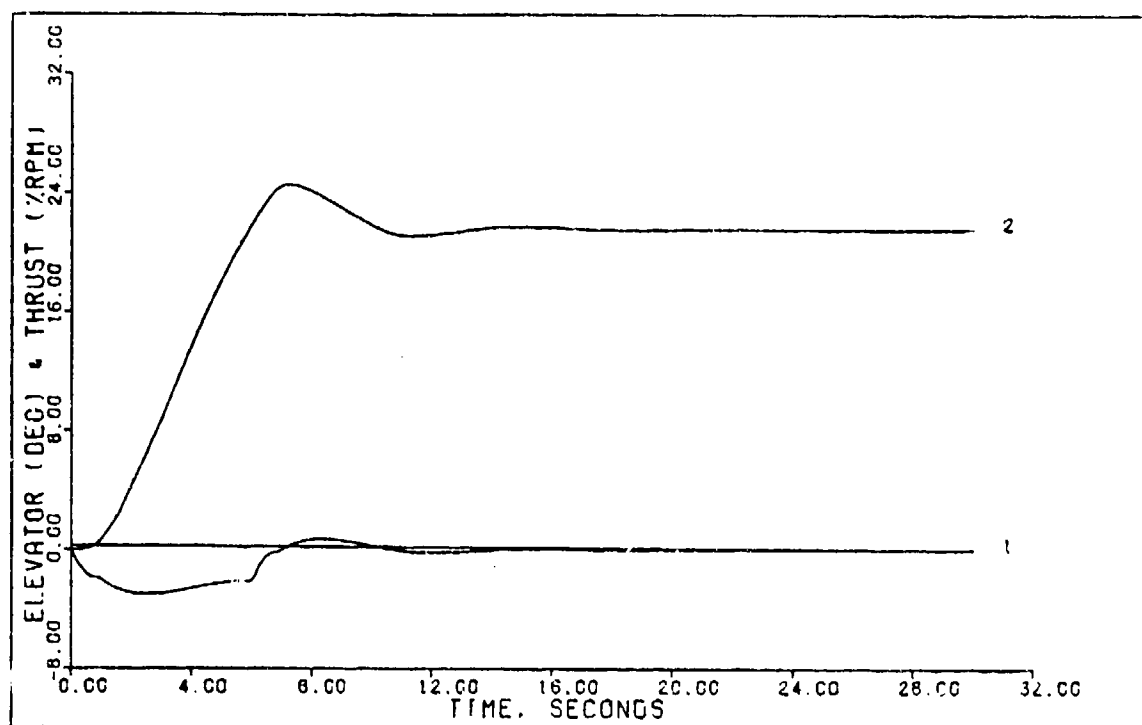


FIGURE 5-18c: Robust Controller Flight Condition #3, Normal Climb (Control 1: Elevator; Control 2: Thrust)

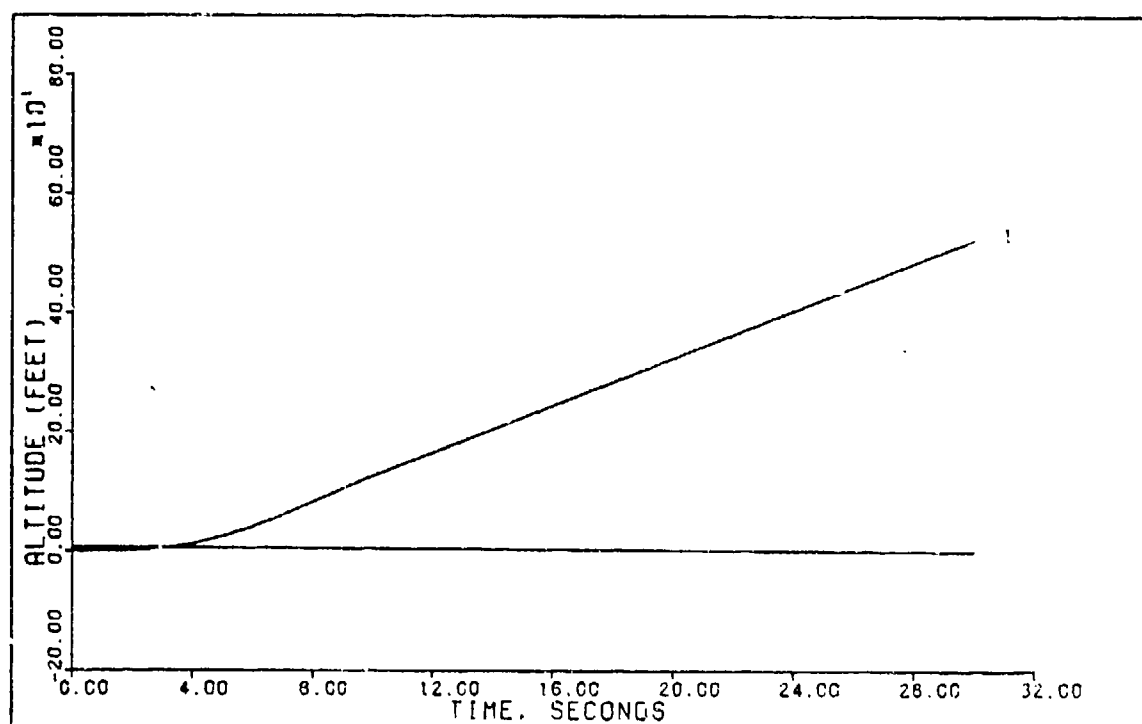


FIGURE 5-18d: Robust Controller Flight Condition #3, Normal Climb (State 1: Altitude)

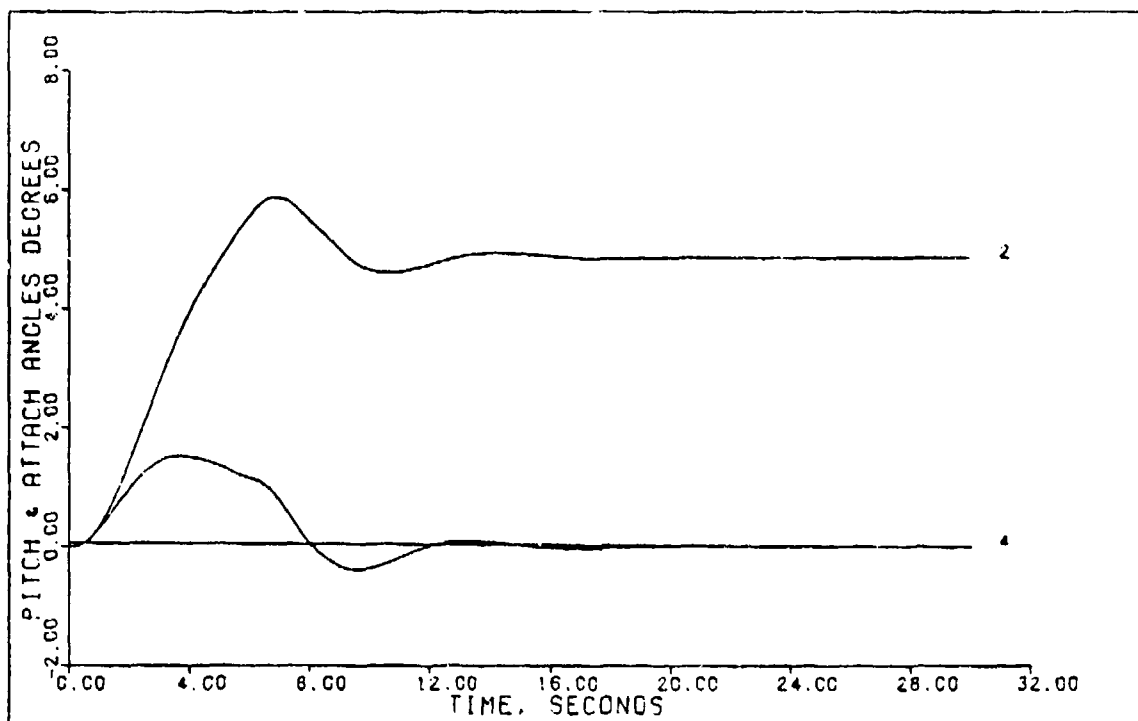


FIGURE 5-18e: Robust Controller Flight Condition #3, Normal Climb (State 2: Pitch Angle; State 4: Attack Angle)

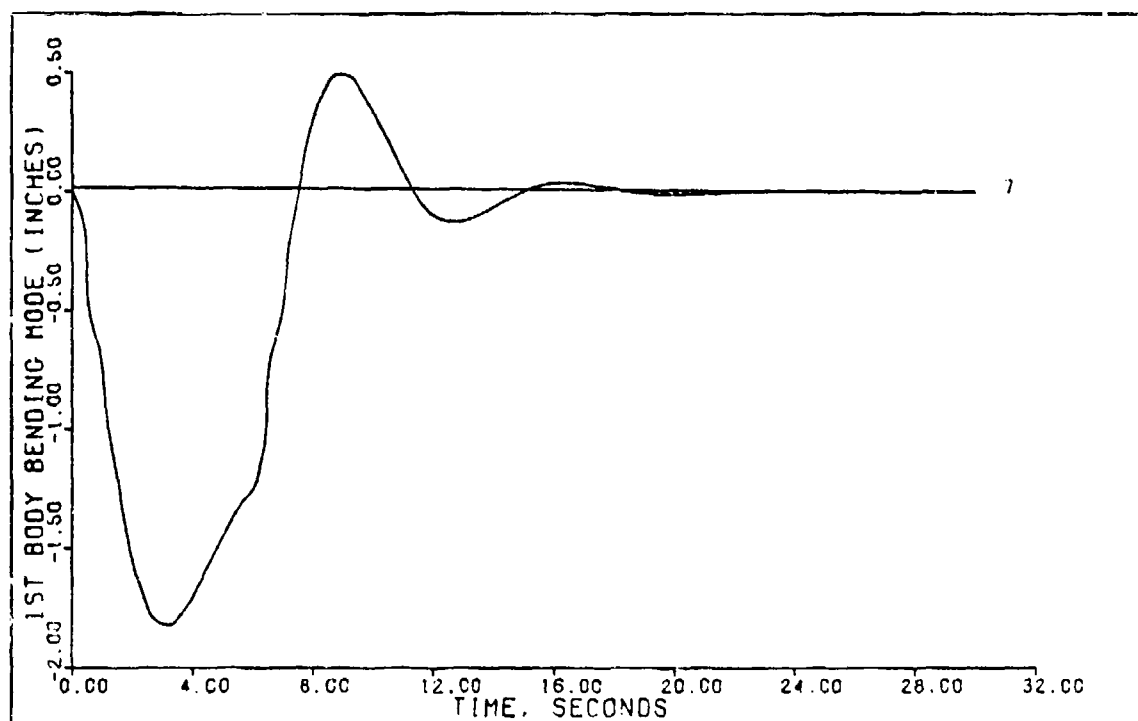


FIGURE 5-18f: Robust Controller Flight Condition #3, Normal Climb (State 7: 1st Body Bending Mode)

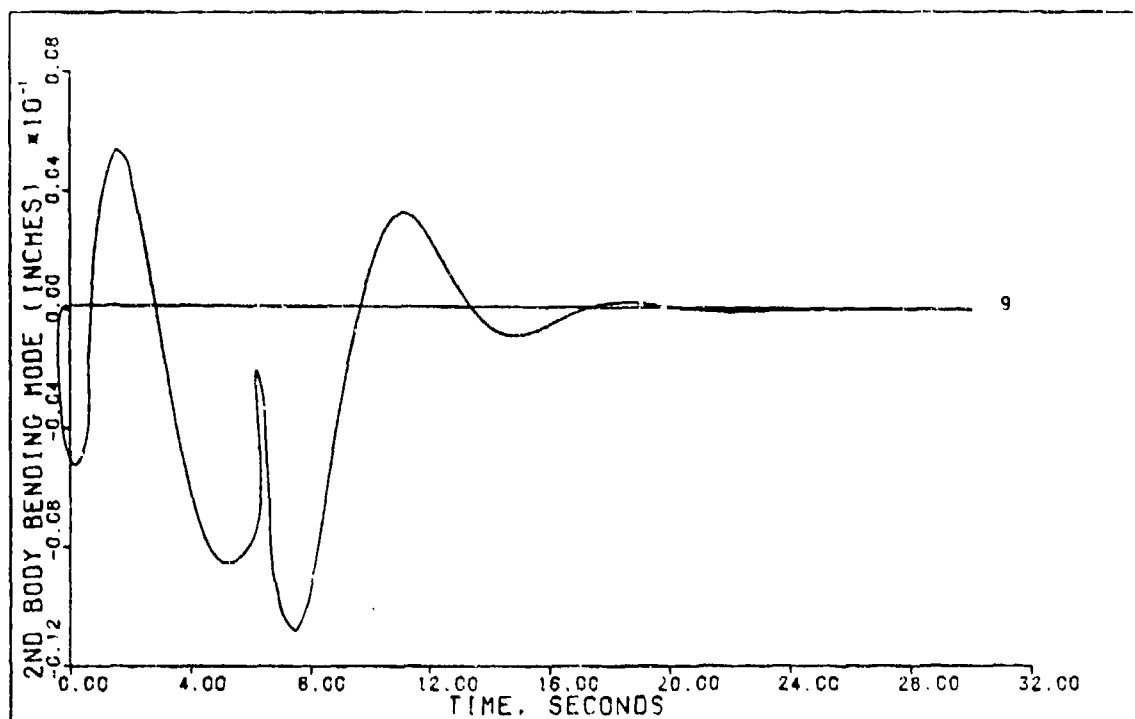


FIGURE 5-18g: Robust Controller Flight Condition #3,  
Normal Climb (State 9: 2nd Body Bending  
Mode)

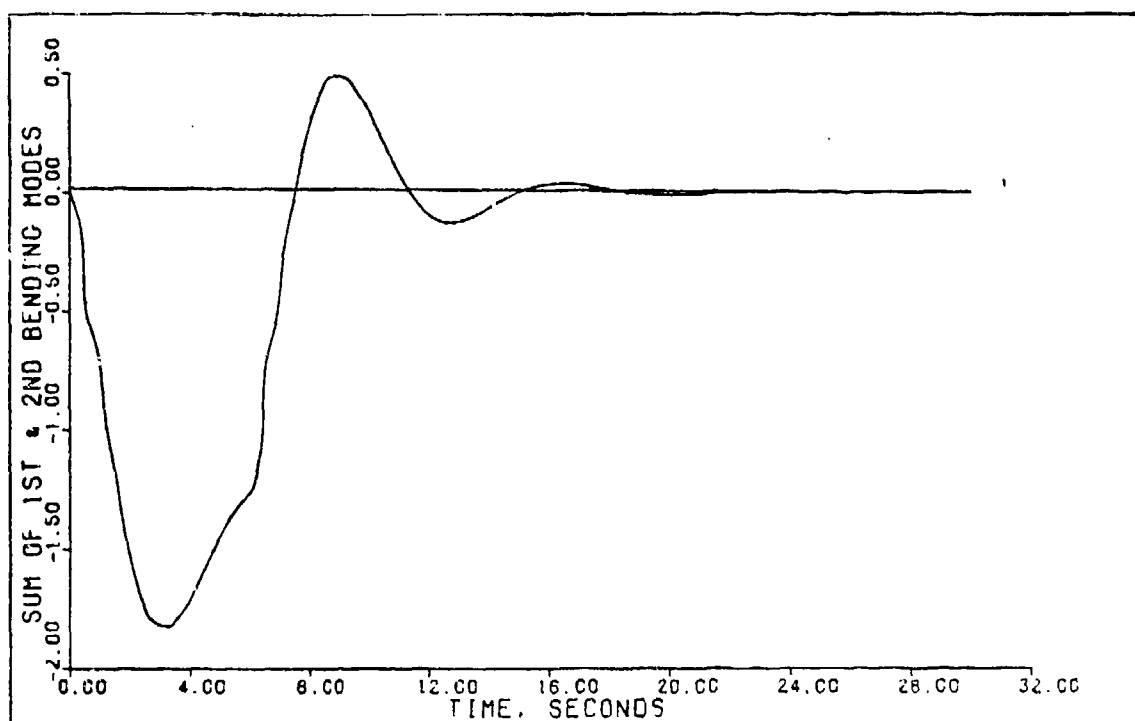


FIGURE 5-18h: Robust Controller Flight Condition #3,  
Normal Climb (Sum of 1st & 2nd Bending  
Modes)

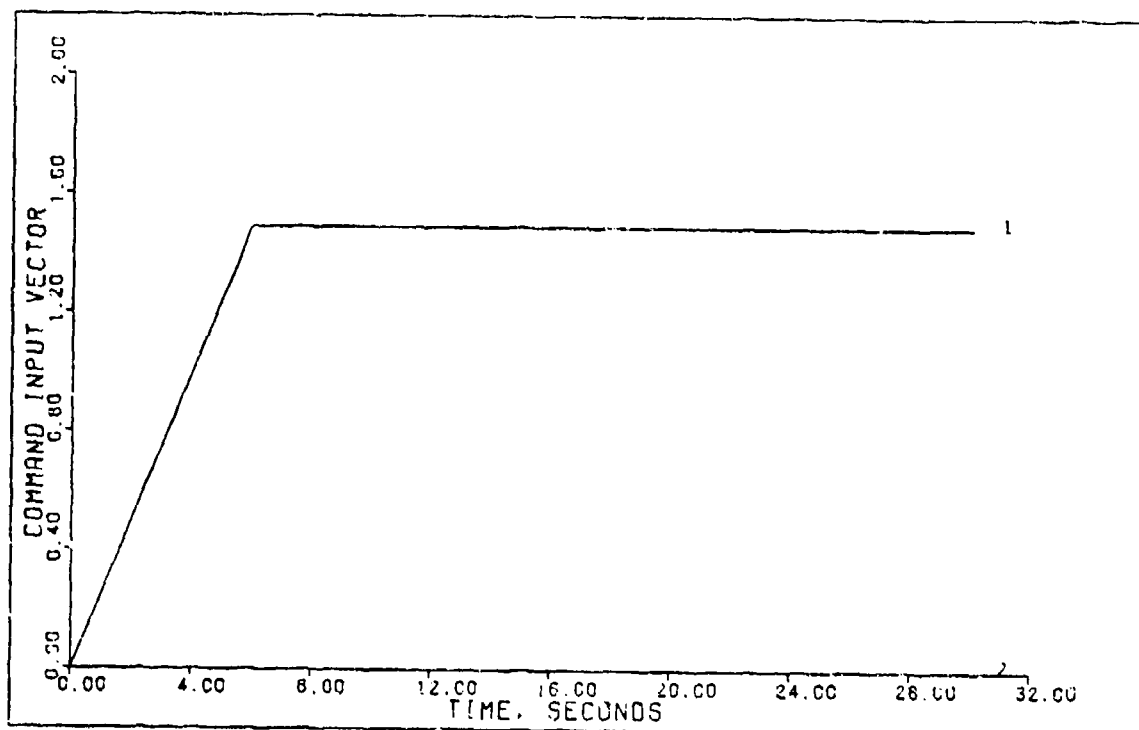


FIGURE 5-19a: Robust Controller Flight Condition #2, Normal Climb (Command Input Vector)

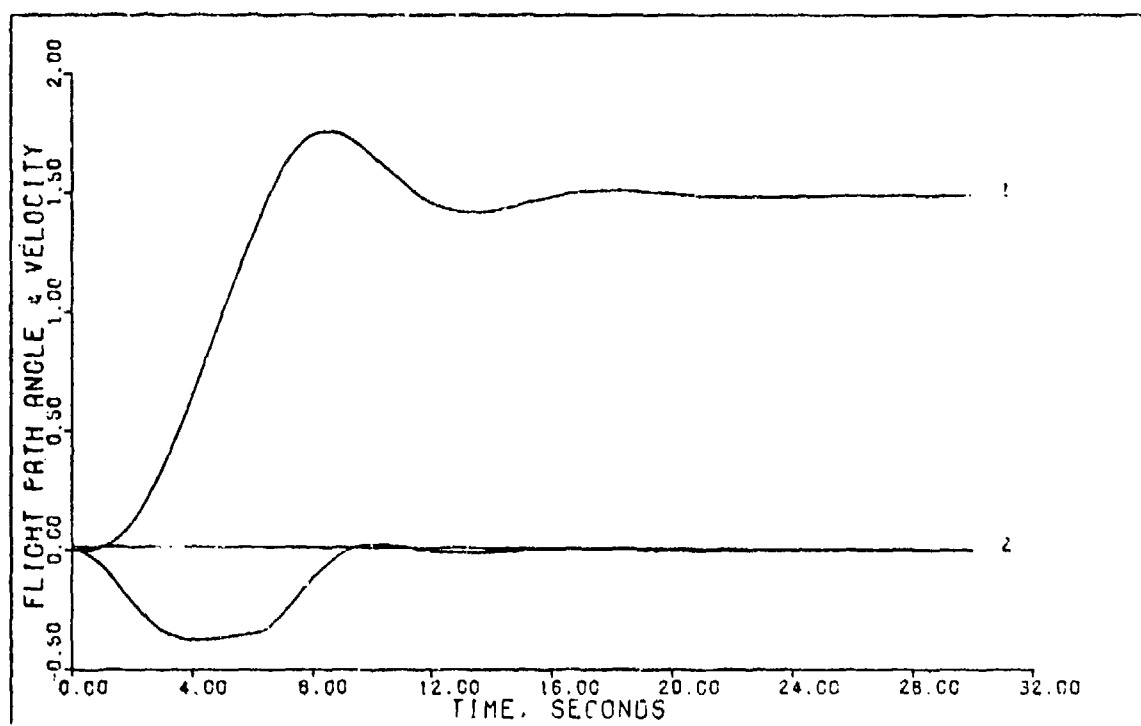


FIGURE 5-19b: Robust Controller Flight Condition #2, Normal Climb (Output 1: Flight Path Angle; Output 2: Velocity)

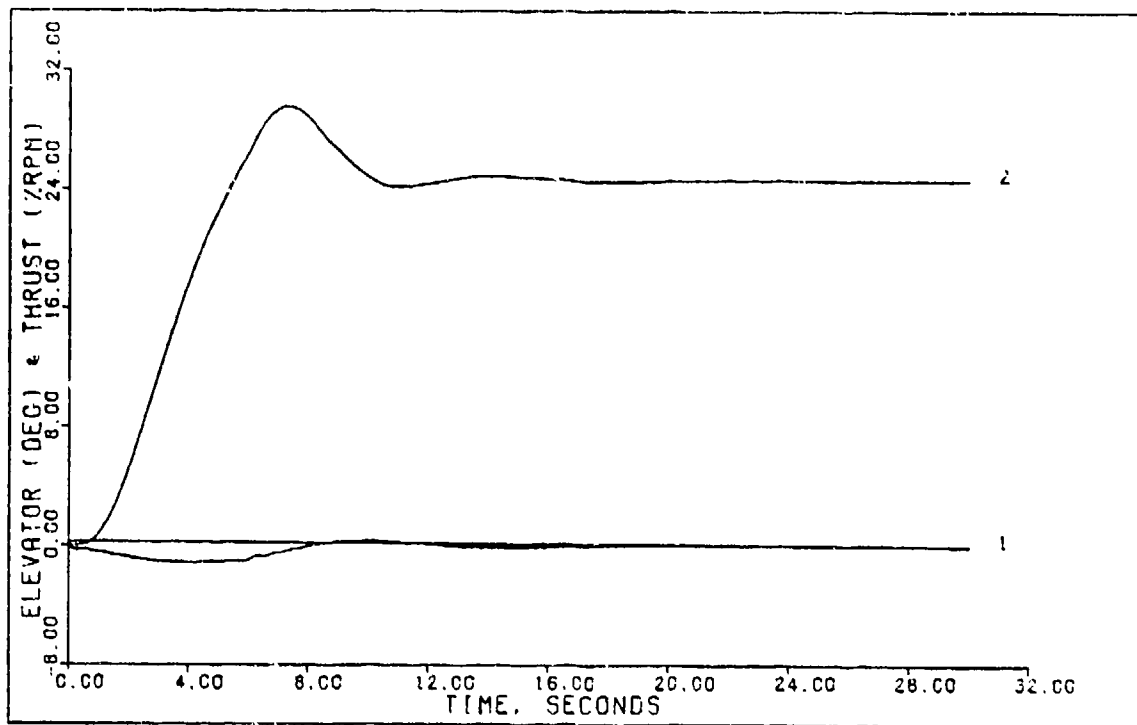


FIGURE 5-19c: Robust Controller Flight Condition #2, Normal Climb (Control 1: Elevator; Control 2: Thrust)

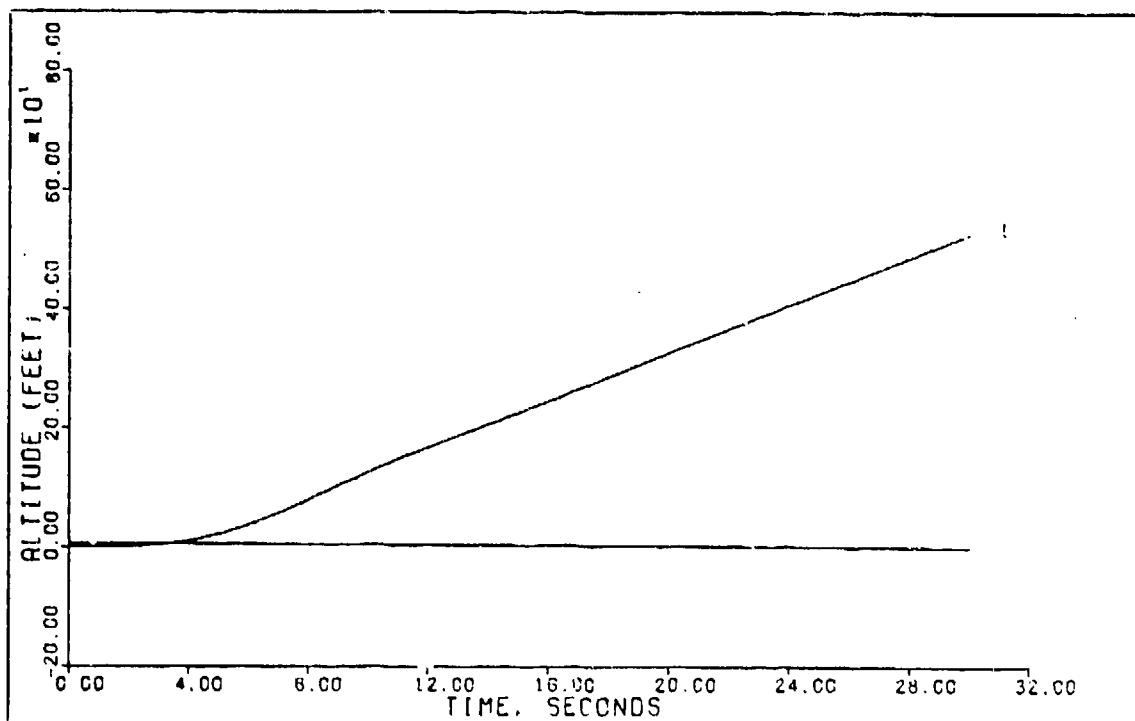


FIGURE 5-19d: Robust Controller Flight Condition #2, Normal Climb (State 1: Altitude)

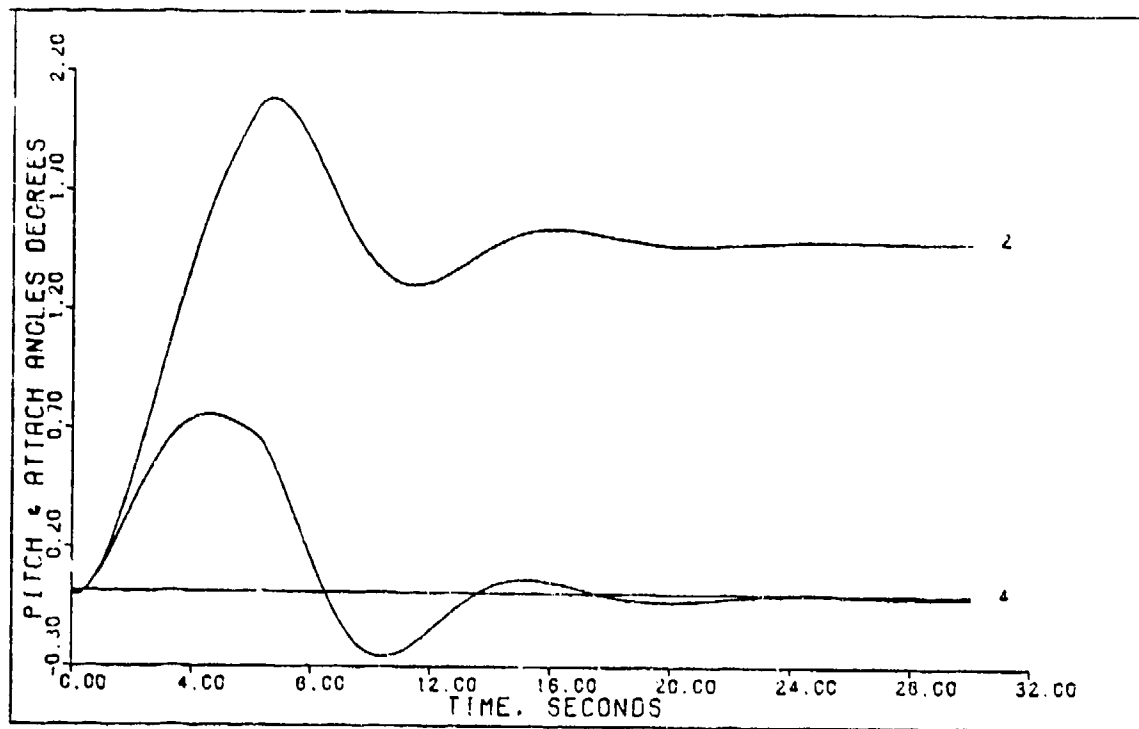


FIGURE 5-19e: Robust Controller Flight Condition #2,  
Normal Climb (State 2: Pitch Angle;  
State 4: Attack Angle)

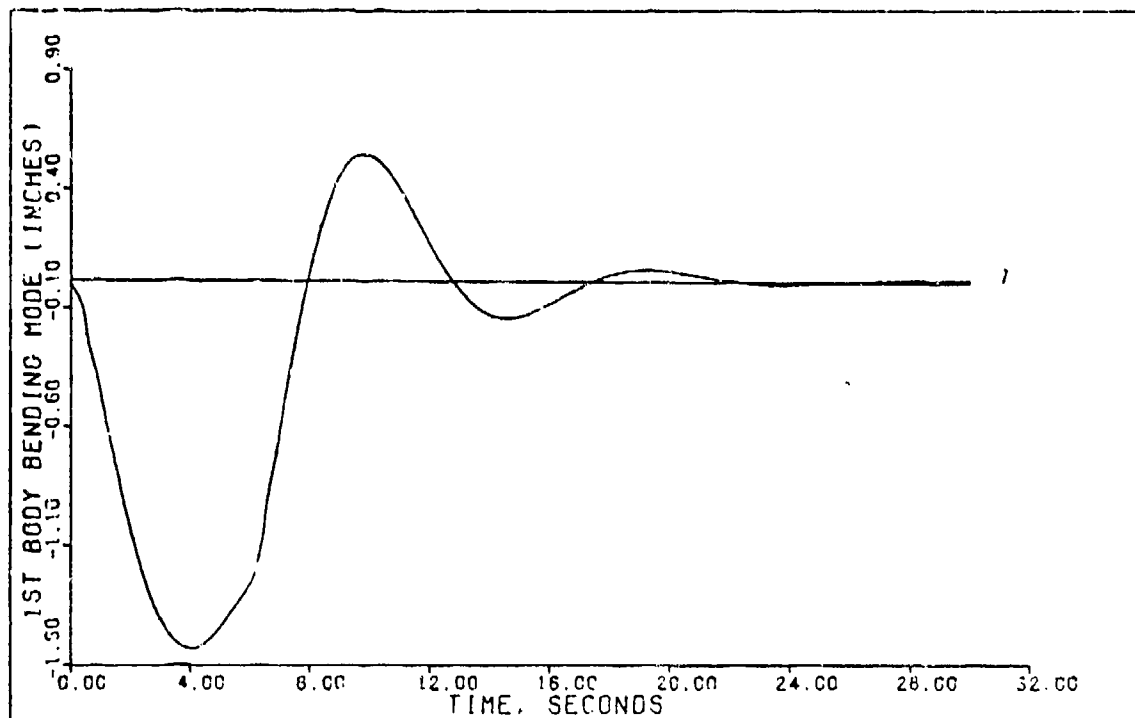


FIGURE 5-19f: Robust Controller Flight Condition #2,  
Normal Climb (State 7: 1st Body Bending  
Mode)



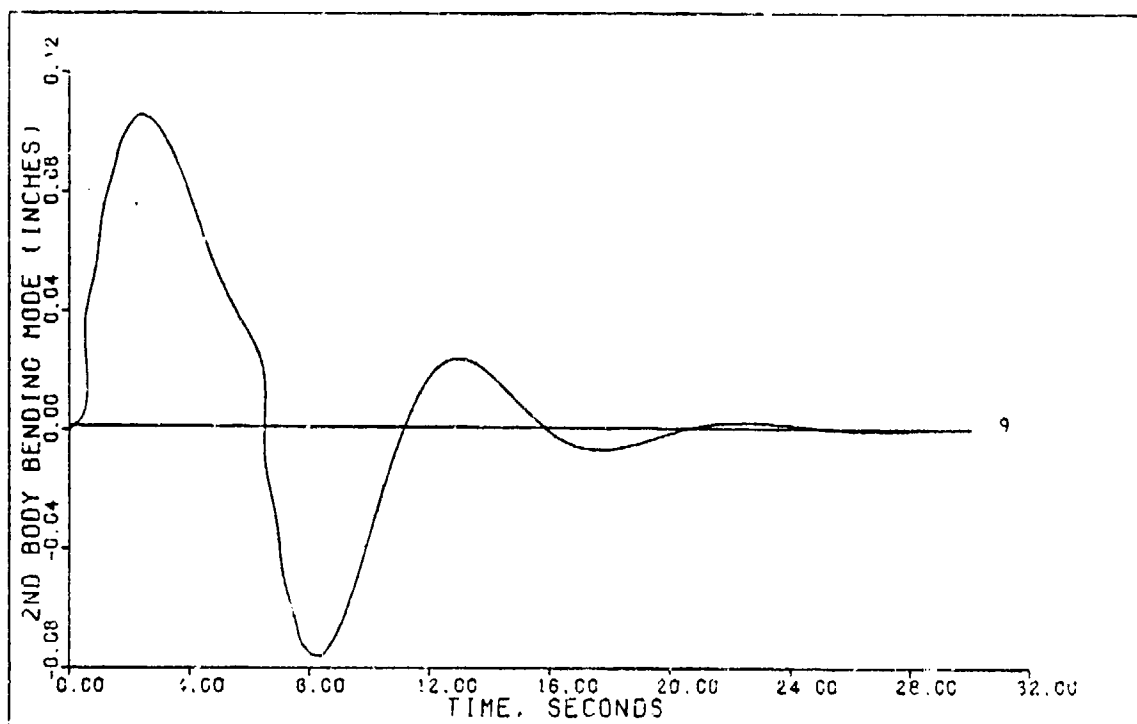


FIGURE 5-19g: Robust Controller Flight Condition #2, Normal Climb (State 9: 2nd Body Bending Mode)

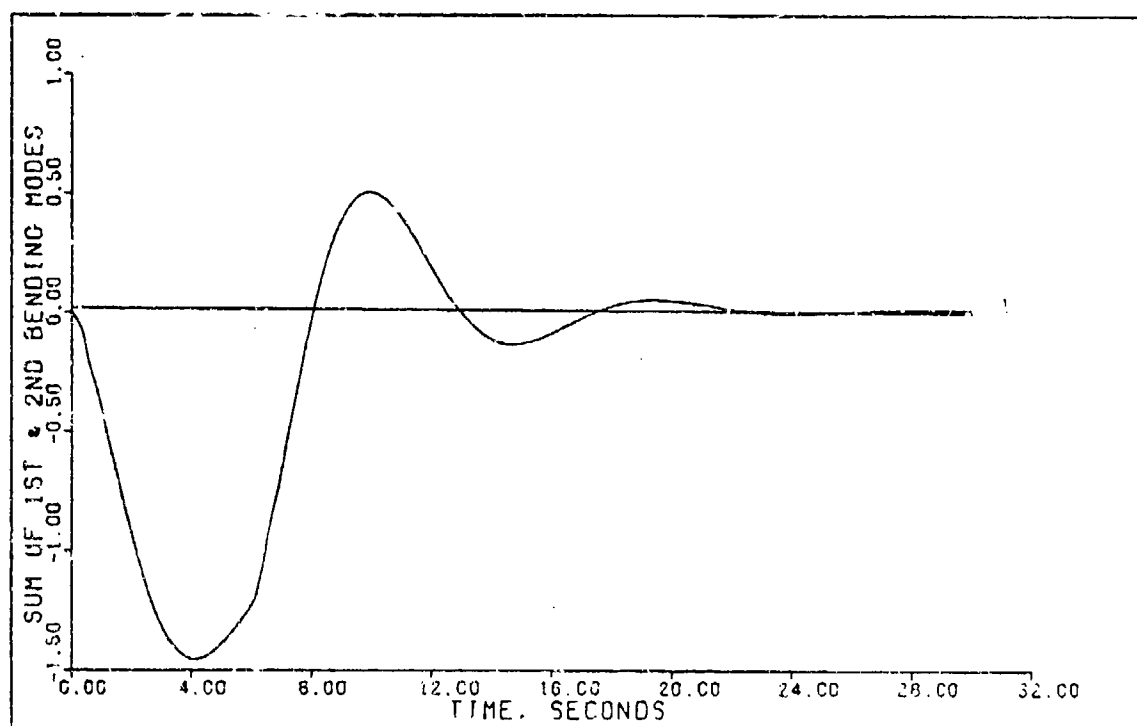


FIGURE 5-19h: Robust Controller Flight Condition #2, Normal Climb (Sum of 1st & 2nd Bending Modes)

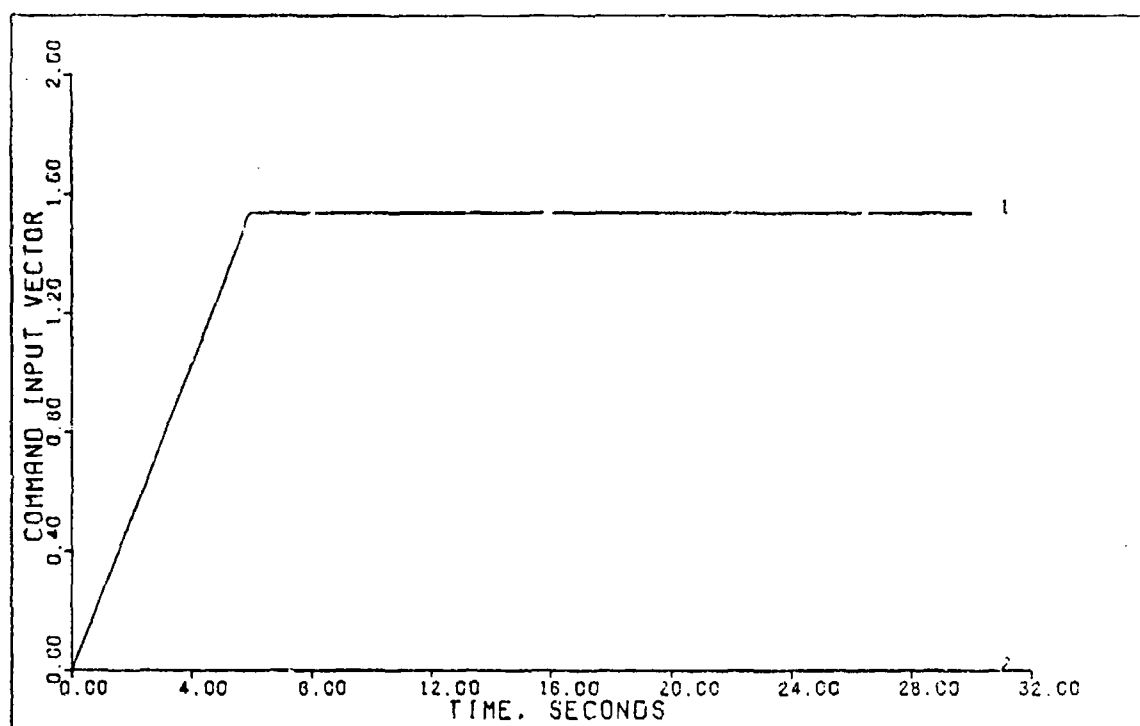


FIGURE 5-20a: Robust Controller Flight Condition #1, Normal Climb (Command Input Vector)

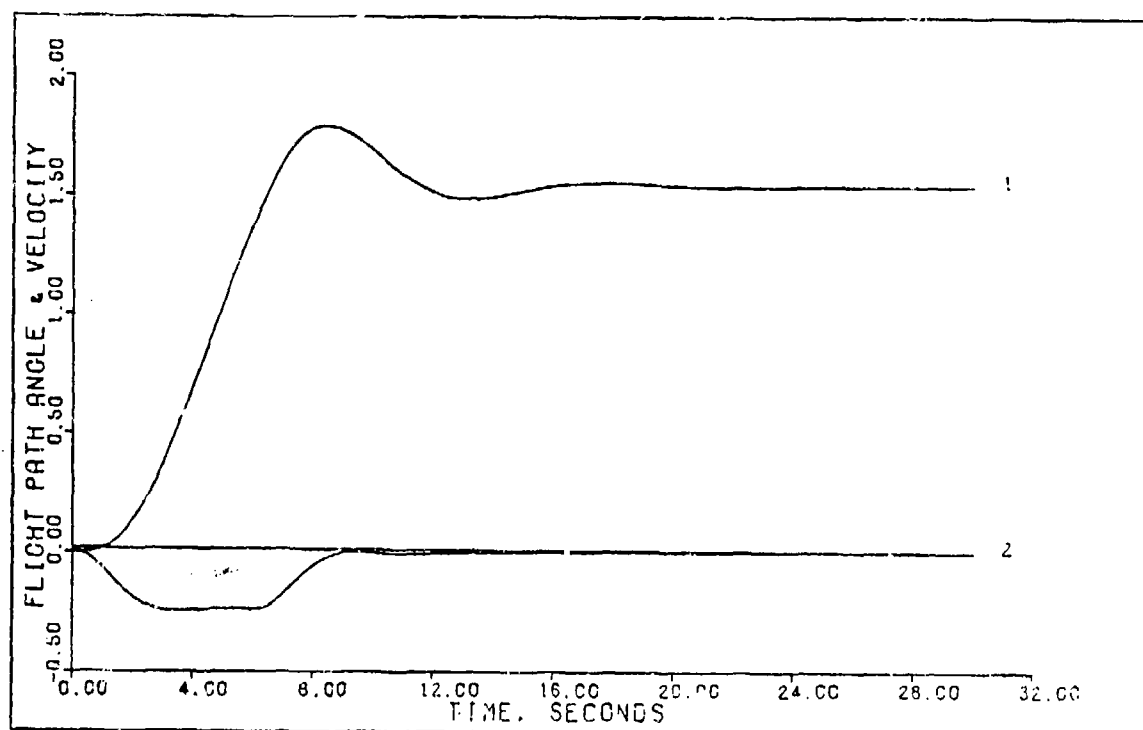


FIGURE 5-20b: Robust Controller Flight Condition #1, Normal Climb (Output 1: Flight Path Angle; Output 2: Velocity)

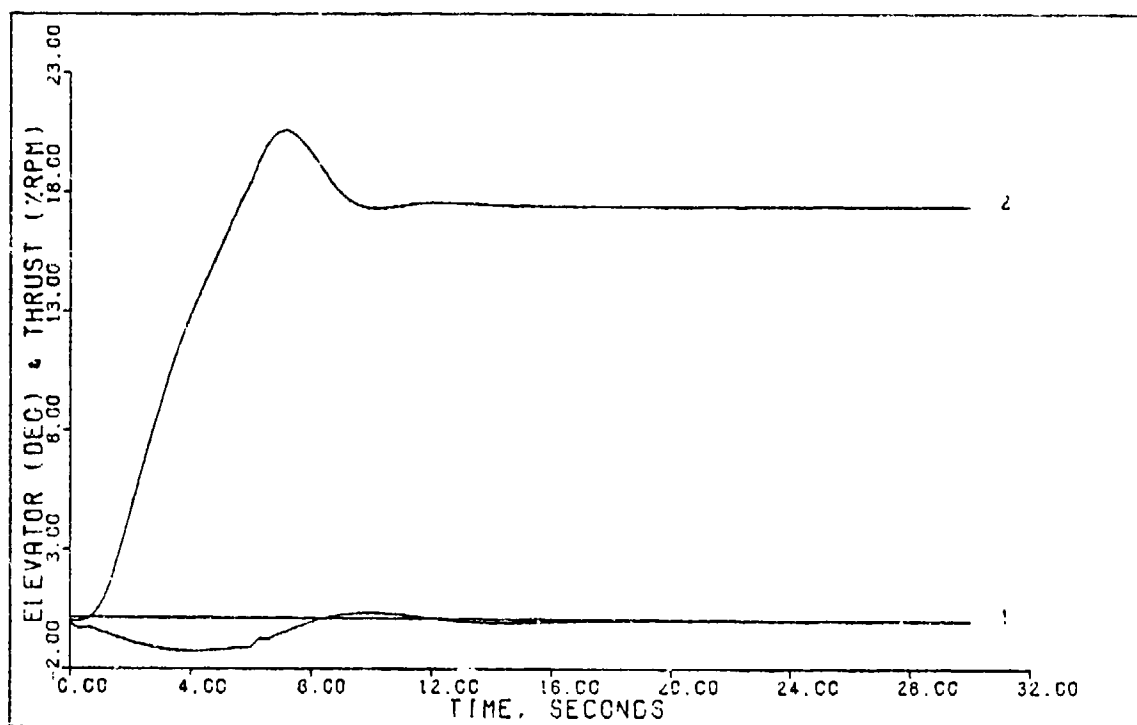


FIGURE 5-20c: Robust Controller Flight Condition #1, Normal Climb (Control 1: Elevator; Control 2: Thrust)

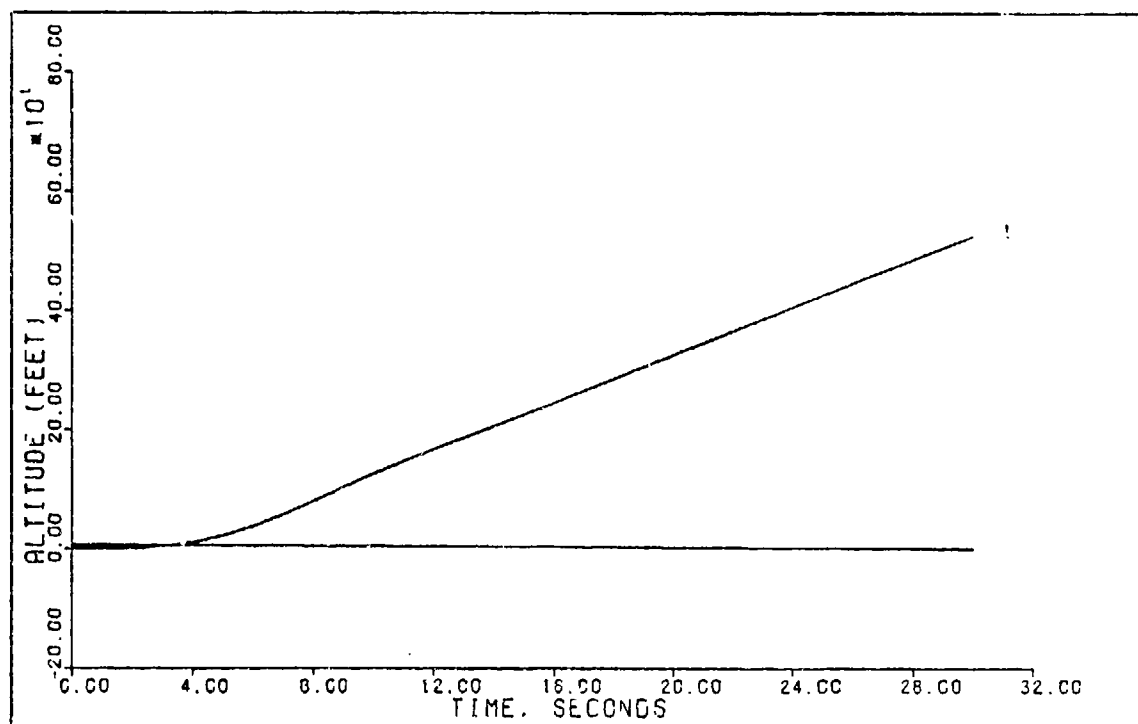


FIGURE 5-20d: Robust Controller Flight Condition #1, Normal Climb (State 1: Altitude)

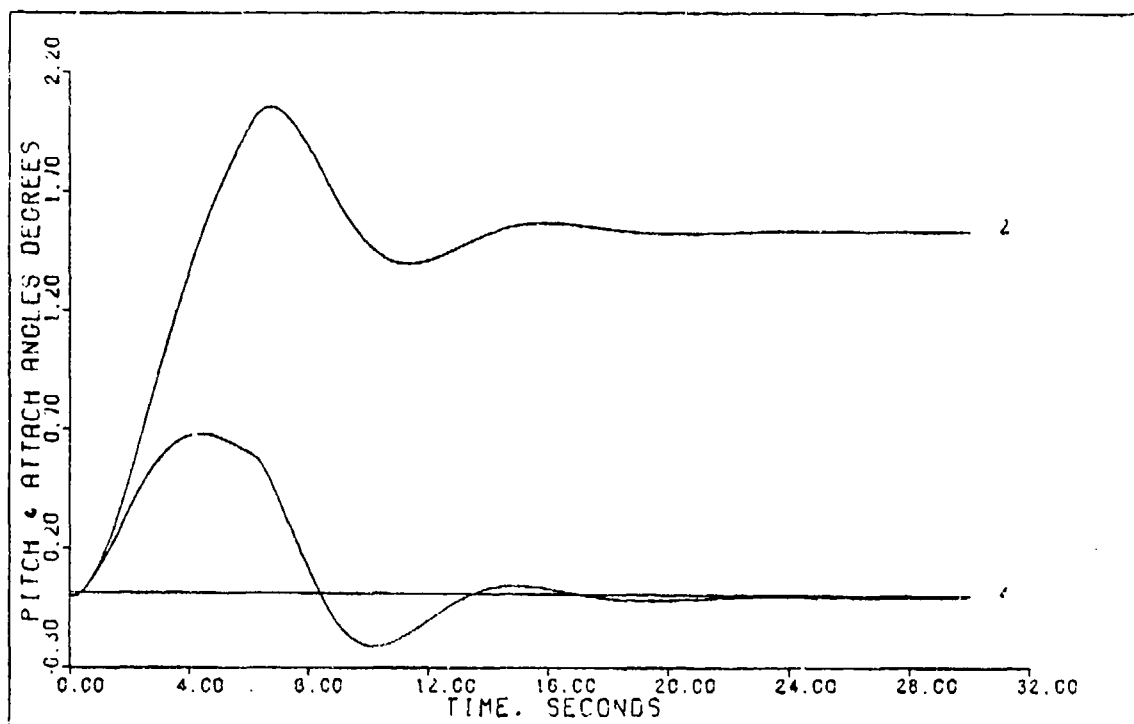


FIGURE 5-20e: Robust Controller Flight Condition #1,  
Normal Climb (State 2: Pitch Angle;  
State 4: Attack Angle)

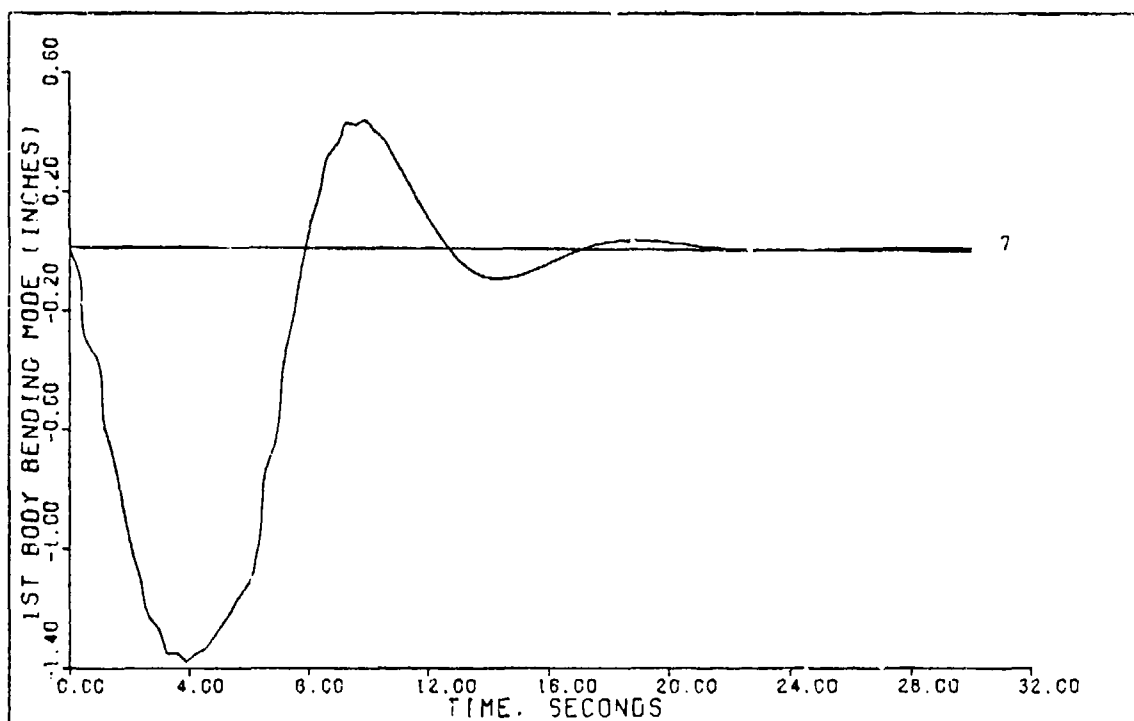


FIGURE 5-20f: Robust Controller Flight Condition #1,  
Normal Climb (State 7: 1st Body Bending  
Mode)

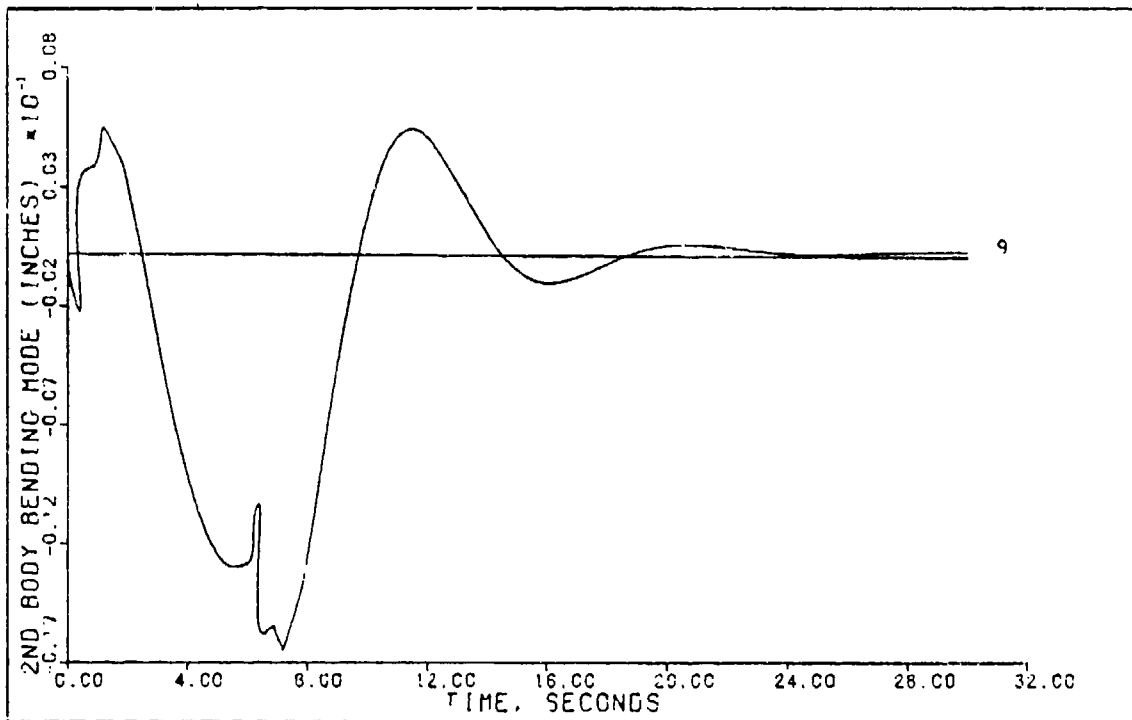


FIGURE 5-20g: Robust Controller Flight Condition #1, Normal Climb (State 9: 2nd Body Bending Mode)

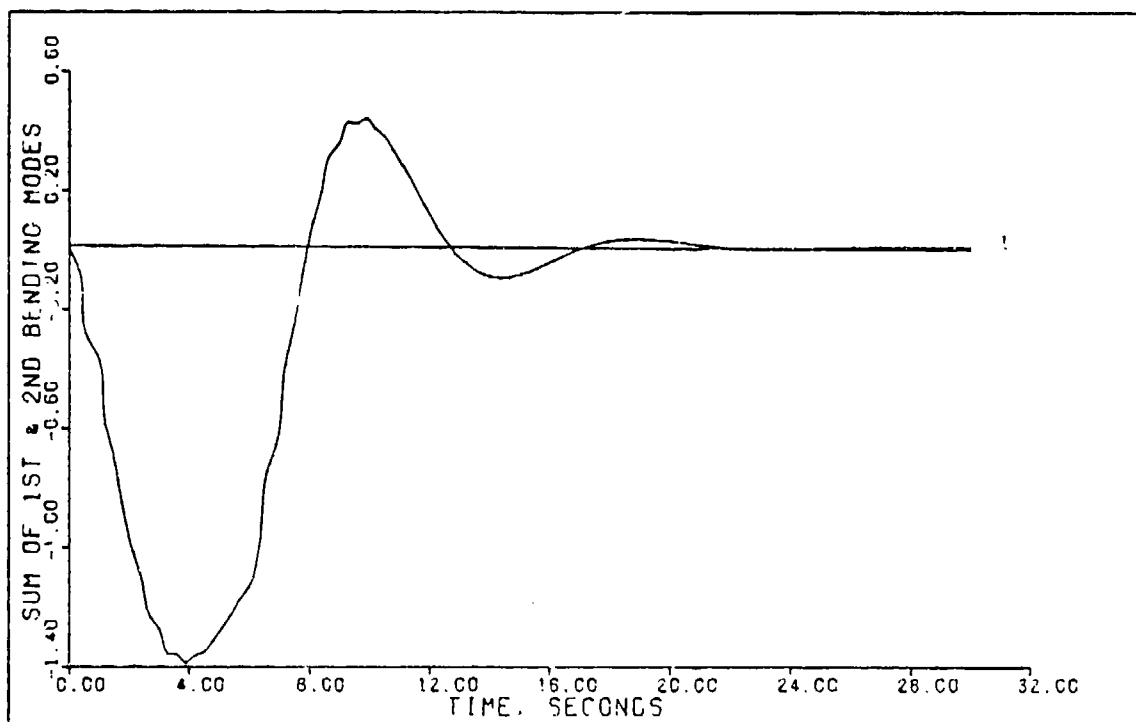


FIGURE 5-20h: Robust Controller Flight Condition #1, Normal Climb (Sum of 1st & 2nd Bending Modes)

Table 5-20  
Simulation Results For  
Robust Controller Flight Condition #1 Normal Climb

Input/ Output	Peak Value	Final Value	$t_p$ (sec)	$t_s$ (sec)
$\gamma$ (deg)	1.786	1.54	8.4	15.0
$u$ (ft/sec)	-0.247	--	3.6	--
$\delta_e$ (deg)	-1.25	--	--	--
$\delta_T$ (%RPM)	20.5	--	--	--

Robust Controller, Pitch Pointing Pitch pointing proved to be a difficult maneuver to perform from a robustness standpoint. In fact a robust controller that produces satisfactory results for all three flight conditions cannot be found. However, another purpose of this section is to show the effect of minimizing the  $K_0$  and  $K_1$  matrices used to perform maneuvers for flight condition #3. Using the controller given by Equations (5-109) thru (5-115) with  $K_0$  and  $K_1$  changed to Equations (5-126) and (5-127) which represent the minimum form, the maneuver is again simulated. Figures 5-21a thru 5-21h and Table 5-21 show the results of this minimum K controller. These results again show that selective elements of the  $K_0$  and  $K_1$  matrices can be set to zero without affecting simulation results.

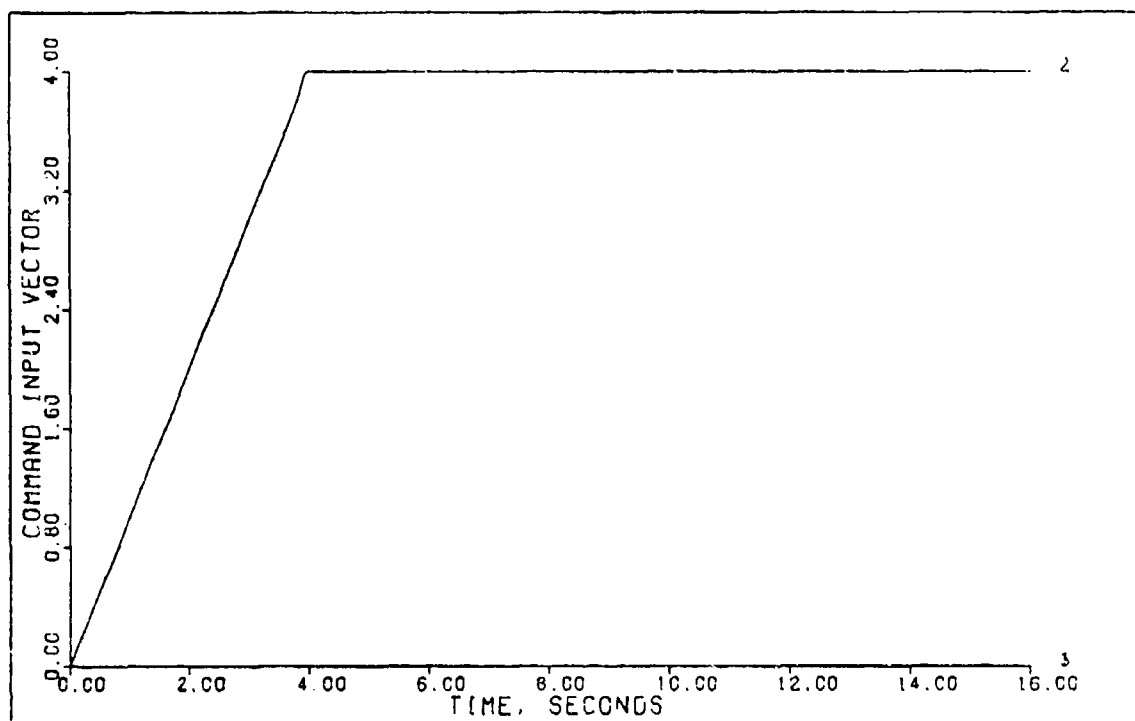


FIGURE 5-21a: Flight Condition #3, Pitch Pointing With Time Delay, Minimum K (Command Input Vector)

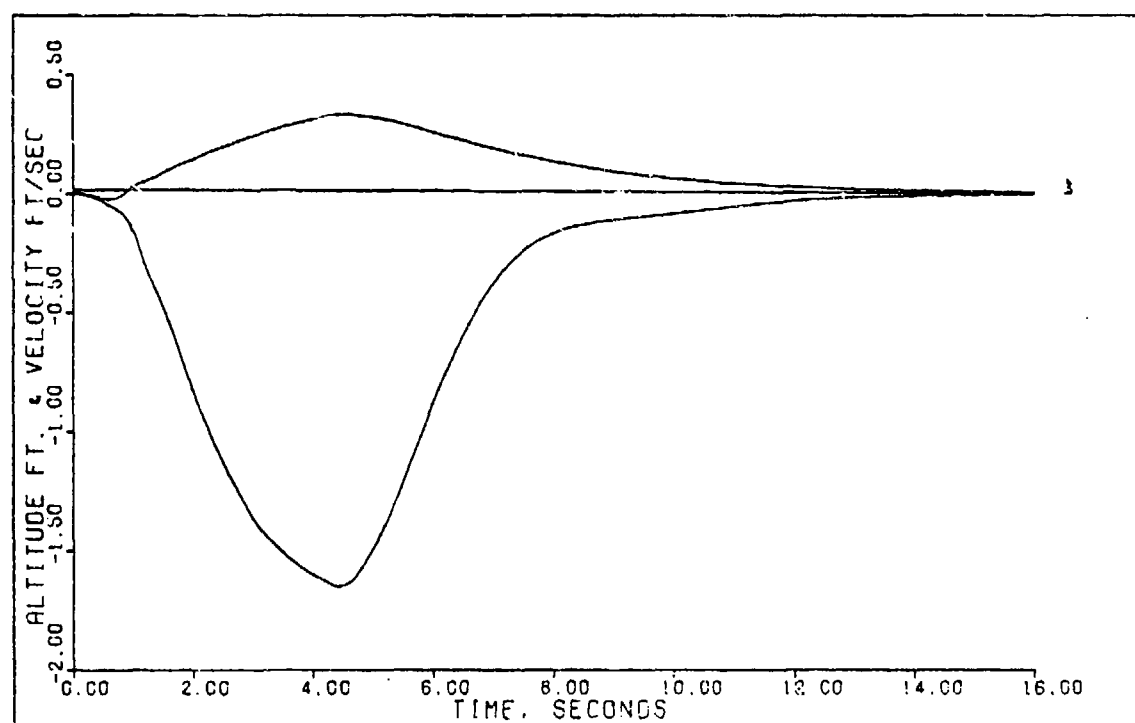


FIGURE 5-21b: Flight Condition #3, Pitch Pointing With Time Delay, Minimum K (Output 1: Altitude; Output 2: Velocity)

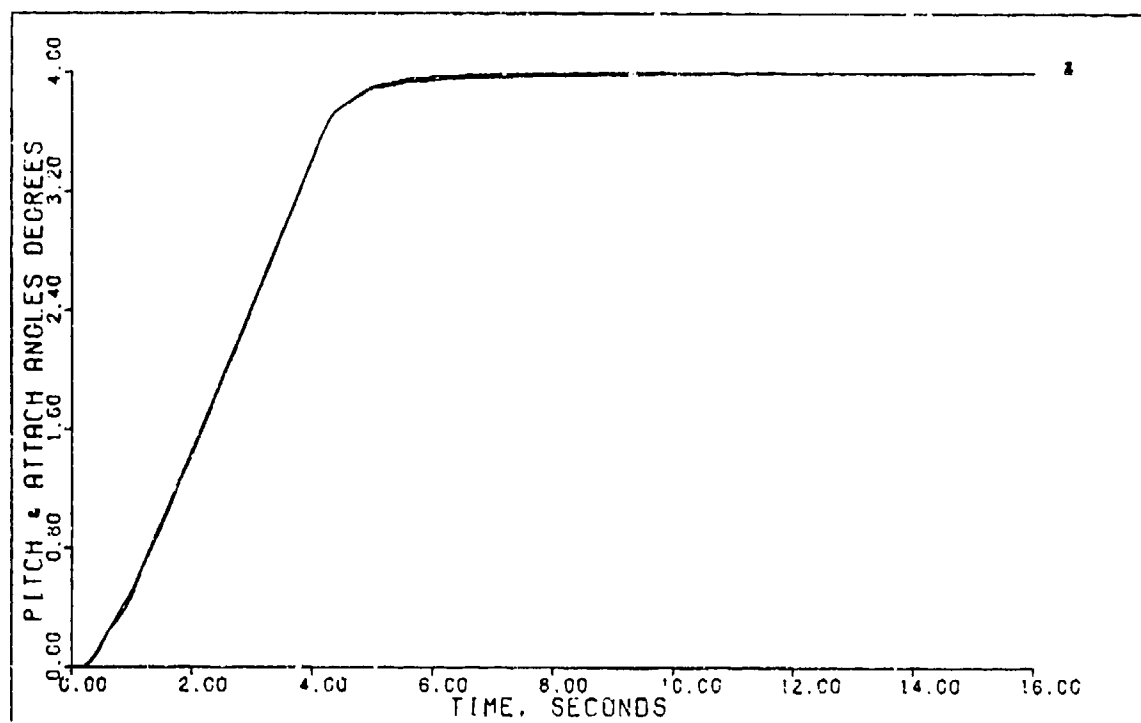


FIGURE 5-21c: Flight Condition #3, Pitch Pointing With Time Delay, Minimum K (State 2: Pitch Angle; State 4: Attack Angle)

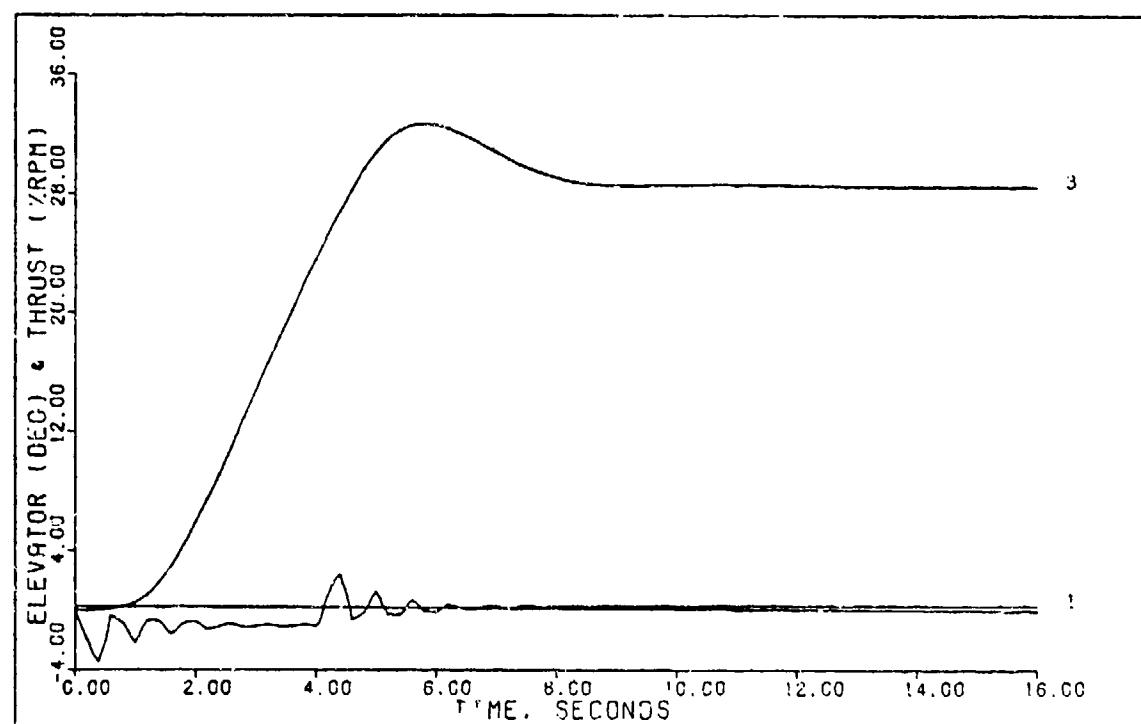


FIGURE 5-21d: Flight Condition #3, Pitch Pointing With Time Delay, Minimum K (Control 1: Elevator; Control 2: Thrust)



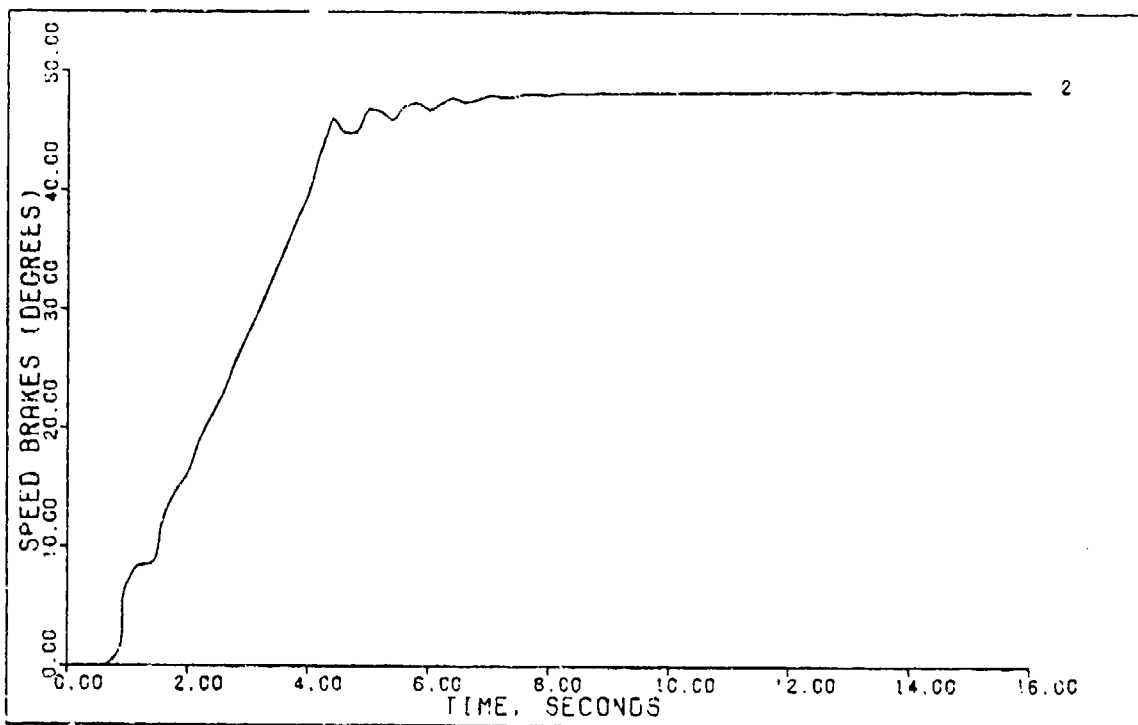


FIGURE 5-21e: Flight Condition #3, Pitch Pointing With Time Delay, Minimum K (Control 3: Speed Brakes)

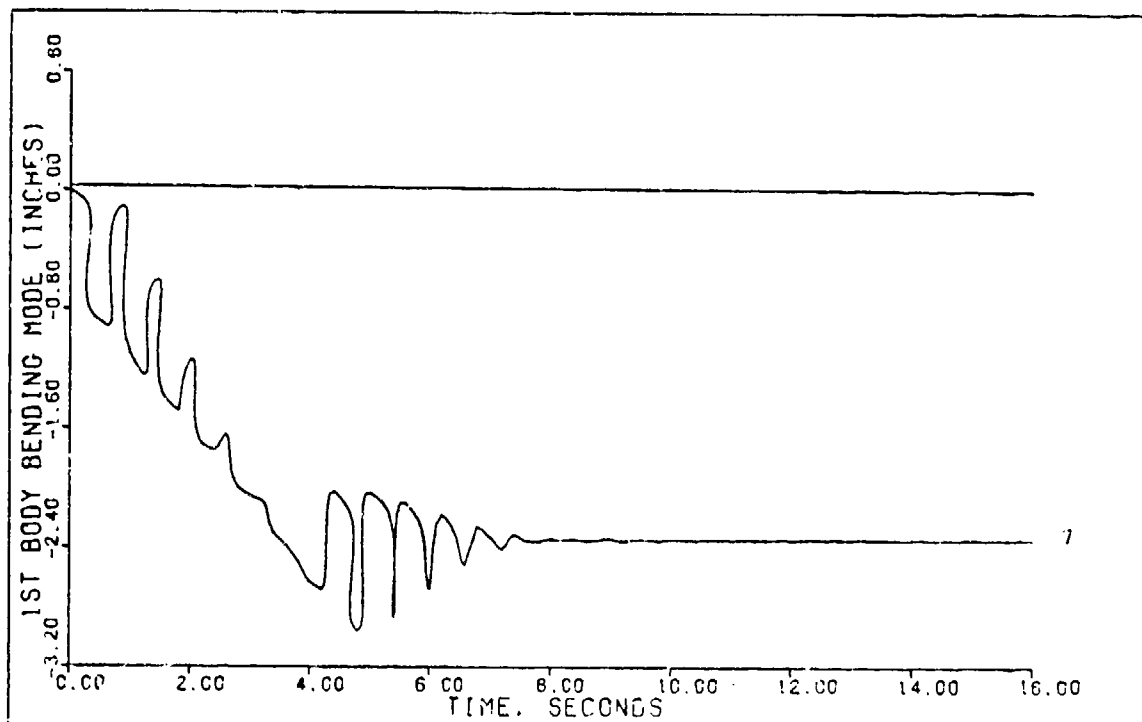


FIGURE 5-21f: Flight Condition #3, Pitch Pointing With Time Delay, Minimum K (State 7: 1st Body Bending Mode)

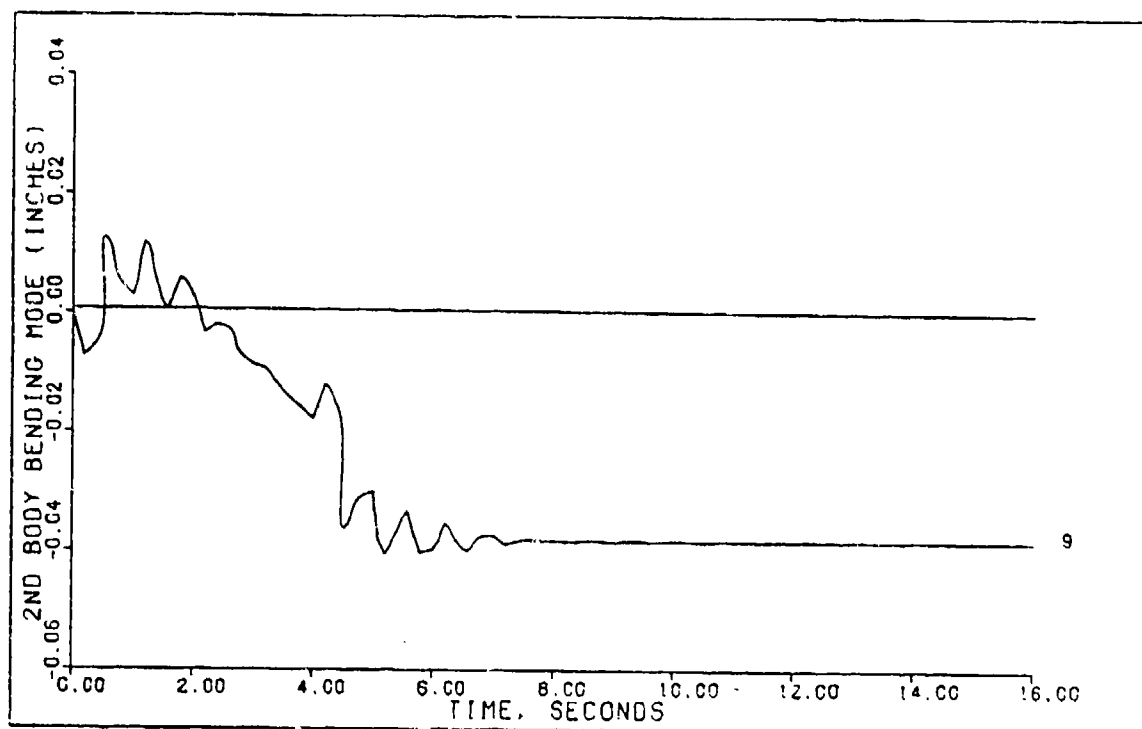


FIGURE 5-21g: Flight Condition #3, Pitch Pointing With Time Delay, Minimum K (State 9: 2nd Body Bending Mode)

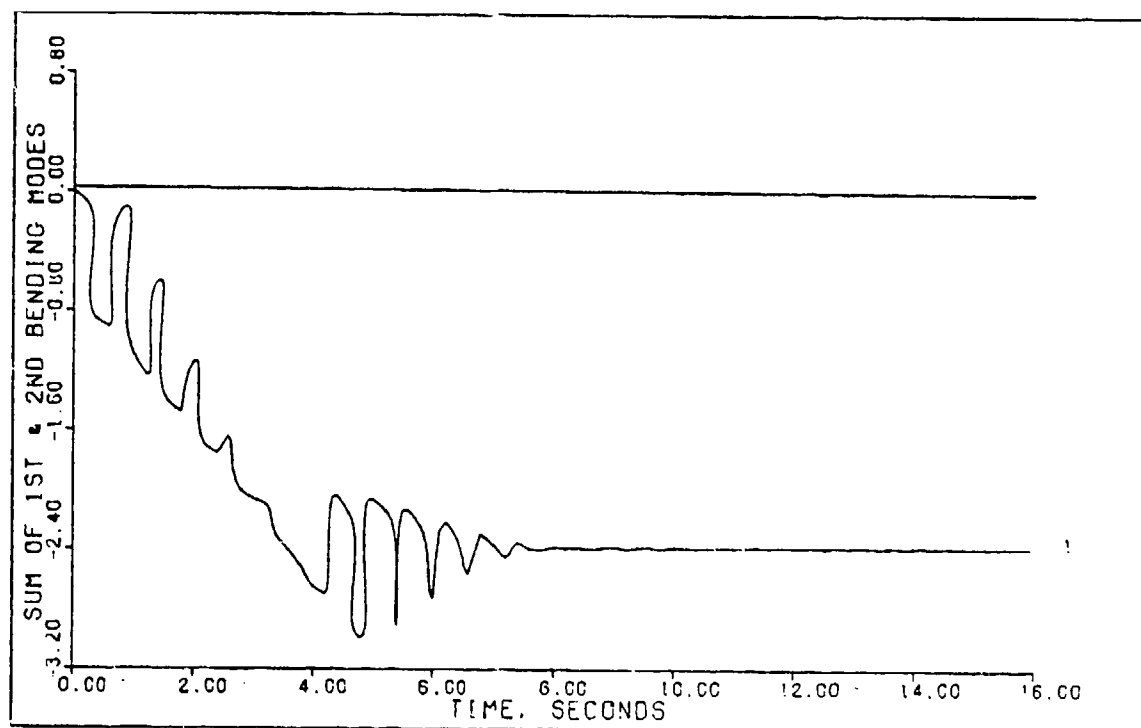


FIGURE 5-21h: Flight Condition #3, Pitch Pointing With Time Delay, Minimum K (Sum of 1st and 2nd Bending Modes)

Table 5-21  
Simulation Results For Pitch Pointing  
With Time Delay Flight Condition #3 Minimum K

Input/ Output	Peak Value	Final Value	$t_p$ (sec)	$t_s$ (sec)
h (ft)	0.598	0.0	4.6	--
$\theta$ (deg)	4.0	4.0	16.0	5.2
u (ft/sec)	-0.899	0.0	3.0	--
$\delta_e$ (deg)	5.0	--	--	--
$\delta_{sb}$ (deg)	52.0	--	--	--
$\delta_T$ (%RPM)	32.0	--	--	--

### Conclusion

This chapter presents the design results for the KC-135A aircraft. Design procedures along with tracker control laws are presented for each of the three flight conditions studied. Simulation results in the form of Calcomp plots for the maneuvers of flight condition #3 are also presented. Plots for the maneuvers of flight conditions #1 and #2 are given in Appendix C. Also included in the chapter are the effect of computational time delay on the maneuvers performed for flight condition #3. Finally robustness is checked, using what is called minimum K designs.

## VI. CONCLUSION AND RECOMMENDATIONS

### Thesis Summary

This thesis is designed to demonstrate the use of Professor Brian Porter's multivariable control law techniques in synthesizing digital controllers for the KC-135A.

Chapter I presents an introduction to the study area. Chapter II gives a brief overview of the control law theory for unknown, known/regular, known/irregular, and B\* design techniques. Chapter III describes the KC-135A aircraft. Chapter IV introduces the concepts of computational time delay and presents the modifications made to MULTI to incorporate a time delay. Chapter V describes the actual development and analysis of the control laws developed for the KC-135A. This includes presentation and discussion of the effects of computational time delay on control law performance. Also included in Chapter V is the development of a robust controller for each flight maneuver, which is capable of performing a single maneuver over the entire range of flight conditions. This robust controller is of the minimum K form.

Appendix A presents the development on the aircraft equations of motion along with tabular listings of stability axes and body axes derivatives for the KC-135A describing each of the three flight conditions studied. Appendix B gives an example of the output of the computer program CAT

used to transform stability axes derivatives to body axes. Simulation data for each of the maneuvers performed for flight conditions one and two are presented in Appendix C. Appendix D describes a fix incorporated by this author to provide properly scaled calcomp plots when using the computer program MULTI. Appendix E describes the debugging of the fortran code for MULTI that was necessary in order to incorporate the computational time delay of Chapter IV. Appendix F presents a method of transforming state equations to the  $O-B_2$  form of Chapter II.

### Conclusions

This research work demonstrates that tracker control laws can be synthesized for the KC-135A aircraft using the singular perturbation methods developed by Professor Brian Porter. The controllers designed are able to tightly track the command inputs and at the same time provide for a high degree of output decoupling.

As more constraints are placed on the system, such as control surface actuators and computational time delays, it becomes increasingly difficult to provide for desired output tracking without inducing unacceptable control surface deflections. In almost all cases some compromise has to be made between system performance and control surface deflections. Chapter V points out the occurrence of these compromises for the maneuvers of flight condition # 3 as they occur.

Chapter V also introduces a reduced form for the control laws developed. The reduced models are called minimum K designs. The results of these minimum K controllers demonstrate the feasibility of reducing the required number of feedback gains.

Results of the robustness test again show the sensitivity of the control surfaces to parameter changes. This control surface sensitivity, that keeps occurring, suggest the importance of actuator models. Simple first order actuators are used in this study but higher order models including some sort of prefilter may be required.

The use of MULTI in the development of multivariable tracker controllers produces relatively good design with a very moderate expenditure of manpower. Once the user becomes familiar with the use of MULTI and the effect of parameter change on design results, a design can easily be performed in an afternoon. The only disadvantage to this method proved to be the sensitivity of the control surface deflections, apparently caused by the high-gain nature of the design.

Several days before the due date for this thesis an error was discovered in the fortran code for the simulation portion of MULTI. This error has since been corrected. The error causes some of the correct simulation results to differ from those given in Chapter V. This discovery was made too late for the results to be included in this thesis. However, some of the changes are worth noting. First the

settling times for the given maneuvers increase slightly, approximately 0.2 seconds. This however could probably be reduced, if desired, by redesigning the controllers. Second, and most important, the sideslip maneuver in Chapter V is performed with a controller that differs from the one used to perform the coordinated turn. The reason for this change is given in Chapter v. However, with the code changed to correct for the error, this problem no longer exists and the controller used to perform the coordinated turn will now work equally as well for the sideslip maneuver. Other changes that occur are very small and would not significantly modify the results given in Chapter V.

### Recommendations

The recommendations that are presented in the following paragraph are a direct result of problems encountered in the completion of this thesis. These problems resulted in an indepth study of the computer code for MULTI, especially in the code involving the simulation and calcomp routines. Thus, some of the recommendations pertain to MULTI itself.

Appendix A gives the state space representation for the lateral model. In the designs presented in Chapter V the outputs are chosen as angles, specifically the roll angle and the sideslip. This results in the matrix product  $CB$  having rank deficiency. Thus the need for an irregular design requiring a measurement matrix. If instead of angles, rates are used, specifically roll rate and yaw rate

the matrix product  $CB$  would have full rank and the measurement matrix would not be required. This design however has transmission zeros in the right half of the  $s$ -plane. A design was attempted on this model, however, limited results were obtained since the aircraft proved to be unstable. By increasing the sampling time to 0.1 seconds the aircraft became stable provided no actuators were used. Thus the first recommendation is for more research to be conducted on plants having unstable transmission zeros in order to determine the feasibility of the design methods on this type of system.

An accurate means of locating transmission zeros for plants not in the  $0-B_2$  form of Equations (2-22) and (2-23) is needed. However, if the plant can be expressed in the form of these equations, then the transmission zeros can be found by using Equation (2-41) for regular plants or Equation (2-63) for irregular plants. Thus an option in MULTI that would transform state equations to the  $0-B_2$  form of Equations (2-22) and (2-23) would be helpful. This would also allow for easy implementation of Equations (2-41) and (2-63) to determine the exact location of the transmission zeros. Appendix F presents a simple method for determining a transformation matrix that will perform this transformation with minimum affect on the state vector.

Another area that needs additional attention is the implementation of actuator dynamics. Current choices include embedding them in the  $A$  matrix as is done in



Reference 16, or adding them to MULTI via Option # 4. MULTI's simulation, Option # 26, handles these two methods very differently. This stems from the fact that MULTI makes a call to ODE once during each execution of the inner loop of the simulation. Thus, a full analysis of the simulation portion of MULTI pertaining to these differences should be accomplished. This indeed is necessary since the conclusions of this thesis show that actuator dynamics play an important part in the design process.

When using MULTI, if an Option is entered by mistake, it must be allowed to finish since there is no way to exit it without terminating the program. Reference 17 describes another interactive program, TOTAL, that allows for an exit of an unwanted option by inserting a \$ as a response to any requested prompt. This produces an extremely user friendly atmosphere that would surely be beneficial to future MULTI users.

Finally MULTI currently is restricted to 100k of core memory in order to run interactively on the Cyber. Addition of the recommended options, discussed earlier, could cause MULTI to exceed this limit since it is currently approaching it. Thus a major modification of the program to provide for more efficient use of memory allocations is essential. Concentration of this effort should be placed on the simulation and Calcomp routines.

## Bibliography

1. Chandler, Phillip. "Proposed AFIT Thesis Topic #I-29" Handout. Wright-Patterson AFB, Ohio: AFWAL/FIGL, April 1983.
2. Porter, B. and A. Bradshaw. "Singular Perturbation Methods in the Design of Tracking Systems Incorporating Fast-Sampling Error-Actuated Controllers," International Journal of System Science 12(10): 1181-1192 (October 1981).
3. Masi, Michael A. Digital Multivariable Tracker Control Laws For The C-141-A Starlifter Aircraft MS Thesis. Air Force Institute of Technology, Wright-Patterson AFB, Ohio; December 1982. (AFIT/GE/EE/82D-47)
4. Porter, Douglas S. Design and Analysis of a Multivariable Digital Controller for the A-7D DIGITAC II Aircraft and the Development of an Interactive Computer Design Program MS Thesis. Air Force Institute of Technology, Wright-Patterson AFB, Ohio; December 1981. (AFIT/GE/EE/81D-48)
5. Porter, B. Design of High Performance Tracking Systems USAME/DC/120/81. Air Force Flight Dynamics Laboratory, Wright-Patterson AFB, Ohio. October 1981.
6. Porter, B. Design of Set Point Tracking And Disturbance Rejection Controllers for Unknown Multivariable Plants Progress Report for Period 15 November 1980 to 31 December 1980. USAME/DC/101/81. Air Force Flight Dynamics Laboratory, Wright-Patterson AFB, Ohio. January 1981.
7. Lewis, Tom. High-Gain Error Actuated Flight Control Systems for Continuous Multivariable Plants MS Thesis. Air Force Institute of Technology, Wright-Patterson AFB, Ohio; December 1982.
8. Ridgely, D. E., S. Banda, and J. J. D'Azzo. "Decoupling of High-Gain Multivariable Tracking Systems." Paper No. AIAA-83-0280, Presented at AIAA 21st Aerospace Sciences Meeting, January 10-13, 1983/Reno, Nevada.
9. Porter, B. "Design of Turnable Non-Undershooting Servomechanisms," Correspondence with Dr. J. J. D'Azzo, Wright-Patterson AFB, Ohio: Air Force Institute of Technology, 1981.
10. Boeing Company. KC/EC/RC-135 Aerodynamic Characteristics Mission Simulators Document Number D3-9782-2, Contract No. F34601-74-A-001 May 1976.

11. USAF Technical Order, KC-135A Dash-1 T.O. 1C-135(K)A-1, Change 47, Tinker Air Force Base, Oklahoma, Dec. 1981.
12. Blackelock, John H. Automatic Control of Aircraft and Missiles New York: John Wiley and Sons, Inc., 1965.
13. Boeing Company. KC/EC/RC-135 Aerodynamic Characteristics Document Number D3-9090, Contract No. F34601-74-A-001 April 1976.
14. Porter, B., A. Bradshaw, A. Garis, and A. Woodhead "Microprocessor Implementation of Fast-Sampling Direct Digital Flight-Mode Controllers." AGARD-CP-321 pages 3-1 thru 3-8; October 1982.
15. Roskam, J. Airplane Flight Dynamics and Automatic Flight Controls Lawrence, Kansas: Roskam Aviation And Engineering Corporation, 1976.
16. Barfield, A. Finley. Multivariable Control Laws for the AFIT/F-16 MS Thesis. Air Force Institute of Technology, Wright-Patterson AFB, Ohio; July 1983 (AFIT/CE/EE/83S-4)
17. Larimer, S. J. TOTAL-An Interactive Computer-Aided Design Program for Digital and Continuous Control System Analysis and Synthesis MS Thesis. Wright-Patterson AFB, Ohio; Air Force Institute of Technology, March 1978.

APPENDIX A  
AIRCRAFT EQUATIONS  
OF MOTION

Introduction

This appendix presents the models of the KC-135A aircraft for the three flight conditions given in Chapter III. The models are developed using linearized equations of motion and are represented as continuous state space models.

Assumptions

The following assumptions apply to the equations of motion as they appear in this Appendix.

1. The equations are assumed to have no coupling between motion in the lateral directional plane and the longitudinal plane.
2. The X, Y, and Z body axes lie in the plane of symmetry and the origin of the axis system is located at the center of gravity of the aircraft.
3. Aircraft mass is assumed to remain constant for each flight condition.
4. The aircraft is a rigid body.
5. The earth is an inertial reference.
6. The equations are perturbation equations and represent the aircraft for small perturbations about the trimmed flight condition.
7. The flow is quasisteady.
8. Thrust acts only in the X-axis direction.

### Equations of Motion (Body Axes)

Using the assumptions stated above the linearized longitudinal equations of motion are:

$$\begin{aligned} \dot{u} = & -g\theta\cos\theta + X_u u + X_\alpha \dot{\alpha} + X_{\dot{\alpha}} \dot{\alpha} + X_q q - U_0 \alpha_0 g \\ & + X_{\delta_e} \delta_e + X_{\delta_{sb}} \delta_{sb} + X_{\delta_T} \delta_T \end{aligned} \quad (A-1)$$

$$\begin{aligned} \dot{w} = & U_0 g - g\theta\sin\theta_0 + Z_u u + Z_\alpha \dot{\alpha} + Z_q q + Z_{\delta_e} \delta_e \\ & + Z_{\delta_{sb}} \delta_{sb} \end{aligned} \quad (A-2)$$

$$\dot{q} = M_u u + M_\alpha \dot{\alpha} + M_q q + M_{\delta_e} \delta_e + M_{\delta_{sb}} \delta_{sb} \quad (A-3)$$

$$\dot{\theta} = q \quad (A-4)$$

$$\dot{h} = U_0 (\theta - \alpha) \quad (A-5)$$

Where  $\delta_e$ ,  $\delta_{sb}$ , and  $\delta_T$  represent displacements in elevator, speed brakes, and thrust respectively. Equation (A-5) is derived from Figure A-1 using small angle approximation.

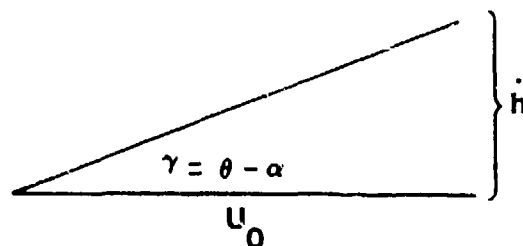


Figure A-1: Geometry of a Climb

Using the same assumptions the linearized lateral equations of motion are:

$$\dot{v} = U_0 r + g \phi \cos \phi_0 + Y_{\beta} \beta + Y_p p + U_0 \alpha_0 p + Y_r r + Y_{\delta_r} \delta_r + Y_{\delta_w} \delta_w \quad (A-6)$$

$$\dot{p} = (I_{xz}/I_{zz}) \dot{r} + L_{\beta} \beta + L_p p + L_r r + L_{\delta_r} \delta_r + L_{\delta_w} \delta_w \quad (A-7)$$

$$\dot{r} = (I_{xz}/I_{xx}) \dot{p} + N_{\beta} \beta + N_p p + N_r r + N_{\delta_r} \delta_r + N_{\delta_w} \delta_w \quad (A-8)$$

$$\dot{\phi} = p$$

#### Conversion of Stability Axes to Body Axes

Control derivatives are given in Reference 13 as non-dimensional stability axes coefficients. These derivatives are converted to body axes and then dimensionalized in a manner found in Reference 15. The equations used to convert longitudinal stability axis derivatives to body axes are:

$$(C_{Z_{\alpha}})_b = (-C_{L_{\alpha}} - C_D) \cos^2 \alpha_0 + (-C_D - 2C_D) \sin^2 \alpha_0 + (-C_{L_u} - C_L - C_{D_{\alpha}}) \cos \alpha_0 \sin \alpha_0 \quad (A-10)$$

$$(C_{Z_q})_b = -C_{L_q} \cos \alpha_0 \quad (A-11)$$

$$(C_{Z_u})_b = (-C_{L_u} - 2C_L) \cos^2 \alpha_0 + (C_{D_{\alpha}} - C_L) \sin^2 \alpha_0 + (C_{L_{\alpha}} - C_{D_u} - C_D) \cos \alpha_0 \sin \alpha_0 \quad (A-12)$$

$$(C_{Z_{\delta}})_b = -C_{L_{\delta}} \cos \alpha_0 - C_{D_{\delta}} \sin \alpha_0 \quad (A-13)$$

$$(C_{X_\alpha})_b = (-C_{D_\alpha} + C_L) \cos^2 \alpha_0 + (C_{L_u} + 2C_L) \sin^2 \alpha_0 \\ + (-C_{D_u} - C_D + C_{L_\alpha}) \cos \alpha_0 \sin \alpha_0 \quad (A-14)$$

$$(C_{X_q})_b = C_{L_q} \sin \alpha_0 \quad (A-15)$$

$$(C_{X_u})_b = (-C_{D_u} - 2C_D) \cos^2 \alpha_0 + (-C_{L_\alpha} - C_D) \sin^2 \alpha_0 \\ + (C_{D_\alpha} + C_{L_u} + C_L) \cos \alpha_0 \sin \alpha_0 \quad (A-16)$$

$$(C_{X_\delta})_b = -C_{D_\delta} \cos \alpha_0 + C_{L_\delta} \sin \alpha_0 \quad (A-17)$$

$$(C_{M_\alpha})_b = C_{M_\alpha} \cos \alpha_0 + (C_M + 2C_M) \sin \alpha_0 \quad (A-18)$$

$$(C_{M_\alpha})_b = C_{M_\alpha} \cos \alpha_0 \quad (A-19)$$

$$(C_{M_u})_b = (C_{M_u} + 2C_M) \cos \alpha_0 - C_{M_\alpha} \sin \alpha_0 \quad (A-20)$$

$$(C_{M_q})_b = C_{M_q} \quad (A-21)$$

$$(C_{M_\delta})_b = C_{M_\delta} \quad (A-22)$$

Where  $( )_b$  is used to distinguish body axes from stability axes. The equations used to convert lateral derivatives to body axes are:

$$(C_{l_\beta})_b = C_{L_\beta} \cos \alpha_0 - C_{N_\beta} \sin \alpha_0 \quad (A-23)$$

$$(C_{l_p})_b = C_{l_p} \cos^2 \alpha_0 + C_{n_r} \sin^2 \alpha_0 \\ - (C_{l_r} + C_{n_p}) \sin \alpha_0 \cos \alpha_0 \quad (A-24)$$

$$(C_{l_r})_b = C_{l_r} \cos^2 \alpha_0 - (C_{n_r} - C_{l_p}) \sin \alpha_0 \cos \alpha_0 \\ + C_{n_p} \sin^2 \alpha_0 \quad (A-25)$$

$$(C_{l_{\delta}})_b = C_{L_{\delta}} \cos \alpha_0 - C_{n_{\delta}} \sin \alpha_0 \quad (A-26)$$

$$(C_{n_{\beta}})_b = C_{n_{\beta}} \cos \alpha_0 + C_{l_{\beta}} \sin \alpha_0 \quad (A-27)$$

$$(C_{n_p})_b = C_{n_p} \cos^2 \alpha_0 - (C_{n_r} - C_{l_p}) \sin \alpha_0 \cos \alpha_0 - C_{l_r} \sin^2 \alpha_0 \quad (A-28)$$

$$(C_{n_r})_b = C_{n_r} \cos^2 \alpha_0 + (C_{l_r} + C_{n_p}) \sin \alpha_0 \cos \alpha_0 + C_{l_p} \sin^2 \alpha_0 \quad (A-29)$$

$$(C_{n_{\delta}})_b = C_{n_{\delta}} \cos \alpha_0 + C_{l_{\delta}} \sin \alpha_0 \quad (A-30)$$

$$(C_{y_{\beta}})_b = C_{y_{\beta}} \quad (A-31)$$

$$(C_{y_p})_b = C_{y_p} \cos \alpha_0 - C_{y_r} \sin \alpha_0 \quad (A-32)$$

$$(C_{y_r})_b = C_{y_r} \cos \alpha_0 + C_{y_p} \sin \alpha_0 \quad (A-33)$$

$$(C_{y_{\delta}})_b = C_{y_{\delta}} \quad (A-34)$$

#### Dimensionalized Body Axes Equations

Once the conversion to body axes is made it is desirable to dimensionalize the derivatives. The equations for dimensionalization of the longitudinal control derivatives as given in Reference 17 are as follows:

$$z_{\alpha} = z C_{z_{\alpha}} \quad (A-35)$$

$$z_q = [(z c)/(2U_0)] C_{z_q} \quad (A-36)$$

$$z_u = (z/U_0) C_{z_u} \quad (A-37)$$



$$Z_{\delta} = Z C_{Z_{\delta}} \quad (A-38)$$

$$X_{\alpha} = X C_{X_{\alpha}} \quad (A-39)$$

$$X_q = [(X c)/(2U_0)] C_{X_q} \quad (A-40)$$

$$X_u = (X/U_0) C_{X_u} \quad (A-41)$$

$$X_{\delta} = X C_{X_{\delta}} \quad (A-42)$$

$$M_{\dot{\alpha}} = M(C_{M_{\dot{\alpha}}})_b \quad (A-43)$$

$$M_{\alpha} = [(M c)/(2U_0)] (C_{M_{\alpha}})_b \quad (A-44)$$

$$M_q = [(M c)/(2U_0)] (C_{M_q})_b \quad (A-45)$$

$$M_u = (M/U_0) (C_{M_u})_b \quad (A-46)$$

$$M_{\delta} = M(C_{M_{\delta}})_b \quad (A-47)$$

Where  $Z=(qs)/m$ ,  $X=(qs)/m$ ,  $M=(qsc)/I_{yy}$ , and  $q$ =dynamic pressure,  $s$ =surface area of the wing,  $m$ =mass of the aircraft, and  $I_{yy}$ =body axes moment of inertia about the  $y$ -axis. The equations for dimensionalization of the lateral control derivatives as given in Reference 17 are as follows:

$$N_{\beta} = N(C_{n_{\beta}})_b \quad (A-48)$$

$$N_p = [(N b)/(2U_0)] (C_{n_p})_b \quad (A-49)$$

$$N_r = [(N b)/(2U_0)] (C_{n_r})_b \quad (A-50)$$

$$N_{\delta} = N(C_{n_{\delta}})_b \quad (A-51)$$

$$L_{\beta} = L(C_{l_{\beta}})_b \quad (A-52)$$

$$L_p = [(L b)/(2U_0)](C_{l_p})_b \quad (A-53)$$

$$L_r = [(L b)/(2U_0)](C_{l_r})_b \quad (A-54)$$

$$L_{\delta} = L(C_{l_{\delta}})_b \quad (A-55)$$

$$Y_{\beta} = Y(C_{y_{\beta}})_b \quad (A-56)$$

$$Y_p = [(Y b)/(2U_0)](C_{y_p})_b \quad (A-57)$$

$$Y_r = [(Y b)/(2U_0)](C_{y_r})_b \quad (A-58)$$

$$Y_{\delta} = Y(C_{y_{\delta}})_b \quad (A-59)$$

Where  $N=(qSb)/(I_{zz})$ ,  $L=(qSb)/(I_{xx})$ , and  $Y=(qSb)/m$  and  $q$ =dynamic pressure,  $s$ =surface area of wing,  $m$ =mass of the aircraft,  $b$ =wind span,  $I_{zz}$ =body axes moment of inertia about  $z$ -axis, and  $I_{xx}$ =body axes moment of inertia about  $x$ -axis.

### State Space Representation

It is desired to represent Equations (A-1) thru (A-9) in state space form. In doing so there are a total of nine aircraft states, two bending mode states, five outputs and five inputs. The complete state model is obtained by using Equations (A-1) thru (A-9) and dimensional body axis derivatives obtained from Equations (A-10) thru (A-59) along with the following assumptions:

$$1. \quad X_{\dot{\alpha}} = Z_{\dot{\alpha}} = 0$$

$$2. \quad U_0 = \text{constant and } V_0 = W_0 = 0$$

$$3. \quad \phi_0 = P_0 = Q_0 = R_0 = 0$$

$$4. \quad \dot{w} = U_0 \quad \text{and} \quad \dot{w} = U_0 \dot{\alpha}$$

$$5. \quad v = U_0 \beta \quad \text{and} \quad \dot{v} = U_0 \dot{\beta}$$

The state space model in matrix form is

$$\dot{x} = Ax + Bu \quad (A-60)$$

$$y = Cx \quad (A-61)$$

where

$$\dot{x} = [\dot{\phi} \dot{\beta} \dot{p} \dot{r} \dot{h} \dot{\theta} \dot{u} \dot{\alpha} \dot{q} \dot{e} \dot{e}]^T$$

$$x = [\phi \beta p r h \theta u \alpha q e e]^T$$

$$u = [\delta_r \delta_w \delta_e \delta_{sb} \delta_T]^T$$

$$y = [\phi \beta h \theta u]^T$$

$$A = \begin{bmatrix} 0 & 0 & 1 & 0 & 0 & 0 & 0 & 0 & 0 & 0 & 0 \\ Y'_{\phi} & Y'_{\beta} & Y'_{p} & Y'_{r} & 0 & 0 & 0 & 0 & 0 & 0 & 0 \\ 0 & L'_{\beta} & L'_{p} & L'_{r} & 0 & 0 & 0 & 0 & 0 & 0 & 0 \\ 0 & N'_{\beta} & N'_{p} & N'_{r} & 0 & 0 & 0 & 0 & 0 & 0 & 0 \\ 0 & 0 & 0 & 0 & 0 & U'_0 & 0 & -U'_0 & 0 & 0 & 0 \\ 0 & 0 & 0 & 0 & 0 & 0 & 0 & 0 & 1 & 0 & 0 \\ 0 & 0 & 0 & 0 & 0 & X'_{\theta} & X_u & X_{\alpha} & X'_q & 0 & 0 \\ 0 & 0 & 0 & 0 & 0 & Z'_{\theta} & Z'_u & Z'_{\alpha} & Z'_q & 0 & 0 \\ 0 & 0 & 0 & 0 & 0 & M'_{\theta} & M'_u & M'_{\alpha} & M'_q & 0 & 0 \\ 0 & 0 & 0 & 0 & 0 & 0 & 0 & 0 & 0 & 0 & 0 \\ 0 & 0 & 0 & 0 & 0 & 0 & 0 & e_{\alpha} & e_q & e & \dot{e} \end{bmatrix}$$

$$B = \begin{bmatrix} 0 & 0 & 0 & 0 & 0 \\ Y'_{\delta_r} & Y'_{\delta_w} & 0 & 0 & 0 \\ L'_{\delta_r} & L'_{\delta_w} & 0 & 0 & 0 \\ N'_{\delta_r} & N'_{\delta_w} & 0 & 0 & 0 \\ 0 & 0 & 0 & 0 & 0 \\ 0 & 0 & 0 & 0 & 0 \\ 0 & 0 & X_{\delta_e} & X_{\delta_{sb}} & X_{\delta_T} \\ 0 & 0 & Z'_{\delta_e} & Z'_{\delta_{sb}} & 0 \\ 0 & 0 & M'_{\delta_e} & M'_{\delta_{sb}} & 0 \\ 0 & 0 & 0 & 0 & 0 \\ 0 & 0 & e_{\delta_e} & 0 & 0 \end{bmatrix}$$

C is maneuver dependent and is discussed in Chapter V.

Appropriate dimensional body axes derivatives are changed to the prime notation using:

$$X'_\theta = -g \cos \theta_0 \quad (A-62)$$

$$X'_q = X_q - U_0 \alpha_0 \quad (A-63)$$

$$Z'_\theta = (-g/U_0) \sin \theta_0 \quad (A-64)$$

$$Z'_u = Z_u/U_0 \quad (A-65)$$

$$Z'_q = (Z_q/U_0) + 1 \quad (A-66)$$

$$Z'_\alpha = Z_\alpha/U_0 \quad (A-67)$$

$$Z'_\delta = Z_\delta/U_0 \quad (A-68)$$

$$M'_\theta = M_\alpha Z_\theta \quad (A-69)$$

$$M'_u = M_u + M_\alpha (Z_u/U_0) \quad (A-70)$$

$$M'_x = M_\alpha + M_\alpha (Z_\alpha/U_0) \quad (A-71)$$

$$M'_q = M_q + M_\alpha [(Z_q/U_0) + 1] \quad (A-72)$$

$$M'_0 = M_\delta + M_{\dot{\alpha}}(Z_\delta/U_0) \quad (A-73)$$

$$Y'_\phi = g/\eta_0 \quad (A-74)$$

$$Y'_\beta = Y_\beta/U_0 \quad (A-75)$$

$$Y'_p = (Y_p/U_0) + \alpha_0 \quad (A-76)$$

$$Y'_r = (Y_r/U_0) - 1 \quad (A-77)$$

$$Y'_\delta = Y_\delta/U_0 \quad (A-78)$$

$$L'_i = \frac{L_i + (I_{xz}/I_{xx})N_i}{1 - (I_{xz}^2)/(I_{xx}I_{zz})} \quad (A-79)$$

$$N'_i = \frac{N_i + (I_{xz}/I_{zz})L_i}{1 - (I_{xz}^2)/(I_{xx}I_{zz})} \quad (A-80)$$

$$U'_0 = (U_0)/57.3 \quad (A-81)$$

Note that  $i$  in Equations (A-79) and (A-80) represents  $\beta$ ,  $p$ ,  $r$ ,  $\delta_r$ , and  $\delta_w$  and that  $\delta$  in Equations (A-68), (A-73) and (A-78) implies  $\delta_e$ ,  $\delta_{sb}$ ,  $\delta_r$ , or  $\delta_w$  as appropriate. Also body axes inertias are used.

Actual transformation from non-dimensional stability axes derivatives to dimensional body axes is accomplished using a computer program created by A. Finley Barfield (Ref. 16) which utilizes the equations summarized in this appendix. A sample run of this program for flight condition #2 is shown in Appendix B. Data received from this program has the units of radians, radians per second, and feet per second. This data is converted, by the author, into units of degrees, degrees per second, and feet per second. Body axes derivatives for all three flight conditions studied are listed in the tables that follow.

Percent thrust is modeled in terms of thrust available and is given by

$$X = \frac{\text{Thrust Available}}{(\text{Mass})100} \frac{\text{ft/sec}^2}{\% \text{ RPM}} \quad (\text{A-82})$$

where  $m=g/w$  is the mass of the aircraft and thrust available is measured in pounds.

#### KC-135A Aircraft Models

The three flight conditions as discussed in Chapter III are:

- Condition #1. High altitude, high speed cruise at Mach 0.77 and 45,000 feet
- Condition #2. Medium altitude, heavy weight cruise at Mach 0.77 and 28,500 feet
- Condition #3. Landing configuration at Mach 0.21 and sea level

Pertinent aircraft data for each of the three flight conditions as found in Reference 10 and 11 is listed in Table A-1. The nondimensional stability axes derivatives as found in Reference 13 are listed in Tables A-2, A-3, and A-4 for conditions #1, #2, and #3 respectively. The dimensional body axes derivatives for the A and B matrices of Equation (A-60) are listed in Table A-5, A-6, and A-7 for conditions #1, #2, and #3 respectively. All derivatives not listed in these table are assumed to be zero.

Table A-1  
KC-135A Aircraft Data

Condition	#1	#2	#2	Units
Altitude	45,000	28,500	sea level	ft
Mach # (true)	0.77	0.77	0.21	--
Weight	130,000	284,000	130,000	lbs
Center of Gravity	32.1	24.2	32.1	%MAC
q	124.8	279.7	65.9	lbs/ft <sup>2</sup>
S (wing area)	2433	2433	2433	ft <sup>2</sup>
b (wing span)	130.83	130.83	130.83	ft
c (wing MAC)	20.16	20.16	20.16	ft
U <sub>0</sub> (true)	745	745	745	ft/sec
$\theta_0$ (body)	2.4	2.4	-0.1	deg
$\alpha_0$ (wing)	4.4	4.4	4.4	deg
$\alpha_0$ (body)	2.4	2.4	2.4	deg
I <sub>xx</sub> <sup>*</sup>	2,050,000	2,930,000	2,050,000	slug ft <sup>2</sup>
I <sub>yy</sub>	2,460,000	4,660,000	2,460,000	slug ft <sup>2</sup>
I <sub>zz</sub>	4,360,000	7,480,000	4,360,000	slug ft <sup>2</sup>
I <sub>xz</sub>	--	--	--	--

\* inertias are body axes

Table A-2  
Non-dimensional Stability Axes Derivatives  
For Flight Condition #1.

$C_L$	0.426	$C_M$	0.0	$C_D$	0.024
$C_{L_u}$	0.0	$C_{M_{\dot{\alpha}}}$	-6.79	$C_{D_u}$	0.0
$C_{L_\alpha}$	5.329	$C_{M_\alpha}$	-1.1747	$C_{D_\alpha}$	0.2417
$C_{L_q}$	5.1545	$C_{M_q}$	-15.65		
$C_{L_{\delta_e}}$	0.2114	$C_{M_{\delta_e}}$	-0.6647	$C_{D_{\delta_e}}$	0.0
$C_{L_{\delta_{sb}}}$	-0.3189	$C_{M_{\delta_{sb}}}$	0.07259	$C_{D_{\delta_{sb}}}$	0.0497
$C_{l_\beta}$	-0.223	$C_{n_\beta}$	0.166	$C_{y_\beta}$	-0.762
$C_{l_p}$	-0.435	$C_{n_p}$	-0.005	$C_{y_p}$	-0.233
$C_{l_r}$	0.155	$C_{n_r}$	-0.194	$C_{y_r}$	0.428
$C_{l_{\delta_r}}$	0.0315	$C_{n_{\delta_r}}$	-0.113	$C_{y_{\delta_r}}$	0.264
$C_{l_{\delta_w}}$	0.0189	$C_{n_{\delta_w}}$	0.00149	$C_{y_{\delta_w}}$	-0.0074

units are radians<sup>-1</sup>



Table A-3  
Non-dimensional Stability Axes Derivatives  
For Flight Condition #2.

$C_L$	0.426	$C_M$	0.0	$C_D$	0.024
$C_{L_u}$	0.0	$C_{M\dot{\alpha}}$	-6.57	$C_{D_u}$	0.0
$C_{L_\alpha}$	4.727	$C_{M_\alpha}$	-0.8595	$C_{D_\alpha}$	0.2143
$C_{L_q}$	4.825	$C_{M_q}$	-14.65		
$C_{L_{\delta_e}}$	0.1862	$C_{M_{\delta_e}}$	-0.5988	$C_{D_{\delta_e}}$	0.0
$C_{L_{\delta_{sb}}}$	-0.2751	$C_{M_{\delta_{sb}}}$	0.07639	$C_{D_{\delta_{sb}}}$	0.04779
$C_{l_\beta}$	-0.198	$C_{n_\beta}$	0.166	$C_{y_\beta}$	-0.752
$C_{l_p}$	-0.345	$C_{n_p}$	-0.005	$C_{y_p}$	-0.211
$C_{l_r}$	0.155	$C_{n_r}$	-0.194	$C_{y_r}$	0.428
$C_{l_{\delta_r}}$	0.0315	$C_{n_{\delta_r}}$	-0.113	$C_{y_{\delta_r}}$	0.264
$C_{l_{\delta_w}}$	0.0153	$C_{n_{\delta_w}}$	0.00149	$C_{y_{\delta_w}}$	-0.0074

units are radians<sup>-1</sup>

Table A-4  
Non-dimensional Stability Axes Derivatives  
For Flight Condition #3.

$C_L$	0.8108	$C_M$	0.0	$C_D$	0.0905
$C_{L_u}$	0.0	$C_{M\dot{\alpha}}$	-5.52	$C_{D_u}$	0.0
$C_{L_\alpha}$	4.475	$C_{M_\alpha}$	-1.0027	$C_{D_\alpha}$	0.3863
$C_{L_q}$	4.6275	$C_{M_q}$	-14.05		
$C_{L_{\delta_e}}$	0.2222	$C_{M_{\delta_e}}$	-0.7105	$C_{D_{\delta_e}}$	0.0
$C_{L_{\delta_s}}$	-0.3857	$C_{M_{\delta_s}}$	0.0879	$C_{D_{\delta_s}}$	0.075
$C_{l_\beta}$	-0.229	$C_{n_\beta}$	0.132	$C_{y_\beta}$	-0.768
$C_{l_p}$	-0.385	$C_{n_p}$	-0.055	$C_{y_p}$	-0.202
$C_{l_r}$	0.248	$C_{n_r}$	-0.186	$C_{y_r}$	0.38
$C_{l_{\delta_r}}$	0.0287	$C_{n_{\delta_r}}$	-0.098	$C_{y_{\delta_r}}$	0.226
$C_{l_{\delta_w}}$	0.0372	$C_{n_{\delta_w}}$	0.0024	$C_{y_{\delta_w}}$	-0.0143

units are radians<sup>-1</sup>

Table A-5  
Dimensional A and B Matrix Coefficients  
For Flight Condition #1.

$X_u$	-0.0029646	1/sec	$L'_\beta$	-4.4499	1/sec <sup>2</sup>
$X_\alpha$	0.53477	$\frac{\text{ft/sec}^2}{\text{deg}}$	$L'_p$	-0.75011	1/sec
$X'_q$	-0.53477	$\frac{\text{ft/sec}}{\text{deg}}$	$L'_r$	0.24613	1/sec
$X'_\theta$	-0.56146	$\frac{\text{ft/sec}^2}{\text{deg}}$	$L'_{\delta_r}$	0.61895	1/sec <sup>2</sup>
$X_{\delta_e}$	0.011617	$\frac{\text{ft/sec}^2}{\text{deg}}$	$L'_{\delta_w}$	0.36464	1/sec <sup>2</sup>
$X_{\delta_{sb}}$	-0.082712	$\frac{\text{ft/sec}^2}{\text{deg}}$	$N'_\beta$	1.42597	1/sec <sup>2</sup>
$X_{\delta_T}$	0.0495	$\frac{\text{ft/sec}}{\% \text{RPM}}$	$N'_p$	-0.012277	1/sec
$M'_u$	0.010529	$\frac{\text{deg}}{\text{ft}(\text{sec})}$	$N'_r$	-0.15052	1/sec
$M'_\alpha$	-2.7963	1/sec <sup>2</sup>	$N'_{\delta_r}$	-0.90838	1/sec <sup>2</sup>
$M'_q$	-0.7537	1/sec	$N'_{\delta_w}$	0.20771	1/sec <sup>2</sup>
$M'_\theta$	0.00041339	1/sec <sup>2</sup>	$Y'_\beta$	-0.076917	1/sec
$M'_{\delta_e}$	-1.64897	1/sec <sup>2</sup>	$Y'_p$	0.039665	---
$M'_{\delta_{sb}}$	0.173339	1/sec <sup>2</sup>	$Y'_r$	-0.99629	---
$Z'_u$	-0.004883	deg/ft	$Y'_{\delta_r}$	0.026647	1/sec
$Z'_\alpha$	-0.54223	1/sec	$Y'_{\delta_w}$	-0.00074615	1/sec
$Z'_q$	0.992966	---	$Y'_\phi$	0.04322	1/sec
$Z'_\theta$	-0.0018099	1/sec	$Z'_{\delta_{sb}}$	0.031962	1/sec
$Z'_{\delta_e}$	-0.021319	1/sec	$U_u$	13.001745	$\frac{\text{ft/sec}}{\text{deg}}$

Table A-6  
Dimensional A and B Matrix Coefficients  
Flight Condition #2.

$X_u$	-0.0029479	1/sec	$L'_\beta$	-6.22193	1/sec <sup>2</sup>
$X_\alpha$	0.551527	$\frac{\text{ft/sec}^2}{\text{deg}}$	$L'_p$	-0.904936	1/sec
$X'_q$	-0.560066	$\frac{\text{ft/sec}}{\text{deg}}$	$L'_r$	0.382638	1/sec
$X'_\theta$	-0.56146	$\frac{\text{ft/sec}^2}{\text{deg}}$	$L'_{\delta_r}$	0.97056	1/sec <sup>2</sup>
$X_{\delta_e}$	0.010498	$\frac{\text{ft/sec}^2}{\text{deg}}$	$L'_{\delta_w}$	0.46253	1/sec <sup>2</sup>
$X_{\delta_{sb}}$	-0.079813	$\frac{\text{ft/sec}^2}{\text{deg}}$	$N'_\beta$	1.87524	1/sec <sup>2</sup>
$X_{\delta_T}$	0.034	$\frac{\text{ft/sec}}{\% \text{RPM}}$	$N'_p$	-0.011695	1/sec
$M'_u$	0.0091035	$\frac{\text{deg}}{\text{ft}(\text{sec})}$	$N'_r$	-0.189843	1/sec
$M'_\alpha$	-2.40739	1/sec <sup>2</sup>	$N'_{\delta_r}$	-1.18668	1/sec <sup>2</sup>
$M'_q$	-0.814938	1/sec	$N'_{\delta_w}$	0.02541	1/sec <sup>2</sup>
$M'_\theta$	0.000441868	1/sec <sup>2</sup>	$Y'_\beta$	-0.07625	1/sec
$M'_{\delta_e}$	-0.018616	1/sec <sup>2</sup>	$Y'_p$	0.0399458	---
$M'_{\delta_{sb}}$	0.0273034	1/sec <sup>2</sup>	$Y'_r$	-0.996444	---
$Z'_u$	-0.0048649	deg/ft	$Y'_{\delta_r}$	0.02642	1/sec
$Z'_\alpha$	-0.477268	1/sec	$Y'_{\delta_w}$	-0.0007397	1/sec
$Z'_q$	0.993693	---	$Y'_\phi$	0.0417639	1/sec
$Z'_\theta$	-0.00174889	1/sec	$Z'_{\delta_{sb}}$	0.218002	1/sec
$Z'_{\delta_e}$	-1.758	1/sec	$U'_0$	13.4555	$\frac{\text{ft/sec}}{\text{deg}}$

Table A-7  
Dimensional A and B Matrix Coefficients  
For Flight Condition #3.

$X_u$	-0.0234233	1/sec	$L'_\beta$	-2.39756	1/sec <sup>2</sup>
$X_\alpha$	0.4228202	$\frac{\text{ft/sec}}{\text{deg}}$	$L'_p$	-1.11861	1/sec
$X'_q$	-0.1660307	$\frac{\text{ft/sec}}{\text{deg}}$	$L'_r$	0.681707	1/sec
$X_\theta$	-0.5619546	$\frac{\text{ft/sec}}{\text{deg}}$	$L'_{\delta_r}$	0.335391	1/sec <sup>2</sup>
$X_{\delta_e}$	0.0064484	$\frac{\text{ft/sec}}{\text{deg}}$	$L'_{\delta_w}$	0.379249	1/sec <sup>2</sup>
$X_{\delta_{sb}}$	-0.063125	$\frac{\text{ft/sec}}{\text{deg}}$	$N'_\beta$	0.588344	1/sec <sup>2</sup>
$X_{\delta_T}$	0.1268	$\frac{\text{ft/sec}}{\% \text{RPM}}$	$N'_p$	-0.0852618	1/sec
$M'_u$	0.0318452	$\frac{\text{deg}}{\text{ft(sec)}}$	$N'_r$	-0.238751	1/sec
$M'_\alpha$	-1.07422	1/sec <sup>2</sup>	$N'_{\delta_r}$	-0.0190339	1/sec <sup>2</sup>
$M'_q$	-1.09229	1/sec	$N'_{\delta_w}$	-0.46518	1/sec <sup>2</sup>
$M'_\theta$	-0.00007434	1/sec <sup>2</sup>	$Y'_\beta$	-0.129778	1/sec
$M'_{\delta_e}$	-0.921844	1/sec <sup>2</sup>	$Y'_l$	0.0316453	---
$M'_{\delta_{sb}}$	0.095412	1/sec <sup>2</sup>	$Y'_r$	-0.982538	---
$Z'_u$	-0.0591737	deg/ft	$Y'_{\delta_r}$	0.03819	1/sec
$Z'_\alpha$	-0.778653	1/sec	$Y'_{\delta_w}$	-0.0024207	1/sec
$Z'_q$	0.966486	---	$Y'_\phi$	0.1370213	1/sec
$Z'_\theta$	0.000239147	1/sec	$Z'_{\delta_{sb}}$	0.064588	1/sec
$Z'_{\delta_e}$	-0.0375145	1/sec	$U'_0$	4.101222	$\frac{\text{ft/sec}}{\text{deg}}$

### Body Bending (Ref. 10)

One of the assumptions made in the development of the equations of motion is that the aircraft is a rigid body. As a first step in eliminating the rigid body assumption, this thesis models the 1st and 2nd body bending modes for the longitudinal case. The purpose of this model is to allow observation of the bending that takes place while performing a maneuver, but not to take into account the effects of the bending. Body bending can affect sensor readings, such as accelerometers, gyros, ect., if these sensors are placed in a position where bending occurs. Structural vibrations and body bending may also have an affect upon the performance of the crew by increasing fatigue. The body bending listed in this section identifies crew station motions due to structural elasticity and vibration. The structural bending mode equation is of the form:

$$I\ddot{e} + [(2\zeta w_n I) + (\rho_0 V_0 C_e)]\dot{e} + [w_n^2 I + \rho_0 V^2 C_e]e = -\rho_0 V^2 C_{q\dot{q}} - \rho_0 V^2 C_{\alpha\dot{\alpha}} - \rho_0 V^2 C_{\delta_e\dot{\delta}_e} \quad (A-83)$$

where

$I$  = mass moment of inertia, slugs-in<sup>2</sup>

$e$  = elastic mode displacement, inches

$\zeta$  = viscous damping

$w_n$  = frequency, radians/second

$V_0$  = true airspeed, inches/sec

C = derivative for structural modes

q = pitch accelerations, degrees/sec<sup>2</sup>

$\alpha$  = angle of attack, degrees

$\delta_e$  = elevator displacement, degrees

Using data found in Reference 10 the first and second bending mode equations for each flight condition become:

Condition #1:

1st Bending Mode

$$\ddot{e} + 1.313\dot{e} + 132.886e = -118.73q - 148.29\alpha + 28.496\delta_e$$

2nd Bending Mode

$$\ddot{e} + 1.1084\dot{e} + 543.60e = 23.51q - 10.37\alpha + 5.518\delta_e$$

Condition #2

1st Bending Mode

$$\ddot{e} + 1.5306\dot{e} + 250.593e = -268.548q - 299.365\alpha + 48.238\delta_e$$

2nd Bending Mode

$$\ddot{e} + 1.1959\dot{e} + 508.36e = 147.52q - 1/267\alpha + 15.759\delta_e$$

Condition #3

1st Bending Mode

$$\ddot{e} + 1.892\dot{e} + 131.34e = -62.697q - 78.306\alpha + 15.053\delta_e$$

2nd Bending Mode

$$\ddot{e} + 1.225\dot{e} + 545.03e = 12.428q - 5.478\alpha + 2.914\delta_e$$

In adding the bending mode model to the state space representation of the aircraft, two new states are created. They are  $\dot{e}$  and  $e$  where  $e$  would represent the aircraft

bending modeled for the crew station.

### Summary

This appendix summarizes the aircraft equations of motion used in this thesis. The assumptions used in deriving the equations are stated, followed by the equations themselves. Data for the KC-135A is in the form of non-dimensional stability axes derivatives. These are changed to dimensional body axes derivatives using a computer program described in Reference 16 . Tabular listings of all derivatives are given for each of the three flight conditions studied. Also given are the body bending mode equations used to depict bending of the aircraft at the crew station.



## Appendix B

### Sample Run of CAT Program

COMMAND- ATTACH,CAT1, ID=T920366  
CFN IS  
CAT1  
AT CY= 001 SN=AFIT  
COMMAND- CAT1

\*\*\*\*\*  
\*\*\*\*\* AXIS TRANSFORMATION PROGRAM \*\*\*\*\*  
\*\*\*\*\*  
ENTER STABILITY AXIS COEFFICIENTS FOR TRANSFORMATION  
TO BODY AXIS. TRIM ALPHA IS NEEDED FOR CONVERSION.  
MOMENT COEFFICIENTS AND SIDEFORCE COEFFICIENTS NOT  
REQUESTED REMAIN UNCHANGED.  
NOTE: ALL COEFFICIENTS ARE REQUESTED WHEN COMPUTING  
DIMENSIONAL DERIVATIVES.  
\*\*\*\*\*  
TO TRANSFORM ONLY LONGITUDINAL DATA - TYPE LONG  
TO TRANSFORM ONLY LATERAL-DIRECTIONAL DATA - TYPE LAT  
TO TRANSFORM BOTH LONG AND LAT-DIR DATA - TYPE BOTH  
KEYWORD =BOTH

ARE DIMENSIONAL BODY AXIS DERIVATIVES REQUIRED ? (YES/NO)YES

\*\*\*\*\*  
Q (DYNAMIC PRESSURE - LBS/FT2) =124.3  
  
S (WING REFERENCE AREA - FT2) =2433  
  
C (WING MEAN AERODYNAMIC CORD - FT) =20.16  
  
B (WING SPAN - FT) =130.83  
  
VT (TRIM VELOCITY - FT/SEC) =745  
  
THETA (PITCH ANGLE - DEGS) =2.4  
  
W (WEIGHT - LBS) =130000  
  
INERTIAS MUST BE INPUT IN BODY AXIS.  
IXX (SLUG-FT2) =2050000  
  
IYY (SLUG-FT2) =2460000  
  
IZZ (SLUG-FT2) =4360000  
  
IXZ (SLUG-FT2) =0  
  
\*\*\*\*\*

# AIRCRAFT PARAMETERS

Q (DYNAMIC PRESSURE - LBS/FT<sup>2</sup>) = 124.800  
 S (WING REFERENCE AREA - FT<sup>2</sup>) = 2433.00  
 C (WING MEAN AERODYNAMIC CORD - FT) = 20.1600  
 B (WING SPAN - FT) = 130.830  
 VT (TRIM VELOCITY - FT/SEC) = 745.000  
 THETA = 2.40000  
 W (WEIGHT - LBS) = 130000.  
 IXX (SLUG-FT<sup>2</sup>) = .205000E+07  
 IYY (SLUG-FT<sup>2</sup>) = .246000E+07  
 IZZ (SLUG-FT<sup>2</sup>) = .436000E+07  
 Ixz (SLUG-FT<sup>2</sup>) = 0.

\*\*\*\*\*  
 IS THE ENTERED DATA CORRECT ? (YES/NO)YES

\*\*\*\*\*  
 ALPHA (DEG) =2.4

CL =.4260

CLA (1/DEG) =.093

CLDE (1/DEG) =.003689

CLDF (1/DEG) =-.005567

CLQ (1/RAD) =5.1545

CLAD (1/RAD) =0

CLU (1/(FT/SEC)) =0

CD =.0240

CDA (1/DEG) =.004218

CDE (1/DEG) =0

CDDE (1/DEG) =.0008674

CDU (1/(FT/SEC)) =0

CM =0

CMA (1/DEG) =-.0205

CMDE (1/DEG) =-.0116

CMDF (1/DEG) =.001267

CMQ (1/RAD) =-15.65

CMAD (1/RAD) =-6.79

CNU (1/(FT/SEC)) =0

\*\*\*\*\*

LONGITUDINAL STABILITY AXIS COEFFICIENTS

ALPHA = 2.40000

CL = .426000	CM = 0.	CD = .240000E-01
CLA = .930000E-01	CMA = -.205000E-01	CDA = .421000E-02
CLDE = .360000E-02	CMDE = -.116000E-01	CDDE = 0.
CLDF = -.556700E-02	CMDF = .126700E-02	CDDF = .867400E-03
CLQ = 5.15450	CMQ = -15.6500	
CLAD = 0.	CMAD = -6.79000	
CLU = 0.	CNU = 0.	CDU = 0.

\*\*\*\*\*

IS THE ENTERED DATA CORRECT ? (YES/NO)YES

\*\*\*\*\*

LONGITUDINAL BODY AXIS COEFFICIENTS (1/RAD)

CZ = -.426631		CX = -.613992E-02
CZA = -5.37114	CMA = -1.17353	CXA = .407432
CZDE = -.211179		CXDE = .885101E-02
CZDF = .316605		CXDF = -.630117E-01
CZQ = -5.14998		CXQ = .215048
CZAD = 0.	CMAD = -6.78404	CXAD = 0.
CZU = -.628894	CNU = .491836E-01	CXU = -.293671E-01

\*\*\*\*\*

LONG BODY AXIS DIMENSIONAL DERIVATIVES

Z = -129542.	M = 0.	X = -1864.32
ZA = -403.958	MA = -2.92017	XA = 30.6425
ZDE = -15.8025	MDE = -1.65384	XDE = .665675
ZDF = 23.8115	MDF = .180639	XDF = -4.73904
ZQ = -5.24057	MQ = -.526903	XQ = .219645
ZAD = 0.	MAD = -.228405	XAD = 0.
ZU = -.634878E-01	MU = .164283E-03	XU = -.296465E-02

\*\*\*\*\*

LONG BODY AXIS PRIMED DIMENSIONAL DERIVATIVES

ZA' = -.542225	MA' = -2.79632	XA' = 30.6425
ZDE' = -.213188E-01	MDE' = -1.64897	XDE' = .665675
ZDF' = .319617E-01	MDF' = .173339	XDF' = -4.73904
ZQ' = .992966	MQ' = -.753701	XQ' = -30.9868
ZU' = -.852186E-04	MU' = .183748E-03	XU' = -.296465E-02
ZTHETA' = -.180993E-02	HTHETA' = .413396E-03	XTHETA' = -32.1710

\*\*\*\*\*

CNB (1/DEG) =.002897

CNP (1/RAD) =-.005

CNR (1/RAD) =-.194

CNDR (1/DEG) =-.001972

CNDA (1/DEG) =.000026

CNDOT (1/DEG) =0  
 CNDC (1/DEG) =0  
 CLB (1/DEG) =-.00389  
 CLP (1/RAD) =-.4350  
 CLR (1/RAD) =.155  
 CLDR (1/DEG) =.0005497  
 CLDA (1/DEG) =.0003298  
 CLDDT (1/DEG) =0  
 CLDC (1/DEG) =0  
 CYB (1/DEG) =-.013298  
 CYP (1/RAD) =-.233  
 CYR (1/RAD) =.428  
 CYDR (1/DEG) =.004607  
 CYDA (1/DEG) =-.000129  
 CYDDT (1/DEG) =0  
 CYDC (1/DEG) =0

\*\*\*\*\*

#### LAT-DIR STABILITY AXIS COEFFICIENTS

CNB = .289700E-02	CLB = -.389000E-02	CYB = -.132980E-01
CNP = -.500000E-02	CLP = -.435000	CYP = -.233000
CNR = -.194000	CLR = .155000	CYR = .428000
CNDR = -.197200E-02	CLDR = .549700E-03	CYDR = .460700E-02
CNDA = .260000E-04	CLDA = .329800E-03	CYDA = -.129000E-03
CNDDT = 0.	CLDDT = 0.	CYDDT = 0.
CNDC = 0.	CLDC = 0.	CYDC = 0.

\*\*\*\*\*

IS THE ENTERED DATA CORRECT ? (YES/NO)YES

\*\*\*\*\*

#### LAT-DIR BODY AXIS COEFFICIENTS

CNB = .156507	CLB = -.229636	CYB = -.761919
CNP = -.153462E-01	CLP = -.440853	CYP = -.250718
CNR = -.188147	CLR = .144654	CYR = .417868
CNDR = -.996992E-01	CLDR = .319410E-01	CYDR = .263962
CNDA = .227967E-02	CLDA = .188172E-01	CYDA = -.739116E-02
CNDDT = 0.	CLDDT = 0.	CYDDT = 0.

```

CNDC = 0.          CLDC = 0.          CYDC = 0.
*****
LAT-DIR BODY AXIS DIMENSIONAL DERIVATIVES
NB = 1.42597       LB = -4.44996       YB = -57.3031
NP = -.122772E-01  LP = -.750111       YP = -1.65568
NR = -.150520       LR = .246128       YR = 2.73949
NDR = -.908384      LDR = .618955      YDR = 19.8523
NDA = .207706E-01  LDA = .364641       YDA = -.555881
NDDT = 0.          LDDT = 0.          YDDT = 0.
NDC = 0.          LDC = 0.          YDC = 0.
*****
LAT-DIR BODY AXIS PRIMED DIMENSIONAL DERIVATIVES
NR' = 1.42597       LB' = -4.44996       YB' = -.759169E-01
NP' = -.122772E-01  LP' = -.750111       YP' = .396655E-01
NR' = -.150520       LR' = .246128       YR' = -.996296
NDR' = -.908384      LDR' = .618955      YDR' = .266473E-01
NDA' = .207706E-01  LDA' = .364641       YDA' = -.746149E-03
NDDT' = 0.          LDDT' = 0.          YDDT' = 0.
NDC' = 0.          LDC' = 0.          YDC' = 0.
*****
IS ANOTHER PROGRAM RUN DESIRED ? (YES/NO)NO

*****
END CAT
024300 MAXIMUM EXECUTION FL.
0.312 CP SECONDS EXECUTION TIME.

```

# APPENDIX C

## Simulation Results For Flight Conditions #1 and #2

Table C-1  
Simulation Results For  
Flight Condition #2 Coordinated Turn

Input/ Output	Peak Value	Final Value	$t_p$ (sec)	$t_s$ (sec)
$\phi$ (deg)	30.48	30.048	6.8	5.2
$\beta$ (deg)	0.0018	-0.0013	4.4	14.0
$r$ (deg/sec)	1.30	1.19	4.2	5.8
$\delta_r$ (deg)	-0.37	--	--	--
$\delta_w$ (deg)	22.0	--	--	--

Table C-2  
Simulation of Results For  
Flight Condition #2 Sideslip

Input/ Output	Peak Value	Final Value	$t_p$ (sec)	$t_s$ (sec)
$\phi$ (deg)	-0.925	0.0	8.4	--
$\beta$ (deg)	5.05	5.0	16.0	8.8
$\delta_r$ (deg)	8.3	--	--	--
$\delta_w$ (deg)	50.0	--	--	--

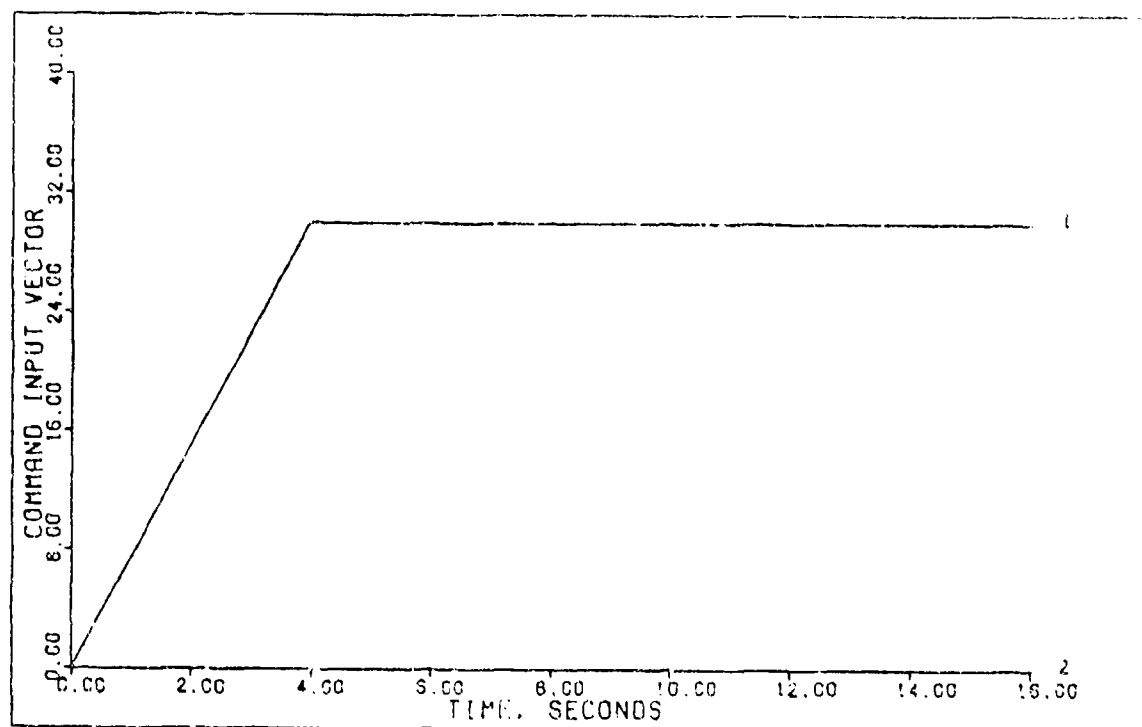


FIGURE C-1a: Flight Condition #2, Coordinated Turn  
(Command Input Vector)

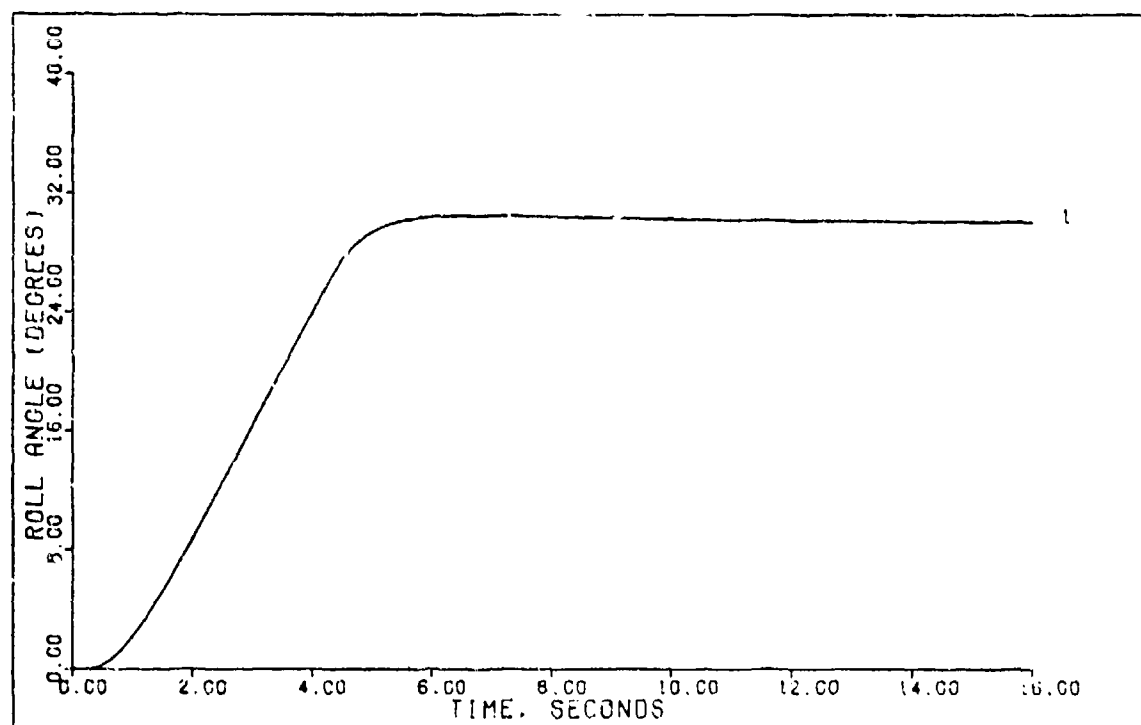


FIGURE C-1b: Flight Condition #2, Coordinated Turn  
(Output 1: Roll Angle)

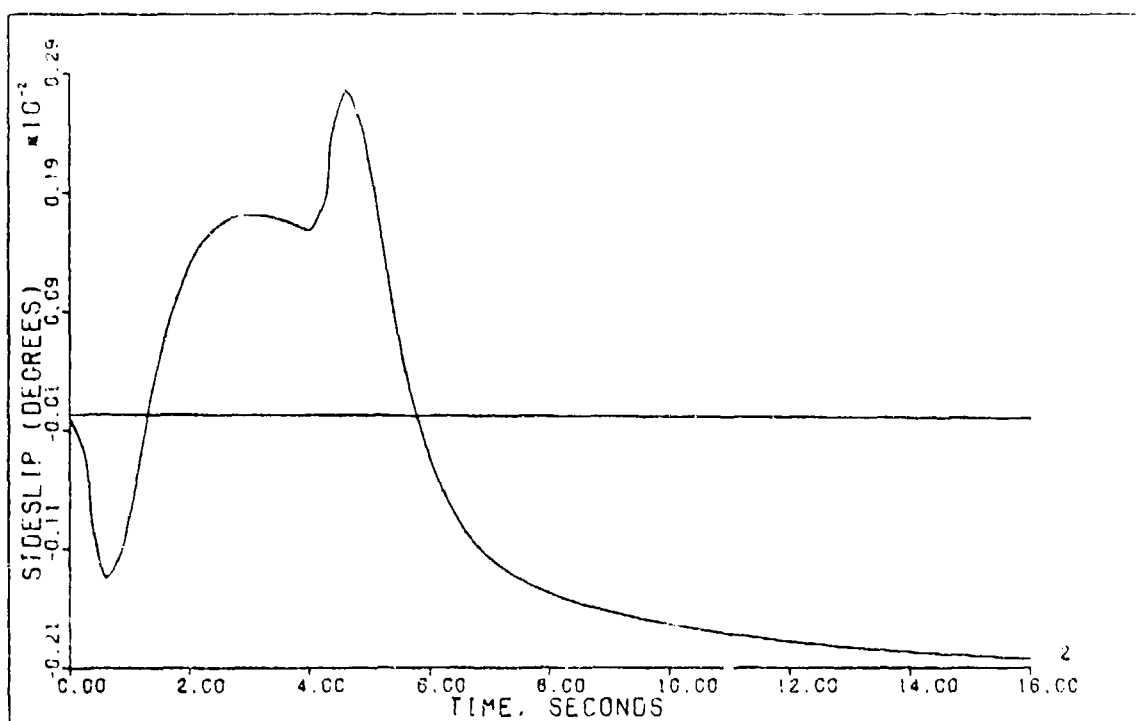


FIGURE C-1c: Flight Condition #2, Coordinated Turn  
(Output 2: Sideslip)

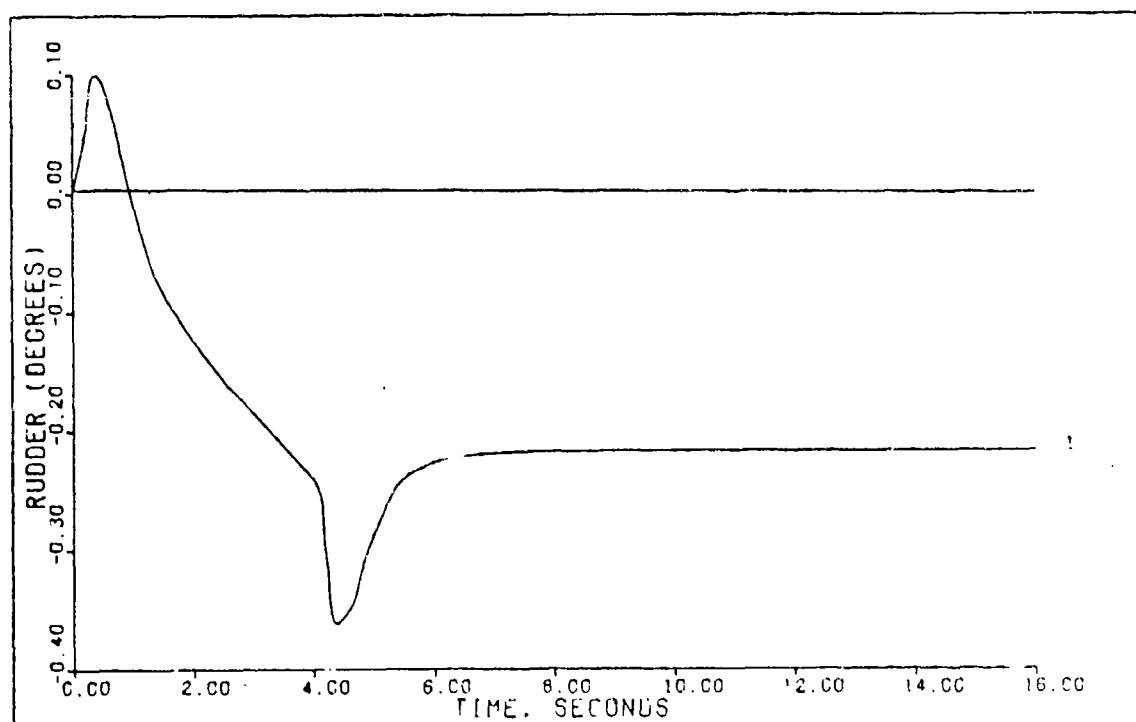


FIGURE C-1d: Flight Condition #2, Coordinated Turn  
(Control 1: Rudder)



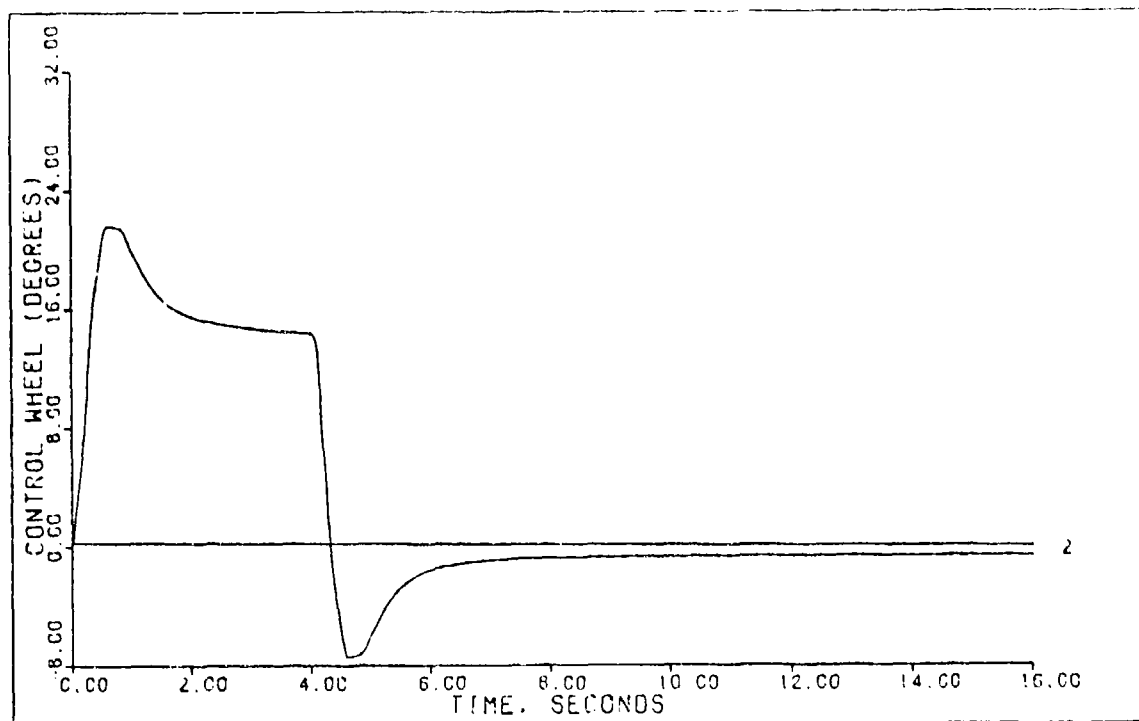


FIGURE C-1e: Flight Condition #2, Coordinated Turn  
(Control 2: Control Wheel)

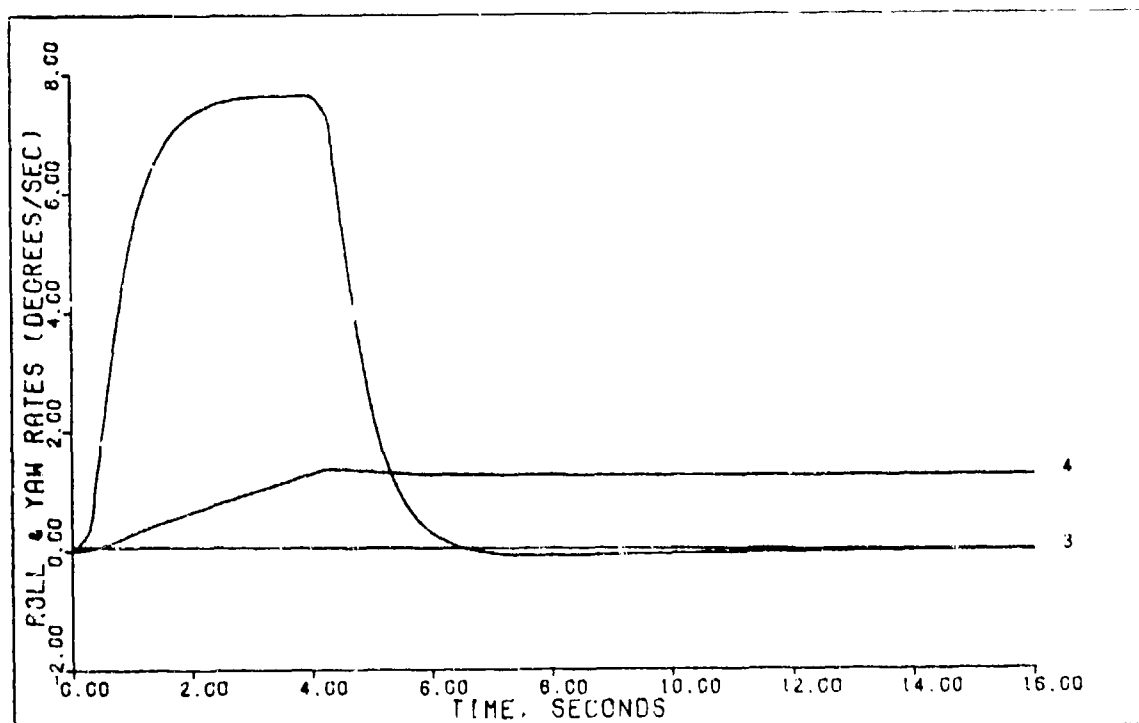


FIGURE C-1f: Flight Condition #2, Coordinated Turn  
(State 3: Roll Rate; State 4: Yaw Rate)

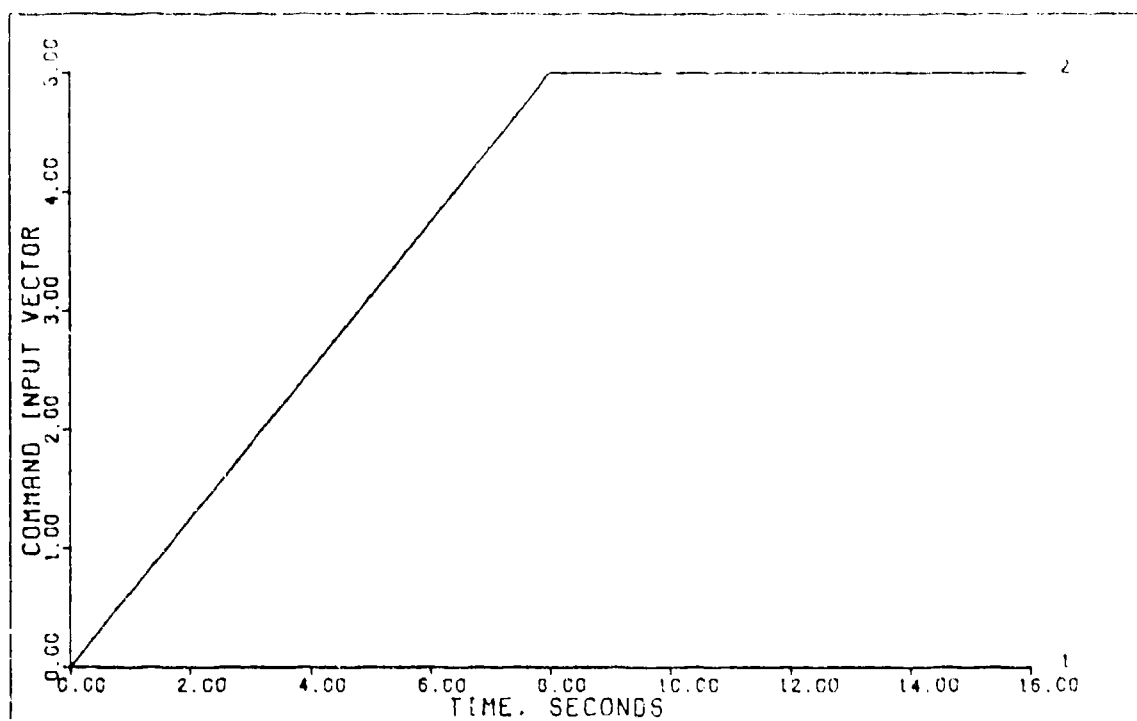


FIGURE C-2a: Flight Condition #2, Sideslip  
(Command Input Vector)

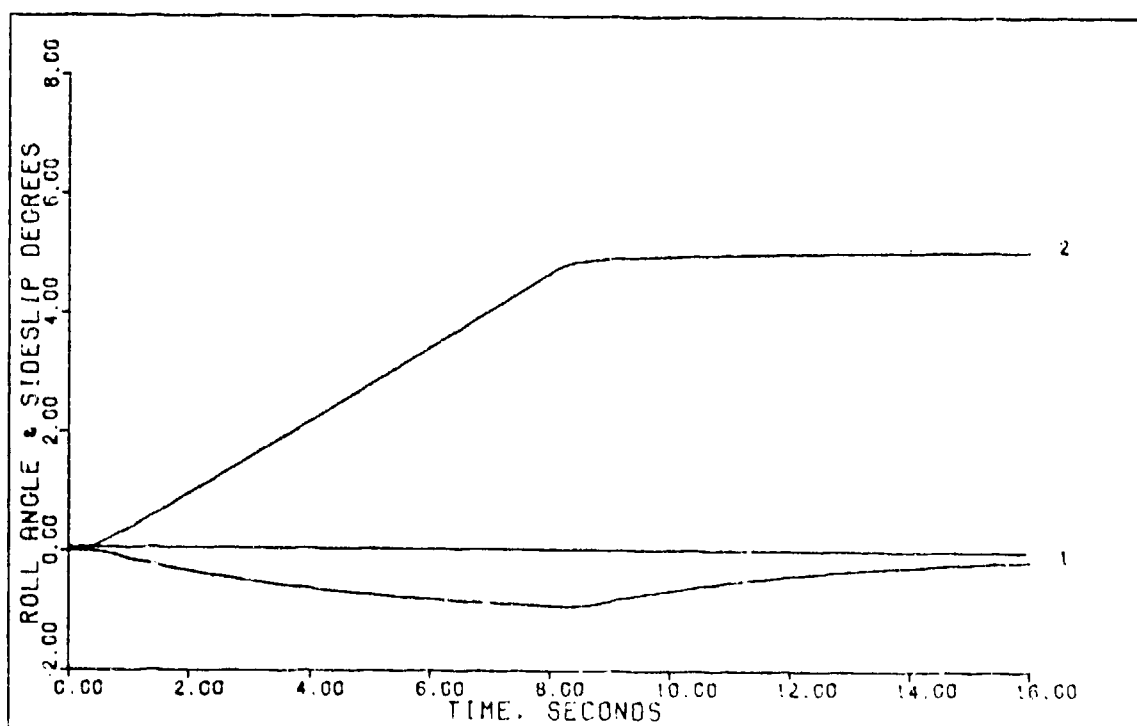


FIGURE C-2b: Flight Condition #2, Sideslip  
(Output 1: Roll Angle; Output 2: Sideslip)

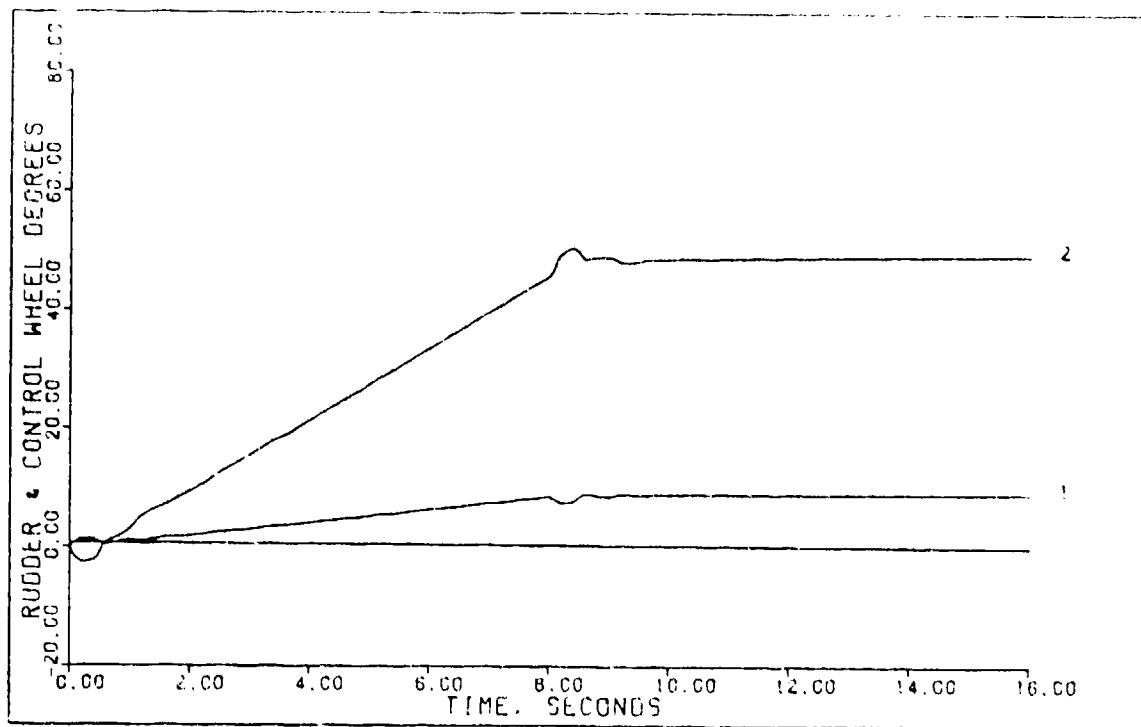


FIGURE C-2c: Flight Condition #2, Sideslip  
(Control 1: Rudder; Control 2: Control Wheel)

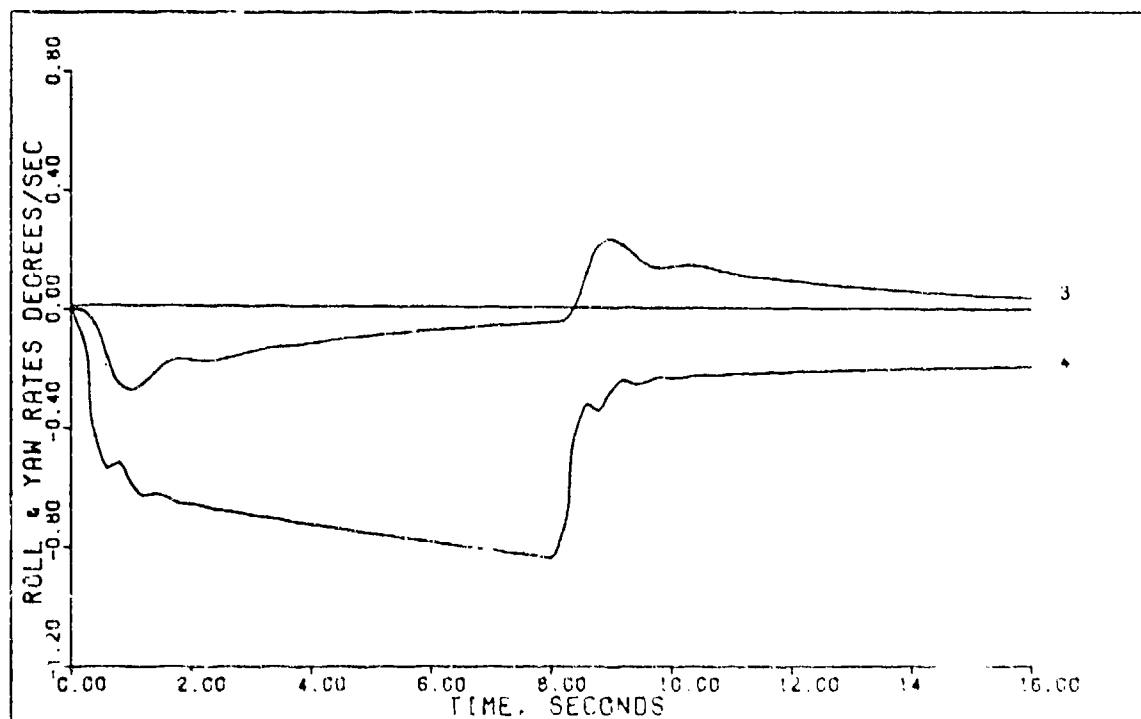


FIGURE C-2d: Flight Condition #2, Sideslip  
(State 3: Roll Rate; State 4: Yaw Rate)

Table C-3  
Simulation Results For  
Flight Condition #2 Normal Climb

Input/ Output	Peak Value	Final Value	$t_p$ (sec)	$t_s$ (sec)
$\gamma$ (deg)	1.73	1.49	8.4	14.7
$u$ (ft/sec)	-0.231	0.0	3.3	--
$\delta_e$ (deg)	-1.0	--	--	--
$\delta_T$ (%RPM)	29.0	--	--	--

Table C-4  
Simulation Results For  
Flight Condition #2 Pitch Pointing

Input/ Output	Peak Value	Final Value	$t_p$ (sec)	$t_s$ (sec)
$h$ (ft)	0.147	0.0	4.4	--
$\theta$ (deg)	1.01	1.0	16.0	5.0
$u$ (ft/sec)	-0.192	0.0	1.6	--
$\delta_e$ (deg)	1.5	--	--	--
$\delta_{sb}$ (deg)	18.0	--	--	--
$\delta_T$ (%RPM)	48.0	--	--	--

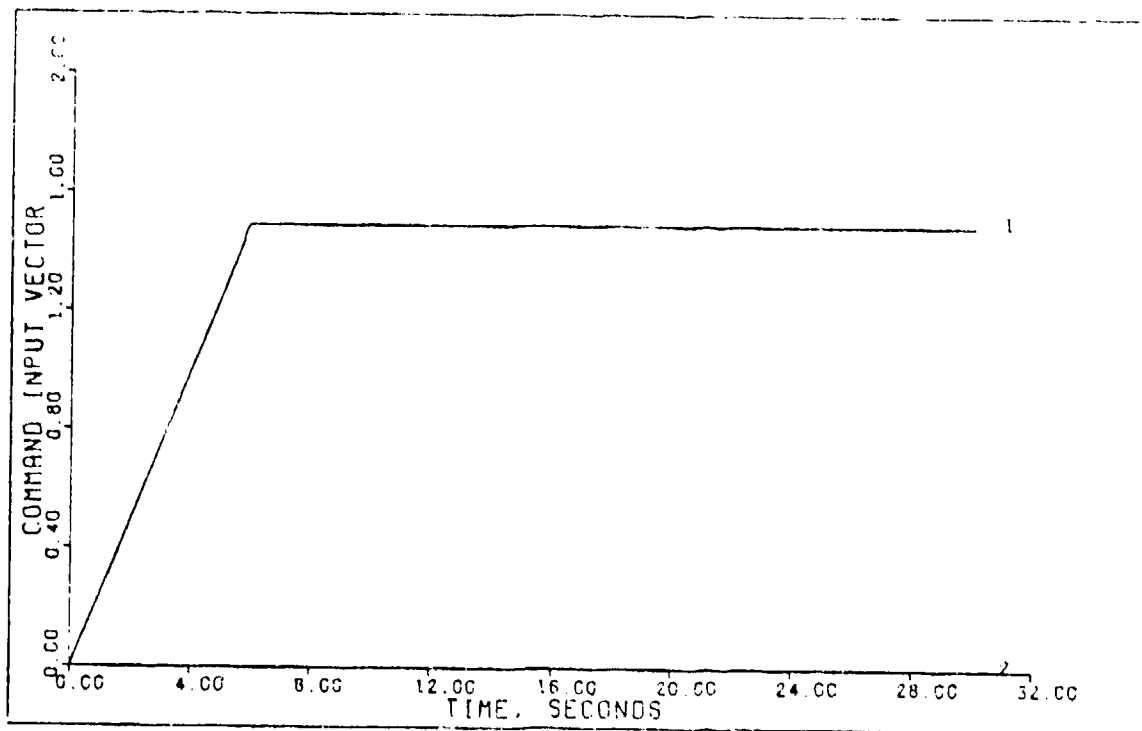


FIGURE C-3a: Flight Condition #2, Normal Climb  
(Command Input Vector)

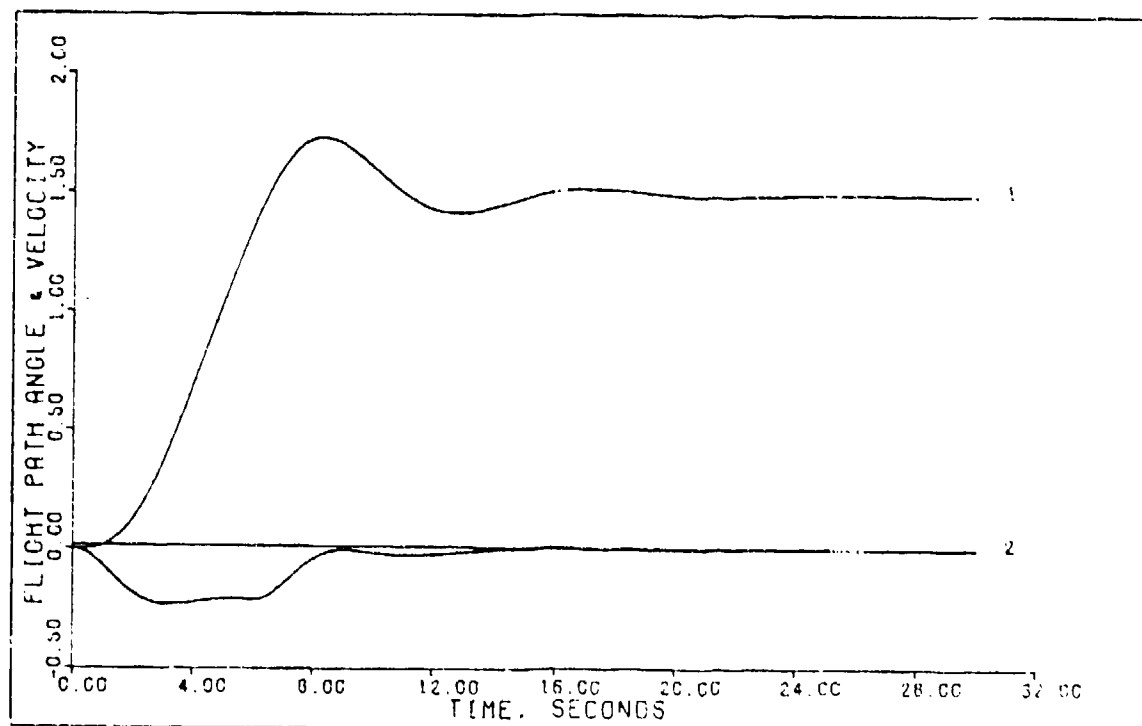


FIGURE C-3b: Flight Condition #2, Normal Climb  
(Output 1: Flight Path Angle;  
Output 2: Velocity)

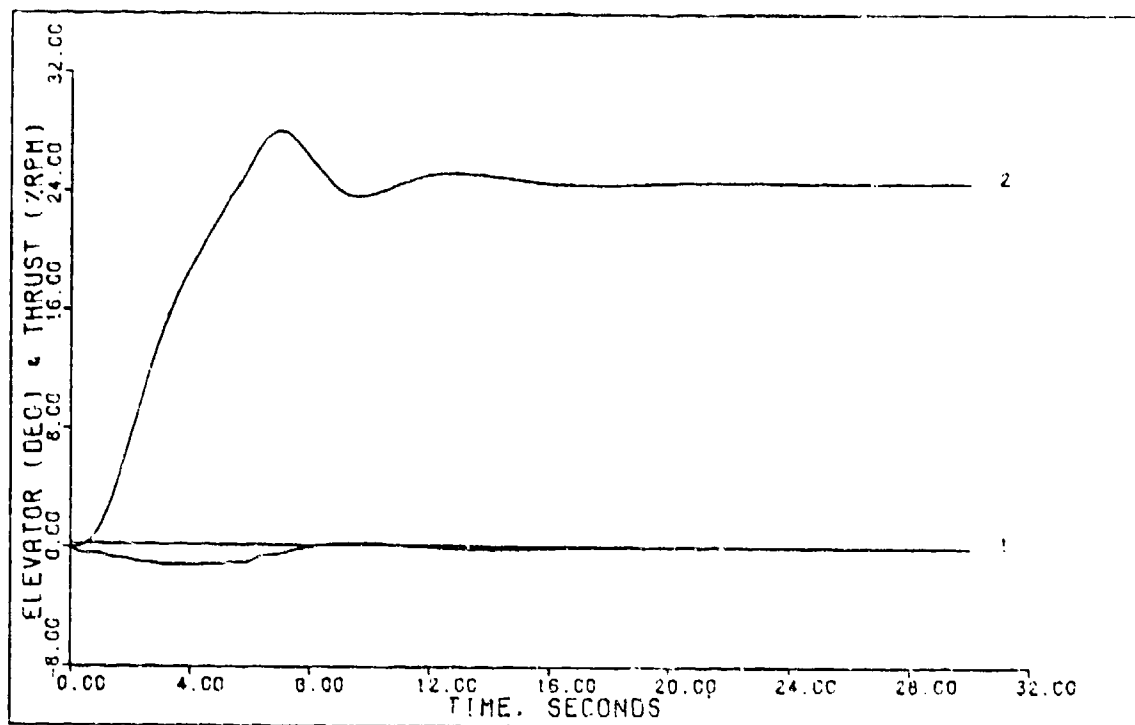


FIGURE C-3c: Flight Condition #2, Normal Climb  
(Control 1: Elevator; Control 2: Thrust)

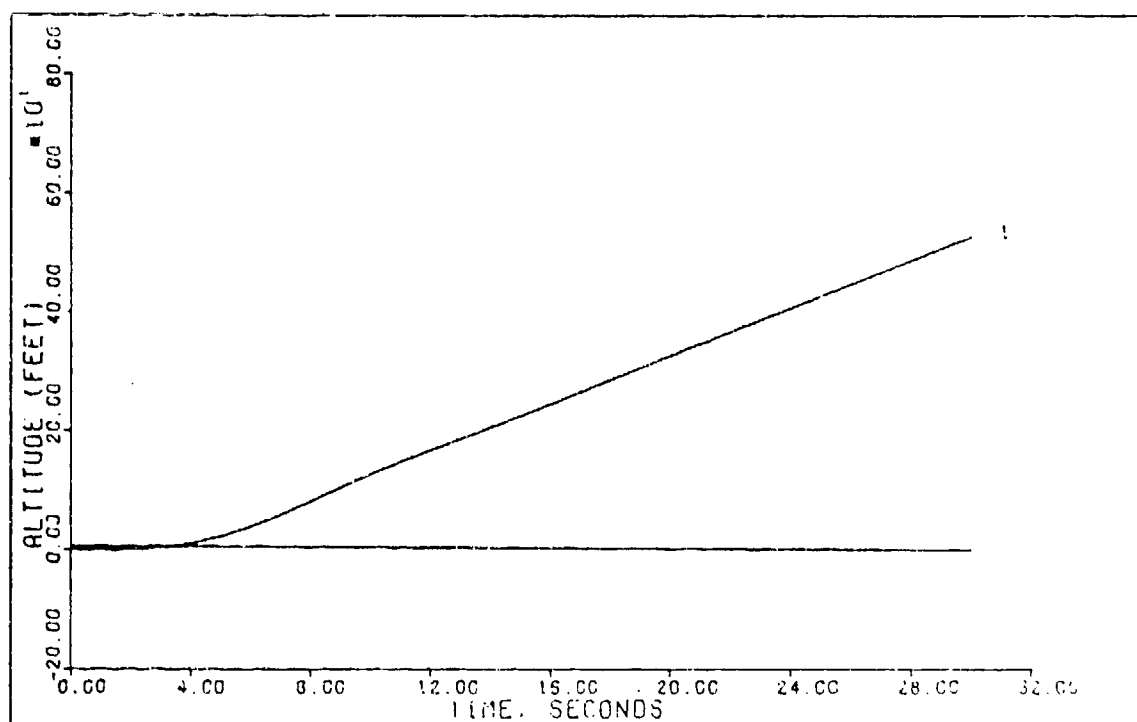


FIGURE C-3d: Flight Condition #2, Normal Climb  
(State 1: Altitude)

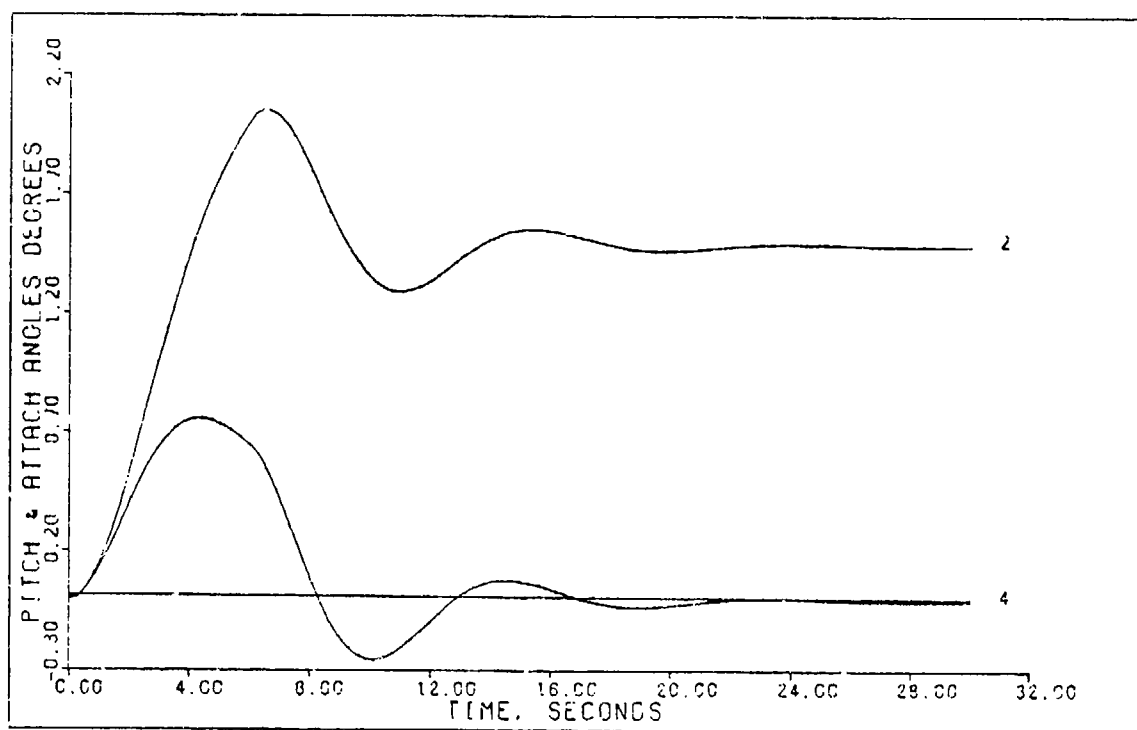


FIGURE C-3e: Flight Condition #2, Normal Climb  
(State 2: Pitch Angle; State 4: Attack Angle)

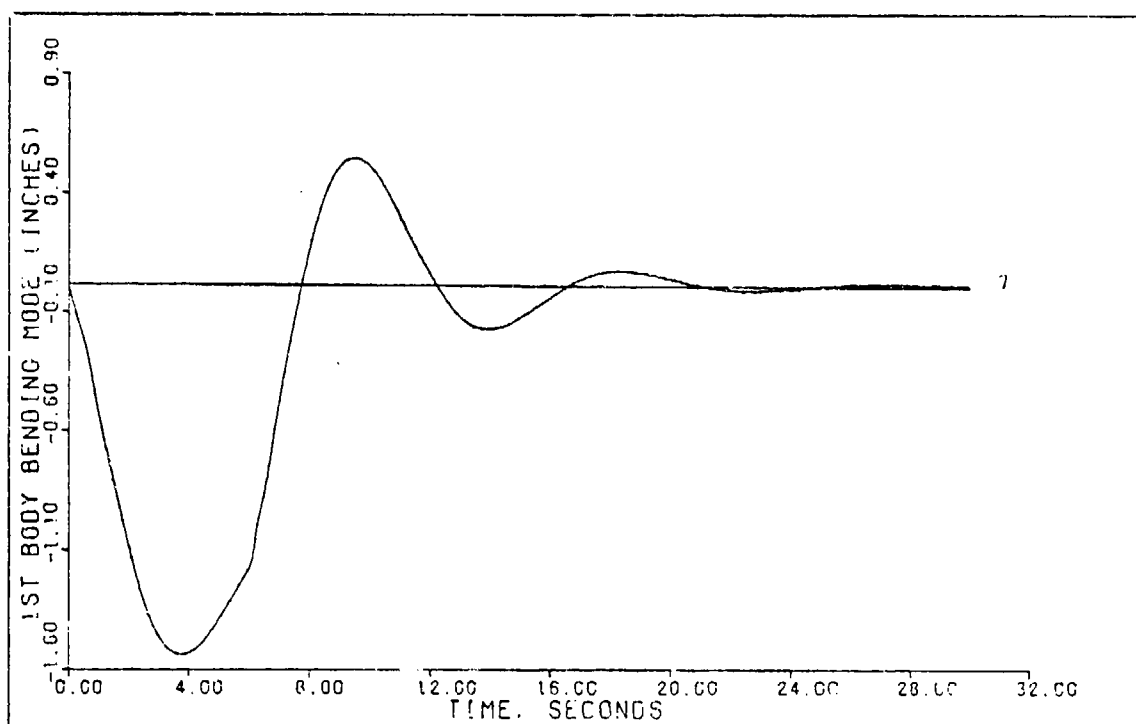


FIGURE C-3f: Flight Condition #2, Normal Climb  
(State 7: 1st Body Bending Mode)

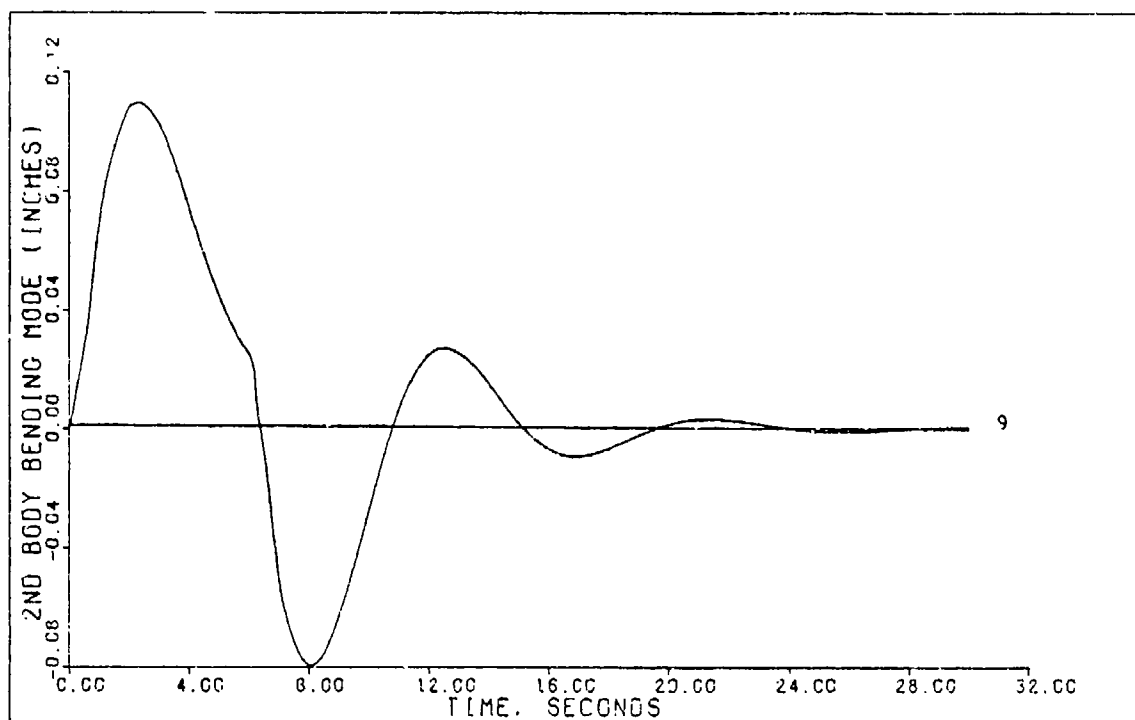


FIGURE C-3g: Flight Condition #2, Normal Climb  
(State 9: 2nd Body Bending Mode)

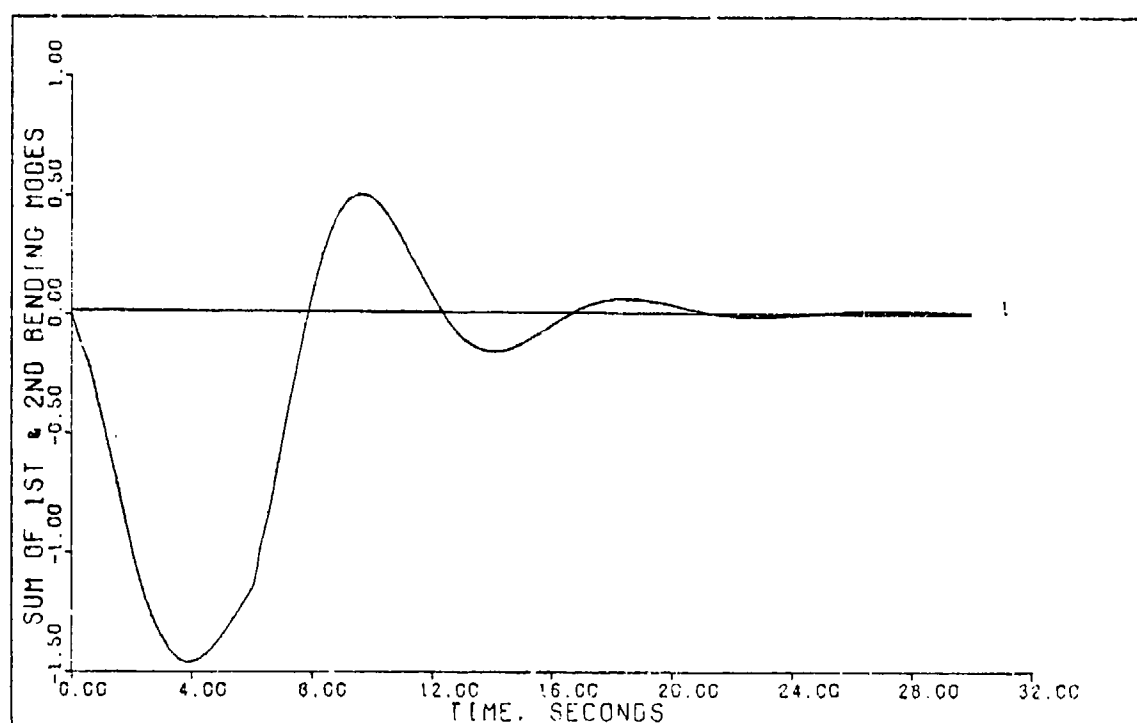


FIGURE C-3h: Flight Condition #2, Normal Climb  
(Sum of 1st & 2nd Bending Modes)



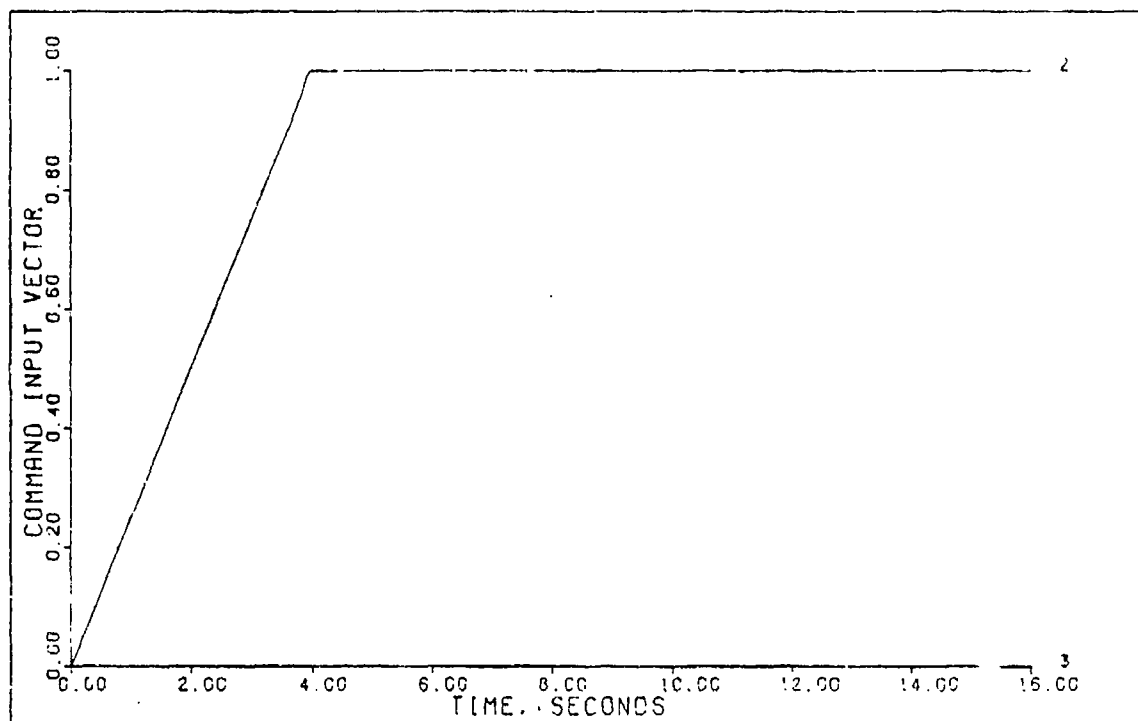


FIGURE C-4a: Flight Condition #2, Pitch Pointing  
(Command Input Vector)

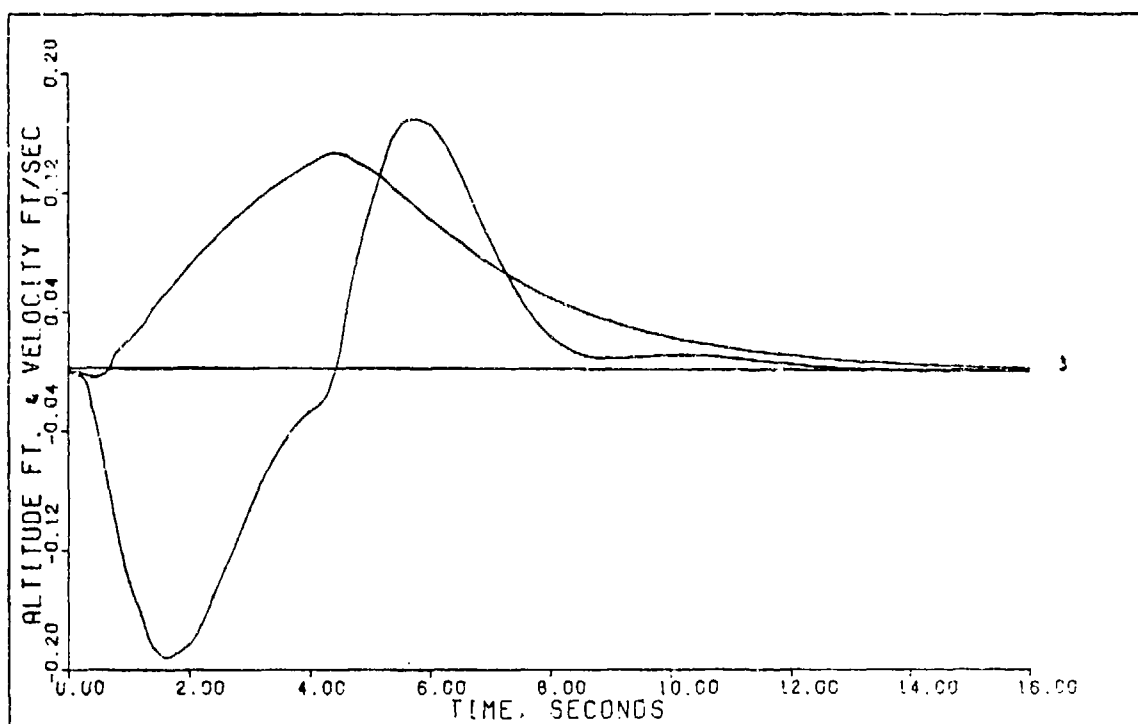


FIGURE C-4b: Flight Condition #2, Pitch Pointing  
(Output 1: Altitude; Output 2: Velocity)

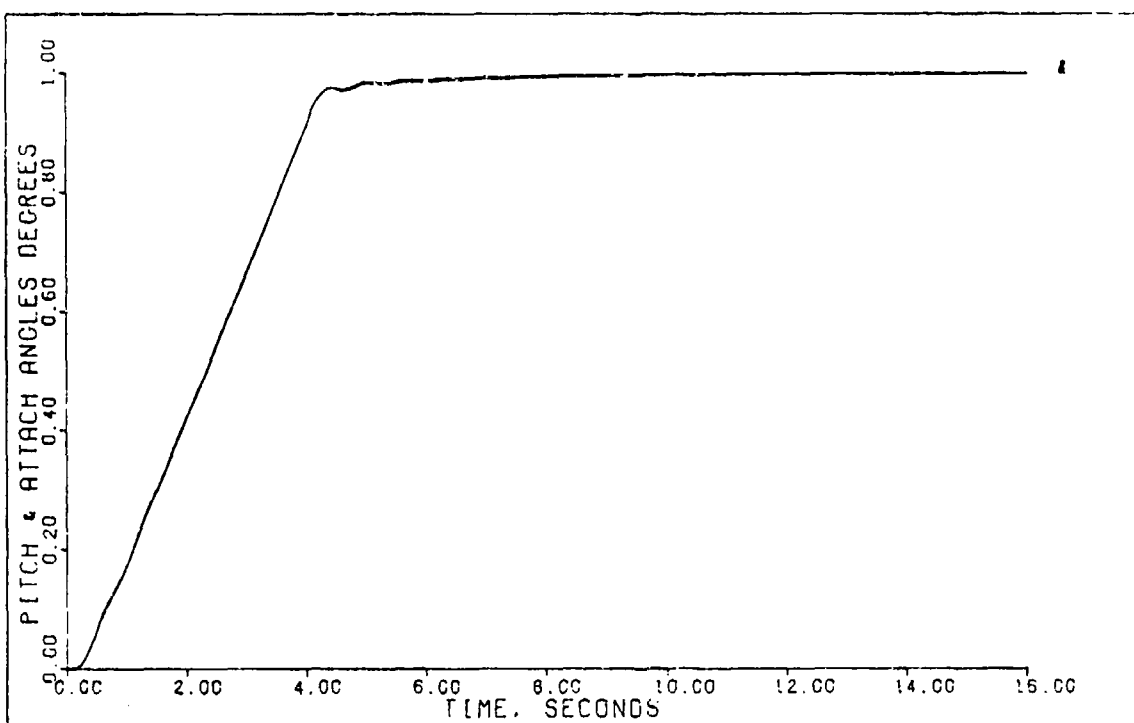


FIGURE C-4c: Flight Condition #2, Pitch Pointing  
(State 2: Pitch Angle; State 4: Attack Angle)

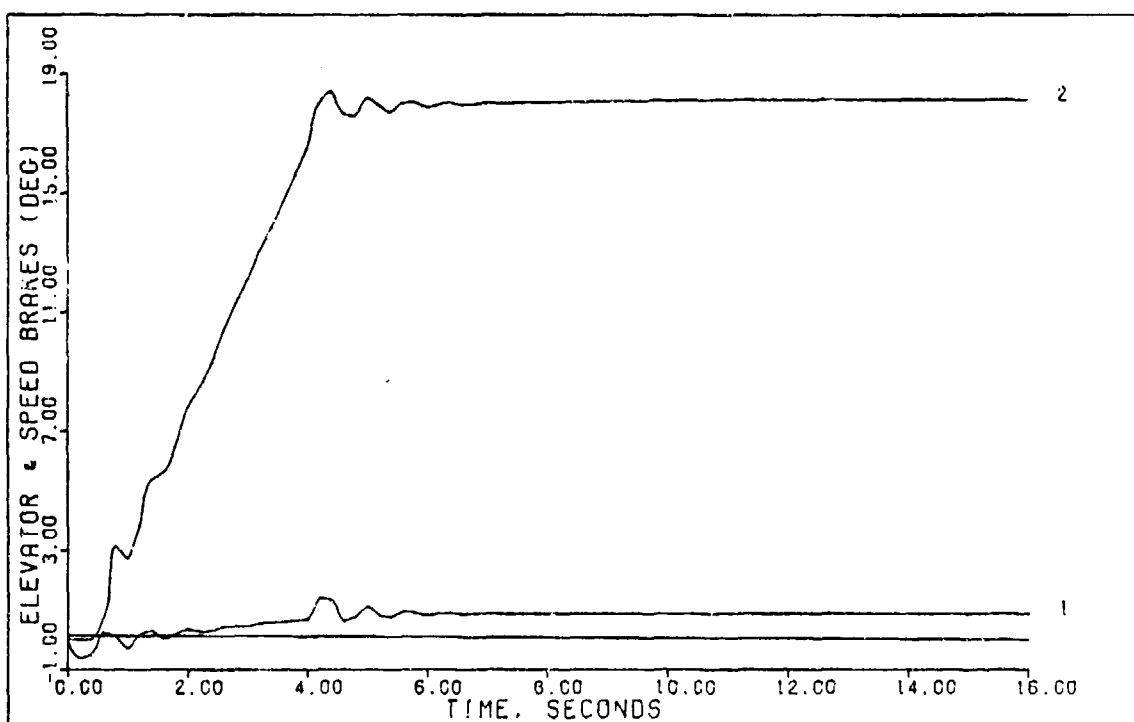


FIGURE C-4d: Flight Condition #2, Pitch Pointing  
(Control 1: Elevator; Control 2: Speed Brakes)

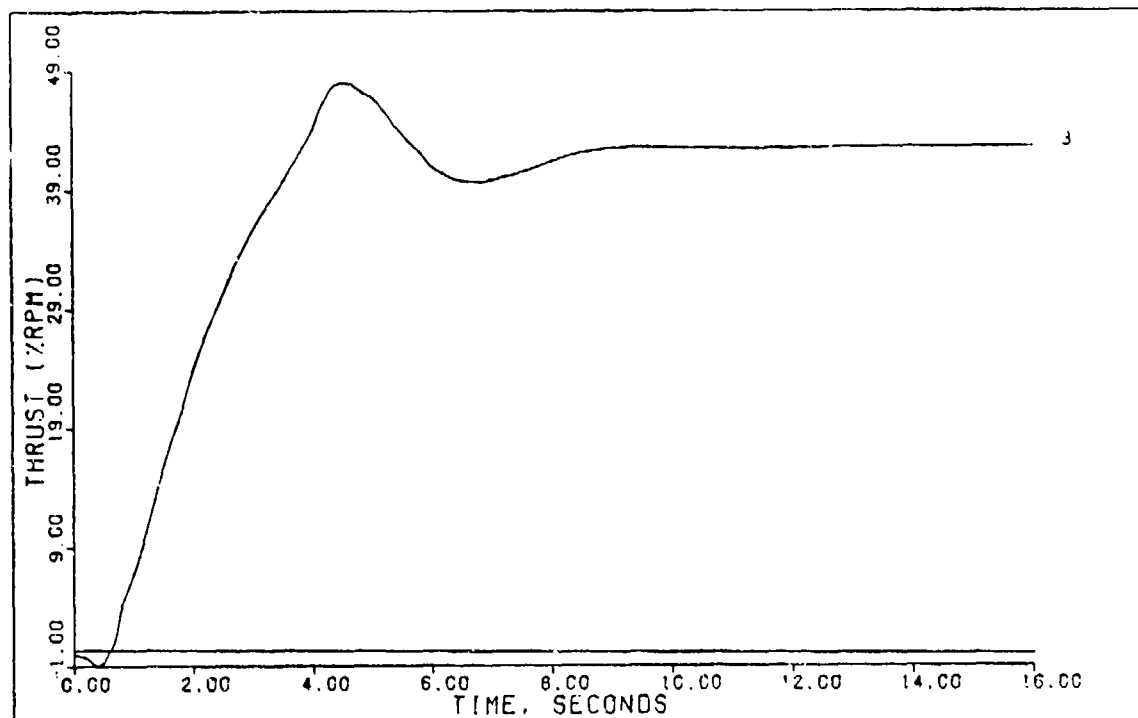


FIGURE C-4e: Flight Condition #2, Pitch Pointing  
(Control 3: Thrust)

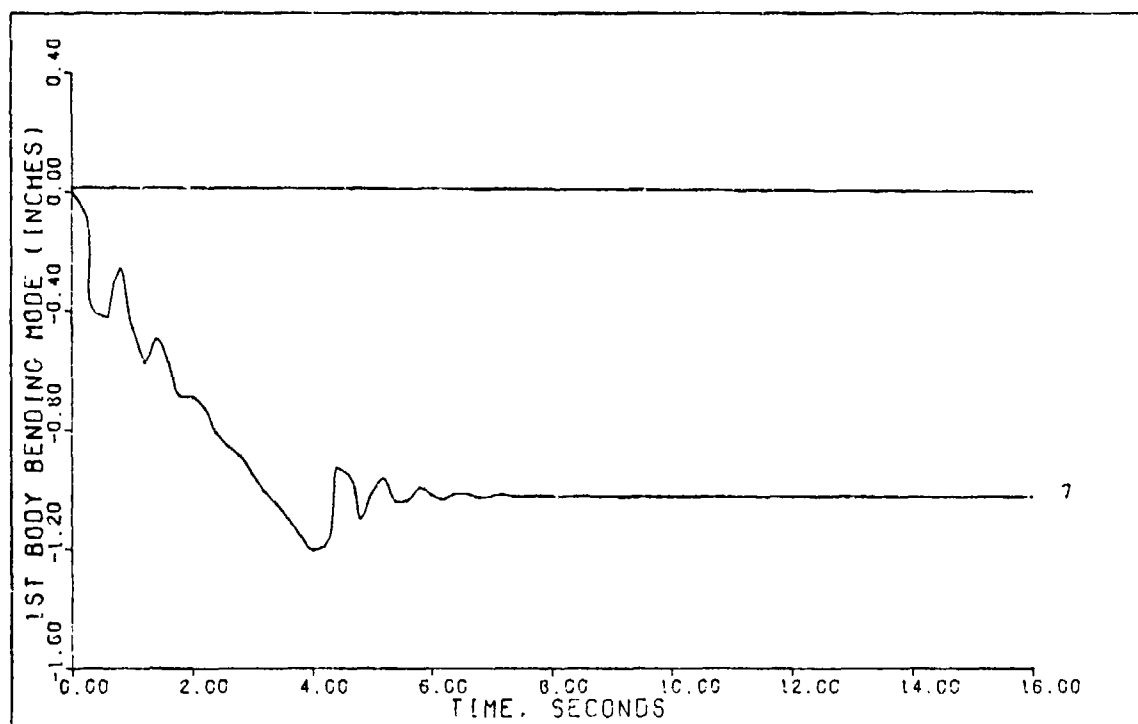


FIGURE C-4f: Flight Condition #2, Pitch Pointing  
(State 7: 1st Body Bending Mode)

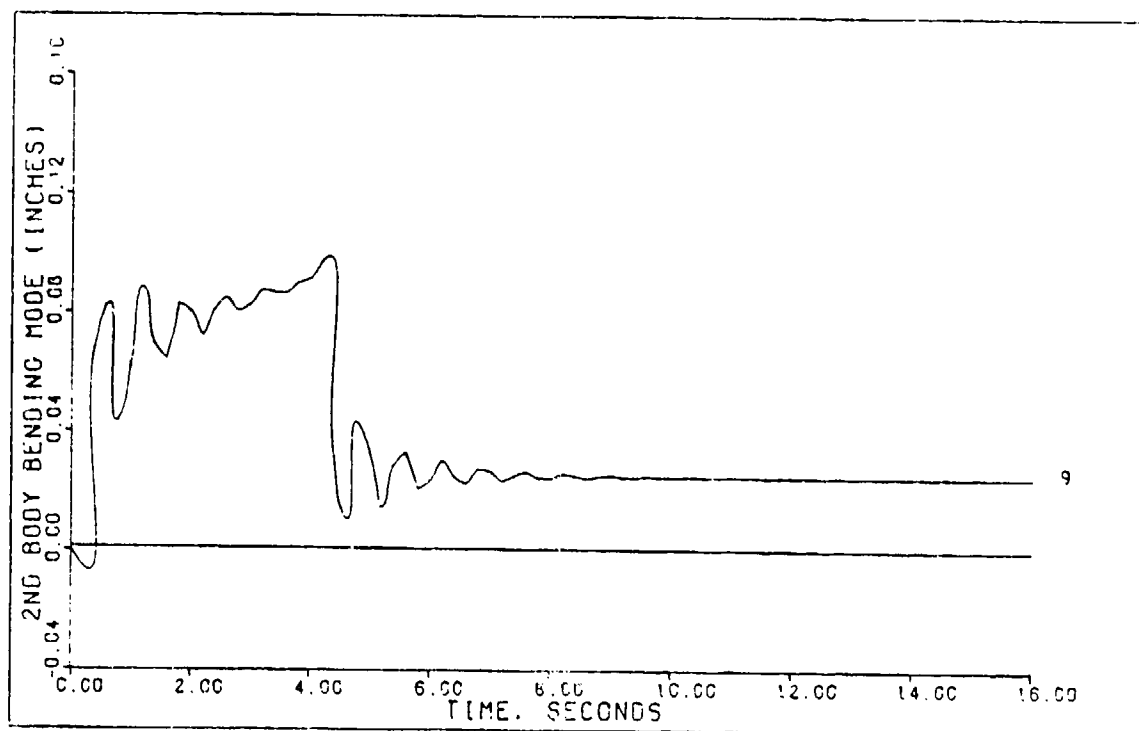


FIGURE C-4g: Flight Condition #2, Pitch Pointing  
(State 9: 2nd Body Bending Mode)

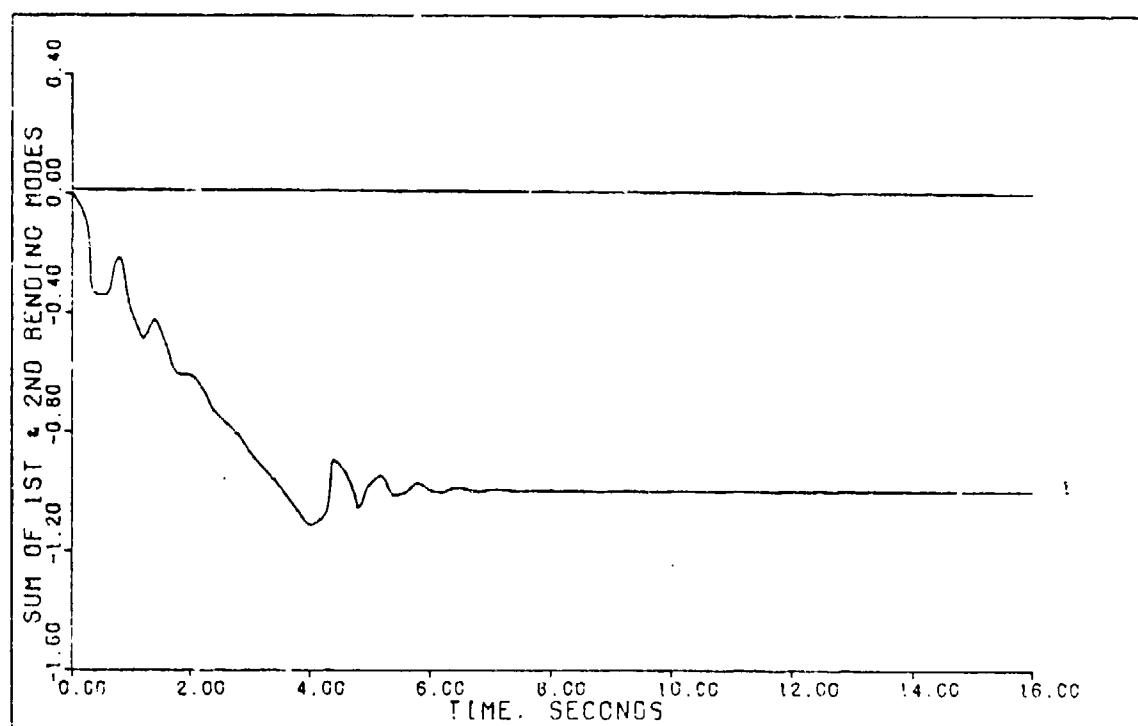


FIGURE C-4h: Flight Condition #2, Pitch Pointing  
(Sum of 1st & 2nd Bending Modes)

Table C-5  
Simulation Results For  
Flight Condition #1 Coordinated Turn

Input/ Output	Peak Value	Final Value	$t_p$ (sec)	$t_s$ (sec)
$\phi$ (deg)	30.36	30.0	6.6	5.2
$\beta$ (deg)	-0.0028	-0.00237	7.4	14.0
$r$ (deg/sec)	1.3	1.24	4.2	5.5
$\delta_r$ (deg)	-0.52	--	--	--
$\delta_w$ (deg)	27.8	--	--	--

Table C-6  
Simulation Results For  
Flight Condition #1 Sideslip

Input/ Output	Peak Value	Final Value	$t_p$ (sec)	$t_s$ (sec)
$\phi$ (deg)	-0.665	0.0	8.4	--
$\beta$ (deg)	5.06	5.0	1.6	8.6
$\delta_r$ (deg)	8.0	--	--	--
$\delta_w$ (deg)	48.0	--	--	--

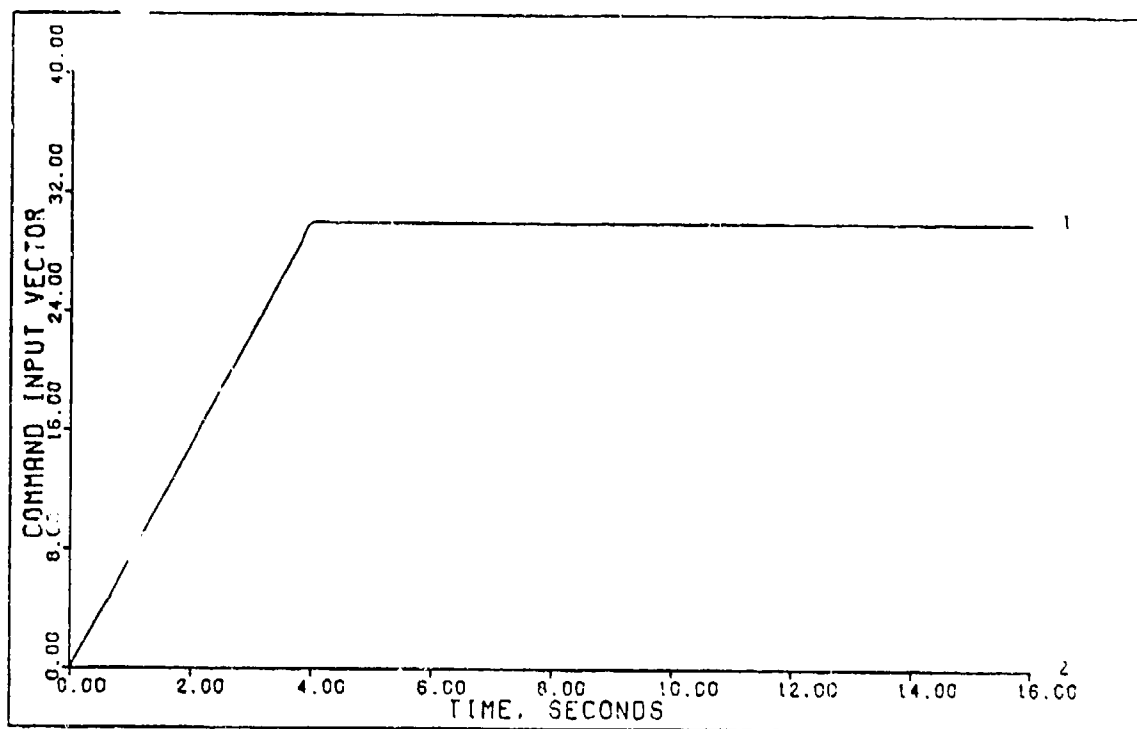


FIGURE C-5a: Flight Condition #1, Coordinated Turn  
(Command Input Vector)

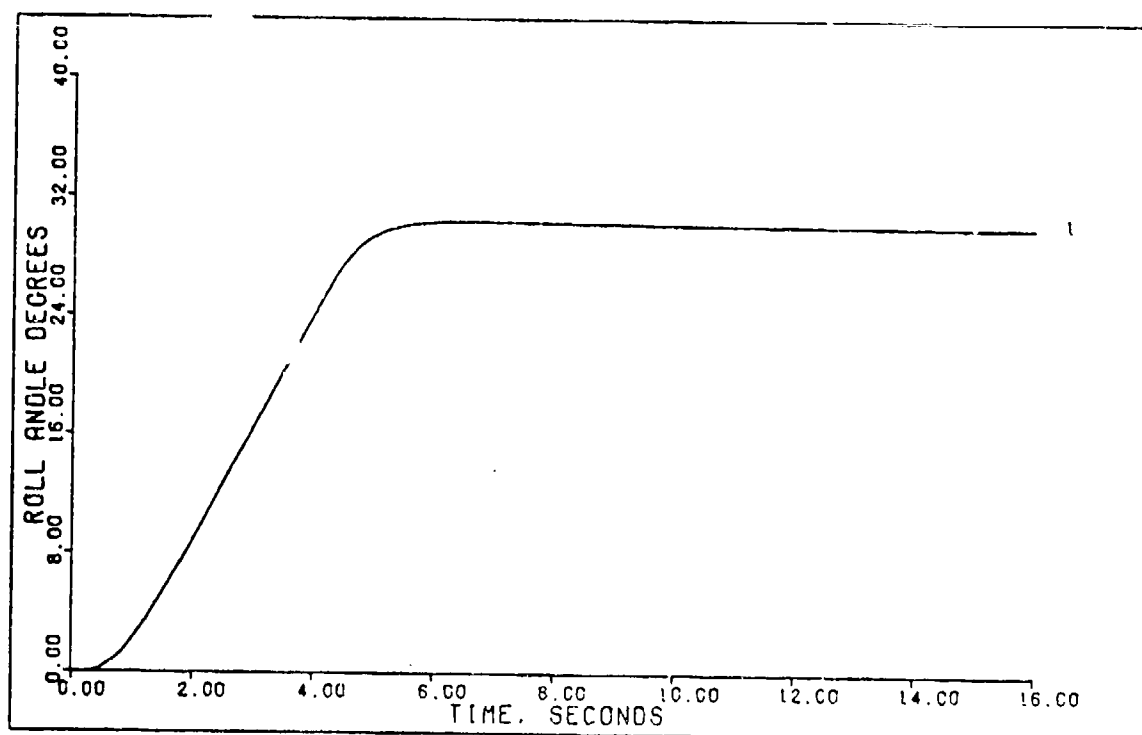


FIGURE C-5b: Flight Condition #1, Coordinated Turn  
(Output 1: Roll Angle)

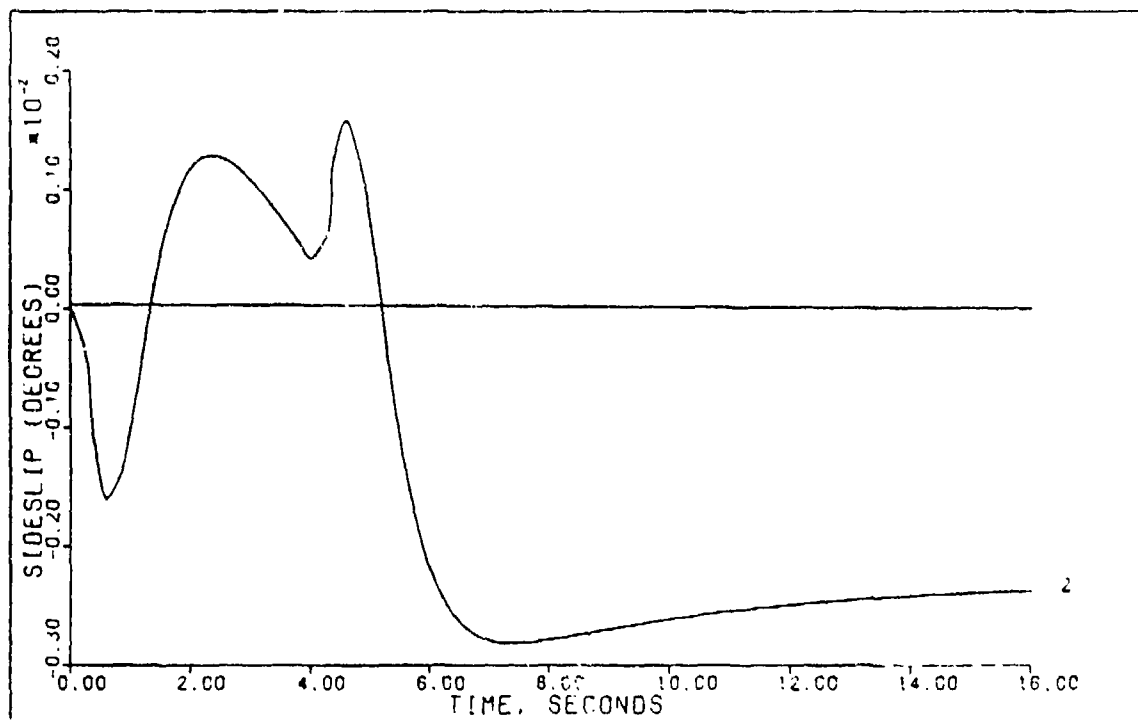


FIGURE C-5c: Flight Condition #1, Coordinated Turn  
(Output 2: Sideslip)

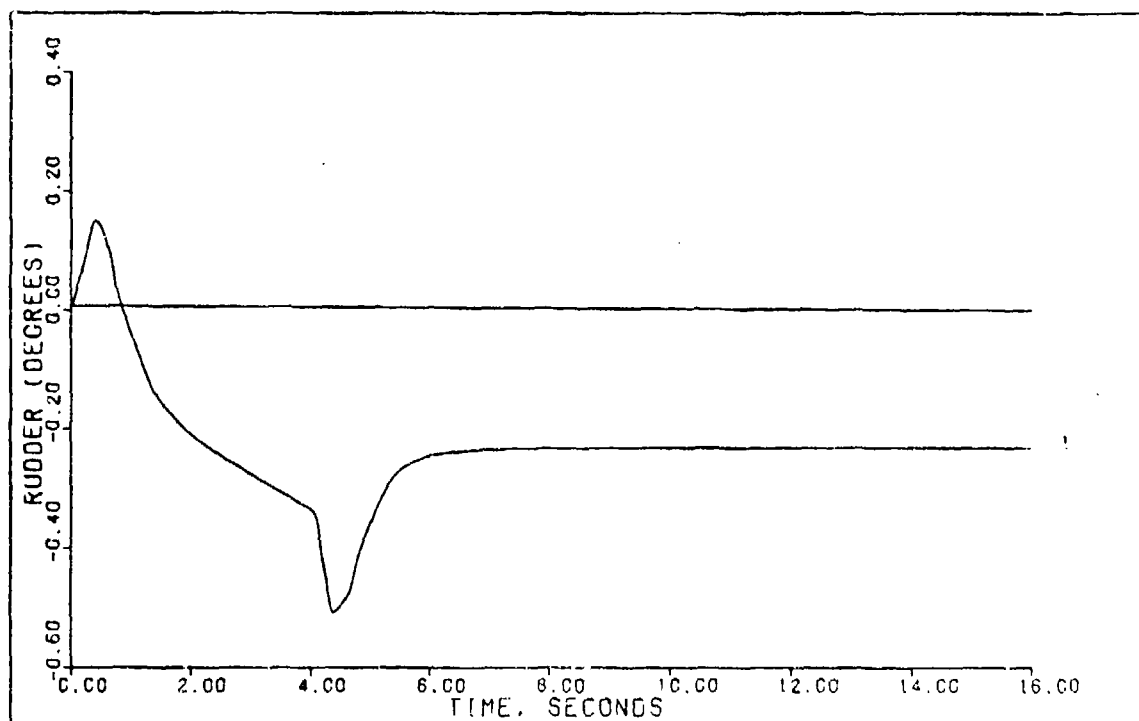


FIGURE C-5d: Flight Condition #1, Coordinated Turn  
(Control 1: Rudder)

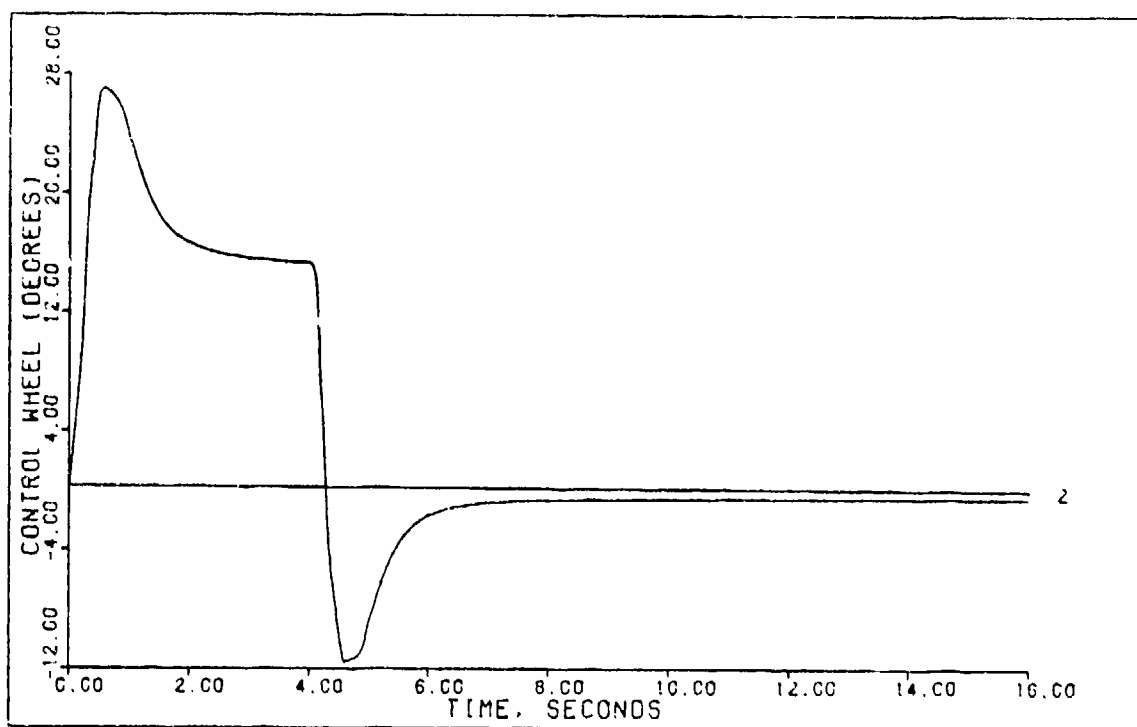


FIGURE C-5e: Flight Condition #1, Coordinated Turn  
(Control 2: Control Wheel)

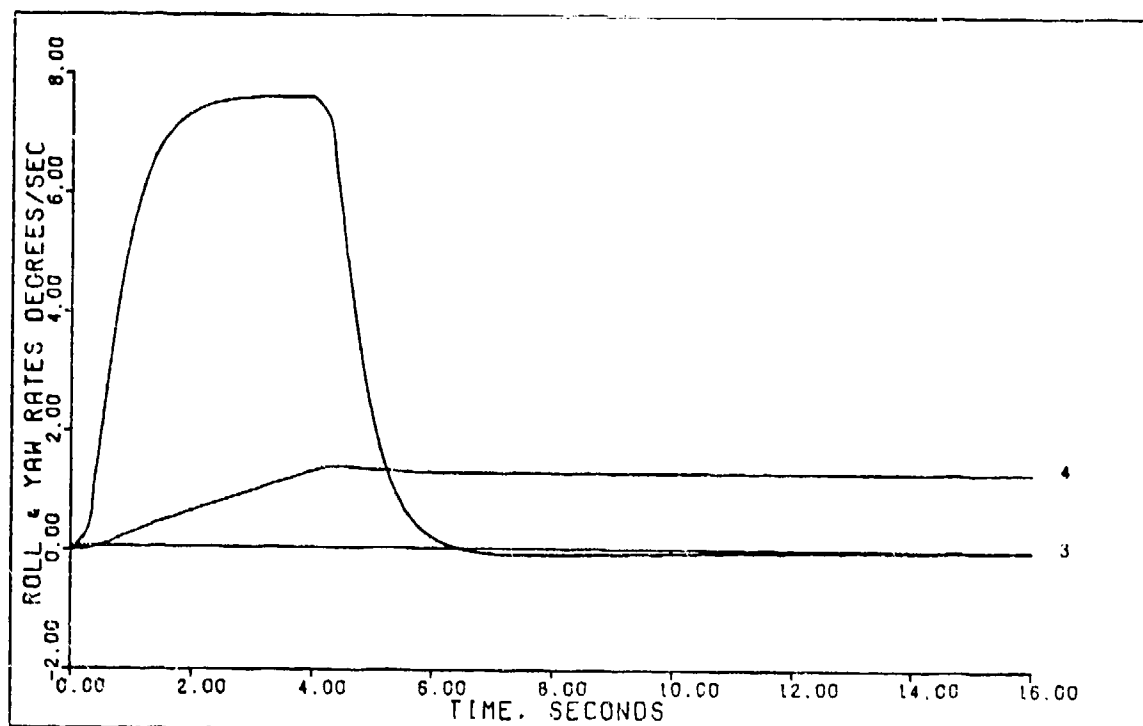


FIGURE C-5f: Flight Condition #1, Coordinated Turn  
(State 3: Roll Rate; State 4: Yaw Rate)



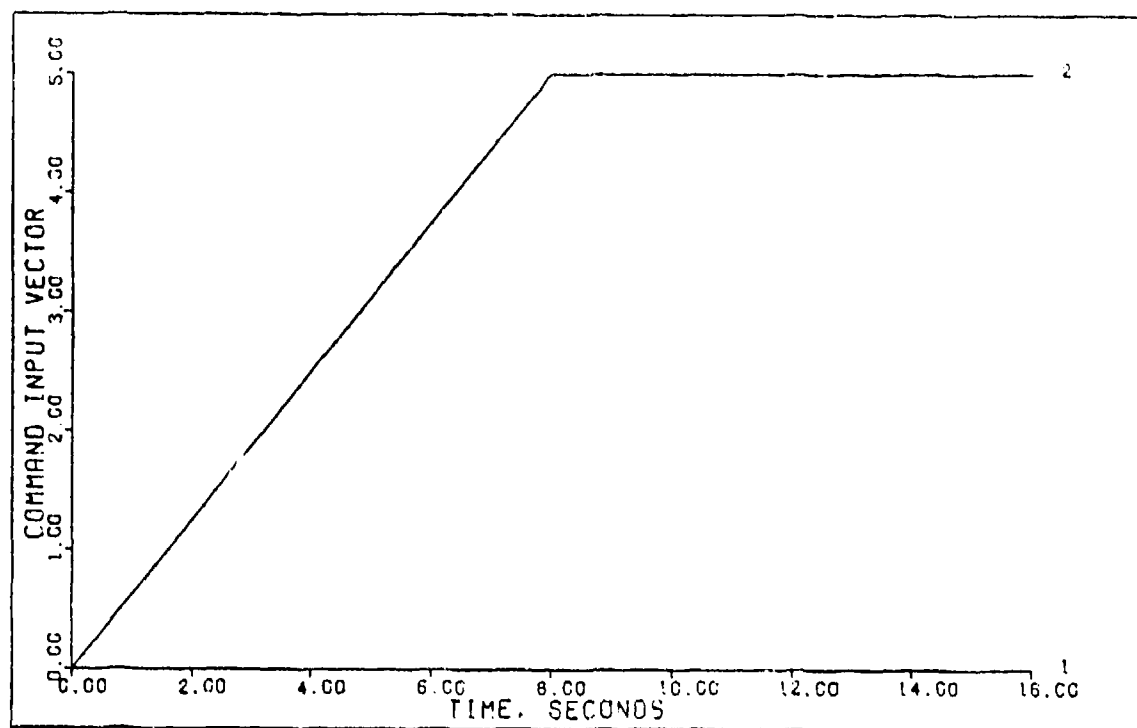


FIGURE C-6a: Flight Condition #1, Sideslip  
(Command Input Vector)

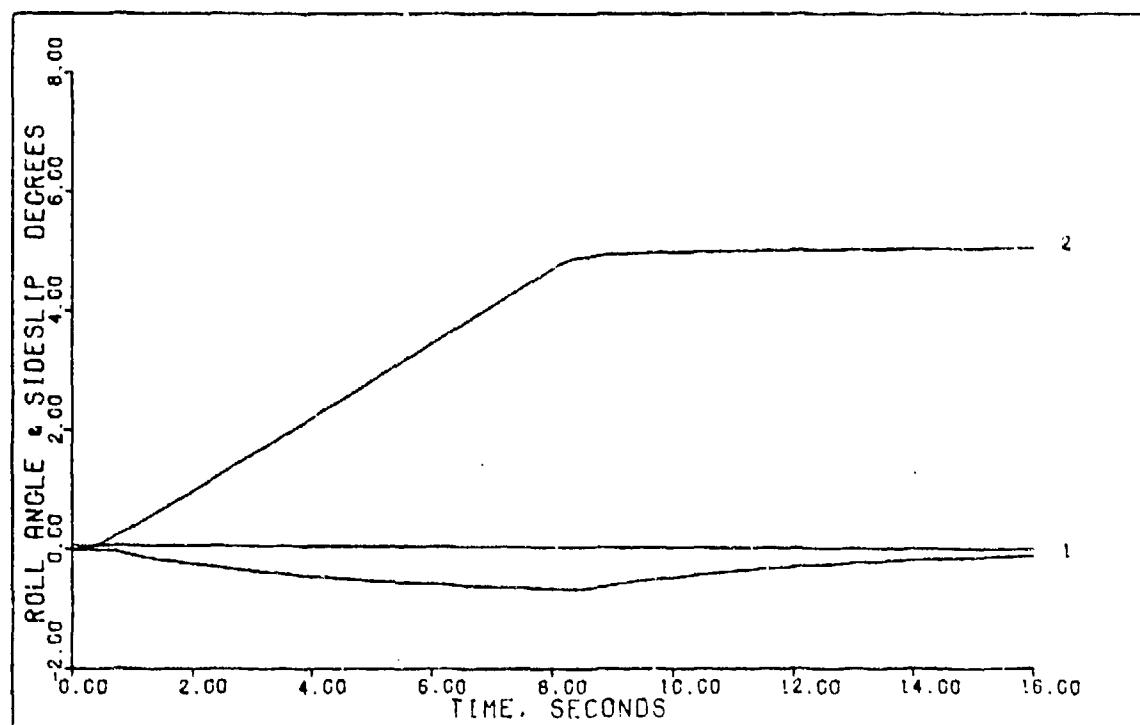


FIGURE C-6b: Flight Condition #1, Sideslip  
(Output 1: Roll Angle; Output 2: Sideslip)

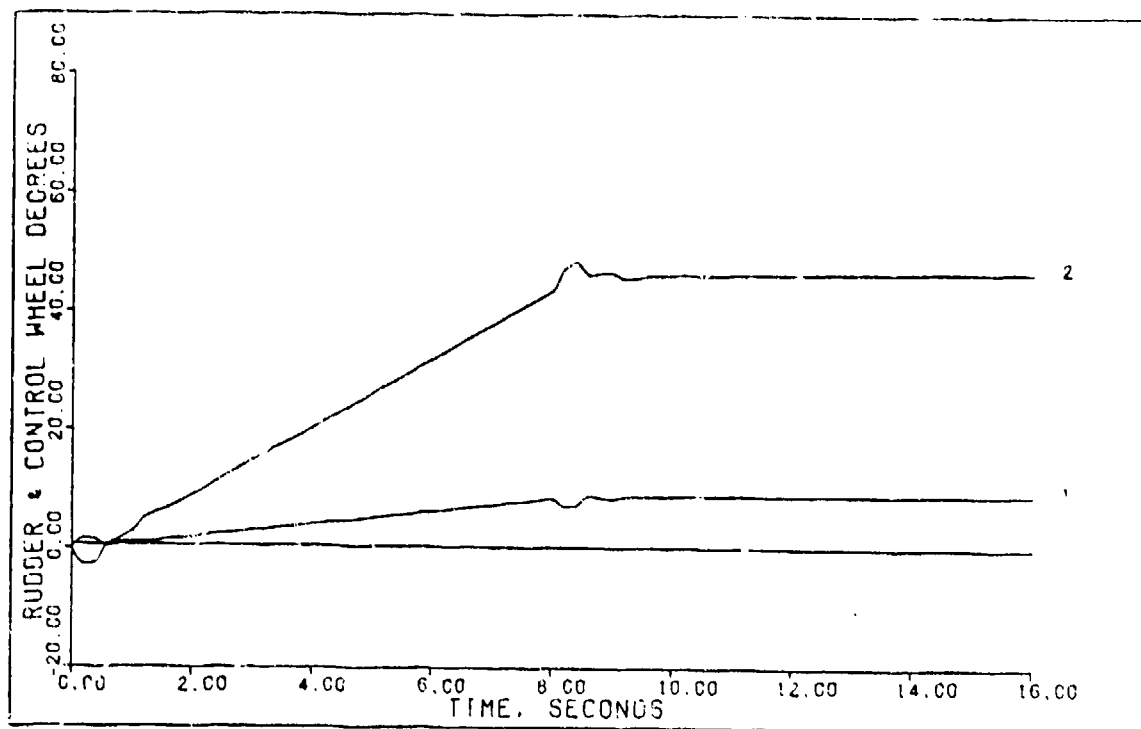


FIGURE C-6c: Flight Condition #1, Sideslip  
(Control 1: Rudder; Control 2: Control Wheel)

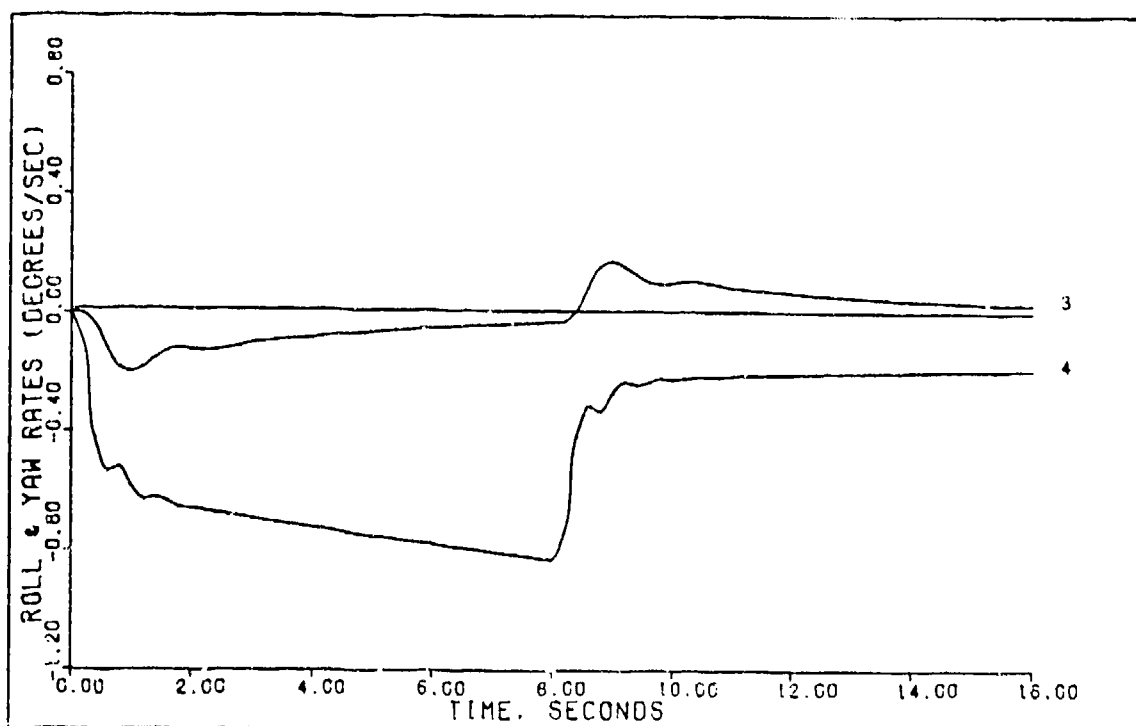


FIGURE C-6d: Flight Condition #1, Sideslip  
(State 3: Roll Rate; State 4: Yaw Rate)

Table C-7  
Simulation Results For  
Flight Condition #1 Normal Climb

Input/ Output	Peak Value	Final Value	$t_p$ (sec)	$t_s$ (sec)
$\gamma$ (deg)	1.76	1.54	8.4	14.4
$u$ (ft/sec)	-0.112	0.0	6.0	--
$\delta_e$ (deg)	1.3	--	--	--
$\delta_T$ (%RPM)	19.0	--	--	--

Table C-8  
Simulation Results For  
Flight Condition #1 Pitch Pointing

Input/ Output	Peak Value	Final Value	$t_p$ (deg)	$t_s$ (deg)
$h$ (ft)	-0.16	0.0	4.2	--
$\theta$ (deg)	1.01	1.0	16.0	5.2
$u$ (ft/sec)	-0.18	0.0	1.9	--
$\delta_e$ (deg)	1.2	--	--	--
$\delta_{sb}$ (deg)	17.0	--	--	--
$\delta_T$ (%RPM)	32.5	--	--	--

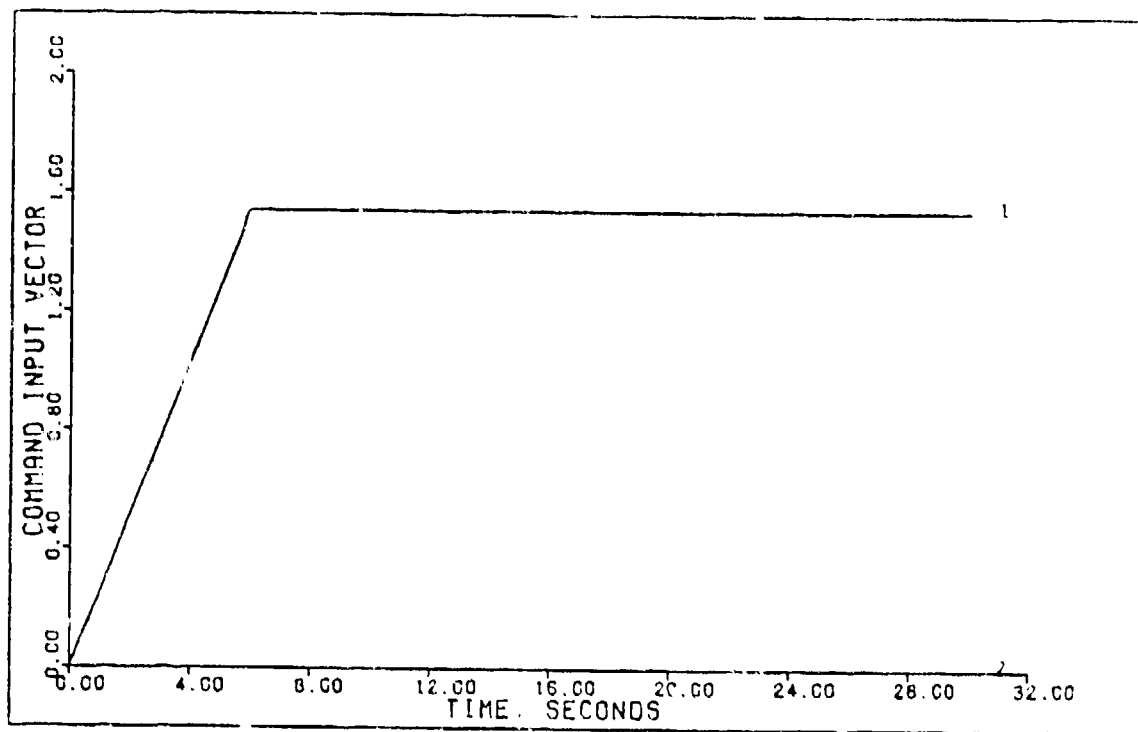


FIGURE C-7a: Flight Condition #1, Normal Climb  
(Command Input Vector)

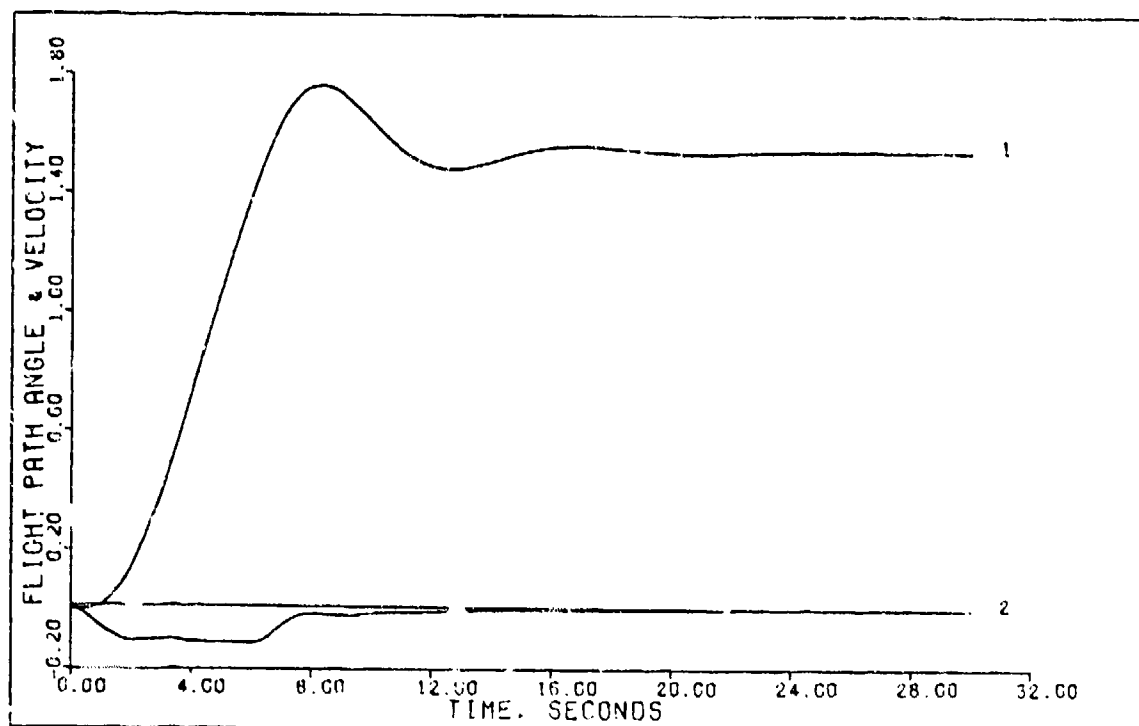


FIGURE C-7b: Flight Condition #1, Normal Climb  
(Output 1: Flight Path Angle;  
Output 2: Velocity)

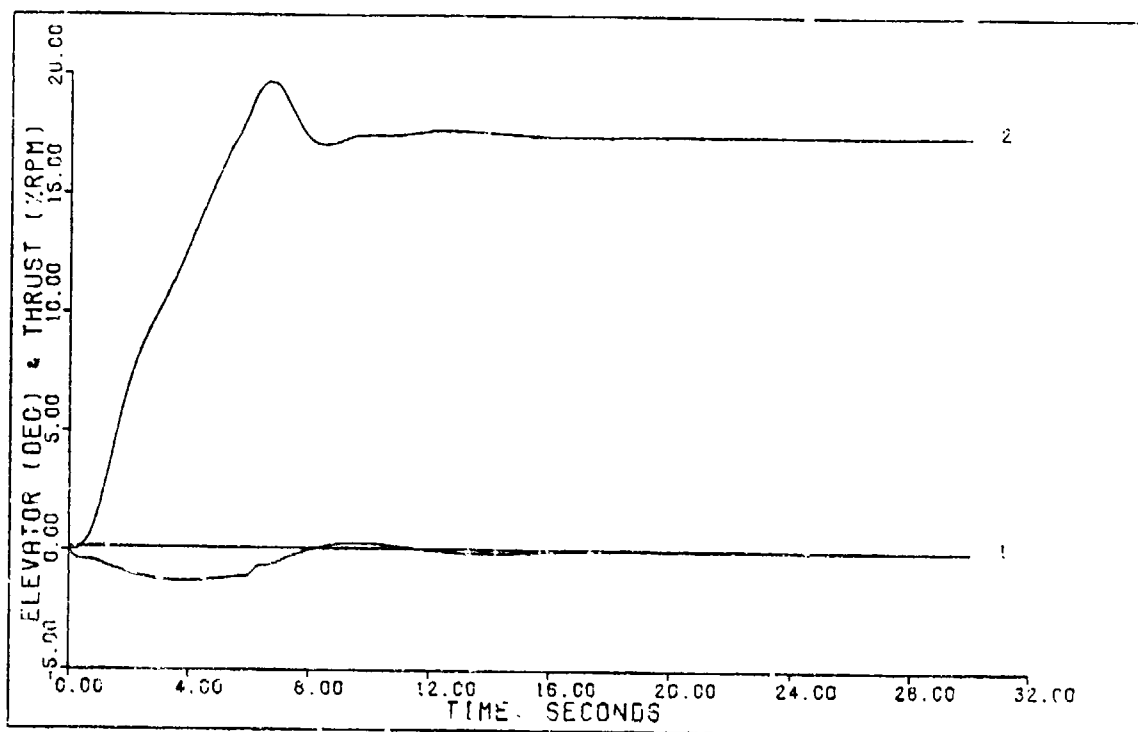


FIGURE C-7c: Flight Condition #1, Normal Climb  
(Control 1: Elevator; Control 2: Thrust)

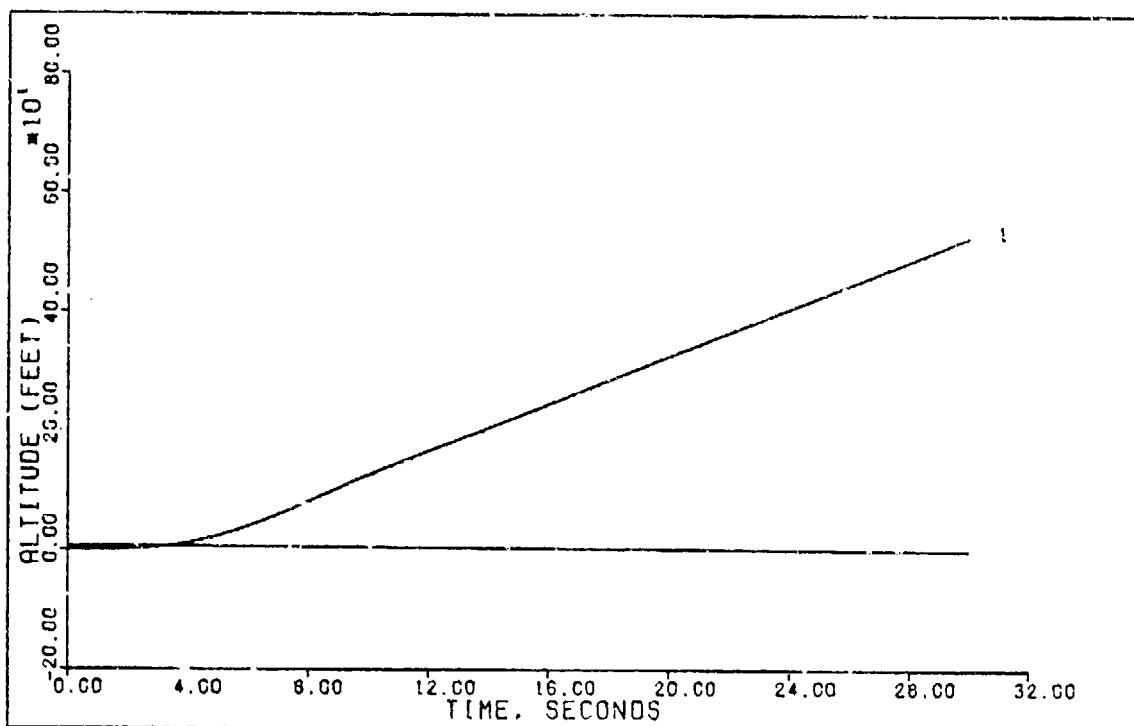


FIGURE C-7d: Flight Condition #1, Normal Climb  
(State 1: Altitude)

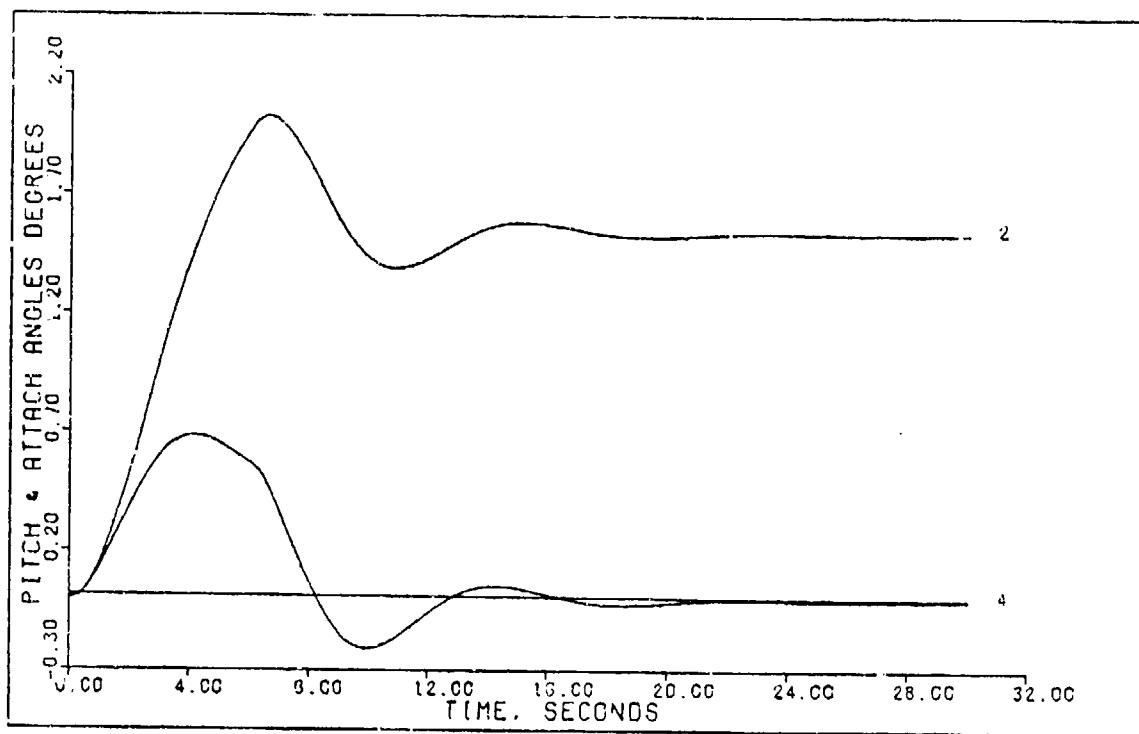


FIGURE C-7e: Flight Condition #1, Normal Climb  
(State 2: Pitch Angle; State 4: Attack Angle)

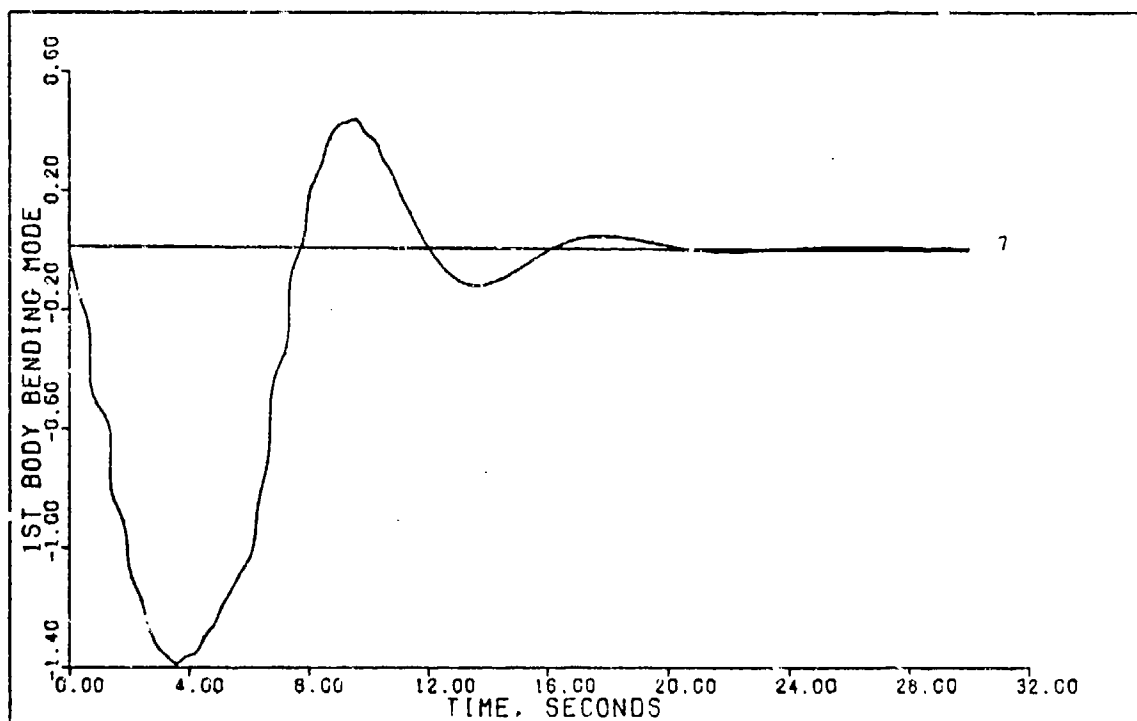


FIGURE C-7f: Flight Condition #1, Normal Climb  
(State 7: 1st Body Bending Mode)

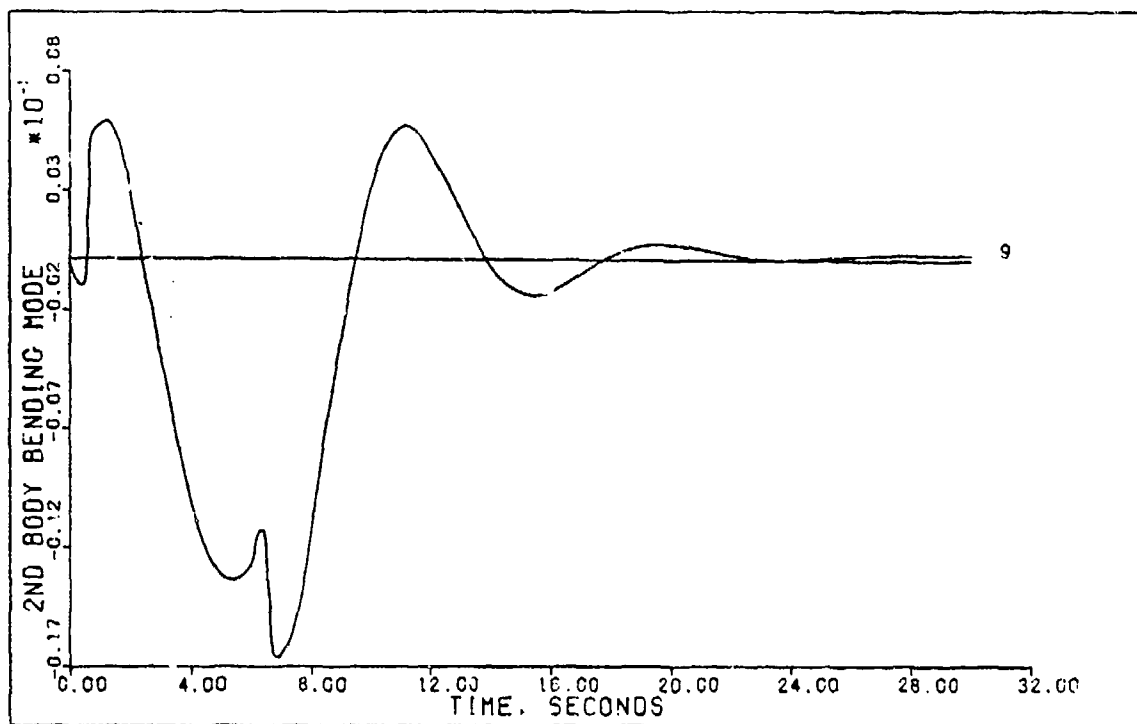


FIGURE C-7g: Flight Condition #1, Normal Climb  
(State 9: 2nd Body Bending Mode)

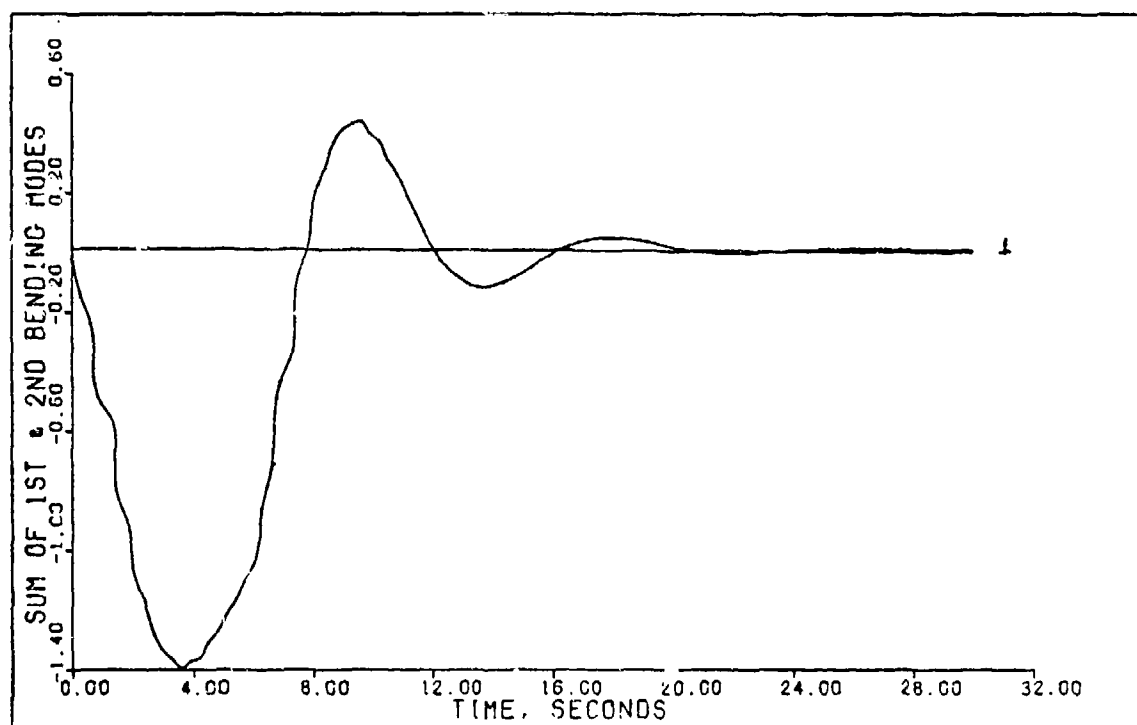


FIGURE C-7h: Flight Condition #1, Normal Climb  
(Sum of 1st & 2nd Bending Modes)

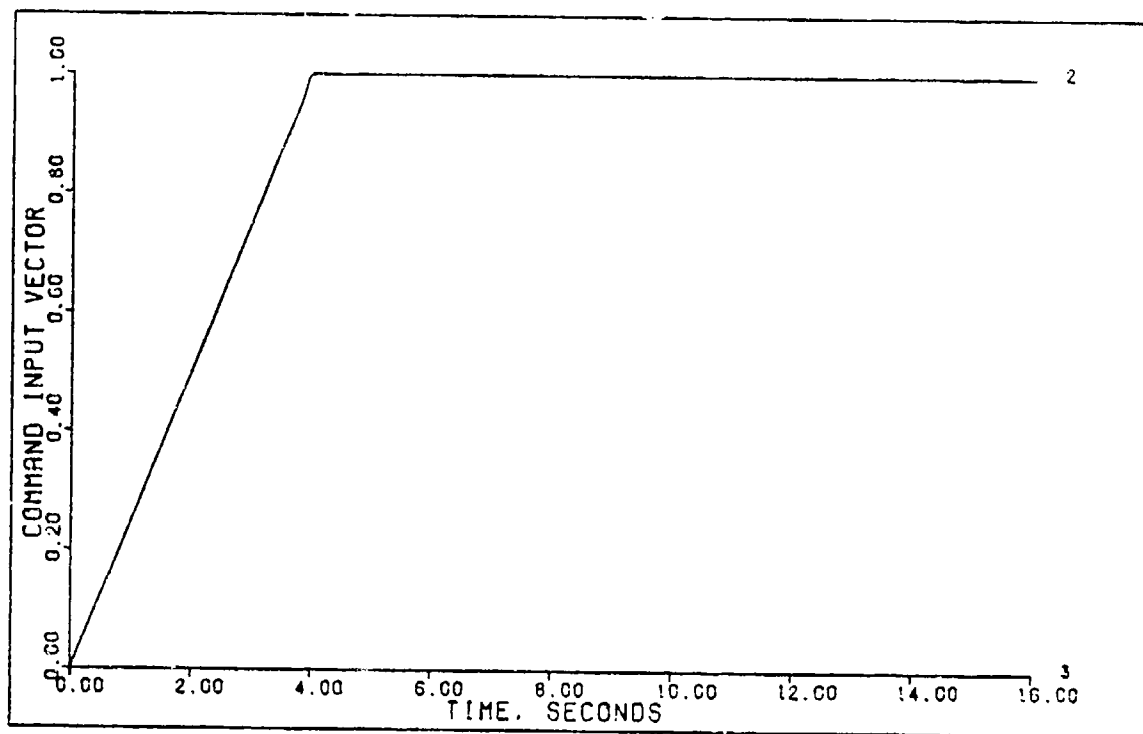


FIGURE C-8a: Flight Condition #1, Pitch Pointing  
(Command Input Vector)

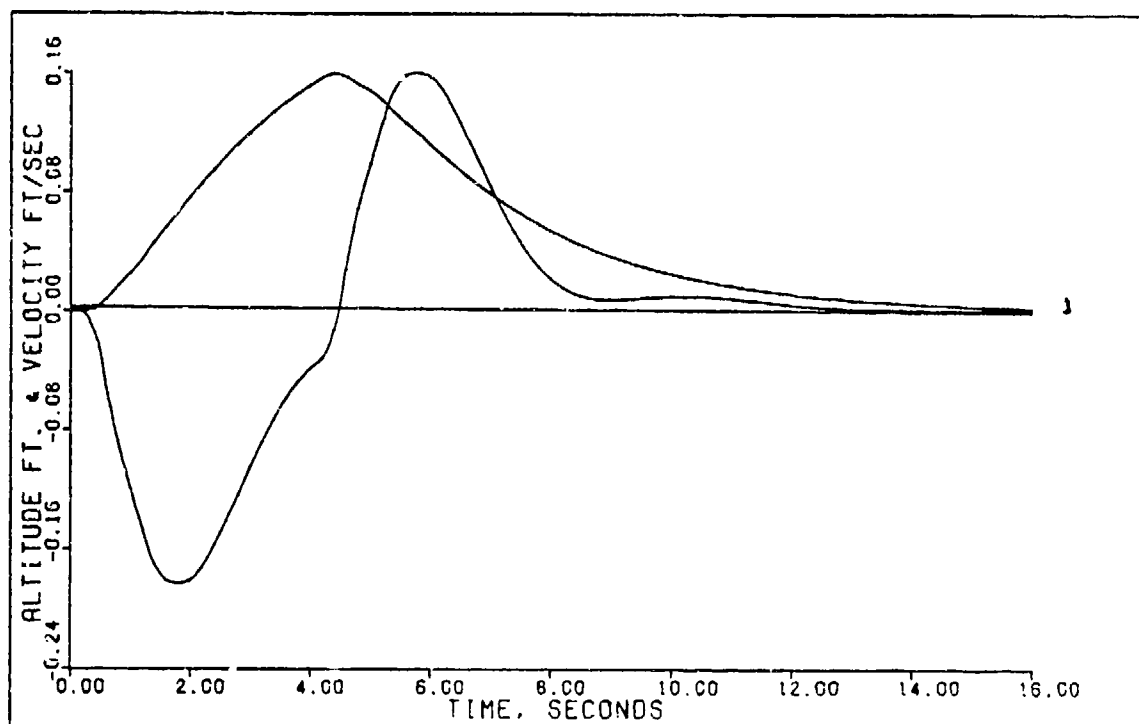


FIGURE C-8b: Flight Condition #1, Pitch Pointing  
(Output 1: Altitude; Output 2: Velocity)



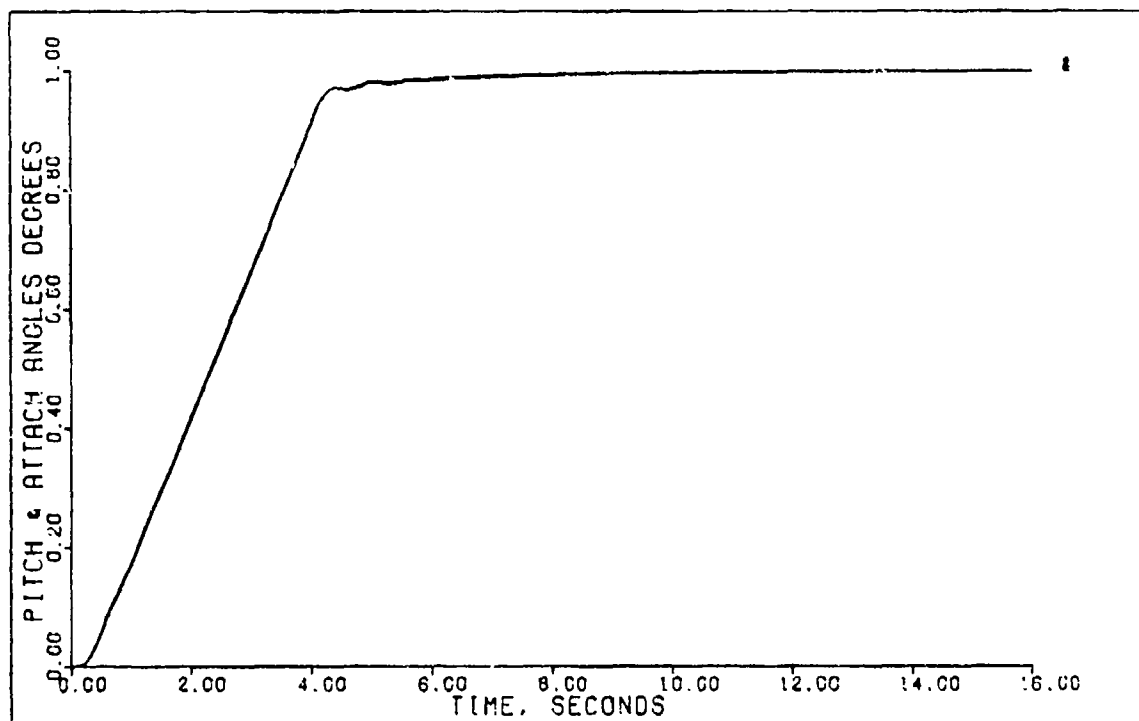


FIGURE C-8c: Flight Condition #1, Pitch Pointing  
(State 2: Pitch Angle; State 4: Attack Angle)

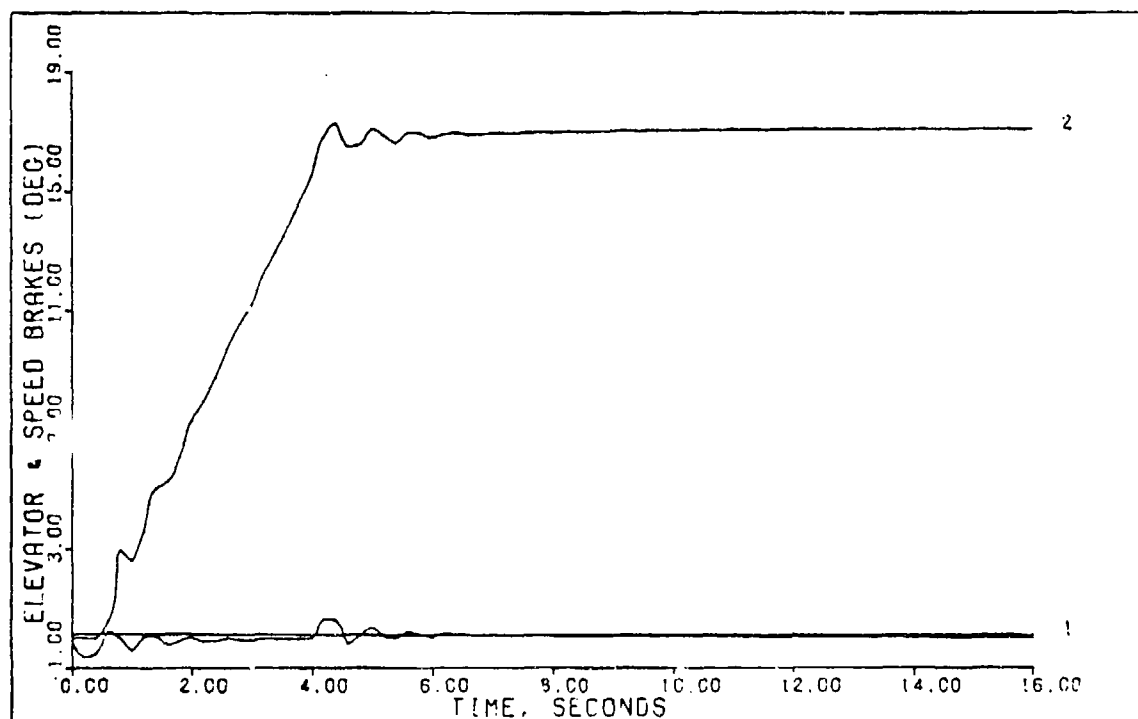


FIGURE C-8d: Flight Condition #1, Pitch Pointing  
(Control 1: Elevator; Control 2: Speed Brakes)

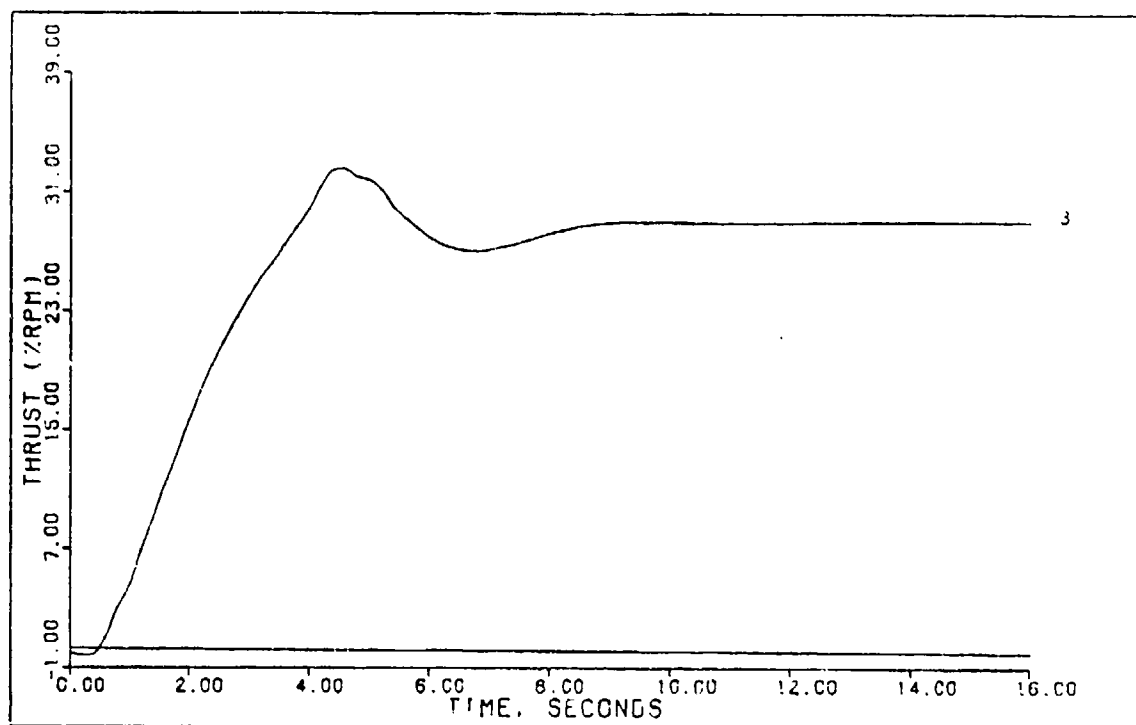


FIGURE C-8e: Flight Condition #1, Pitch Pointing  
(Control 3: Thrust)

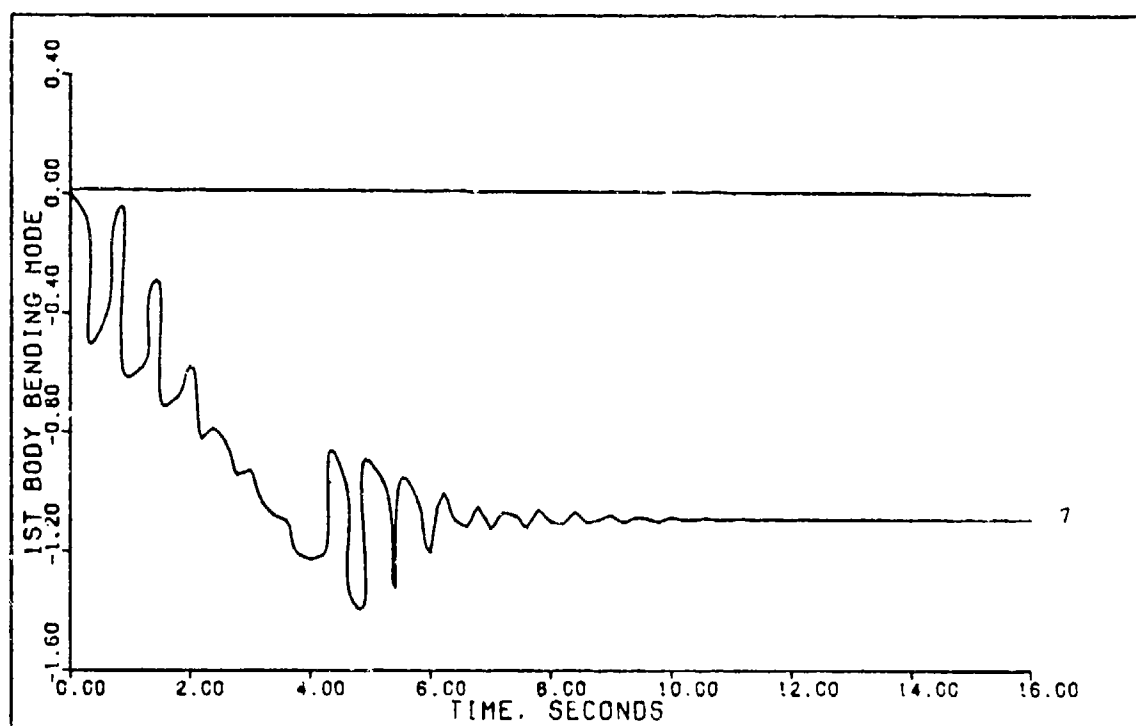


FIGURE C-8f: Flight Condition #1, Pitch Pointing  
(State 7: 1st Body Bending Mode)

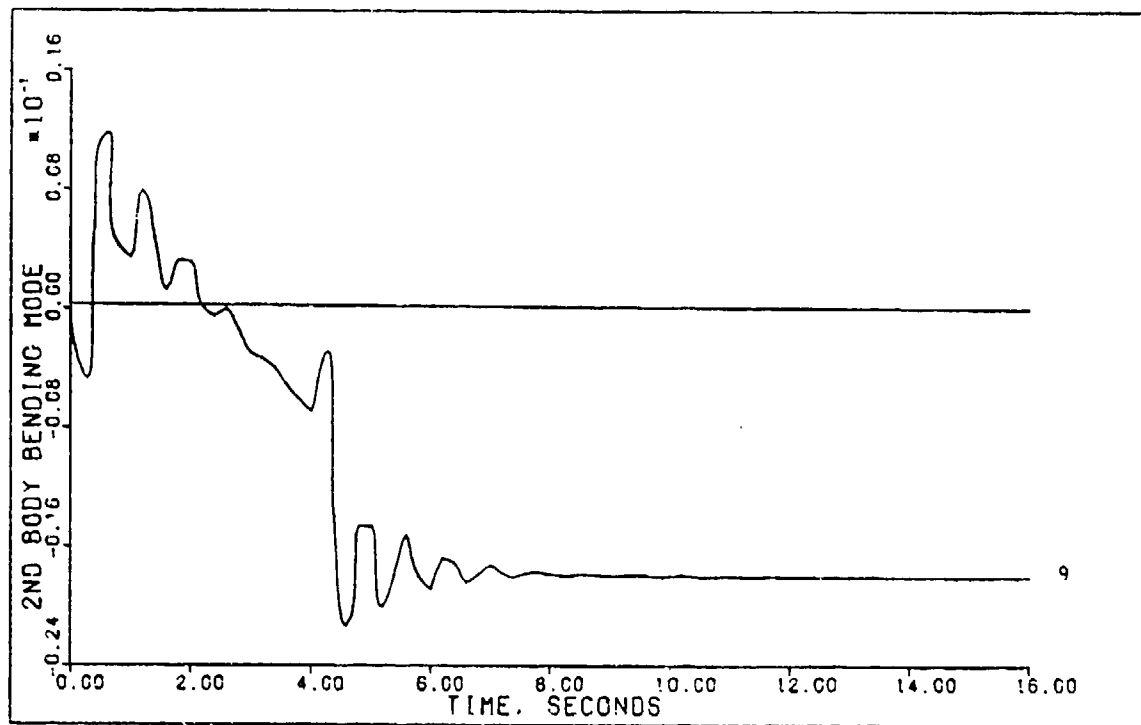


FIGURE C-8g: Flight Condition #1, Pitch Pointing  
(State 9: 2nd Body Bending Mode)

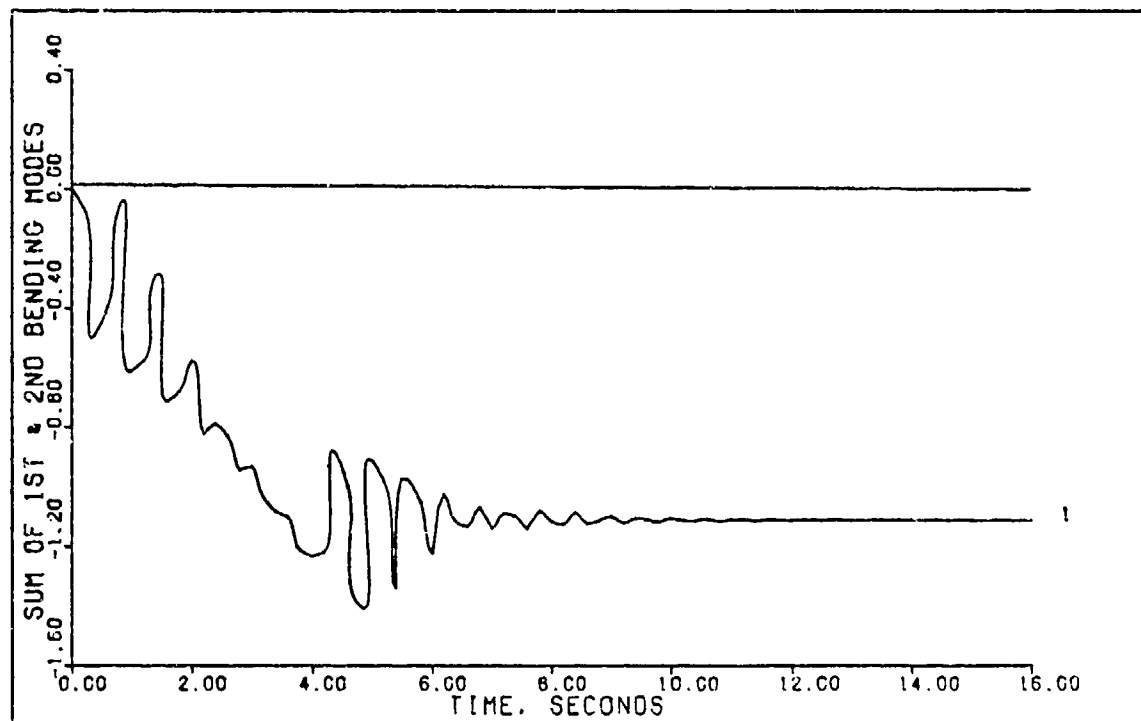


FIGURE C-8h: Flight Condition #1, Pitch Pointing  
(Sum of 1st & 2nd Bending Modes)

APPENDIX D  
CALCOMP PLOTS

Introduction

As designs approached the final stage, calcomp plots showing flight control system performance were generated using OPTION #34 and #35. Comparision of terminal generated plots and those recieved from the calcomp plotter showed that plots whose y-axis were properly scaled on the terminal were some times improperly scaled by the calcomp plotter. This was more evident when attempting to plot curves that had only small deviations from zero. In some cases the y axis scaling produced curves that were hardly distinguishable from the zero line. See Figure D-1 as an example.

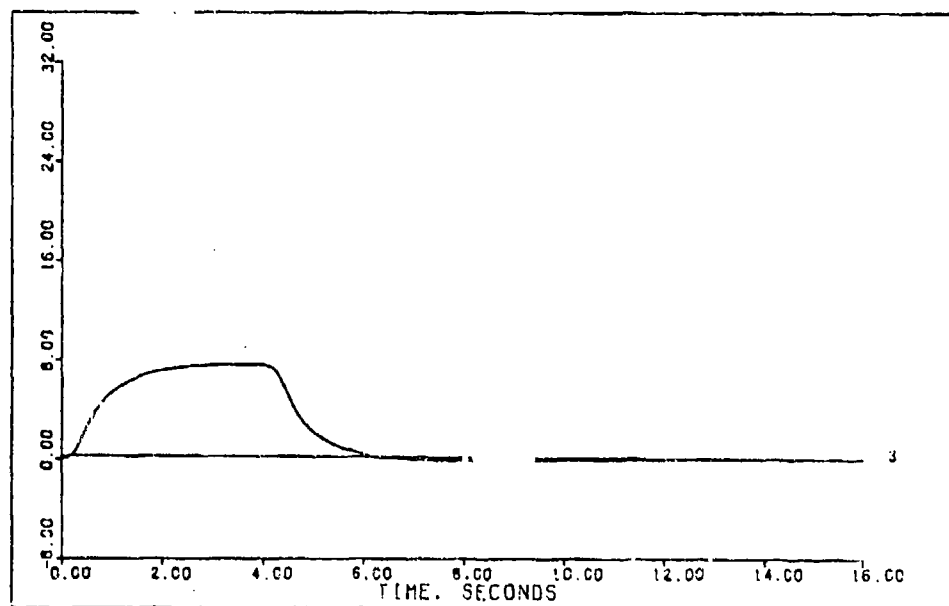


FIGURE D-1: Improperly Scaled Calcomp Plot

Discussions with earlier users of MULTI verified that a problem with the calcomp plots did indeed exist. However, no one in the past had made any attempt to investigate the problem.

This appendix identifies a problem with the calcomp plot routines found in MULTI and explains a fix that is now incorporated to eliminate that problem.

#### Analysis of the Calcomp Routine

An analysis was made of the Fortran code in the plot options of MULTI to determine why such plots as the one shown in Fig. D-1 were being generated. When any of the options in the thirties is called (i.e. 31,32,33,34,35,35), the first thing accomplished in MULTI is the generation and storage of the data to be plotted. All plot data is generated from the packed data that is generated in the simulation, OPTION #26. This data consists of a maximum of 101 data points. When the plot data is generated it is stored in a matrix called PLMAT which is 103 rows by 4 columns. At this point rows 102 and 103 are zero. Each column of PLMAT represents a collection of data that is sent to the calcomp plotter and is used to generate one curve. A maximum of 4 curves can be printed on each plot and these are explained in the MULTI Users Manual, Reference 4.

Once data has been stored in PLMAT the appropriate columns are searched to determine the maximum and minimum values for that data being plotted. If two curves are to

appear on the calcomp plot, then two columns of PLMAT are searched; if three curves, then three columns and so forth. The maximum and minimum values as determined from this process are placed in the number one and two positions of a new vector called Y-axis which is 103 elements long. This vector was formerly filled with 99 data points from the second column of PLMAT. At this point Y-axis consists of 101 points, where 99 of them are just fill points from column two of PLMAT and points 102 and 103 are zero. Next a call to SCALE is made with the array Y-axis as the passed data. SCALE is a subroutine of the calcomp plotter that determines the minimum, maximum, and a "delta" increment for a set of points. The delta selected is limited to 1,2,4,5, or 8 times a power of ten. SCALE returns to MULTI the Y-axis data consisting of 101 data points previously generated plus, in position 102, the minimum as determined from the call to SCALE and in position 103 the delta also determined by SCALE. Multi then assigns the 102 and 103 values of Y-axis to the 102 and 103 rows of PLMAT, in each of the columns to be plotted. Once this has been completed each column of PLMAT represents all data required by the calcomp plotter to generate a single curve. This includes 101 data points, the minimum value, and delta as determined by SCALE. The error that caused plots as shown in Figure D-1 was generated by the call to SCALE. SCALE uses Y-axis to determine a minimum and a delta value. Y-axis consisted of 99 data points that may or may not be plotted since they

came from column two of PLMAT. This column is plotted only if two curves are generated on the same graph. Since column one of PLMAT would always be used to generate a curve on the calcomp plot, the code was changed to use this column instead of column two when filling the data into Y-axis. This code change eliminates the bug that existed in the calcomp plot routines.

#### Summary

An error in MULTI's Fortran code formerly generated calcomp plot files that gave improperly scaled calcomp plots under certain circumstances. This error was tracked down and eliminated.

## APPENDIX E

### Debugging of Multi Fortran Code

Chapter 4 gives a summary of the fortran code changes necessary to incorporate a computational time delay. Once these changes were made a sample run of the program was accomplished using the examples given in Reference 14. These examples used a computational time delay of one sampling period. Comparison of the results from the trial run of MULTI and the results given in Reference 14 showed that a problem initially existed with MULTI. This was evident since MULTI showed an unstable system for the stable system of Reference 14. Thus it became necessary to perform error checking on the Fortran Code for MULTI. As a means of doing this error checking, temporary print statements were added to the simulation portion of MULTI to print  $s(kT)$ ,  $r(kT)$  and  $u(kT)$  as given by Equations (4-1), (4-2) and (4-3). A sample run of multi was again accomplished using the same example. Comparison of the results of these extra print statements with hand calculated results showed that the computer code was performing the computational delay and it's compensation correctly as given by Equations (4-2) and (4-3). Further investigation revealed that the error vector,  $e(kT)$ , used in generation of the control law was one sampling period behind the rest of the information being used. Once this small deviation was corrected, results from MULTI compared favorably with those given by Reference 14.



## APPENDIX F

### Transformation Matrix

#### Introduction

This Appendix presents a method, in theory only, for transforming a system of state equations into the  $0-B_2$  form of Equations (2-22) and (2-23).

#### Transformation Matrix

The problem under consideration centers around the B matrix that is not in the form of Equation (2-22) and cannot be put into this form by simply rearrangement of the states. An example of this type of matrix is given in Appendix A and applies to the lateral equations used in this thesis. For this case the B matrix is of the form

$$B = \begin{bmatrix} 0 & 0 \\ B_{21} & B_{22} \\ B_{31} & B_{32} \\ B_{41} & B_{42} \end{bmatrix} \quad (D-1)$$

where B is an nxm matrix with n equal to the number of states and m equal to the number of inputs.

The desired result is a transformation matrix T that transforms Equation (D-1) into the  $0-B_2$  form of Equation (2-22). The proposed form for this T matrix is shown in Equation (D-2).

$$\begin{bmatrix} 0 \\ B_2 \end{bmatrix} = \begin{bmatrix} 0 & 0 \\ B_{31} & B_{32} \\ B_{41} & B_{42} \end{bmatrix} = \begin{bmatrix} 1 & 0 & 0 & 0 \\ 0 & 1 & T_{23} & T_{24} \\ 0 & 0 & 1 & 0 \\ 0 & 0 & 1 & 0 \end{bmatrix} \begin{bmatrix} 0 & 0 \\ B_{21} & B_{22} \\ B_{31} & B_{32} \\ B_{41} & B_{42} \end{bmatrix} \quad (D-2)$$

Notice the simple structure of the T matrix, ones on the principle diagonal and only two undetermined elements,  $T_{23}$  and  $T_{24}$ . Notice also that the  $B$  of Equations (D-2) contains the last two rows of the original B matrix. This will always be the case when T is of the form shown in Equation (D-2). Expanding Equation (D-2) results in the following two equations.

$$B_{21} + T_{23}B_{31} + T_{24}B_{41} = 0 \quad (D-3)$$

$$B_{22} + T_{23}B_{32} + T_{24}B_{42} = 0 \quad (D-4)$$

Equations (D-3) and (D-4) represent a system of two equations and two unknowns ( $T_{23}$  and  $T_{24}$ ) for which there is a unique solution. Once T is found the new system is given by the state equations:

$$\dot{z} = A'z + \begin{bmatrix} 0 \\ B_2 \end{bmatrix} u \quad (D-5)$$

$$y = C'z \quad (D-6)$$

where

$$A' = TAT^{-1} \quad (D-7)$$

$$C' = CT^{-1} \quad (D-8)$$

and

$$z = Tx \quad (D-9)$$

Notice that the new state vector  $z$  has all but one of the states of the original system and the remaining state is a linear combination of the other states.

For higher order systems the following general statements can be applied. Forcing the principle diagonal elements of  $T$  to be exactly one results in a system of equations that will always yield a unique solution for the unknown elements of  $T$ . The  $0-B_2$  matrix that results from the transformation will always contain the bottom  $m$  rows of the original  $B$  matrix. The new state vector will have  $n-m-f$  state that are a combination of the original states. Where  $f$  is equal to the number of zero rows of the original  $B$  matrix. The remaining states will always be the same as the original system.

### VITA

William J. Locken was born in Parkston, South Dakota on 6 June 1951. After graduation from Hanson High School he attended South Dakota State University, Brookings, South Dakota, from September 1969 to December 1973. He received his Bachelor of Science Degree in Electrical Engineering from SDSU. He was commissioned as a Distinguished Graduate through the Air Force ROTC program from which he received a two-year scholarship.

After completing Undergraduate Pilot Training at Craig AFB, Alabama in July 1975 he was assigned to the 28th Bombardment Wing, 28th Air Refueling Squadron, Ellsworth AFB, South Dakota. He currently has a Senior Pilot rating with approximately 2000 hours of jet aircraft time.

He entered the Graduate Electrical Engineering program at the School of Engineering, Air Force Institute of Technology in June 1982. His next assignment is with the 6585 Test Group (AFSC) Holloman AFB, New Mexico

Permanent Home Address: Box 68  
Dimock, South Dakota  
57331

UNCLASSIFIED

SECURITY CLASSIFICATION OF THIS PAGE

AD-A141 118

## REPORT DOCUMENTATION PAGE

REPORT SECURITY CLASSIFICATION UNCLASSIFIED			1b. RESTRICTIVE MARKINGS	
2a. SECURITY CLASSIFICATION AUTHORITY			3. DISTRIBUTION/AVAILABILITY OF REPORT Approved for public release; distribution unlimited.	
2b. DECLASSIFICATION/DOWNGRADING SCHEDULE				
4. PERFORMING ORGANIZATION REPORT NUMBER(S) AFIT/GE/EE/83D-40			5. MONITORING ORGANIZATION REPORT NUMBER(S)	
6a. NAME OF PERFORMING ORGANIZATION School of Engineering		6b. OFFICE SYMBOL (If applicable) AFIT/ENG	7a. NAME OF MONITORING ORGANIZATION	
7c. ADDRESS (City, State and ZIP Code) Air Force Institute of Technology Wright-Patterson AFB, Ohio 45433			7b. ADDRESS (City, State and ZIP Code)	
8a. NAME OF FUNDING/SPONSORING ORGANIZATION		8b. OFFICE SYMBOL (If applicable)	9. PROCUREMENT INSTRUMENT IDENTIFICATION NUMBER	
8c. ADDRESS (City, State and ZIP Code)			10. SOURCE OF FUNDING NOS.	
11. TITLE (Include Security Classification) See Box 19			PROGRAM ELEMENT NO.	TASK NO.
			PROJECT NO.	WORK UNIT NO.
12. PERSONAL AUTHOR(S) William J. Locken, B.S., Capt, USAF				
13a. TYPE OF REPORT MS Thesis	13b. TIME COVERED FROM _____ TO _____	14. DATE OF REPORT (Yr., Mo., Day) 1983 December	15. PAGE COUNT 250	
16. SUPPLEMENTARY NOTATION				
17. COSATI CODES			18. SUBJECT TERMS (Continue on reverse if necessary and identify by block number)	
FIELD	GROUP	SUB. GR.	Multivariable Flight Control Digital P.I. Controller	
19. ABSTRACT (Continue on reverse if necessary and identify by block number)				
Title: DIGITAL MULTIVARIABLE CONTROL LAWS FOR THE KC-135A			Approved for public release: LAW, AFR 180-17, LYNN E. WOLAVER Dean for Research and Professional Development, Air Force Institute of Technology (AFIT), Wright-Patterson AFB, OH 45433 7 MAY 84	
Thesis Chairman: Professor John J. D'Azzo Deputy Department Head Electrical Engineering Department Air Force Institute of Technology				
20. DISTRIBUTION/AVAILABILITY OF ABSTRACT UNCLASSIFIED/UNLIMITED <input checked="" type="checkbox"/> SAME AS RPT. <input type="checkbox"/> DTIC USERS <input type="checkbox"/>			21. ABSTRACT SECURITY CLASSIFICATION UNCLASSIFIED	
22a. NAME OF RESPONSIBLE INDIVIDUAL John J. D'Azzo, Professor, AFIT			22b. TELEPHONE NUMBER (Include Area Code) 513-255-3576	22c. OFFICE SYMBOL AFIT/ENG

DD FORM 1473, 83 APR

EDITION OF 1 JAN 73 IS OBSOLETE.

UNCLASSIFIED

SECURITY CLASSIFICATION OF THIS PAGE

Multivariable design technique developed by Professor Brian Porter of the University of Salford, England, are used to develop digital control laws for the KC-135A. Control laws are developed for each of three diverse flight conditions. MULTI, a computer program used in the design, is modified to account for computational time delay. The effects of a computational time delay on the controllers developed are presented.

The controllers developed, using these techniques, utilize output feedback with proportional plus integral control. Because of the structure of the system, measurement variables, in addition to the outputs, are necessary. A reduced controller is modeled by setting some of the required feedback gains to zero. A comparison of the results of the reduced controller to the complete controller is presented.

A robustness controller is tested by performing specific maneuvers at more than one flight condition. The robust controller is of the reduced form and is required to perform under the constraints of the computational time delay.

This thesis concludes that actuator dynamics play a significant role in the development of control laws, and as a result 2nd order or higher actuator models should be used in future studies.